

Effects of dopamine on BDNF / TrkB mediated signaling and plasticity on cortico-striatal synapses

Effekte von Dopamin auf BDNF / TrkB vermittelte Signalwege und Plastizität an cortico-striatalen Synapsen



**Doctoral thesis for a doctoral degree
at the Institute of Clinical Neurobiology
University Hospital Würzburg
and
The Graduate School of Life Sciences,
Julius-Maximilians-Universität Würzburg,
Section: Neuroscience**

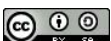
Submitted by

Thomas Andreska

from

Bad Salzungen, Germany

Würzburg, August 2018



Submitted on: 29 August 2018

Members of the *promotion-committee*:

Chairperson: Prof. Dr. Utz Fischer

Primary Supervisor: Prof. Dr. Michael Sendtner

Supervisor (Second): Prof. Dr. Esther Asan

Supervisor (Third): Prof. Dr. Jens Volkmann

Supervisor (Fourth): Prof. Dr. Charlotte Förster

Date of Public Defence:

Date of Receipt of Certificates:

„Wyrđ bið ful aræd!”

Table of contents

1. Summary	6
2. Zusammenfassung	8
3. Introduction	10
3.1. The Basal Ganglia Circuit	10
3.2. The neurotrophic factor BDNF is required for striatal development and function	13
3.3. Classification of cortical layers and subcortical projection neurons	15
3.4. Two classes of striatal medium spiny projection neurons with opposing functions	16
3.5 Dopamine mediated signaling in striatal MSNs is facilitated by two opposing GPCRs	18
3.6 Dopamine receptors are able to mediate surface expression of transmembrane proteins	21
3.7. A link between BDNF and dopamine signaling	23
3.8 Aim of the study	26
4. Material & Methods	30
4.1 Materials	30
4.1.1 Animals	30
4.1.2 Technical devices	31
4.1.3 Expendable materials	33
4.1.4 Chemicals	34
4.1.5 Buffers and media	37
4.1.5.1 Cell culture	37
4.1.5.2 Immunocytochemistry (ICC) and Immunohistochemistry (IHC)	37
4.1.5.3 Fluorescence <i>in situ</i> hybridization (FISH)	38
4.1.5.4 Western Blot analysis, Surface Biotinylation, Immunoprecipitation	40
4.1.5.5 BDNF ELISA	42
4.1.5.6 Polymerase Chain Reaction (PCR)	43
4.1.6 PCR Primers and Oligo-probes for FISH	43
4.1.6.1 PCR Primers - Genotyping	43
4.1.6.2 PCR Primers - qRT-PCR	44
4.1.6.3 Oligo Probes for FISH	44
4.1.7 PrimaryAntibodies	44
4.1.7.1 Mouse derived primary antibodies	44
4.1.7.2 Rabbit derived primary antibodies	45

4.1.7.3 Goat derived primary antibodies	46
4.1.7.4 Chicken derived primary antibodies	46
4.1.7.5 Rat derived primary antibodies	46
4.1.8 SecondaryAntibodies	47
4.1.8.1 Fluorescent secondary antibodies.....	47
4.1.8.2 Enzyme linked secondary antibodies	47
4.1.9 Kits.....	48
4.1.10 Software	48
4.2 Methods	49
4.2.1 Cell culture.....	49
4.2.1.1 Coating of cell culture coverslips.....	49
4.2.1.2 Tissue preparation	49
4.2.1.3 Stimulation of striatal MSN cell cultures	51
4.2.2 BDNF / TrkB Immunohistochemistry (IHC).....	51
4.2.2.1 Tissue preparation	51
4.2.2.2 30µm free floating vibratome brain slices.....	52
4.2.2.3 BDNF / TrkB Immunohistochemistry staining protocol.....	52
4.2.3 Immunocytochemistry (ICC)	53
4.2.4 Immunocytochemistry (ICC) with Fluorescence <i>in situ</i> Hybridisation (FISH).....	54
4.2.5 Western Blot analysis of tissue samples obtained from mouse or rat.....	55
4.2.5.1 Tissue preparation from animals	55
4.2.5.2 Tissue dissociation / lysis	56
4.2.5.3 Sonification	56
4.2.5.4 BCA Assay for calculation of protein content	56
4.2.5.5 SDS - gel running.....	57
4.2.5.6 Gel loading and electrophoresis	58
4.2.5.7 Preparation of PVDF (nitrocellulose) membrane (5x8.3cm)	58
4.2.5.8 Blotting.....	59
4.2.5.9 Blocking and primary antibody incubation.....	59
4.2.5.10 Secondary antibody incubation and detection.....	60
4.2.5.11 Loading control and re-probing.....	60
4.2.5.12 Storage.....	61
4.2.6 Immunoprecipitation of TrkB and Western Blot analysis from tissue samples	61
4.2.6.1 Pre-clearing and protein binding	61

4.2.6.2 Pulldown and purification	61
4.2.7 TrkB surface biotinylation in striatal MSNs (primary & FACS)	62
4.2.7.1 Cell culture	62
4.2.7.2 Biotinylation.....	62
4.2.7.3 Cell lysis.....	62
4.2.7.4 Avidin mediated pull-down.....	63
4.2.7.5 Purification of surface proteins	63
4.2.8 BDNF ELISA.....	64
4.2.8.1 Tissue preparation from animals	64
4.2.8.2 Tissue dissociation/lysis for ELISA	64
4.2.8.3 Sonification	64
4.2.8.4 Coating of 96 well ELISA plate with "collecting antibody"	64
4.2.8.5 ELISA - plate blocking	64
4.2.8.6 BDNF standard curve and plate loading	65
4.2.8.7 Second antibody incubation and detection.....	66
4.2.9 RNA purification and qRT-PCR analysis.....	66
4.2.9.1 RNA purification from tissue samples	66
4.2.9.2 RNA purification from cell culture	67
4.2.9.3 RNA quality control and DNA digestion.....	68
4.2.9.4 Digestion of genomic DNA (gDNA) in purified RNA samples	69
4.2.9.5 cDNA synthesis from RNA by RT-PCR.....	69
4.2.9.6 qRT-PCR for <i>Gapdh</i>	70
4.2.9.7 qRT-PCR for <i>Gfp</i>	71
4.2.9.8 qRT-PCR for mouse <i>TrkB</i> Full Length.....	71
4.2.9.9 qRT-PCR for mouse <i>TrkB T1</i>	72
4.2.9.10 qRT-PCR for rat <i>TrkB</i>	73
4.2.10 Genotyping.....	74
4.2.10.1 PCR for NFL-Cre BDNF ^{fl/ko}	74
A) NFL-Cre PCR.....	74
B) BDNF k.o. PCR.....	74
C) BDNF loxP PCR.....	75
D) BDNF - remaining loxP site after Cre - recombination	76
4.2.10.2 <i>BDNF-myc</i> PCR	77
4.2.10.3 Ntrk Rohrer (<i>TrkB</i> ^{-/-}) PCR.....	77

4.2.10.4 <i>Drd1-EGFP</i> PCR	78
4.2.10.5 <i>Drd1-Td-Tomato</i> PCR.....	79
4.2.10.6 <i>Drd2-EGFP</i> PCR	80
4.2.11 Imaging and image preparation	80
5. Results	81
5.1 Optimization of BDNF Detection.....	81
5.2 BDNF expression in Cortex and Midbrain.....	87
5.3 BDNF expression in somatomotor cortical areas involved in the control of voluntary movement	92
5.4 BDNF expression in pre- and infralimbic cortex involved in motivational regulation ..	98
5.5 Verification of BDNF-IR in the striatum	103
5.6 Detection of BDNF in presynaptic VGluT1 positive cortico-striatal terminals.....	105
5.7 BDNF expression in midbrain dopaminergic neurons	111
5.8 BDNF/TrkB mediated plasticity in rodent striatum	113
5.9 Verification of TrkB antibody specificity	115
5.10 6-OHDA induced ablation of dopamine in nigrostriatal projections	122
5.11 TrkB forms intracellular aggregates in striatal MSNs in the absence of dopamine ...	124
5.12 TrkB aggregates specifically form in MSNs of the direct pathway	128
5.13 TrkB aggregates occur in the endocytic rather than in the secretory pathway.....	129
5.14 The number of TrkB aggregates remains stable over time.....	137
5.15 Translocation of TrkB in striatal MSNs <i>in vitro</i>	141
5.16 Fluorescence-activated cell sorting (FACS) using transgenic mice enables specific enrichment of iMSNs <i>in vitro</i>	142
5.17 Activation of DRD2 by the high-affinity agonist Sumanitrole prevents TrkB surface expression	153
5.18 Stimulation of DRD2 with Sumanitrole causes induction of pTrkB.....	157
6. Discussion	161
6.1 Developmental expression of BDNF in layer V subcortical projection neurons of the motor cortex.....	161
6.2 BDNF expression in cortical neurons is reflected by BDNF expression in cortico-striatal terminals	167
6.3 BDNF expression in the limbic cortex	169
6.4 BDNF expression in cortical areas of the ventral mPFC.....	170
6.5 BDNF expression in layer VI somatosensory cortex	171
6.6 Translocation and transactivation of TrkB in striatal medium spiny neurons.....	173

7. References	182
8. Appendix	201
8.1 Table of figures.....	201
8.2 Table of tables	202
8.3 Abbreviations.....	203
Akt kinase / Protein kinase B	203
9. Affidavit	206
10. Curriculum Vitae.....	207
11. Acknowledgments	208

1. Summary

Progressive loss of voluntary movement control is the central symptom of Parkinson's disease (PD). Even today, we are not yet able to cure PD. This is mainly due to a lack of understanding the mechanisms of movement control, network activity and plasticity in motor circuits, in particular between the cerebral cortex and the striatum. Brain-derived neurotrophic factor (BDNF) has emerged as one of the most important factors for the development and survival of neurons, as well as for synaptic plasticity. It is thus an important target for the development of new therapeutic strategies against neurodegenerative diseases. Together with its receptor, the Tropomyosin receptor kinase B (TrkB), it is critically involved in development and function of the striatum. Nevertheless, little is known about the localization of BDNF within presynaptic terminals in the striatum, as well as the types of neurons that produce BDNF in the cerebral cortex. Furthermore, the influence of midbrain derived dopamine on the control of BDNF / TrkB interaction in striatal medium spiny neurons (MSNs) remains elusive so far. Dopamine, however, appears to play an important role, as its absence leads to drastic changes in striatal synaptic plasticity. This suggests that dopamine could regulate synaptic activity in the striatum via modulation of BDNF / TrkB function. To answer these questions, we have developed a sensitive and reliable protocol for the immunohistochemical detection of endogenous BDNF. We find that the majority of striatal BDNF is provided by glutamatergic, cortex derived afferents and not dopaminergic inputs from the midbrain. In fact, we found BDNF in cell bodies of neurons in layers II-III and V of the primary and secondary motor cortex as well as layer V of the somatosensory cortex. These are the brain areas that send dense projections to the dorsolateral striatum for control of voluntary movement. Furthermore, we could show that these projection neurons significantly downregulate the expression of BDNF during the juvenile development of mice between 3 and 12 weeks.

In parallel, we found a modulatory effect of dopamine on the translocation of TrkB to the cell surface in postsynaptic striatal Medium Spiny Neurons (MSNs). In MSNs of the direct pathway (dMSNs), which express dopamine receptor 1 (DRD1), we observed the formation of TrkB aggregates in the 6-hydroxydopamine (6-OHDA) model of PD. This suggests that DRD1 activity controls TrkB surface expression in these neurons. In contrast, we found that DRD2 activation has opposite effects in MSNs of the indirect pathway (iMSNs). Activation of DRD2 promotes a rapid decrease in TrkB surface expression which was reversible and depended on cAMP. In parallel, stimulation of DRD2 led to induction of phospho-TrkB (pTrkB). This effect was significantly slower than the effect on TrkB surface expression and indicates that TrkB is transactivated by DRD2. Together, our data provide evidence that dopamine triggers dual modes of plasticity on striatal MSNs by acting on TrkB surface expression in DRD1 and DRD2 expressing MSNs. This surface expression of the receptor is crucial for the binding of BDNF, which is released from corticostriatal afferents. This leads to the induction of TrkB-mediated downstream signal transduction cascades and long-term potentiation (LTP). Therefore, the dopamine-mediated translocation of TrkB could be a mediator that modulates the balance between dopaminergic and glutamatergic signaling to allow synaptic plasticity in a spatiotemporal manner. This information and the fact that TrkB is segregated to persistent aggregates in PD could help to improve our understanding of voluntary movement control and to develop new therapeutic strategies beyond those focusing on dopaminergic supply.

2. Zusammenfassung

Der fortschreitende Verlust der willkürlichen Bewegungskontrolle ist ein zentrales Symptom der Parkinson-Krankheit (PD). Auch heute sind wir noch nicht in der Lage, PD zu heilen. Dafür verantwortlich ist hauptsächlich ein mangelndes Verständnis von Mechanismen der Bewegungskontrolle, Netzwerkaktivität und Plastizität in motorischen Schaltkreisen, insbesondere zwischen Hirnrinde und Striatum. Der neurotrophe Faktor BDNF ist einer der wichtigsten Faktoren für die Entwicklung und das Überleben von Neuronen sowie für synaptische Plastizität im zentralen Nervensystem. BDNF ist daher ein Target für die Entwicklung neuer therapeutischer Strategien gegen neurodegenerative Erkrankungen. Zusammen mit seinem Rezeptor, der Tropomyosin-Rezeptorkinase B (TrkB), ist BDNF maßgeblich an der Entwicklung und Funktion des Striatums beteiligt. Dennoch ist nur wenig bekannt, wo BDNF an Synapsen im Striatum lokalisiert ist, und wo BDNF in Neuronen der Hirnrinde synthetisiert wird. Außerdem ist der Einfluss von Dopamin aus dem Mittelhirn auf die Kontrolle der BDNF / TrkB-Interaktion in striatalen Medium-Spiny-Neuronen (MSNs) bisher unklar. Dopamin scheint jedoch eine wichtige Rolle zu spielen, da dessen Abwesenheit zu drastischen Veränderungen der striatalen Plastizität führt. Dopamin könnte synaptische Plastizität im Striatum über eine Modulation der BDNF / TrkB-Interaktion regulieren. Um diese Fragen beantworten zu können, haben wir ein sensibles und zuverlässiges Protokoll für den immunhistochemischen Nachweis von endogenem BDNF entwickelt. Wir fanden heraus, dass BDNF im Striatum vor allem in glutamatergen Synapsen von Projektion aus dem Kortex lokalisiert ist und nicht in Terminalen dopaminergener Neurone aus dem Mittelhirn. Tatsächlich fanden wir BDNF in den Zellkörpern von Neuronen in den Schichten II-III und V des primären und sekundären motorischen Kortex sowie Schicht V des somatosensorischen Kortex. Es sind jene Hirnareale, welche dichte Projektionen zum dorsolateralen Striatum senden und entscheidend an der Steuerung von willkürlichen Bewegungen beteiligt sind. Weiterhin konnten wir zeigen, dass eben jene Projektionsneurone die Bildung von BDNF

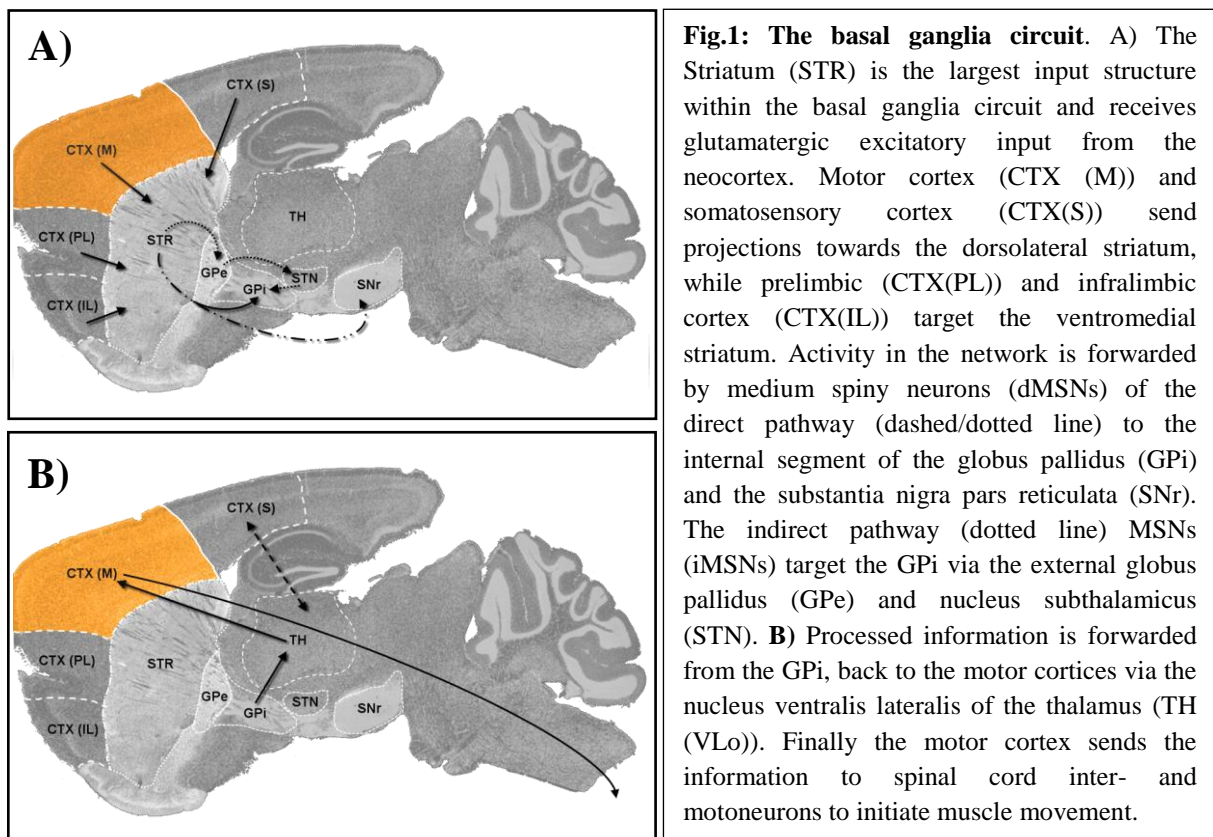
während der juvenilen Entwicklung von Mäusen zwischen 3 und 12 Wochen signifikant herunter regulieren.

In striatalen MSN fanden wir zudem einen modulatorischen Effekt von Dopamin auf die Translokation von TrkB zur Zelloberfläche. In MSNs des direkten Signalweges (dMSNs), welche Dopaminrezeptor 1 (DRD1) exprimieren, konnten wir die Bildung von TrkB-Aggregaten im 6-Hydroxydopamin (6-OHDA) - Rattenmodell der Parkinson Erkrankung beobachten. Dies deutet darauf hin, dass die DRD1-Aktivität die TrkB-Oberflächenexpression in diesen Neuronen steuert. Im Gegensatz dazu fanden wir heraus, dass die DRD2-Aktivierung in MSNs des indirekten Signalweges (iMSNs) eine gegensätzliche Wirkung hat. Die Aktivierung von DRD2 führt zu einer schnellen Reduktion der TrkB-Oberflächenexpression, die reversibel und von cAMP abhängig ist. Außerdem führte die Stimulation von DRD2 zu einer Induktion von Phospho-TrkB (pTrkB). Dieser Effekt war deutlich langsamer als die Wirkung auf die TrkB-Oberflächenexpression und deutet auf eine Transaktivierung von TrkB über DRD2 hin. Insgesamt scheint Dopamin entgegengesetzte Plastizitätsmodi in striatalen MSNs auszulösen, indem es auf die TrkB-Oberflächenexpression in DRD1- und DRD2-exprimierenden MSNs einwirkt. Diese Oberflächenexpression des Rezeptors ist entscheidend für die Bindung von BDNF, welches aus kortiko-striatalen Afferenzen freigesetzt wird. Dies führt zur Induktion von TrkB-vermittelten-Signaltransduktionskaskaden und Langzeitpotenzierung (LTP). Daher könnte die dopamin-vermittelte Translokation von TrkB das Gleichgewicht zwischen dopaminergen und glutamatergen Signalen modulieren, um die synaptische Plastizität in einer räumlich-zeitlich abgestimmten Weise zu ermöglichen. Diese Information und die Tatsache, dass TrkB bei PD stabile Aggregate bildet, könnte dazu beitragen, unser Verständnis der willkürlichen Bewegungskontrolle zu verbessern und neue therapeutische Strategien zu entwickeln, die über jene hinausgehen, welche sich auf die dopaminerge Versorgung konzentrieren.

3. Introduction

3.1. The Basal Ganglia Circuit

Voluntary movement initiation is processed within the primary motoric loop through the basal ganglia circuit (**Fig. 1**). This loop involves the cerebral cortex, striatum, globus pallidus, thalamus and substantia nigra in the midbrain. Within this motor-loop, the striatum is the largest receptive component into the basal ganglia which receives excitatory, somatotopically organized, glutamatergic input from the motor and somatosensory cortices (Kunzle, 1975; Tanji and Evarts, 1976; Kunzle, 1977; Tanji et al., 1980; Weinrich and Wise, 1982; Alexander et al., 1986).



Both regions densely innervate dorsolateral and ventromedial regions of the striatum which represent areas involved in limb movement control (Webster, 1961; Kunzle, 1975, 1977; Wise and Jones, 1977; Cospito and Kultas-Ilinsky, 1981; Alexander et al., 1986; Donoghue and Herkenham, 1986; McGeorge and Faull, 1989; West et al., 1990; Kanazawa et al., 1993;

Kimura et al., 1993; Yin and Knowlton, 2006) In addition to the primary motor cortex, further innervation to the dorsolateral striatum arises from the pre- and supplementary (secondary) motor areas of the cortex (Tanji and Evarts, 1976; Wise and Jones, 1977; Kunzle, 1978; Tanji et al., 1980; Weinrich and Wise, 1982; Miyata and Sasaki, 1984; Selemon and Goldman-Rakic, 1985). This region-specific organization of activity is also represented within the globus pallidus and further encodes information about direction and intensity of the intended movement (Cowan and Powell, 1966; Nauta and Mehler, 1966; Szabo, 1967; Johnson and Rosvold, 1971; DeVito et al., 1980; Georgopoulos et al., 1983; Crutcher and DeLong, 1984; Parent et al., 1984; DeLong et al., 1985; Liles, 1985). These projections from the striatum (caudate-putamen) to the globus pallidus are separated into direct pathway projections, innervating the internal segment of the globus pallidus (GPi) (Chesselet and Graybiel, 1983; Penney and Young, 1983; Alexander and Crutcher, 1990; Gerfen, 1992; Gerfen and Surmeier, 2011) and the substantia nigra (Nauta and Mehler, 1966; Szabo, 1967; Parent et al., 1983; Alexander et al., 1986), while indirect pathway neurons innervate the GPi via the external segment of the globus pallidus (GPe) and the nucleus subthalamicus (STN) (Chesselet and Graybiel, 1983; Penney and Young, 1983; Beckstead and Kersey, 1985; Alexander and Crutcher, 1990; Gerfen et al., 1990; Gerfen, 1992, 2006; Gerfen and Surmeier, 2011). Similarly, an activity initiated within cortical motor areas is followed, temporally delayed, by the caudate putamen and globus pallidus (Georgopoulos et al., 1983; Crutcher and DeLong, 1984; DeLong et al., 1984; Alexander et al., 1986). Activity in the GPi in turn is forwarded to the nucleus ventralis lateralis of the thalamus (VLo) (Nauta and Mehler, 1966; Kuo and Carpenter, 1973; Kim et al., 1976; DeVito and Anderson, 1982), from which dense projections are directed back to the supplementary motor cortex (Schell and Strick, 1984; Alexander et al., 1986). From here, the information is finally forwarded to spinal cord inter- and motor-neurons to initiate the output of the motor program (Hallett and Khoshbin, 1980; DeLong et al., 1984; Alexander et al., 1986; West et al., 1990). In summary, the striatum

receives afferent input virtually from the whole neocortex, especially primary and supplementary (secondary) motor cortex (Tanji and Evarts, 1976; Tanji et al., 1980; Weinrich and Wise, 1982), somatosensory cortex and arcuate cortex, as well as from the substantia nigra (Alexander et al., 1986). These inputs into the basal ganglia are processed within the globus pallidus and thalamus and are finally projected to the secondary motor cortex, the output structure which forwards information about movement initiation to the primary motor cortex as well as to spinal cord interneurons and motor-neurons (Biber et al., 1978; Muakkassa and Strick, 1979; Murray and Coulter, 1981; Palmer et al., 1981; Macpherson et al., 1982; Schell and Strick, 1984; Alexander et al., 1986). Thus the secondary motor cortex seems to play an important role in programming coordinated movement patterns and is further involved in their initiation which was also indicated by increased activity during planning and execution of complex movements (Roland et al., 1980). For this reason it has been suggested that distinct motor programs are written in motor cortices, fine-tuned in striatum and globus pallidus which add information about correct speed and direction of the programs which are then finally carried out by spinal cord mediated muscle contraction or relaxation (Hallett and Khoshbin, 1980; DeLong et al., 1984; Alexander et al., 1986; West et al., 1990). All this indicates a delicate interplay between multiple input structures which are integrated into a complex neuronal network, in which single components contribute to the correct coordination and initiation of voluntary movement. Errors within this network can cause severe pathologies. One example is Parkinson's disease which is characterized by a progressive loss of dopaminergic neurons in the substantia nigra pars compacta (Surmeier et al., 2014; Zhai et al., 2018). This reduces the availability of dopamine in the striatum, leading to hypokinetic motor symptoms like rigidity and bradykinesia, but also tremor (Zhai et al., 2018). Since its discovery in 1817, by James Parkinson (Parkinson, 2002), much effort has been conducted in order to understand this disease and develop therapeutic strategies. Today we know that PD occurs in multiple variants, amongst which mutations in the α -syn nuclein gene are critical

factors for the development of the disease (Polymeropoulos et al., 1997; Spillantini et al., 1997; Kruger et al., 1998; Zarranz et al., 2004). Facilitating the production of dopamine by the remaining dopaminergic neurons through the application of Levodopa (L-Dopa) turned out to be an effective treatment at early disease stages (Lang and Lozano, 1998a, b). Nevertheless, increased dosage and progressive loss of dopaminergic neurons tend to induce side effects like L-Dopa induced dyskinesia (Obeso et al., 2000; Picconi et al., 2003; Zhai et al., 2018). In late-stage PD, when medication is not able to improve the symptoms anymore, deep brain stimulation turned out to be an efficient tool to equalize failure in activity in the basal ganglia circuit (Kumar et al., 1998; Deep-Brain Stimulation for Parkinson's Disease Study et al., 2001; Rodriguez-Oroz et al., 2005; Benabid et al., 2009). However, even 200 years after its first scientific description, we are still unable to stop disease progression or to cure PD. This indicates the need for a better understanding of the network connectivity and conducted activity, in order to develop better therapeutic strategies.

3.2. The neurotrophic factor BDNF is required for striatal development and function

New therapeutic strategies have arrived with the discovery of neurotrophic factors and their ability to promote neuronal survival, growth, and differentiation, starting with the work of Rita Levi-Montalcini in the 1950's (Levi-Montalcini and Hamburger, 1951; Cohen et al., 1954). This marked the origin of the discovery of a whole family of neurotrophic factors, amongst which Brain-Derived Neurotrophic Factor (BDNF) (Barde et al., 1982) turned out to be the most promising candidate for developing therapeutic approaches for neurodegenerative diseases. This is due to the ability of BDNF to promote neuronal differentiation, survival and in particular to its function in modulating synaptic plasticity within the adult brain, through binding to receptor tyrosine kinase B (TrkB) (Barde et al., 1982; Soppet et al., 1991; Barbacid, 1994; Thoenen, 1995; Poo, 2001; Luikart and Parada, 2006; Minichiello, 2009).

Global ablation of this factor leads to early postnatal death by failure in sensory neuron development (Ernfors et al., 1994; Jones et al., 1994; Conover et al., 1995; Liu et al., 1995; Erickson et al., 1996; Liebl et al., 1997; Brady et al., 1999). To investigate the role of BDNF in the adult CNS and PNS, strategies for conditional postnatal BDNF ablation had to be developed. These approaches provided new insights into the role of BDNF for the development and function of different brain areas (Rauskolb et al., 2010). Even though densely expressed in the hippocampus (Ernfors et al., 1990b; Ernfors et al., 1990a; Hofer et al., 1990; Phillips et al., 1990; Wetmore et al., 1990; Conner et al., 1997; Yan et al., 1997; Dieni et al., 2012), ablation of BDNF had little impact on hippocampal morphology. Instead, depletion of BDNF in the adult mouse causes severe morphological changes in other brain regions, in particular, the striatum (Rauskolb et al., 2010). The striatum itself does not contain BDNF expressing cells, but rather depends on external BDNF import, mainly from cortex and possibly midbrain (Altar et al., 1997; Conner et al., 1997; Yan et al., 1997; Gorski et al., 2003; Baquet et al., 2004; Li et al., 2012). Indeed BDNF mRNA and protein have been observed in cortical layers II, III, V and VI (Conner et al., 1997; Yan et al., 1997). In the absence of BDNF (Rauskolb et al., 2010) or TrkB (Baydyuk et al., 2011) the striatum shows a massive decrease in volume, accompanied by decreased dendritic architecture and spine loss on GABAergic, striatal medium spiny neurons (MSNs). On the functional level, BDNF / TrkB signaling appears critically involved in striatal modes of plasticity, especially LTP induction in cortico-striatal synapses (Jia et al., 2010; Park et al., 2014; Plotkin et al., 2014). Thus, the majority of BDNF which is responsible for maintenance of morphology and synaptic function within the striatum seems to be derived from subcortical projection neurons within the neocortex. Nevertheless, the direct visualization of endogenous BDNF remained difficult, due to the very low protein levels and lack of reliable methods for immunohistochemical detection of this protein.

3.3. Classification of cortical layers and subcortical projection neurons

The cortex of higher mammals is structured on the morphological level into distinct layers. Within these cortical layers, several types of pyramidal neurons which constitute ~75-85% (Tsiola et al., 2003; Voelker et al., 2004; Molnar and Cheung, 2006), as well as inter- and non-pyramidal neurons constituting ~15-25% (Hendry et al., 1987; Meinecke and Peters, 1987; Markram et al., 2004) of all neurons are located in direct neighborhood. Nevertheless, cortical neurons within discrete layers are functionally different which makes it difficult to specifically identify neurons of the same functional subtype. This is reflected by the fact that markers which identify these discrete subpopulations are extremely rare. One way to distinguish neurons of distinct layers is based on differences in their morphology. Layer V subcortical projection neurons are distinguished by the degree of their dendritic branching. Type I or tufted neurons express high levels of neurofilament proteins and usually constitute corticobulbar and corticospinal projection neurons (Voelker et al., 2004; Molnar and Cheung, 2006). Type II, or non-tufted pyramidal projection neurons, are of higher interest since they directly target the striatum and also form connections within the cortex (Voelker et al., 2004; Molnar and Cheung, 2006). Both populations express CTIP2, a protein of yet unknown function which is a neuronal subtype-specific, rather than a simple layer specific marker (Arlotta et al., 2005). It is highly enriched in subcortical projection neurons of layer V, to a lesser extent in layer VI cortico-thalamic neurons, but not in cortico-cortical projection neurons (Arlotta et al., 2005; Molyneaux et al., 2007). Among the neurons in layer V it is also expressed in corticospinal motor neurons (CSMN), where it is important for the formation of axonal fibers, even though, it is not exclusively expressed by this subpopulation of projection neurons (Arlotta et al., 2005). The DNA binding protein Cux-1, another layer specific marker, is expressed in upper layers II-IV (Nieto et al., 2004). Together Cux-1 and CTIP-2 can be used as markers to identify pyramidal projection neurons of layer II-III and layer V which also govern those subcortical projection neurons innervating the striatum.

3.4. Two classes of striatal medium spiny projection neurons with opposing functions

Afferent fibers from subcortical projection neurons of the somatomotor cortex enter the basal ganglia circuit by entry into its largest receptive component, the striatum. In this structure sensorimotor, cognitive and motivational inputs arrive and experience an initial processing step which leads to the essential initiation of motivational cues, action and movement initiation, habit formation, skill and motor learning (Graybiel et al., 1994; Mink, 1996; Tepper and Bolam, 2004; Bertran-Gonzalez et al., 2010). The dorsolateral part of the striatum is involved in the control of movement (Webster, 1961; Wise and Jones, 1977; Cospito and Kultas-Ilinsky, 1981; Kelley et al., 1982; Donoghue and Herkenham, 1986; McGeorge and Faull, 1989; West et al., 1990; Kanazawa et al., 1993; Kimura et al., 1993; Yin and Knowlton, 2006), while its ventral part, the nucleus accumbens, integrates motivational information and reward-related habits (Reep et al., 2003; Yin and Knowlton, 2006; Belin et al., 2009). The incoming information is processed by two segregated neuronal populations of striatal medium spiny neurons (MSNs) which are both GABAergic. These neurons define 90-95% of all striatal neurons (Kawaguchi, 1997; Bolam et al., 2000; Tepper and Bolam, 2004). The remaining 5-10% are neuropeptide Y (NPY), Parvalbumin or ChAT-positive interneurons (Kawaguchi, 1997; Bolam et al., 2000; Tepper and Bolam, 2004). Striatal MSNs can be subdivided into two major counteracting subpopulations. Striatonigral MSNs specifically express DRD1, substance P and dynorphin and define the “Direct pathway” due to their direct projections to the midbrain and globus pallidus (**Fig. 1, 2**) (Chesselet and Graybiel, 1983; Penney and Young, 1983; Alexander and Crutcher, 1990; Gerfen, 1992; Gerfen and Surmeier, 2011). In contrast, projections of striatopallidal “Indirect pathway” MSNs terminate in the lateral or external segments of the globus pallidus and these neurons express DRD2 together with enkephalin (**Fig. 1, 2**) (Chesselet and Graybiel, 1983; Penney and Young, 1983; Beckstead and Kersey, 1985; Alexander and Crutcher, 1990; Gerfen et al., 1990; Gerfen,

1992, 2006; Gerfen and Surmeier, 2011). Striatal MSNs exhibit unique properties since they have structurally and functionally closely coupled receptive cellular components for glutamatergic, cortical and thalamic, as well as dopaminergic circuitries. This dopamine input arises from the midbrain, especially the ventral tegmental area (VTA) and the substantia nigra pars compacta (SNc) (Anden et al., 1964; Beckstead et al., 1979). Dopamine is a catecholaminergic neurotransmitter in the mammalian CNS, with widespread functions (Tritsch and Sabatini, 2012).

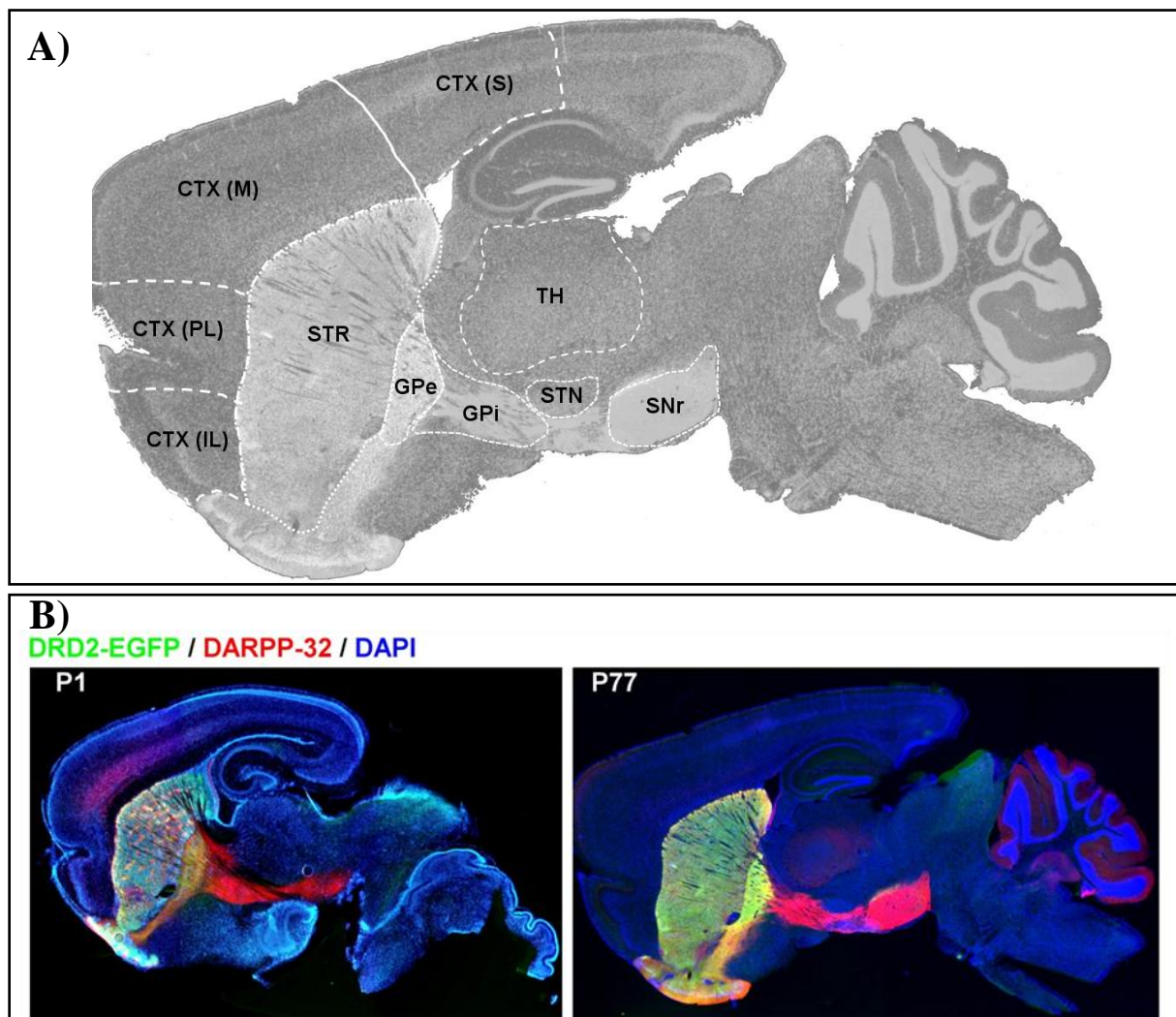


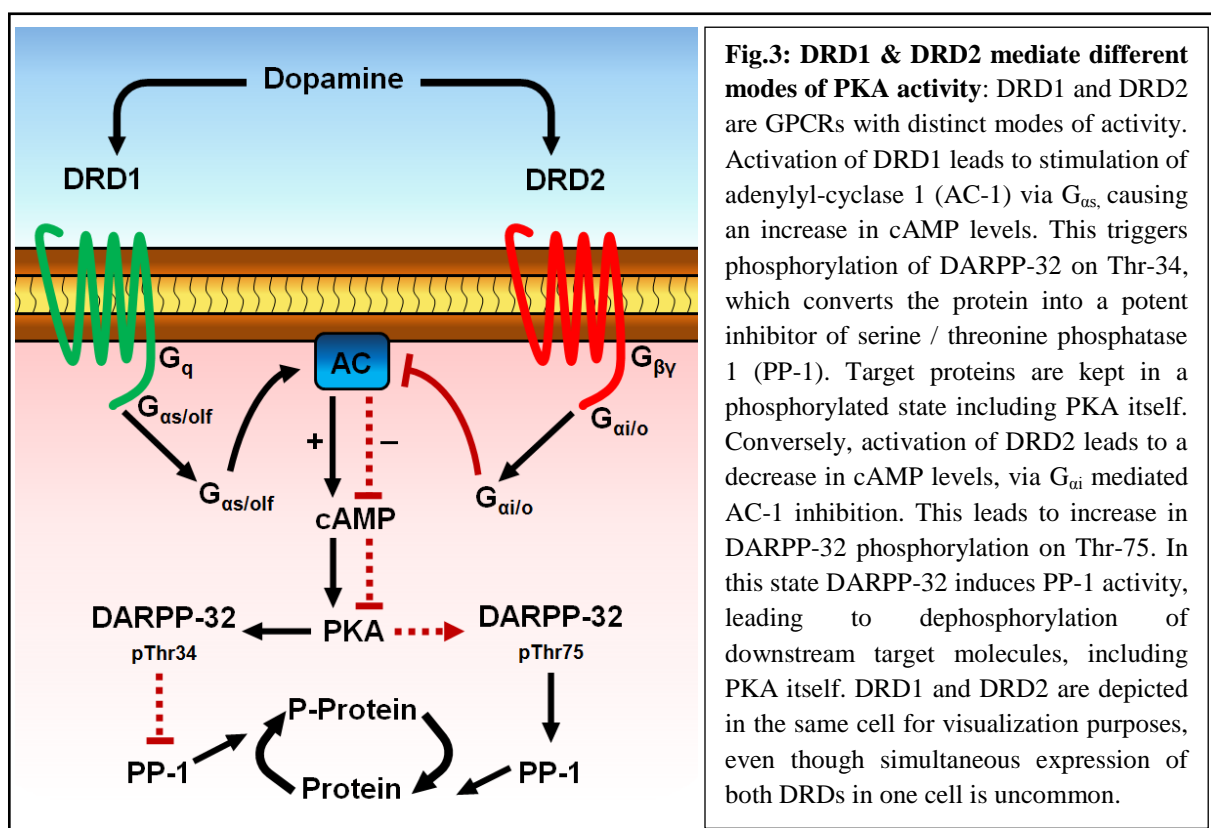
Fig.2: Projections of the Direct and Indirect pathway in mouse Striatum. A) Representative scheme illustrating components of the basal ganglia circuit (sagittal slice from adult brain - same image as P77 in B). B) Representative immunohistochemical stainings of sagittal brain slices from BAC transgenic DRD2-EGFP mice (see also Fig. 38C). Left side shows an early postnatal P1, right side an adult P77 (11wk) brain. Transgenic DRD2-EGFP expression is shown in green, DARPP-32 in red. Nuclei were stained with DAPI. DRD2-EGFP highlights striatal neurons of the indirect pathway, whose projections terminate in the external segment of globus pallidus. DARPP-32 is expressed in all striatal medium spiny neurons. Thus it also indicates direct pathway MSN projections to the midbrain. Abbreviations: primary somatosensory cortex - CTX(S); Primary and secondary motor cortex - CTX(M); prelimbic cortex - CTX(PL); infralimbic cortex - CTX(IL); Striatum - STR; external segment of globus pallidus - GPe; internal segment of globus pallidus - GPi; Nucleus Subthalamicus - STN; substantia nigra pars reticulata - SNr; thalamus - TH.

Dopamine is not only involved in the control of movement and motivation, its inaccurate signaling is linked to many neurological and psychiatric disorders like Parkinson's disease (PD), Tourette's syndrome, schizophrenia, addiction and obsessive-compulsive disorders (Tritsch and Sabatini, 2012). It is also a crucial mediator of higher cognitive functions, such as learning and memory, involved in the control of motor functions, attention, decision making and many aspects of reward (Tritsch and Sabatini, 2012). The main effects of dopamine are mediated by DRD1 and DRD2 which are the most frequently expressed dopamine receptors in the striatum. They show a 5% overlap in the dorsal striatum, and 15% overlap in MSNs of the ventral striatum, meaning their expression profiles are cell-type specific in distinct MSN types (Kebabian and Calne, 1979; Stoof and Kebabian, 1984; Beckstead, 1988; Gerfen et al., 1990; Hersch et al., 1995; Yung et al., 1995; Bertran-Gonzalez et al., 2008; Heiman et al., 2008; Lobo et al., 2010; Tritsch and Sabatini, 2012). Of both receptors, DRD2 shows a 10-100 fold higher affinity to dopamine, compared to DRD1 (Beaulieu and Gainetdinov, 2011).

3.5 Dopamine mediated signaling in striatal MSNs is facilitated by two opposing GPCRs

The main effects of dopamine in the striatum are mediated by DRD1 and DRD2. Both are the most frequently expressed dopamine receptors in the striatum and their expression profiles are cell-type specific in distinct MSN types (Kebabian and Calne, 1979; Stoof and Kebabian, 1984; Beckstead, 1988; Gerfen et al., 1990; Hersch et al., 1995; Yung et al., 1995; Bertran-Gonzalez et al., 2008; Heiman et al., 2008; Lobo et al., 2010; Tritsch and Sabatini, 2012). Both receptors belong to the family of G protein-coupled receptors (GPCRs). Nevertheless, they differ in the composition of their attached G proteins. DRD1 belongs to the family of G_{α_s} coupled receptors, able to stimulate adenylyl-cyclase (AC-1) activity, increase cAMP levels

and facilitate PKA activity (**Fig. 3**)¹ (Memo et al., 1986; Dearry et al., 1990; Monsma et al., 1990; Zhou et al., 1990; Sugamori et al., 1994; Demchyshyn et al., 1995). In contrast GPCRs coupled to G_{ai} subunits, like DRD2, inhibit AC-1 activity, decrease cAMP levels and attenuate PKA activity (**Fig. 3**) (De Camilli et al., 1979; Onali et al., 1981; Enjalbert and Bockaert, 1983; McDonald et al., 1984; Onali et al., 1985; Shen et al., 2016). All of the modes of dopaminergic and glutamatergic signaling on striatal MSNs involve a factor, commonly shared among MSNs, "dopamine and cAMP-regulated phosphoprotein of 32kDa" (DARPP-32) (**Fig. 2B**) (Fienberg and Greengard, 2000; Svenningsson et al., 2004). It serves as an intra-



cellular phosphoprotein, able to induce or inhibit further signaling cascades, depending on the site of phosphorylation in the molecule itself. For instance, PKA mediated phosphorylation of Thr34, as a result of DRD1 activation in dMSNs, converts DARPP-32 into a potent inhibitor of serine / threonine phosphatase 1 (PP-1) (Hemmings et al., 1984d; Hemmings et al., 1984c; Hemmings et al., 1984a; Hemmings et al., 1984b; Walaas and Greengard, 1984; Nishi et al.,

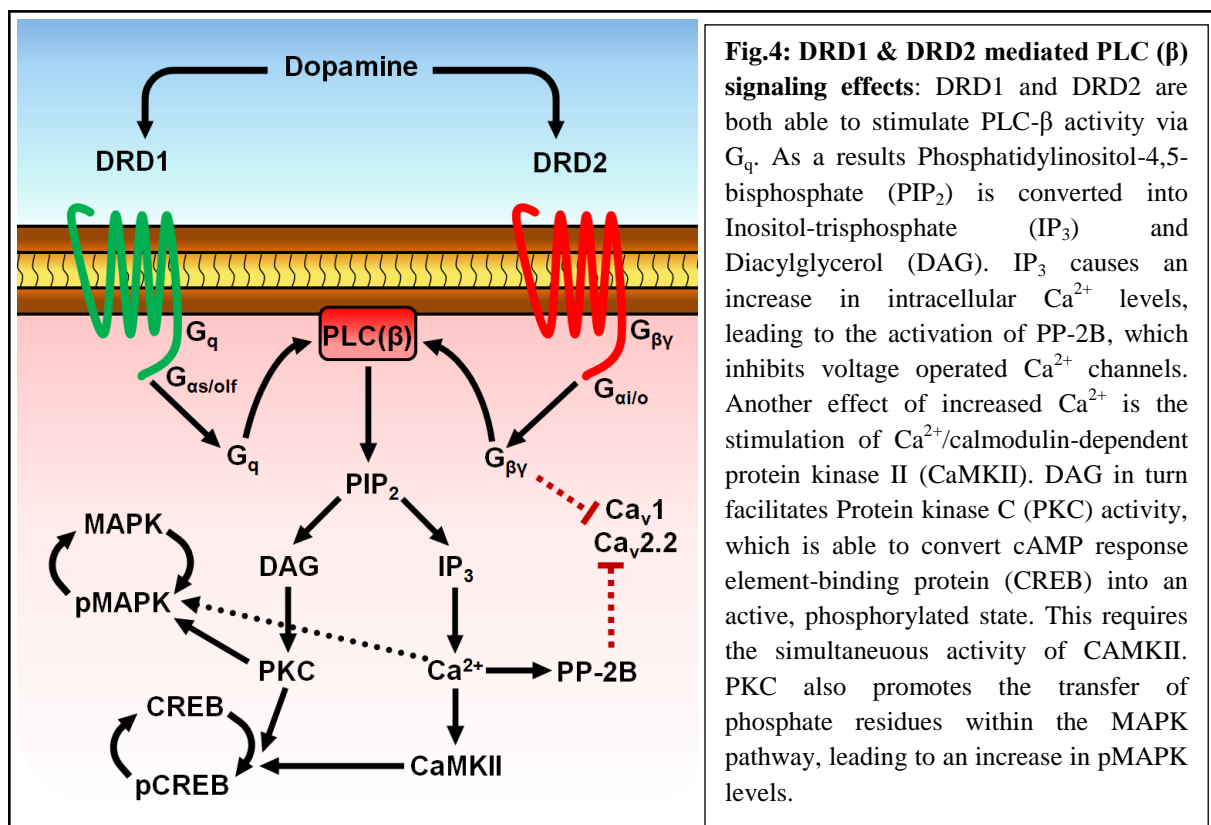
¹ Fig. 3 was reproduced and modified from (Tritsch and Sabatini, 2012)

1997; Fienberg and Greengard, 2000; Bateup et al., 2008). Thus, it mediates the preservation of phosphorylated sites of PP-1 target proteins, including PKA itself and facilitates its activity in this way (**Fig. 3**). On the other hand activation of DRD2 in iMSNs leads to the phosphorylation of DARPP-32 on Thr-75 and dephosphorylation on Thr-34 which converts it into an inhibitor of PKA (Nishi et al., 1997; Fienberg and Greengard, 2000; Bateup et al., 2008) (**Fig. 3**). Furthermore, DARPP-32 k.o. mice show a complete absence of both forms of synaptic plasticity, LTP, and longterm-depression (LTD), in striatal MSNs and a significant attenuation of corticostriatal excitatory postsynaptic potentiation (EPSPs) (Calabresi et al., 2000; Fienberg and Greengard, 2000). Thus under experimental conditions, DARPP-32 activity was shown to be required for induction of synaptic plasticity. Furthermore, inhibition of either PKA or PKC is required to prevent high-frequency stimulation (HFS)-induced LTP and LTD (Calabresi et al., 2000). This information already postulates an important role of dopamine signaling in striatal MSNs which regulates antagonistic intracellular signaling mechanisms, leading to distinct network functions of dMSNs and iMSNs.

Another important intracellular signaling cascade mediated by DRDs is independent of cAMP and targets phospholipase C (PLC) via G_q and $G_{\beta\gamma}$ subunits to convert Phosphatidylinositol 4,5-bisphosphate (PIP_2) into diacylglycerol (DAG) and inositol 1,4,5-trisphosphate (IP_3) (**Fig. 4**)² (Wang et al., 1995; Yu et al., 1996; Yan et al., 1999). IP_3 elevates intracellular Ca^{2+} levels by release from intracellular stores, in particular, the endoplasmatic reticulum (ER). These elevated Ca^{2+} levels facilitate Serine/Threonine-protein phosphatase 2B (PP-2B) activity which blocks voltage-operated Ca^{2+} channels. On the other hand, Ca^{2+} /calmodulin-dependent protein kinase II (CaMKII) also gets activated. If CaMKII activity occurs in concert with DAG mediated induction of protein kinase C (PKC), then cAMP response element-binding protein (CREB) is converted into its active form, phospho-CREB

² Fig. 4 was reproduced and modified from (Tritsch and Sabatini, 2012)

(pCREB) (Yan et al., 1999). Induction of pCREB modulates gene expression, induces transcription and is thus responsible for morphological and functional changes of synaptic connections which constitute central properties of LTP induction. At the same time activation of PKC, downstream of GPCRs is able to induce pMAPK (Berg et al., 1992; Yan et al., 1999; Lee and Chao, 2001). On the other hand, DRD2 is able to inhibit L-type Ca^{2+} channels which have been shown to play a role in spine loss on iMSNs in PD (Day et al., 2006).



3.6 Dopamine receptors are able to mediate surface expression of transmembrane proteins

Dopamine receptor activation can modulate the surface expression of neurotransmitter receptors and thus influence synaptic function on a biochemical and electrophysiological level (Tritsch and Sabatini, 2012). DRD1 is able to potentiate extrasynaptic *N*-methyl-D-aspartate receptor (NMDA-R) activity, by an increase in surface trafficking and phosphorylation of NMDA-Rs (Flores-Hernandez et al., 2002; Braithwaite et al., 2006; Hallett et al., 2006; Gao

and Wolf, 2008). As a result, dopamine is able to indirectly modulate voltage operated Ca^{2+} channels via DRD1 and change synaptic Ca^{2+} signaling via NMDA-R potentiation, leading to Mg^{2+} release and NMDA-R activation (Cepeda et al., 1998; Fienberg and Greengard, 2000). In contrast, DRD2 activation leads to a decrease in NMDA-R mediated Ca^{2+} influx which is suggested to be mediated via a PKA dependent mechanism and control of NMDA-R downstream signaling (Skeberdis et al., 2006; Chalifoux and Carter, 2010; Higley and Sabatini, 2010). Thus NMDA-R mediated synaptic signaling may be bi-directionally regulated by DRD1 and DRD2 (Fienberg and Greengard, 2000; Tritsch and Sabatini, 2012). Similar observations were also made for the surface expression and function of the α -amino-3-hydroxy-5-methyl-4-isoxazolepropionic acid receptor (AMPA-Rs). PKA mediated AMPA-R phosphorylation, causes increased open probability and surface expression (Fienberg and Greengard, 2000; Shepherd and Huganir, 2007) which is promoted by DRD1 activation (Fienberg and Greengard, 2000; Sun et al., 2008) but prevented by DRD2 activation (**Fig. 3**) (Fienberg and Greengard, 2000; Sun et al., 2005).

3.7. A link between BDNF and dopamine signaling

As mentioned above, BDNF knock out in cortical neurons (Rauskolb et al., 2010), as well as a TrkB knockout in striatal neurons (Baydyuk et al., 2011), cause a significant decrease in striatal volume by defective development of MSN dendrites and spine degeneration. BDNF is a high-affinity ligand for TrkB (Barbacid, 1994), leading to activation of several signaling cascades, including the PI3K/Akt, MAPK or PLC- γ pathways (Barbacid, 1994; Kaplan and Miller, 2000; Schlessinger, 2000; Huang and Reichardt, 2001). These pathways influence gene expression, and via transcription activity but also other direct cytoplasmic signaling mechanisms cause neuronal survival, dendrite and axon growth (Schlessinger, 2000; Poo, 2001). BDNF mediated TrkB activation also modulates synaptic activity. In particular, it is required for the induction of LTP (Poo, 2001; Minichiello, 2009; Jia et al., 2010). However, TrkB is also activated by other ligands such as Neurotrophin-3, and by transactivation through other tyrosine kinase receptors such as Epidermal growth factor receptor (EGFR) and GPCRs, like DRD1 (Iwakura et al., 2008; Puehringer et al., 2013). TrkB downstream signaling is involved in several pathophysiologic processes, neurodegenerative diseases, and mood disorders, affecting neuronal networks (Gupta et al., 2013; Zhang et al., 2014; Zhang et al., 2016). Distinct striatal subregions are affiliated with mood disorders, compulsive drug seeking in addiction, Parkinson's disease and Chorea Huntington. Thus, BDNF / TrkB interaction might play a crucial role in the pathophysiology of these diseases (Jeanblanc et al., 2009; Lesscher and Vanderschuren, 2012; Price and Drevets, 2012). Interestingly the neuropathological changes in the striatum of BDNF or TrkB deficient mouse models resemble the alterations caused by the absence of striatal dopamine supply in PD models. The ablation of dopamine also induces massive spine loss on striatal neurons (Day et al., 2006; Gerfen, 2006) and interferes with LTP and LTD in striatal MSNs (Shen et al., 2008; Shen et al., 2016; Zhai et al., 2018). Morphological and functional changes within the striatum are directly linked to both cortical BDNF function as well as to dopamine from the midbrain. This raises

an important question: How is it possible that striatal MSNs transform dopaminergic and glutamatergic synaptic inputs in a spatiotemporal manner and how does BDNF / TrkB contribute to regulation of synaptic plasticity mechanisms like LTP and LTD? Striatal LTP induction is critically linked to postsynaptic NMDAR activation, as well as to TrkB activation (Plotkin et al., 2014). In addition, LTP induction requires activation of either DRD1, in direct pathway MSNs (dMSNs), or A2aR activation in indirect pathway MSNs (iMSNs) (**Fig. 5**) (Shen et al., 2008; Plotkin et al., 2014; Shen et al., 2016). While blockade of either NMDAR or TrkB completely abolishes striatal LTP, inhibition of DRD1 only attenuates LTP, mainly because A2aR activity in iMSNs may still be present (Shen et al., 2008; Plotkin et al., 2014; Zhai et al., 2018).

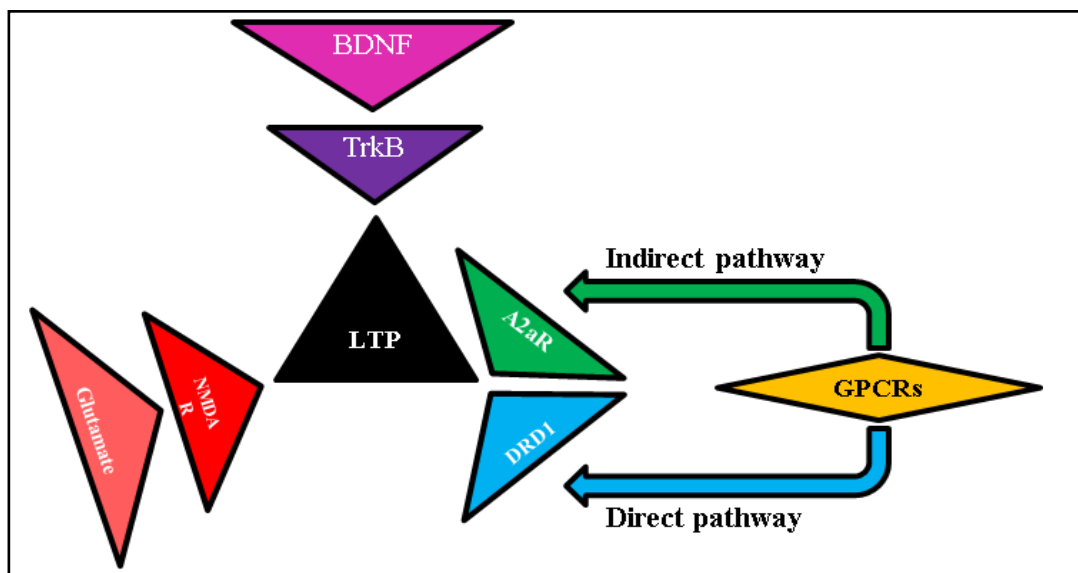
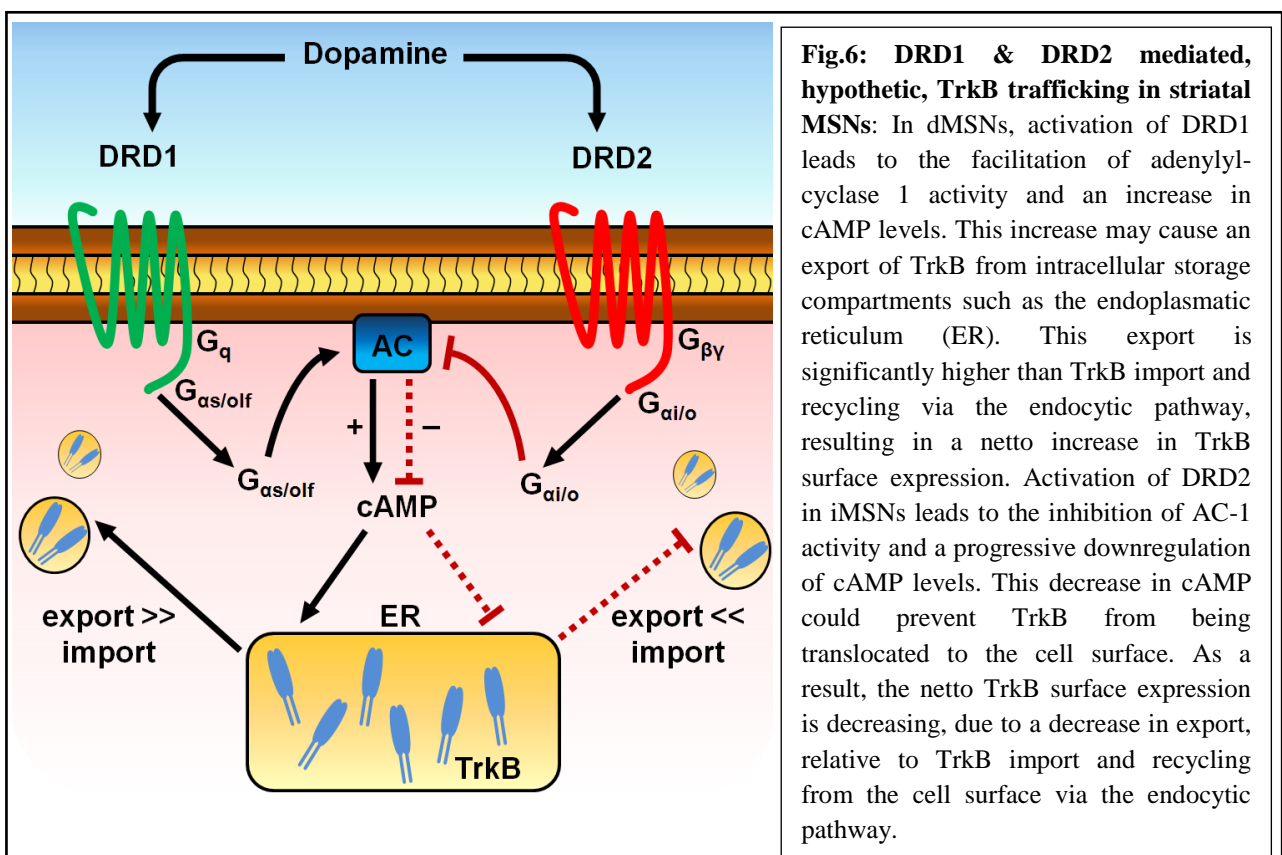


Fig.5: Striatal LTP induction: Striatal LTP requires simultaneous activation of NMDA-R, TrkB and GPCRs. NMDA-R and TrkB activation are crucial elements eliminating LTP completely when either of these receptors is inhibited. GPCRs are also involved into striatal LTP induction, but inhibition of either DRD1 or A2aR decreases LTP efficiency rather than completely abolishing it. Adapted from (Plotkin et al.,2014).

Both receptors, DRD1 and A2aR, belong to the family of $G_{\alpha s}$ GPCRs, able to stimulate adenylyl-cyclase 1 (AC-1) and increase intracellular cAMP levels (**Fig. 3**). Interestingly, TrkB surface expression was shown to be directly linked to cAMP levels (Meyer-Franke et al., 1998) and striatal MSNs indeed show significant TrkB expression (Baydyuk et al., 2011).

For this reason, it is possible, that activation of G_{as} GPCRs in either dMSNs or iMSNs triggers TrkB surface expression, through which the receptor is then able to bind BDNF released in an activity-dependent manner together with glutamate from cortico-striatal afferences. The resulting simultaneous activity of postsynaptic NMDARs, TrkB and G_{as} GPCRs leads to induction of LTP as suggested previously (Plotkin et al., 2014). Now, if the induction of LTP was the only mode of plasticity within the striatum, this would contradict our general understanding of plasticity, in terms of adaptability and flexibility, unless there is an antagonistic modulation via induction of LTD as well. This already implies a model of "bi-directional plasticity at glutamatergic synapses on striatal MSNs" (Fino et al., 2005; Calabresi et al., 2007; Shen et al., 2008; Shen et al., 2016; Zhai et al., 2018). Indeed, induction of LTD has been linked to activation of DRD2 in iMSNs and muscarinic acetylcholine receptor M_4 (M_4R) in dMSNs, both of which belong to the family of G_{ai} GPCRs which inhibit AC-1 and decrease cAMP levels (Fig. 3) (Shen et al., 2008; Shen et al., 2016). So far, the modes of plasticity and the different molecular mechanisms involved in their modulation still remain largely elusive.



It is therefore possible that activation of DRD1 (dMSNs) and DRD2 (iMSNs) is able to trigger TrkB translocation in an opposite manner, via AC-1 activity leading to reduced cAMP levels (**Fig. 6**). While DRD1 facilitates TrkB surface expression, DRD2 might prevent it.

3.8 Aim of the study

The capacity of DRDs to modulate cAMP levels via activation or inhibition of AC-1 (**Fig. 3**) and their ability to control AMPA and NMDA-R surface expression (Flores-Hernandez et al., 2002; Braithwaite et al., 2006; Hallett et al., 2006; Gao and Wolf, 2008) led us to the hypothesis that DRDs may also control TrkB surface expression. It is well known that TrkB surface trafficking depends on intracellular cAMP levels (Meyer-Franke et al., 1998) which are bi-directionally controlled by downstream signaling of dopamine receptors (**Fig. 3, 6**). The control of TrkB surface expression, through dopamine, might be a way to synchronize glutamatergic, cortical and dopaminergic signaling on the same spine. We therefore propose a model in which activation of DRD1 in dMSNs leads to a net increase in TrkB surface expression, via elevation of cAMP levels (Memo et al., 1986; Dearry et al., 1990; Monsma et al., 1990; Zhou et al., 1990; Sugamori et al., 1994; Demchyshyn et al., 1995), since TrkB export might be higher than TrkB import and recycling from the cell surface (**Fig. 6, 7, 8B**). On the other hand, activation of DRD2 in iMSNs might decrease TrkB surface expression, due to attenuating AC-1 activity and subsequently decrease cAMP levels (De Camilli et al., 1979; Onali et al., 1981; Enjalbert and Bockaert, 1983; McDonald et al., 1984; Onali et al., 1985). This could prevent TrkB translocation to the cell surface (**Fig. 6**). This hypothesis, in turn, suggests that if both glutamatergic and dopaminergic afferences are stimulated (**Fig. 8D**), then also postsynaptic NMDA-Rs and DRDs should be active. For the induction of LTP, TrkB activation is critically required (Plotkin et al., 2014). $G_{\alpha s}$ coupled GPCRs might trigger TrkB surface expression which then binds BDNF which is provided from cortico-striatal terminals in a Ca^{2+} dependent manner (Park et al., 2014) (**Fig. 6, 7, 8B, D**). Following the

model proposed for striatal LTP induction (Fig. 5), then NDMA-Rs, GPCRs, and TrkB are simultaneously activated to enable LTP induction, at least in DRD1 expressing dMSNs. Similarly, LTP is not induced if only the corticostriatal afferences are activated, releasing glutamate and BDNF, but TrkB surface expression and activation might be low, due to the absence of dopaminergic signaling (Fig. 8C). The same would be true if only dopamine is released from nigrostriatal afferences that increase TrkB surface expression in dMSNs(Fig.6, 7, 8B). LTP would not be induced in the absence of cortico-striatal glutamate and BDNF

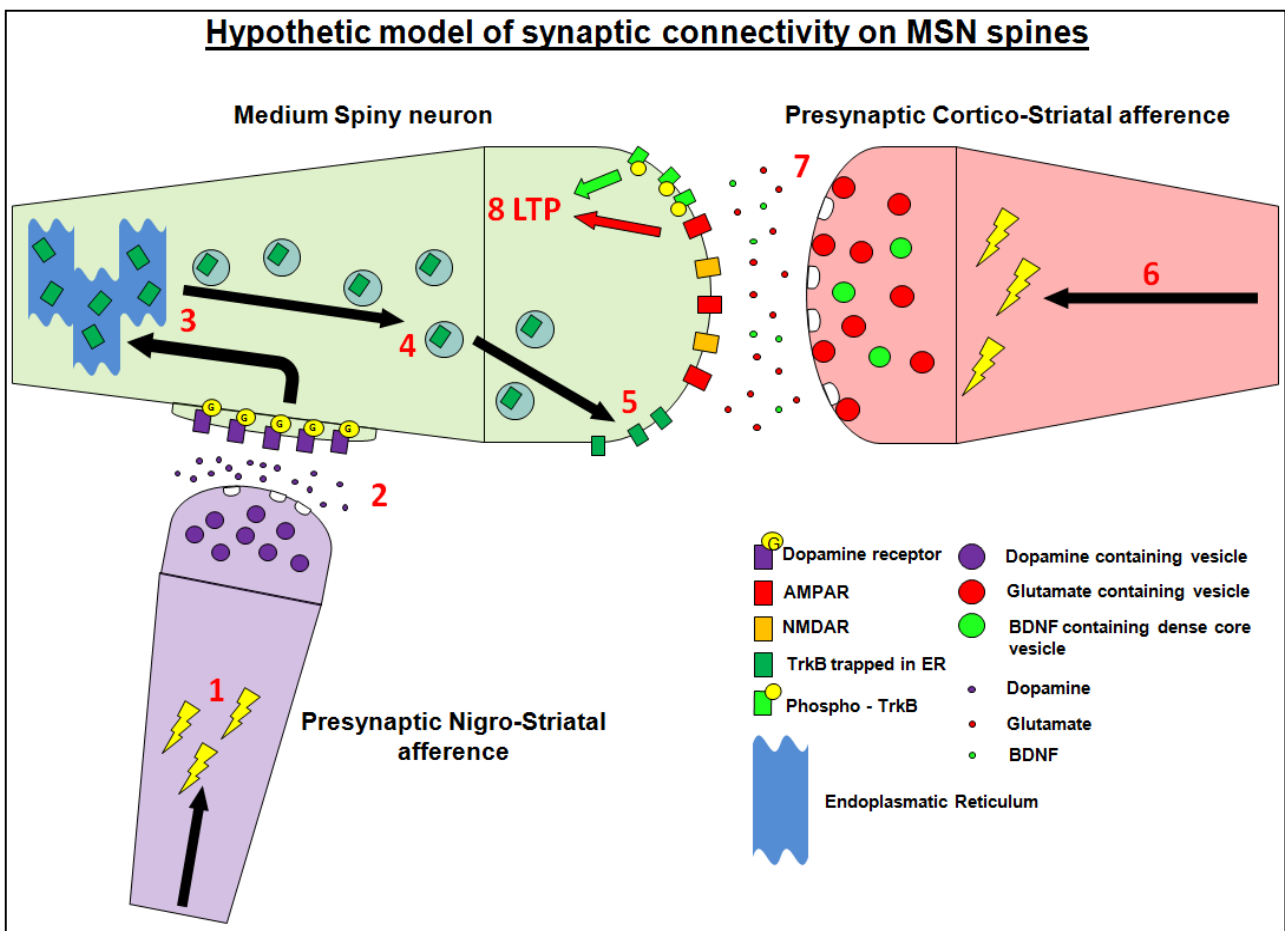
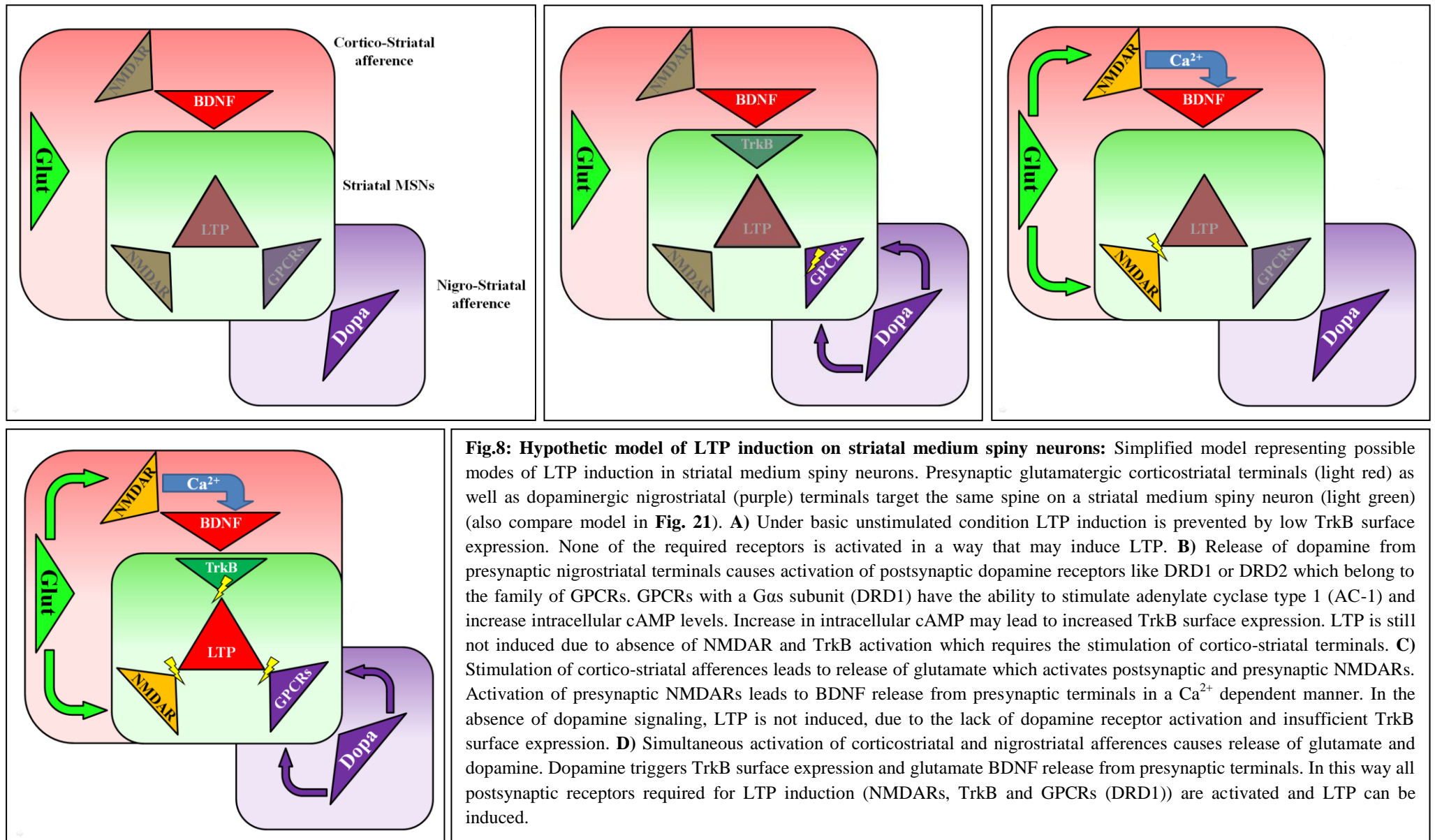


Fig.7: Hypothetic model of synaptic connectivity on striatal medium spiny neurons: Initial excitation of either the nigrostriatal (1) or corticostriatal afference (6) is required to induce signaling cascades leading to LTP induction. In this model, initial stimulation of the nigrostriatal afference and DRD1 activation in dMSNs is depicted (1). This stimulation leads to dopamine release which binds to postsynaptic dopamine receptors (2). The activation of dopamine receptors with a *G_{αs}* subunit, i.e. DRD1 leads to an increase of intracellular cAMP (3). This increase in cAMP leads to the translocation of TrkB from intracellular stores (4) and increases TrkB surface expression (5). A parallel stimulation of the cortico-striatal afference (6) causes a release of glutamate (7), which binds to postsynaptic NMDARs as well as presynaptic NMDARs. This presynaptic NMDAR activation leads to a Ca²⁺ mediated release of BDNF from presynaptic terminals (7). This BDNF binds to postsynaptic TrkB receptors, that are incorporated into the surface membrane through dopamine signaling and now become phosphorylated. Together with NMDAR and AMPAR signaling LTP can now be induced (8).

release in dMSNs. We thus propose a regulatory effect of dopamine signaling on TrkB surface expression in striatal medium spiny neurons, in order to integrate glutamate, dopamine, and neurotrophin signaling in a spatiotemporal manner, to mediate distinct modes of plasticity in MSN spines. First evidence for a direct effect of DRD1 on TrkB surface expression in dMSNs already exists (Iwakura et al., 2008). A role for DRD2 in these modalities of neurotrophin signaling remains rather elusive so far. If the model we propose here is indeed true, then it suggests 4 major assumptions. First, BDNF needs to be expressed in cortico-striatal projection neurons and their presynaptic terminals within the striatum. Second, striatal MSNs targeted by these cortical afferences need to express significant amounts of TrkB. Third, dopamine signaling should increase TrkB surface expression in dMSNs, or prevent it, unless the DRD1 activity is abolished. Fourth, dopamine should decrease TrkB surface expression upon activation of DRD2 in iMSNs which should be prevented by the absence of dopamine. We aimed to test first DRD2 mediated effects on the translocation or retention of TrkB from intracellular compartments to the cell surface. Subsequently, we characterized the transactivation of TrkB via DRD2 activation, independent of BDNF. Interestingly, evidence already exists that DRD1 is able to transactivate TrkB in the absence of BDNF (Iwakura et al., 2008). The aim of the present Ph.D. thesis was to characterize the underlying mechanisms downstream of dopaminergic signaling, as well as the consequences of their absence in PD, on modes of plasticity which are critically linked to BDNF / TrkB interaction. The goal was to provide new information about how information is processed in the basal ganglia, in particular how motor skills might be established by different modes of activity that lead to plastic changes in cortico-striatal synapses. These analyses could help to develop new therapeutic strategies for PD which are independent of dopaminergic neurons and target defective signaling in the striatum itself instead of dopamine production in the midbrain.



4. Material & Methods

4.1 Materials

4.1.1 Animals

Tissue for IHC or ELISA approaches was obtained from 8wk-12wk old male mice from following mouse lines: WT (C57Bl6-J), Bdnf-Myc (Matsumoto et al., 2008) DRD1-EGFP (FVB) [TG(DRD1a-EGFP)X60Gsat] (RRID:MMRRC_000297-MU), DRD1-EGFP (C57Bl6-J), DRD2-EGFP (FVB) [TG(DRD2-EGFP)S118Gsat] (RRID:MMRRC_000230-UNC), DRD2-EGFP (C57Bl6-J), NFL-Cre^{Wt/Tg} / BDNF^{fl/k.o.}. Conditional BDNF k.o. mice were generated by crossing mice expressing cyclic recombinase (CRE) under control of the Neurofilament-Light-Chain promoter (NF-L) (Schweizer et al., 2002) with mice carrying a BDNF Exon V, flanked by two loxP sites, on one allele and a neomycin cassette in the 5' coding region of Exon V on the second allele (Korte et al., 1995). NFL-Cre mediated recombination was found to occur in layer V subcortical projection neurons as well as layer VI cortical neurons (Schweizer et al., 2002). DRD1-EGFP and DRD2-EGFP mice were kept in a heterozygous background since homozygous background causes significant phenotypes in DRD2-EGFP mice (Kramer et al., 2011). All mouse lines were bred in the animal facility of the Institute of Clinical Neurobiology, University Hospital of Würzburg. Animals were provided with food and water in excess amounts. They were maintained at 20–22°C and 55–65% humidity, with a 12 hours light/dark cycle. Tissue, for IHC and WB analysis, derived from unilateral 6-OHDA lesioned adult Sprague Dawley rats were kindly provided by Dr. Marta Rattka. All experiments were performed in accordance with the local veterinary authority (Veterinäeramt der Stadt Würzburg) and Committee on the Ethics of Animal Experiments, i.e., Regierung von Unterfranken, Würzburg.

4.1.2 Technical devices

- 8x Multipette; Eppendorf Research 8 x 30-300 µl; 8180-104
- Bacteria Shaker / Incubator Innova 44 incubator shaker
- Balance Kern 440-47N & ALS 120-4; Kern & Sohn GmbH
Bosch SAE200
- BioMetra Power Pack P25
- BioRad Gel chamber ("Mini-Protean Tetra System" & "Mini-Protean II gel & blotting chamber")
- BioRad Power Pack HC
- Biozero, Keyence BZ8000K, fluorescence microscope
- Blotting: BioRad "Trans-Blot SD – Semi-Dry Transfer Cell"
- Blotting membrane: Immun Blot PVDF membrane (0.2µm) (Cat. No.:162-0177; BioRad)
- Cell culture Hood: Thermo Scientific Safe 2020
Thermo Hera Safe HS12
- combs: 10 well, 1.0mm or 1.5mm; (BioRad; #1653359; Work order: 090809RS)
- combs: 15 well, 1.0mm or 1.5mm; (BioRad; #1653360; Work order: 081809CL)
- ELISA reader Tecan; Infinite M200 Pro
- Eppendorf BIO – Photometer
- Eppendorf Mini Spin
- Eppendorf Centrifuge 5417R
- Eppendorf Centrifuge 5702
- Eppendorf Centrifuge 5804R
- Eppendorf Centrifuge 5810R
- Eppendorf Thermomixer Comfort

- Glass plates: spacer plates 1.0mm; (BioRad; #1653311; Work order: PLN101869)
- Horizon 58 Life Technologies – Gel chamber
- Incubator: Heraeus, Kendro Laboratory Products 50042301
Thermo Scientific Hera cell 240
Binder CB 150 Air-Jacketed CO2 Incubator
- Inova44 incubator shaker – New Brunswick Scientific
- LabNet centrifuge SN06040692
- Leica RM2265 vibratome
- Leica TCS SP5 confocal laser microscope
- Leica VT1000S vibratome
- Nanodrop (Peqlab; Spectrophotometer ND-1000)
- Neubauer improved profondeur counting – chamber (Marienfeld)
- Olympus CKX41 cell culture microscope
- Olympus FluoView 1000 confocal microscope
- Owl And Easy Cast – Gel chamber
- PCR: Eppendorf Mastercycler Gradient
Eppendorf Mastercycler
Eppendorf Mastercycler Nexus X2 & X2e
- Perfusion pump: ISMATEC - Reglo
- pH meter: Seven Easy pH, Mettler Toledo AG, 8603 Schwarzenbach
- Rotofix Centrifuge 32A (Hettich)
- Shaker: BioScan Mini Rocker / Shaker MR-1
Heidolph Duomax 1030
NeoLab Shaker DRS-12
- Short plates (BioRad; #1653308; Work order: PLN101742)

- Sonifier (UP50H Hielscher)
- Stirrer: Labinco Hotplate Stirrer L-81
IKA RH Basic 2
IKAMAG Reo
IKA RCT basic, safety control
- Tissue culture flasks (Greiner, bio-one; #658170; 658175; 658190; 658195)
- Vortexer: NeoLab Vortex Mixer 7-2020
Labinco BV Model L-46
- Waterbath: Memmert WNB22
Assistent WTE var3185

4.1.3 Expendable materials

- 1.5ml tubes - Sarstedt; 20003490
- 2.0ml tubes - Sarstedt; 20003491
- 4 well plate - Nunc; 76740
- 10mm glass coverslips - (Marienfeld Superior™ 0111500)
- 12mm glass coverslip - (Marienfeld Superior™ 0111520)
- 18mm glass coverslip - (Marienfeld Superior™ 0111580)
- 15ml tube - Falcon; 352095
- 50ml tube - Falcon; 352070
- 24 well plate - Sarstedt; 83.3922
- Cell scraper - Sarstedt; 83.1832
- “tissue culture dishes” (Greiner, Cellstar #627 160; 627 170; Greiner bio one)

4.1.4 Chemicals

- 1x PBS Dulbecco's; PAA; H15-002
- 2-Mercaptoethanol Sigma Aldrich; M6250-250ML
- 2-Propanol VWR; 20839.366
- Agarose Biozym LE Agarose; 840004
- Aquapoly mount Polysciences; 18606
- B-27 supplement Gibco; 17504-044
- Betaine Sigma Aldrich; 61962-250G
- Bromophenol-blue Sigma Aldrich; B8026
- Chloroform Sigma Aldrich; 32211-2,5L-M
- Dithiothreitol (DTT) Thermo Scientific; 20291
- Donkey Serum Merck; S30-100ml
- EtBr₂ Sigma Aldrich; E8751
- EtOH Honeywell; 32205-2,5L
- Ethyleneglycol Roth; 9516.1
- FluorSave Reagent Merck, Calbiochem; 345789-20ml
- Formaldehyde Merck; 1.04003.1000
- Formamide Sigma Aldrich; F7503-1L
- Forskolin Sigma Aldrich; F6886-10MG
- Glucose Sigma Aldrich; G6152
- Glutamax Gibco; 35050-038
- Glutaraldehyde (25%) SERVA; 23114.01
- Glycerol Honeywell; 15523-1L
- Glycine Roth; 3790.3
- HBSS Thermo Scientific; 14170-138

- Heparin (25.000) Ratiopharm; N68542.04
- Horse serum Linaris; SHD3250YK
- KCL Roth; 6781.1
- KH_2PO_4 Merck; 1.04873.1000
- L741-626 Sigma Aldrich; L135-10MG
- Laminin Thermo Scientific; 23017-015
- L-Lysine mono hydrochloride Sigma; L5626
- Luminaris HiGreen qPCR Master Mix ThermoFisher; K0991
- MeOH Sigma Aldrich; 32213-2.5L-M
- MgCl_2 Thermo Scientific; F-510MG
- Milkpowder Roth; T145.3
- Na_2HPO_4 Roth; P030.2
- $\text{Na}_2\text{HPO}_4 \times 2\text{H}_2\text{O}$ Merck; 1.06580.1000
- NaCl Roth; 9265.2
- $\text{NaH}_2\text{PO}_4 \times 2\text{H}_2\text{O}$ Merck; 1.06342.1000
- NaOH (1N) Merck; 1091371000
- Neurobasal medium Thermo Scientific; 21103049
- Neutravidin beads Thermo Scientific; 29200
- Nonident NP-40 Sigma Aldrich; 74385-1L
- Paraformaldehyde (PFA) Merck; 1.04005.1000
- PCR Enhancer Invitrogen; 52391
- PCR_x Enhancer System Thermo Scientific; 11495017
- PCR-Reactionbuffer (5-Prime) Quanta-Bio; 2900162
- PCR-Reactionbuffer (VWR) VWR; 5100950-1500
- Phosphatase Inhibitor Roche; 04906837001

• Poly D-L-Ornithine	Sigma Aldrich; P8638-500MG
• Protease Inhibitor	Roche; 04693159001
• Quenching buffer	Thermo Scientific; 1859386
• Quinpirole Hydrobromide	Sigma Aldrich; Q102-25mg
• Saponine	Sigma Aldrich; S7900-25G
• SKF38393	Sigma Aldrich; D047-100MG
• Sodiumcitrate (Trisodium-Citrate)	Sigma Aldrich; S4641 1kg
• Sodiumdeoxychelate	Applichem; A1531.0100
• Sodiumdodecylsulfate (SDS)	Applichem; A2572.1000
• Sodiumfluoride	Sigma Aldrich; S7920
• Sodium Metaperiodate	Sigma Aldrich; 71859
• Sodiumorthovanadate	Sigma Aldrich; S6508-50G
• Sodiumpyrophosphate	Sigma Aldrich; 221368-100G
• Restore™ PLUS Stripping Buffer	Thermo Scientific; 46430
• Sulfo-NHS-SS-Biotin	Thermo Scientific; 21331
• Sumanirole Maleate	Tocris; 2773
• Taq-Polymerase (5-Prime)	QuantaBio; 2200320
• Taq-Polymerase (VWR)	VWR; 5101600-0100
• Tris HCl	Roth; 9090.3
• Triton X100	Sigma Aldrich; 23472-9 & X100-1L
• TRIZMA	Applichem; A1086,1000
• Trizol	Invitrogen; 15596-026
• Trypsin	Worthington; TRL3
• Trypsin inhibitor	Sigma Aldrich; T6522-100MG
• Tween20	Sigma Aldrich; P1379-1L

- Washing Buffer (Surface Biotinylation) Thermo Scientific; 1859389

4.1.5 Buffers and media

4.1.5.1 Cell culture

- 1% Trypsin in HBSS/HEPES 40:1
- 1% Trypsin-Inhibitor in HBSS/HEPES 40:1
- Full medium
 - Neurobasal medium
 - 1:50 B27 supplement
 - 1:100 Glutamax
 - 5% Horse serum
- Maintenance Medium
 - Neurobasal medium
 - 1:50 B27 supplement
 - 1:100 Glutamax

4.1.5.2 Immunocytochemistry (ICC) and Immunohistochemistry (IHC)

- 1xPBS (1l)
 - 80g NaCl
 - 2g KCl
 - 14.4g NaH₂PO₄
 - 2.4g KH₂PO₄
- 1x PBS, 0.4% Heparin
 - 100ml 1xPBS
 - 400µl Heparin
- 4% PFA (1l) pH (6.0, 7.4, 100ml)
 - 4g PFA
 - 50ml dH₂O (~55°C)
 - 3-4 drops NaOH
 - 41ml 0.2M Na₂HPO₄ x 2H₂O
 - 9ml NaH₂PO₄ x 2H₂O

- Antigenretrieval (100ml, pH8.5)
 - 10mM Sodiumcitrate (0.294g)
 - 100ml dH₂O
- Blocking solution (ICC)
 - 1xPBS
 - 10% Donkey Serum
 - 0.1% Triton-X 100 (X100)
 - 0.1% Tween 20
- Blocking solution (IHC)
 - 1xPBS
 - 10% Donkey Serum
 - 0.3% X100
 - 0.1% Tween 20
- Cryoprotection buffer (300ml)
 - 150ml 0.05M Phosphate Buffer
 - 90ml Glycerol,
 - 60ml Ethyleneglycol
- DAPI
 - 0.4µg/ml in 1xPBS
- Washing Buffer (ICC)
 - 1xPBS
 - 0.1% X100
- Washing Buffer (IHC)
 - 1xPBS
 - 0.1% X100
 - 0.3% Tween20

4.1.5.3 Fluorescence *in situ* hybridization (FISH)

- 0.1M Na₂HPO₄
 - 500ml dH₂O
 - 8.9g Na₂HPO₄
- 0.2M Phosphate Buffer (pH 7.4)
 - 500ml dH₂O
 - 17.8g Na₂HPO₄ x 2H₂O

- 2.7g $\text{NaH}_2\text{PO}_4 \times \text{H}_2\text{O}$
- 4% PLP (pH 7.4) (10 ml)
 - 7.5 ml lysine phosphate buffer
 - 2.5 ml 16% PFA
 - 0.135 g glucose
 - 0.021 g sodium (meta) periodate
- 16% PFA (pH 7.4)
 - 16 g paraformaldehyde
 - 3-4 drops NaOH
 - 41ml 0.2M $\text{Na}_2\text{HPO}_4 \times 2\text{H}_2\text{O}$
 - 9ml $\text{NaH}_2\text{PO}_4 \times 2\text{H}_2\text{O}$
 - 50ml dH_2O (~55°C)
- Blocking solution (FISH)
 - 1xPBS
 - 10% Donkey serum
 - 5% sucrose in 1xPBS
 - 0.3% Triton-X 100
 - 200µg/ml Saponin
- Lysine-Phosphate Buffer
 - 100ml dH_2O
 - 3.66g Lysine Hydrochloride
 - 0.1M Na_2HPO_4 until the pH is 7.4
 - 50ml 0.2M PB (pH 7.4)
 - fill with dH_2O to 200ml
- Saponin solution (10 mg/ml stock)
 - 100 mg saponin
 - 10 ml PBS

4.1.5.4 Western Blot analysis, Surface Biotinylation, Immunoprecipitation

- TNE Buffer (Lysis / Extraction buffer) - 0.05M Tris HCl, pH7.5
 - 0.15M NaCl
 - 2% NP-40
 - 0.5% Sodiumdeoxycholate
 - 1mM Sodiumfluoride
 - Protease Inhibitor (1 Tablet)

for detection of phospho-proteins the following might be added:

- Phosphatase Inhibitor (1 Tablet)
- 5mM Sodium-Pyrophosphate
- 100mM Sodium-Othovanadate
- Tris SDS - Separation gel buffer (4x stock) - 1.5M Tris HCl pH 8.8 (182.0g)
 - 0.4% SDS (10ml; 20% SDS stock)
 - dH₂O ad 1l
- Tris SDS - Stacking gel buffer (4x stock) - 0.5M Tris HCl pH6.8 (30.25g)
 - 0.4% SDS (10ml, 20% SDS stock)
- Electrophoresis buffer (10x) pH8.35
 - 125mM Tris Base (TRIZMA) (30.5g)
 - 1.0M Glycine (144g)
 - 0.5% SDS (10g)
 - dH₂O ad 2l
- 10x TBST pH 8.0
 - 100mM Tris HCl (24.22g)
 - 1.5M NaCl (175.32g)
 - 0.5% Tween20 (10ml)
 - dH₂O ad 2l
- WB Transfer buffer (Semi Dry) pH8.3
 - 25mM Tris HCl (50ml 1M Tris)
 - 150mM Glycine (22.72g)

- 10% MeOH (200ml)
- dH₂O ad 2l
- WB Transfer buffer (Wet Blot) pH8.6 - (0.025M TRIS; 0.192M Glycine; 20% MeOH)
 - 100ml 10x TOWBIN
 - 200ml MeOH
 - 700ml dH₂O
- 10x TOWBIN pH8.6
 - 0.25M Tris Base (TRIZMA) (60.4g)
 - 1.92M Glycine (288.0g)
 - dH₂O (1.8l)
- DTT in SDS sample buffer
 - 23.7µl DTT solution
 - 450µl SDS sample buffer
- SDS sample buffer
 - 62.5mM Tris HCl pH6.8
 - 1% SDS
 - 10% Glycerol
- Dithiothreitol (DTT) solution
 - 7.7mg DTT
 - 50µl ddH₂O
- Laemmli buffer (5x)
 - 1M Tris HCl (pH6.8) (2.5ml)
 - 20% SDS (2.5ml)
 - Glycerol (3.0ml)
 - 2-Mercaptoethanol (0.5ml)
 - Bromophenol-blue (200µl)
- IP - Lysis / Wash-buffer 1
 - 0.05M Tris HCl pH7.5
 - 0.15M NaCl
 - 1% Nonident NP-40
 - 0.05% Sodiumdeoxycholate

- Proteinase inhibitor (1 tablet ad 10ml)
 - Phosphatase inhibitor (1 tablet ad 10ml)
- IP Wash-buffer 2
 - 0.05M Tris HCl (pH7.5)
 - 0.5M NaCl
 - 0.1% Nonident NP-40
 - 0.05% Sodiumdeoxycholate
 - Proteinase inhibitor (1 tablet ad 10ml)
 - Phosphatase inhibitor (1 tablet ad 10ml)
- IP Wash-buffer 3
 - 0.01M Tris HCl (pH7.5)
 - 0.1% NP-40
 - 0.05% Sodiumdeoxycholate

4.1.5.5 BDNF ELISA

- ELISA Extraction buffer (20ml, pH4.0)
 - 20ml 0.05M (50mM) Sodiumacetate
 - 1M NaCl
 - 2x proteinase inhibitor tablet ~1 in 10ml
 - 1% BSA (0.2g)
 - 0.1% Triton-X 100 - 100µl (20% X100)
- ELISA Coating buffer (20ml pH9.7)- 20ml dH₂O
 - 50mM NaHCO₃, 50mM Na₂CO₃, pH9.7
 - 50.000ng mouse anti BDNF (mAb#1)
(stock = 3.8µg/µl)
- ELISA blocking buffer
 - 4% BSA in 1xPBS

- ELISA Washing buffer - 250ml 1xPBS
- 0.1 Tween 20 (1250µl of 20% stock)
- ELISA Incubation buffer (50ml pH7.6): - 0.1M Phosphate buffer pH7.6
- 5x Proteinasease inhibitor tablet
- 4% BSA (2g)

4.1.5.6 Polymerase Chain Reaction (PCR)

- 50x TAE Buffer - 484g Tris Base
- 114.2 ml acetic acid
- 200ml 0.5M EDTA
- ad 2l with dH₂O

4.1.6 PCR Primers and Oligo-probes for FISH

4.1.6.1 PCR Primers - Genotyping

Table 1: List of genotyping primers

<u>PCR</u>	<u>Forward Primer</u>	<u>Reverse Primer</u>
BDNF floxed	Bdnf 13 5- GTT GCG TAA GCT GTC TGT GCA CTG TGC -3'	Bdnf 14 5- CAG ACT CAG AGG GCA CTT TGA TGG CTT G -3'
BDNF k.o.	Bdnf_499for 5- GTT TGC GGA GTA TGC TTA T -3'	Bdnf_935rev 5- CAT TGT TTT AAT TCC AAC GCT -3'
BDNF k.o.	BD2A 5- GTG TCT ATC CTT ATG AAT CGC C -3'	BKO-1 5- ATA AGG ACG CGG ACT TGT ACA -3'
BDNF k.o.	BD2A 5- GTG TCT ATC CTT ATG AAT CGC C -3'	3'NEO 5- GAT TCG CAG CGC ATC GCC TT -3'
BDNF myc	Myc for 5- GAC TGC AGT GGA CAT GTC T -3'	Myc rev 5- AGA TTG TAG AAC CAC TGT ACT G -3'
DRD1-Td-Tomato	12153 5- CTT CTG AGG CGG AAA GAA CC -3'	12154 5- TTT CTG ATT GAG AGC ATT CG -3'
DRD1-Td-Tomato	oIMR7338 5- CTA GGC CAC AGA ATT GAA AGA TCT -3'	oIMR73389 5- GTA GGT GGA AAT TCT AGC ATC ATC C -3'
DRD1-EGFP	M297 (Drd1a) F 5- ACC GGA AGT GCT TTC CTT CTG GA -3'	Gensat GFP Rev 5- TAG CGG CTG AAG CAC TGC A -3'
DRD2-EGFP	Drd2F(230) 5- GAG GAA GCA TGC CTT GAA AA -3'	Drd2R(230) 5- TGG TGC AGA TGA ACT TCA GG -3'
NFL-Cre	NFL-SEQ (19mer) 5'-TCG CAG GCT GCG TCA GGA G -3'	pMC-Cre (19mer) 5- GGT ATG CTC AGA AAA CGC C -3'

Ntrk Rohrer (TrkB ^{-/-})	Trkb-c8 5'- ACT GAC ATC CGT AAG CCA GT -3'	Trkb-n2 5'- ATG TCG CCC TGG CTG GCT GAA GTG -3'
Ntrk Rohrer (TrkB ^{-/-})	Trkb-c8 5'- ACT GAC ATC CGT AAG CCA GT -3'	Pgk3-1 5'- GGT TCT AAG TAC TGT GGT TTC C -3'

4.1.6.2 PCR Primers - qRT-PCR

Table 2: List of qRT-PCR primers

PCR	Forward Primer	Reverse Primer
GAPDH	mGAPDHfor 5'- GCA AAT TCA ACG GCA CA -3'	mGAPDHrev 5'- CACCAGTAGACTCCACGAC -3'
GFP	GFP-forward 5'- AAG TTC ATC TGC ACC ACC G -3'	GFP-reverse 5'- TTC TTG AAG AAG ATG GTG CG -3'
TrkB Full Length Rat	TrkB2026_for 5'- GTT GGC GAG ACA TTC CAA G -3'	TrkBkin2204rev 5'- GGG GGT TTT CAA TGA CAG G -3'
TrkB Full Length Mouse	TrkB1940U21 5'- CGG GAG CAT CTC TCG GTC TAT -3'	TrkBkin2074L21 5'- CTG GCA GAG TCA TCG TCG TTG -3'
TrkB T1 Mouse / Rat	T1-1907U19 5'- CGG GAG CAT CTC TCG GTC T -3'	T1-2094L19 5'- GGC GTC AGG CAA CAA GCA C -3'

4.1.6.3 Oligo Probes for FISH

DRD1 Oligonucleotide-probe (1µM) - Affymetrix; VC1-11563

DRD2 Oligonucleotide-probe (1µM) - Affymetrix; VC1-13759

4.1.7 Primary Antibodies

4.1.7.1 Mouse derived primary antibodies

- Mouse anti BDNF (mAb#1) - Provided by Prof. Yves Alain Barde
- Mouse anti BDNF (mAb#9) - Provided by Prof. Yves Alain Barde
- Mouse anti BDNF (mAb#4C8) - Icosagen; 328-100
- Mouse anti BDNF (mAb#3C11) - Icosagen; 327-100
- Mouse anti BDNF (mAb#3B2) - Icosagen; 329-100
- Mouse anti GAD65 - Abcam; 26113
- Mouse anti GFAP - Millipore; 3402

- Mouse anti GM130 - BD Biosciences; 610822
- Mouse anti MAPK (total) - Cell Signaling; 4696S
- Mouse anti p42/44 pMAPK - Cell Signaling; 9106S
- Mouse anti Pan-Cadherin - Sigma Aldrich; C1821
- Mouse anti Rab5 - Synaptic Systems; 108011
- Mouse anti Rab7 - Abcam; AB50533
- Mouse anti TGN-38 - Novus Biologicals; NB300-575-SS
- Mouse anti Ubiquitin - Abcam; AB7254

4.1.7.2 Rabbit derived primary antibodies

- Rabbit anti Akt (total) - Cell Signaling; 9272S
- Rabbit anti pAkt (phosphorylated) - Cell Signaling; 4060P
- Rabbit anti c-Fos - Synaptic Systems; 226003
- Rabbit anti Cux1 (CDP) - Santa Cruz; Sc1324
- Rabbit anti DARPP-32 - Cell Signaling; 2306
- Rabbit anti DARPP-32 (pThr34) - Cell Signaling (12438)
- Rabbit anti DARPP-32 (pThr75) - Cell Signaling; 2301
- Rabbit anti FOXO1 - Cell Signaling; C29H4
- Rabbit anti EGFR - Santa Cruz; Sc-03
- Rabbit anti EGFR (phosphorylated) - Cell Signaling; 3777
- Rabbit anti LC-3B - Cell Signaling; 3863
- Rabbit anti Met-Enk - Immunostar / Acris; 20065
- Rabbit anti myc - Abcam; AB9106
- Rabbit anti myc - Santa Cruz; Sc-789
- Rabbit anti myc - Abcam; AB9132
- Rabbit anti panTrk - Cell Signaling; C17F1

- Rabbit anti pTrk (kinase domain) - Cell Signaling; 4621
- Rabbit anti TH - Millipore; AB152
- Rabbit anti TrkB - Millipore; 07-225
- Rabbit anti TrkB (T1) - Santa Cruz; SC-119
- Rabbit anti SHP-2 - Cell Signaling; 3397
- Rabbit anti Src (total) - Cell Signaling; 2109T
- Rabbit anti Src (phosphorylated) - Cell Signaling; 2101S
- Rabbit anti VGluT1 - Synaptic Systems; 135302

4.1.7.3 Goat derived primary antibodies

- Goat anti Calnexin - SICGEN; AB0037-200
- Goat anti Cathepsin D - Santa Cruz; Sc-6494 G19
- Goat anti DARPP-32 - R&D Systems; AF6259
- Goat anti mTrkB - R&D Systems; AF1494

4.1.7.4 Chicken derived primary antibodies

- Chicken anti Calreticulin - Thermo Scientific; PA1-902A
- Chicken anti GFP - Abcam; AB13970
- Chicken anti TH - Abcam; AB76442

4.1.7.5 Rat derived primary antibodies

- Rat anti CTIP-2 - Abcam; AB18465
- Rat anti HA - Roche; 11867431001

4.1.8 Secondary Antibodies

4.1.8.1 Fluorescent secondary antibodies

- Donkey anti Chicken Alexa488 - Jackson; 703-545-155
- Donkey anti Goat Alexa488 - Jackson; 705-545-147
- Donkey anti Mouse Dylight488 - Thermo Scientific; SA5-10166
- Donkey anti Rabbit Alexa488 - Jackson; 711-545-152
- Donkey anti Rabbit Dylight488 - Jackson; 711-485-152
- Donkey anti Rat Alexa488 - Molecular Probes; A21208

- Donkey anti Chicken Cy3 - Jackson; 703-165-155
- Donkey anti Goat Cy3 - Jackson; 705-165-003
- Donkey anti Mouse Dylight550 - Thermo Scientific; SA5-10167
- Donkey anti Rabbit Cy3 - Jackson; 711-165-152
- Donkey anti Rat Cy3 - Jackson; 712-165-150

- Donkey anti Chicken Alexa647 - Jackson; 703-605-155
- Donkey anti Chicken Dylight649 - Jackson; 703-495-155
- Donkey anti Goat Alexa647 - Jackson; 705-605-003
- Donkey anti Goat Cy5 - Jackson; 705-175-003
- Donkey anti Mouse Cy5 - Jackson; 715-175-150
- Donkey anti Rabbit Alexa647 - Thermo Scientific; A-31573
- Donkey anti Rabbit Dylight649 - Jackson; 711-495-152

4.1.8.2 Enzyme linked secondary antibodies

Donkey anti Goat POD - Jackson; 705-035-003

Horse anti Mouse POD - Cell Signaling; 7076S

Donkey anti Rabbit POD

- Jackson; 711-035-152

4.1.9 Kits

- Ambion Turbo DNA - free kit - Thermo Scientific, AM1907
- BCA Protein Assay Kit - Thermo Scientific; 23225
- cDNA synthesis kit "First Strand" (RT-PCR) - Thermo Scientific ;K1621
- ECL Western Blotting Detection kit - GE Healthcare
- High-Capacity RNA-to-cDNA™ Kit - Thermo Scientific; 4387406
- Pierce Surface biotinylation kit - Thermo Scientific; 89881
- ViewRNA ISH Cell Assay - Thermo Scientific; QVC0001

4.1.10 Software

- Adobe Photoshop 7.0
- ApE plasmid editor
- Endnote X7
- GIMP 2.8
- GraphPad Prism 6.0 for statistical analysis
- ImageJ, Fiji
- Imaris 3D Imaging software by Bitplane
- Leica LAS-AF lite
- Microsoft Office 2010, Excel, Word, PowerPoint
- Oligo 6 primer design
- Olympus FV10-ASW 3.0 Viewer

4.2 Methods

4.2.1 Cell culture

4.2.1.1 Coating of cell culture coverslips

Coverslips should be excessively washed in 100% EtOH and flamed afterwards. In a first step, they are coated with polyornithine hydrobromide (1mg/ml) at 4°C o.n. Coverslips are then washed 4 times with 1xHBSS, followed by a second coating step with laminin, again at 4°C o.n. Before striatal MSNs are plated, the coverslips get washed at least twice with 1xHBSS and one further washing step with the full medium.

4.2.1.2 Tissue preparation

P1-P3 newborn mice are decapitated and cleaned with 70% EtOH. The brains are removed and transferred to 1xHBSS (should be 4°C), in order to dissect the striatum from the brain and transfer it to 1,5ml tubes with 250µl 1xHBSS (on ice). This can be easily done by:

1. bracing the two cortex hemispheres and cut corpus callosum in between
2. start with one hemisphere and move the cerebrum "upside down"
3. the hippocampus is now visible
4. remove the hippocampus completely
5. underneath the striatum becomes obvious - nestling against the cortex
6. cut along the edge between cortex and striatum and move down -
deeper along the cortex
7. the striatum can now be removed
8. move on to the second hemisphere

After tissue preparation, 50µl of 1% trypsin is added to each tube which is incubated at 37°C for 30min, interrupted by gently shaking each 5-10min. The trypsinization is stopped by adding 50µl trypsin-inhibitor. The tissue is now collected in a 15ml tube, preventing extensive liquid transfer. An appropriate amount of "full medium" (~4ml for tissue from 10 animals) is added and the 1st trituration with "large" diameter Pasteur pipette is carried out. Afterwards the tissue is centrifuged for 3min at 400xg. The fragment containing supernatant is carefully removed and discarded, before the same volume of full medium is added again, to perform the 2nd trituration, this time with a "medium" diameter Pasteur pipette. Again the tissue is centrifuged for 3min at 400xg. The supernatant is discarded afterwards. A 3rd trituration round is carried out according to the first two, this time with a "small" diameter Pasteur pipette. Cells and residual clusters are allowed to settling for 60s. Major clumps and aggregates may be removed manually. These cells can now be used for primary cell culture or for fluorescence-activated cell sorting (FACS).

For primary cell culture, a sample of 10µl is obtained and transferred to a counting chamber to estimate the cell density in order to dilute the cells in full medium to the appropriate dilution, before plating them on the prepared glass coverslips.

For FACS, these cells are filtered again and sorted in a BD ARIA III FACS sorter into 15ml Falcon tubes, provided with at least 2ml full medium. After the sorting is finished, the cells are provided with a further 2-3ml pre-warmed (37°C) full medium. Afterwards cells are centrifuged at 400xg for 3min. The supernatant is discarded and FACS MSNs are then diluted in an appropriate volume of the full medium before plating. After the cells are transferred to the glass coverslips they are allowed to attach for ~2h at 37°C, 5% CO₂. Afterwards "full medium" is added to obtain the working volume of the wells on the certain cell culture dish. The cells are then incubated at 37°C, 5% CO₂ for 24h, before the serum containing "full medium" is replaced with the same volume of serum-free "maintenance medium".

4.2.1.3 Stimulation of striatal MSN cell cultures

Striatal MSNs, no matter if they are low-density primary cultures or high-density FACS MSNs are stimulated with the following substances diluted in serum-free maintenance cell culture medium for the timescale indicated in the experiments.

BDNF	10ng/ml
Quinpirole Hydrobromide	1-2 μ M
L741-626	100nM
SKF38393	2 μ M
Sumanirole Maleate	500nM

After the stimulation, the cells are washed with 1xPBS before they are further processed for either ICC or WB (Surface Biotinylation) analysis.

4.2.2 BDNF / TrkB Immunohistochemistry (IHC)

4.2.2.1 Tissue preparation

Mice: - WT C57/B16 J

- NFL-Cre^{Wt/Tg} / BDNF^{fl/k.o.}

- BDNF-myc

- Ntrk Rohrer (TrkB^{-/-})

- D1-GFP [TG(DRD1a-EGFP)X60Gsat] (RRID:MMRRC_000297-MU)

- D2-GFP [TG(DRD2-EGFP)S118Gsat] (RRID:MMRRC_000230-UNC)

Mice are anaesthetized with CO₂. Chest is opened and a "butterfly" needle is injected into the left ventricle. Blood vessels are flushed with 1xPBS, 0.4% Heparin (4°C) for 2-3min. Perfusion is performed with 4% PFA in Phosphate Buffer (pH (6.0 for BDNF) 7.4) for ~8min. Mice are then decapitated and brains are removed from the skull. Tissue needs to be postfixed in 4% PFA at 4°C for 2h. Afterwards brains are washed 4x with 1xPBS and are kept in the same buffer o.n.

4.2.2.2 30µm free floating vibratome brain slices

Brains are embedded in 6% agarose and kept at 4°C for polymerization for ~30min. 30µm free-floating, coronal brain sections are obtained with a LEICA Vibratome VT1000S. Slices are stored in Cryoprotection Buffer (150ml 0.05M Phosphate Buffer, 90ml Glycerol, 60ml Ethylene-Glycol) at -20°C.

4.2.2.3 BDNF / TrkB Immunohistochemistry staining protocol

Antigen retrieval is performed in 10mM C₆H₅Na₃O₇ (pH 8.5) at 80°C for 30min. Afterwards brain slices are equilibrated to RT for 20min followed by 3 washing steps in 1xPBS for 15min each. Blocking and permeabilization are performed in one step by incubating the tissue slices in 1xPBS, 0.3% Triton X100, 0.1% Tween 20 and 10% normal Donkey serum for 2h. Afterwards primary antibodies are diluted in permeabilization and blocking solution as following:

BDNF: - Mouse anti BDNF (mAb#9 Prof. Y.-A. Barde) 0.5-1.0µg/ml

TrkB: - Rabbit anti TrkB (Millipore; 07225) 1.0µg/ml

- Goat anti TrkB (R&D Systems; AF1494) 0.5-1.0µg/ml

Antibodies are incubated on a shaker at 4°C for at least 24h (up to 72h). After the primary antibody solution is removed, the brain slices are further processed by washing 3 times with

1xPBS, 0.1% Triton-X 100, 0.3% Tween20 for 15min each. Thereafter, secondary antibodies are diluted in permeabilization and blocking solution as followed and incubated at RT for 2h:

BDNF: - Donkey anti Mouse DyLight549/550 (~0.625µg/ml)

TrkB: - Donkey anti Rabbit Alexa488 (~0.625µg/ml)

- Donkey anti Rabbit Cy3 (~0.625µg/ml)

- Donkey anti Rabbit Alexa647/DyLight649 (~0.625µg/ml)

After removal of the secondary antibody solution, brain slices are washed 3 times, using 1xPBS, 0.1% Triton-X 100, 0.3% Tween20 at RT, in dark for at least 15min each. Elongated washing procedures with an increased number of individual washing steps are recommended for BDNF-IHC approaches. Nuclear DNA is highlighted by incubation with DAPI in 1xPBS (0.4µg/ml) at RT, in dark for 15min. Afterwards the tissue is washed twice in 1xPBS at RT, in dark for 20min each. Free-floating brain slices are then mounted on Superfrost glass slides in dH₂O. Finally, the tissue is covered with MERCK-FluorSaveTM and a cover glass which is fixed with nail polish and can be stored afterwards at 4°C.

4.2.3 Immunocytochemistry (ICC)

Cell cultures were used for staining intracellular and cell surface proteins. Similarly, fixation of the cells and staining may follow a preceded treatment of the cells. In case of staining for surface proteins, like TrkB, primary antibodies are diluted in NB, B27, Glx, 1% P/S (4°C) and incubated at the same temperature for 30min. as followed:

TrkB: - Rabbit anti TrkB (Millipore; 07225) 1.0µg/ml

- Goat anti TrkB (R&D Systems; AF1494) 0.5-1.0µg/ml

The cells and proteins are directly fixed and cross-linked in 4% PFA (37°C, pH 7.4) at 37°C, for 10min and get washed twice with 1xPBS afterwards. Permeabilization and blocking are performed in 1xPBS, 10% Donkey serum (for surface protein staining) or 1xPBS, 10% Donkey serum, 0.1% Triton-X 100 (for access to intracellular epitopes) at RT for 1h. Intracellular epitopes are then bound by antibodies which are incubated in permeabilization and blocking solution at 4°C o.n. The next day, the cells are washed in 1xPBS, 0.1% Triton-X 100, three times for up to 5min each, before secondary antibodies are applied in permeabilization and blocking solution for up to 1.5h. Afterwards the cells are washed again in 1xPBS for up to 5min each. If required nuclei may be stained by highlighting DNA with DAPI in 1xPBS (0.4µg/ml) which is incubated at RT, in dark for 15min. Afterwards the excess of DAPI is washed off by 1xPBS and dH₂O, before glass coverslips, containing the cells are mounted on superfrost glass slides.

4.2.4 Immunocytochemistry (ICC) with Fluorescence *in situ* Hybridisation (FISH)

Confocal analysis of *in situ* hybridization is used for detection of DRD1 and DRD2 mRNAs in primary or FACS striatal MSN cultures. The procedure is carried out, following the guidelines and instructions by Panomics/Affymetrix. Antisense probes detecting DRD1 or DRD2 transcripts were obtained from Affymetrix. At all steps of the protocol, it is important to prevent the activity of RNase in order to preserve mRNAs in the samples. MSNs are washed 3x with RNase free pre-warmed 1xPBS and are fixed in 4% PLP buffer at RT for 10min. Following 3 further 1xPBS washing steps, the coverslips are then transferred to an "ICC-wet chamber". For permeabilization, 50µl detergent buffer is added to each coverslip for 4min. Afterwards the coverslips are washed 3x with 70µl 1xPBS. Afterwards 1µl Oligo-probes are diluted each in 100µl (40°C pre-warmed) probe diluent. MSNs are incubated with 40µl Oligo-probe containing diluent at 40°C o.n. in a dry incubator. After this incubation period, cells are washed 3x with the supplied washing buffer (Affymetrix kit) at RT. In the

next step, 70µl diluted pre-amplifier (1:25 in 40°C pre-warmed amplifier buffer) are incubated on the cells, at 40°C for 1h, before the cells are washed again 3x with 70µl washing buffer. This procedure is repeated in the same way, using an amplifier (1:25 in amplifier buffer) instead of pre-amplifier. After another 3 washing steps, the probes get labeled, using 70µl label probe mix per coverslip, diluted 1:25 in 40°C label probe diluent QF, incubated on the cells at 40°C for 1h. Again, the label probe mix is washed off, 3 times with 70µl washing buffer. The samples are now prepared for indirect immunofluorescence detection of protein. Therefore, non-specific binding sites are blocked with 70µl 1xPBS, 10% SDS, 200µg/ml Saponine which is incubated at RT for 1h. Now primary antibodies are diluted in blocking solution and are incubated at RT for 1h before they are washed off 3 times with RNase free 1xPBS. Secondary antibodies are diluted in blocking solution as well and get incubated accordingly to the primary antibodies, again followed by 3 washing steps with 1xPBS. Nuclear staining is achieved by incubation of DAPI (20µg/ml in 1xPBS) for 1min followed by two washing steps with 1xPBS. To prevent crystal formation from residual PBS, this is washed off with dH₂O. Afterwards the coverslips are mounted on superfrost glass slides with Merck FluorSave. Samples are stored at 4°C until analysis on a confocal microscope.

4.2.5 Western Blot analysis of tissue samples obtained from mouse or rat

4.2.5.1 Tissue preparation from animals

Adult animals are euthanized in CO₂ and body weights are obtained before decapitation. In case of newborn mice of BDNF^{-/-} or Ntrk Rohrer^{-/-} until the age of P5, animals were quickly decapitated. The brain is removed after opening the skull and placed in 1xPBS or 1xHBSS (4°C). Afterwards Cortex, Hippocampus, Striatum, Cerebellum and midbrain including the remaining tissue are dissected and transferred separately to 2ml tubes which are immediately frozen in liquid nitrogen and stored at -80°C.

4.2.5.2 Tissue dissociation / lysis

Before further processing, the tissue weight / mass is obtained in order to proceed lysis in the correct volume of lysis buffer. Tubes and tissue are then provided with 5x volume of the mass equivalent of the tissue (60mg = 300 μ l) with lysis buffer. Afterwards, the tissue is manually fragmented, using a plastic mortar, while keeping the samples on ice / dry ice all the time.

4.2.5.3 Sonification

In addition to the manual homogenization of the tissue, a Hielscher Sonifyer is used for sonification (cycle 0.5, amplitude 90, 10 pulses) of tissue lysates. After this step, the samples are placed on ice for an incubation of 4x15min. The tissue is vortexed after 15min each, before placing it back on ice for further incubation. Finally, all probes are centrifuged at 4°C and 14.000rpm for 20min. Afterwards the supernatant is stored in new 2.0ml tubes at -20°C.

4.2.5.4 BCA Assay for calculation of protein content

For calculation of the protein content, a BCA assay is performed according to the manufacturer's guidelines, using a Pierce Protein Research BCA kit by Thermo Scientific.

For preparation of the standard-curve BSA standards are set up as followed:

Table 3: Preparation of standard-curve BSA samples

BCA Assay	dH ₂ O (μ l)	BSA (μ l)	Concentration (μ g/ml)
A)	0	300 (original Stock Thermo Scie.)	2000
B)	125	375 (original Stock Thermo Scie.)	1500
C)	325	325 (original Stock Thermo Scie.)	1000
D)	175	175 of B)	750
E)	325	325 of C)	500
F)	325	325 of E)	250
G)	325	325 of F)	125
H)	400	100 of G)	25
I)	400	0	0

According to the manual a "working reagent" is prepared by mixing 17.64ml Reagent A with 360 μ l Reagent B (50:1) resulting in 18ml for 18 reactions. Afterwards, 50 μ l standard-curve

samples are mixed with 950µl "working reagent" ($V_{\text{tot}} = 1\text{ml}$). Accordingly, 5µl protein-tissue samples are diluted in 45µl 1xPBS and mixed with 950µl "working reagent". All probes are incubated in a Thermomixer at 37°C while gently shaking for 30min. The preparation of standard curve dilution in working reagent and the resulting concentration is depicted in the following table.

Table 4: Dilution of standard-curve BSA samples in "working reagent" for photometer analysis

<u>Standard curve dilution (in Working reagent - WR)</u>	<u>Final Concentration in 1ml WR (µg/ml)</u>	<u>Dilution Coefficient</u>
50µl of A) with 950µl WR	100 (stock 2000µg/ml)	20
50µl of B) with 950µl WR	75 (stock 1500µg/ml)	
50µl of C) with 950µl WR	50 (stock 1000µg/ml)	
50µl of D) with 950µl WR	37,5 (stock 750µg/ml)	
50µl of E) with 950µl WR	25 (stock 500µg/ml)	
50µl of F) with 950µl WR	12,5 (stock 250µg/ml)	
50µl of G) with 950µl WR	6,25 (stock 125µg/ml)	
50µl of H) with 950µl WR	1,25 (stock 25µg/ml)	
50µl of I) with 950µl WR	0 (stock 0µg/ml)	

The protein concentration is then calculated from the data obtained in a photometric analysis. Afterwards the volume of tissue samples which contain 30µg protein (used for gel loading) is calculated. Laemmli buffer is added to obtain a total volume of ~15µl and a concentration of 1x Laemmli. All samples are then boiled at 95-99°C for 5min before they are stored at -20°C o. n. Alternatively, samples are directly applied to a polyacrylamide gel.

4.2.5.5 SDS - gel running

1.0mm glass plates are used with 1.0mm combs (BioRad). A mark is made manually at a 5cm distance from the bottom of the glass plate which defines the edge of the separation gel. Both separation and stacking gels are set up according to calculations, using SDS PAGE Calculator (Chang Bioscience). When the separation gel is transferred to the prepared glass plates (in plate mounting system), isopropanol is added on top to ensure an even surface and clear border between both gels. The separation gel is polymerized at RT for 1h. Afterwards the

isopropanol is removed with blotting paper and the stacking gel is made in the same way as mentioned above and added on top of the separation gel, including a comb for preparation of pockets. Polymerization is performed for 15-20min. Afterwards, gels may be further polymerized at 4°C (~2h) before directly using, or they may be wrapped in wet tissues papers and plastic foil in order to store them at 4°C for up to 7 days.

4.2.5.6 Gel loading and electrophoresis

If only one gel is used a dummy plate (BioRad) is placed into the gel chamber which is filled with electrophoresis buffer. Combs are removed and pockets get cleaned, in order to prepare them for probe loading. 8µl of "Page ruler - protein ladder" and the samples are now applied to the gel. The gel running is performed in two separate steps as followed:

Gel running conditions - stacking gel: - 70V for 15-20min until separation gel is reached
by the marker front

Gel running conditions - separation gel: - U=130V; I=20mA (const.)

- increase U to maximum but I constant at 20mA

- t = ~1 - 1.5h

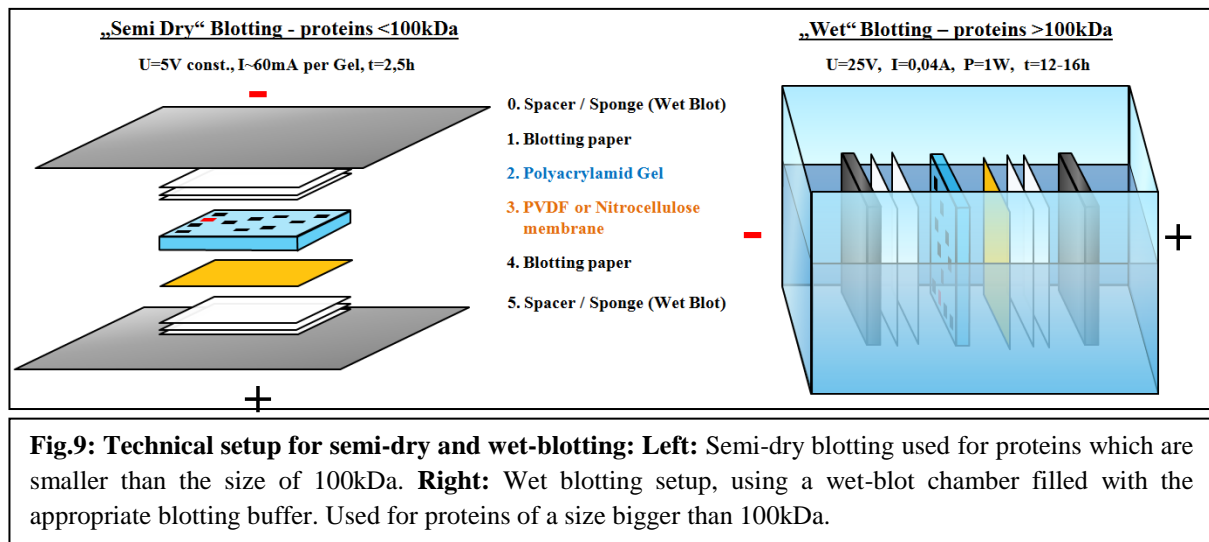
When the gel running is complete, the gels are carefully removed and washed in western blotting transfer buffer until the blotting setup is prepared.

4.2.5.7 Preparation of PVDF (nitrocellulose) membrane (5x8.3cm)

PVDF membranes are incubated in methanol for 30min, before a stepwise transfer to either western (Semi-Dry blotting) or wet blot (Wet blotting) transfer buffer is performed. Furthermore, blotting papers are incubated in transfer buffer according to the preferred method of blotting.

4.2.5.8 Blotting

Two different techniques are used for transfer of proteins from polyacrylamide gels to either PVDF or nitrocellulose membranes. For proteins <100kDa a "semi-dry blotting" method was used, while for proteins >100kDa "wet blotting" is the preferred method (**Fig. 9**). Both methods and the methodological setup are depicted below.



Usually "wet blotting" is used for western blot detection of TrkB (130kDa). The PVDF membranes have a dimension of $5 \times 8.3 \text{cm} = 41,5 \text{cm}^2$ which requires a current of $I=2.5 \text{mA/cm}^2$ at the beginning of the blotting which is decreasing with ongoing time. Wet blotting is performed at 4°C o.n., under permanent stirring of the buffer, to prevent overheating or sedimentation. When blotting is finished, the PVDF membranes are immediately transferred to 1xTBST for 15min.

4.2.5.9 Blocking and primary antibody incubation

PVDF membranes are incubated in 1xTBST, 5% Milk powder, in order to saturate non-specific antibody binding epitopes, for up to 4h. Afterwards the blocking solution is discarded and the blots get washed in 1xTBST. Primary antibodies, diluted in 1xTBST, 0.01% NaN_3 are incubated on the membranes at 4°C on a shaker for up to 72h.

4.2.5.10 Secondary antibody incubation and detection

After use, primary antibody solution is stored in 15ml tube at 4°C, for repeated use. Usually, monoclonal antibodies are not used again, while polyclonal antibodies were used up to 5 times. Blots are then washed 3 times in 1x TBST, for at least 15min each. Afterwards the blots are incubated with 10ml 1x TBST, containing HRP/POD coupled secondary antibodies at a standardized dilution of 1:10.000. This incubation is performed for 1-2h at RT on a shaker. Afterwards the antibody solution is discarded and the membranes are washed again 3 times in 1xTBST for at least 15min each. Proteins on the membranes are detected after incubation with ECL - WB detection reagents (Solution A: Solution B = 1:1 - 500µl each per membrane) for 5min. The detection itself is carried out, using a photo-film equipped cassette, and a KODAK/AGFA developer machine. The certain exposure times vary, depending on protein abundance and antibody-related chemo-luminescence signal.

4.2.5.11 Loading control and re-probing

Immediately after detection, the blots are washed up to 3 times for 45min each in 1xTBST, containing 0.01% NaN₃. The NaN₃ is used for abolishing HRP related chemo-luminescence by destroying the enzymatic activity. After this, further target proteins are aimed for detection, as long as the antibody used for detection is derived from a different host, then the first antibody used for detection. If this is the case, detection of further proteins follows the protocol, starting at step 4.2.5.8, but without repeating the blocking step. If host species and related signal intensity of two different detected proteins are identical, then the antibodies bound to proteins on the membrane are washed off with stripping buffer at RT on a shaker, for up to 30min. Afterwards blots are extensively washed in 1xTBST, before the protocol follows the steps beginning with 4.2.5.8, but including another blocking step.

4.2.5.12 Storage

As a final step, after detecting all relevant proteins on each membrane, these are washed in 1xTBST and finally dH₂O. Afterwards, blots are air dried and shrink-wrapped in plastic foil for long-term storage and possible reactivation.

4.2.6 Immunoprecipitation of TrkB and Western Blot analysis from tissue samples

The striatum, derived from P5 WT and P5 Ntrk Rohrer (TrkB ^{-/-}) animals was used for analysis of TrkB expression via immunoprecipitation. The striatal tissue is lysed according to steps 4.2.5.1 - 4.2.5.4, using IP-Lysis / Wash-buffer 1.

4.2.6.1 Pre-clearing and protein binding

Agarose beads are pre-incubated with 3µg antibody (Rabbit anti-TrkB 07-225) in IP-Lysis / Wash-buffer 1 in a spinning wheel at 4°C for 2h. This has the aim to saturate non-specific binding sites on the agarose beads. Afterwards 300µg of the tissue lysate is added and the IP-setup is incubated in a spinning wheel at 4°C o.n. The setup for each IP is as following:

IP pull-down setup:

- 30µl Protein A agarose
- 3µg primary antibody
- 300µg tissue lysate
- ad 500µl total volume with IP-Lysis / Wash-buffer 1

4.2.6.2 Pulldown and purification

After incubation o.n. samples are spun down at 1000xg for 1min. The supernatant is transferred to a fresh tube and stored as "Flow-Through" at -20°C. Afterwards, the beads containing antibody coupled target proteins (TrkB) are washed in 500µl IP-Lysis / Wash-buffer 1 in a spinning wheel at 4°C for 20min. Afterwards the samples are again centrifuged at 1000xg for 1min. The supernatant is discarded and the washing procedure is repeated in the same way, first with IP Wash-buffer 2 and then with IP Wash-buffer 3. After the final centrifugation at 1000xg at 4°C for 1min, the supernatant is removed completely with a

vacuum pump and an extra thin hollow needle. Afterwards 30µl 2x Laemmli are added and the samples are boiled at 95°C for 5min. Afterwards the samples are stored at -20°C or directly applied for WB analysis, moving on with loading to PAA gels (step 4.2.5.5).

4.2.7 TrkB surface biotinylation in striatal MSNs (primary & FACS)

4.2.7.1 Cell culture

For obtaining significant bands from surface biotinylation an absolute minimum of ~250.000 cells is required. Most experiments were carried out using ~250.000-1.000.000 cells. Cell culture protocols were performed as mentioned above (4.2.1). Cells may be stimulated with pharmaceutical agents before surface biotinylation (4.2.1.3).

4.2.7.2 Biotinylation

After stimulation, cell culture medium is removed completely and cells are washed 3x with 1xPBS (4°C). The temperature needs to be kept constantly at 1-4°C to prevent import or export of membrane proteins. Afterwards the cells are incubated with 2ml Sulfo-NHS-SS-Biotin (0.25mg/ml in 1xPBS) on a shaker at 4°C for 30min. 100µl Quenching buffer (Glycine or Tris based) are added to stop biotinylation and 3 further washes in 2ml 1xTBS are performed to scavenge the residual biotin.

4.2.7.3 Cell lysis

After stopping the biotinylation, the whole volume is removed and 500µl TNE lysis buffer is added to the cells. A cell scraper is used for immediately collecting all cells grown on the coverslips. The cells are transferred to a fresh tube and are incubated at 4°C for 10min, before performing two sonification steps (10 bursts, amplitude 0.5; 80%). In between these sonification steps, the cells are always incubated at 4°C on ice for 10min. Afterwards, the samples are centrifuged at 20.000xg and 4°C for 10min. 10% of the supernatant is stored in a fresh tube as "Input" at -20°C.

4.2.7.4 Avidin mediated pull-down

For Avidin-Biotin mediated pull-down, 50µl Neutravidin beads are washed 3 times with 200µl washing buffer. Afterwards, 450µl biotinylated cell-lysate is added and left for incubation and binding in a spinning wheel at RT for 1h. Afterwards, the samples are centrifuged at 2000xg for 2min and the supernatant is stored as "Flow-Through" in a new tube at -20°C.

4.2.7.5 Purification of surface proteins

The beads are washed 3 times with 200µl washing buffer, interrupted by centrifugation at 2000xg for 2min each. Every single time, the supernatant is discarded. In the final step, 50µl DTT (in SDS-sample buffer) is added to the beads, in order to break the disulfide bond between biotin and the bound surface proteins. The samples are incubated with DTT in a spinning wheel at RT for 1h. Afterwards, the samples are centrifuged at 2000xg for 2min and the samples are stored as "Pull Down" at -20°C. The samples are now prepared for usage in gel-electrophoresis and western blot analysis. For detection of surface TrkB Gel Electrophoresis 8% PAA gels were used. Loading was accompanied as followed:

- 4% Input (20µl + 5µl 5x Laemmli)
- 4% Flow-Through (20µl + 5µl 5x Laemmli)
- 12% Pull Down (15µl + 4µl 5x Laemmli)

All samples are boiled at 99°C for 5min followed by 1min 20.000xg. Electrophoresis is performed in 1x Electrophoresis buffer (25mM Tris, 0.2M Glycine, 0.1% SDS, in dH₂O, pH 8.35) at U=70V for ~ 30min, before switching to U=200V const.; I~20mA per gel. After the gel run samples are blotted (Wet-Blotting) and further prepared according to 4.2.5.6.

4.2.8 BDNF ELISA

4.2.8.1 Tissue preparation from animals

Tissue preparation is performed according to 4.2.5.1

4.2.8.2 Tissue dissociation/lysis for ELISA

The weight of each brain area (Cortex (Ctx), Hippocampus (Hippo), Striatum (Str), Cerebellum (Cereb), Midbrain (Midbr)) was obtained and the samples are provided with the 5x volume of the mass equivalent of the tissue (60µg = 300µl) with ELISA extraction buffer.

4.2.8.3 Sonification

All samples are kept at temperatures between 1-4°C during the whole procedure. A Hielscher Sonifyer is used for homogenization of each sample, using the following settings:

Cycle: 1; Amplitude: 80%; 7 pulses for each tissue sample (~1s)

Afterwards, the tubes are placed on ice for an incubation time of 10min. Thereafter the sonification and incubation step is repeated twice. Finally, all samples are centrifuged at 4°C at 20.000xg for 25min. The supernatant is transferred to new 2.0ml safe-lock tubes and can be used directly for ELISA or long-term storage at -80°C.

4.2.8.4 Coating of 96 well ELISA plate with "collecting antibody"

A 96 well ELISA plate is provided with 200µl/ well-diluted Mouse anti-BDNF (500ng; mAb#1) in ELISA coating buffer. For a whole 96 well plate 19.2ml coating buffer are mixed with 48.000ng mAb#1 (12.6µl from antibody stock). 200µl are transferred to each of the 96 wells, using an 8x multipette. Afterwards the plate is covered in aluminum foil and left for incubation at RT o.n.

4.2.8.5 ELISA - plate blocking

After the coating is completed, coating buffer from the ELISA plate is discarded and the plate is provided with ELISA blocking solution. The wells should be filled completely. Again the plate is covered with aluminum foil and incubated at RT for 2h. In the meantime all samples

are carefully defrosted on ice and again centrifuged at 20.000xg, 4°C, for 25min. In parallel, a standard curve preparation is set up in order to calculate protein concentrations.

4.2.8.6 BDNF standard curve and plate loading

8 safe lock tubes (#1-8) are provided with each 1ml extraction buffer (#1 provided with 2ml) and a BDNF dilution series is established, using a stock solution of recombinant BDNF, as following:

- preparation of tube #1: - 2ml Extraction buffer
- 1.70µl (25.52ng) recombinant BDNF (15µg/ml stock)
- 25.52ng in 2ml \cong 12,75ng in 1ml \cong 638pg in 50µl

After mixing the BDNF solution in tube #1 carefully, transfer 1ml to tube #2. Again, after carefully mixing, 1ml of tube #2 is transferred to tube #3 and so on. Using a new pipette tip for each step is recommended.

Dilution series of recombinant BDNF:

- #1. 2000µl - 638pg BDNF in 50µl
- #2. 1000µl - 319pg BDNF in 50µl
- #3. 1000µl - 160pg BDNF in 50µl
- #4. 1000µl - 80pg BDNF in 50µl
- #5. 1000µl - 40pg BDNF in 50µl
- #6. 1000µl - 20pg BDNF in 50µl
- #7. 1000µl - 10pg BDNF in 50µl
- #8. 1000µl - 0pg BDNF in 50µl (no transfer to this tube)

Now, each of the 96 wells on the ELISA plate is provided with 150µl ELISA incubation buffer. The BDNF standard curve samples are loaded first. Since the analysis is performed in triplicates to identify variances and errors during pipetting, each sample is loaded 3 times. Therefore 50µl of standard curve samples are added to 150µl ELISA incubation buffer in the appropriate well. Afterwards, brain tissue samples are loaded as triplicates, in the same way, using 50µl sample in 150µl ELISA incubation buffer. The whole plate is now incubated in a bacteria shaker (20°C; 25rpm) for 3h.

4.2.8.7 Second antibody incubation and detection

3µl of Mouse anti-BDNF mAb#9, conjugated to HRP is added to 20ml incubation buffer and are gently mixed (use antibody in a range of 1:4000-1:10.000). The primary "detection" antibody is incubated at RT for 3h, before being discarded. Each well is now washed 3 times with 400µl ELISA washing buffer, followed by loading 200µl of secondary antibody solution to each well which is incubated, like the primary antibody at 20°C, 25rpm in a bacteria shaker for 3h. After discarding the secondary antibody, all wells are again washed 3 times with 400µl washing buffer. For the detection, POD-substrate is prepared (ELISA substrate - Roche), by mixing 20ml of solution #1 with 200µl solution #2 (100:1). HRP triggered chemoluminescence is measured with an ELISA reader. The obtained data are summarized in an EXCEL file for preparation of statistics, using GraphPad Prism software.

4.2.9 RNA purification and qRT-PCR analysis

4.2.9.1 RNA purification from tissue samples

Purification of RNA was performed according to the original protocol, using a Trizol-lysis, based on acidic guanidinium thiocyanate - phenol - chloroform extraction, described by (Chomczynski and Sacchi, 1987). During the phase separation, the upper aqueous phase contains RNA at pH4-6, as well as RNA/DNA hybrids and DNA at pH7-8. The lower organic phase contains lipids and proteins that may also be bound to DNA at pH4-6. Guanidinium

thiocyanate is a chaotropic agent which is able to denaturize proteins and enzymes including RNase, thus leaving nucleic acids untouched. For RNA extraction from tissue, whole brains from P1 mice (DRD1-EGFP, DRD2-EGFP, FVB-WT), or single brain areas from rat brain, are dissected and frozen in liquid nitrogen in 2ml tubes. For the whole procedure, the tissue is kept on dry ice all the time. 400µl Trizol is added to each sample which is homogenized manually by using a mortar. Afterwards 160µl Chloroform is added and mixed to the homogenate which is then centrifuged at 15.250xg at 4°C for 15min. In parallel new tubes are provided with 500µl Isopropanol. The aqueous phase of the supernatant, containing RNA is transferred to new tubes with isopropanol which will precipitate nucleic acids. The mixture is incubated for 10min at RT and centrifuged at 15.250xg at 4°C for another 10min. The supernatant is removed and 500µl 70% EtOH is added to the pellet which is then centrifuged at 15.250xg at 4°C for 5min. The supernatant needs to be discarded and the washing procedure with EtOH is repeated in order to remove salt from nucleic acids. Afterwards the pellet is dried at RT for ~20-25min, before dissolving it in 50µl RNase free H₂O. The concentration of nucleic acids is obtained with a Nanodrop. If the density is too high, the samples are further diluted with RNase free H₂O. All samples are stored at -80°C (RNA - no long-term storage possible).

4.2.9.2 RNA purification from cell culture

Similar to 4.2.9.1, the purification of RNA from cells was also performed using a Trizol-lysis, based on acidic guanidinium thiocyanate - phenol - chloroform extraction. Initially, the cells are washed twice with 1x PBS, followed by the application of 1ml Trizol (12-18mm glass coverslips). The cells are collected, using a cell scraper and mixed afterwards with 400µl chloroform in a new safe lock tube. The lysate is gently vortexed and centrifuged at 15.250xg at 4°C for 15min. Afterwards, the aqueous phase is transferred to a new tube with 500µl Isopropanol. For precipitation, the mixture is incubated at RT for 10min, followed by a centrifugation at 15.250xg and 4°C for 10min. The supernatant is discarded and the pellets are

washed 2-3 times with 70% EtOH, intermitted by 5min centrifugation at 15.250xg and 4°C. After the final washing step, the pellet is dried at 37°C, before dissolving in 50µl ultra pure, nuclease-free dH₂O.

4.2.9.3 RNA quality control and DNA digestion

The integrity of the purified RNA is confirmed by RNA gel analysis (Northern Blot) in order to identify 5S, 18S, 28S rRNA. RNA gels are prepared as followed:

- 1.6% agarose gel in 1xTAE (100ml, 1,6g Agarose, 8µl EtBr)
- run gel in 1xTAE
- wash gel chamber with 3% H₂O₂

For gel loading the samples are set up as followed:

- 500ng nucleic acids from RNA purification
- 7µl Formaldehyde
- 3µl Formamide
- 1.5µl 10x TAE buffer
- 1µl EtBr₂

All samples are incubated for 10min at 70°C and placed on ice shortly, before directly applying them to the RNA gel together with 8µl 100bp gene ruler marker. The gel run is performed at U=120V for 20-25min. 18S and 28S rRNA bands should be evident to ensure sufficient quality. Smear on the gel might be due to a high salt concentration which can be prevented by additional EtOH washing steps during RNA extraction. The purified RNA is very likely to still contain gDNA (genomic DNA) which needs to be degraded in the next step.

4.2.9.4 Digestion of genomic DNA (gDNA) in purified RNA samples

If gDNA is not degraded, it will cause false results, due to amplification during PCR.

Therefore, DNase mediated digestion of gDNA was performed, using an "Ambion Turbo DNA - free kit". Therefore 10µg of nucleic acids are diluted in 50µl RNase free dH₂O. 0.1x volume (5µl) of DNase buffer and 1,5µl DNase are added for incubation at 37°C for 30min. Thereafter again 1,5µl DNase is added and the incubation is repeated. After the digestion, 3µl DNase inactivation reagent is added, samples are vortexed gently and incubated at RT for 5min. This is followed by a centrifugation at 10.000xg at RT for 2min. The supernatant is then transferred to new tubes and stored as "pure RNA" at -80°C.

4.2.9.5 cDNA synthesis from RNA by RT-PCR

RNA needs to be diluted to 10µg in 50µl RNase free dH₂O. Therefore the exact concentration of RNA after digestion of gDNA is obtained with a nanodrop. For RT-PCR, 500ng RNA is mixed with 1µl random hexamer from RT-PCR kit. For RT-PCR

- Run RT-PCR program:
- 5min 65°C
 - cool down on ice; short spin down
 - add:
 - 4µl 5x reaction buffer
 - 1µl RiboLock RNase inhibitor
 - 2µl 10mM dNTP mix
 - 2µlM-MuLV-Reverse Transcriptase
 - mix gently and spin down
 - 5min at 25°C; 60min at 37°C

The amplified cDNA is stored at -20°C or -80°C. The mRNA is reverse transcribed into stable cDNA which allows easy handling, storage and specific analysis of transcribed genes, using specific primer pairs for certain genes of interest.

4.2.9.6 qRT-PCR for *Gapdh*

GAPDH serves as an internal control for accuracy and basis for calculation of relative mRNA ratios. A "-RT" control without performing the reverse transcriptase step, preventing cDNA synthesis, as well as a negative control using dH₂O instead of nucleic acids, were used as negative controls.

Expected band size: ~141bp

Q-PCR approach:

- 2µl *Gapdh* primer (10µM each)
- 6µl dH₂O
- 10µl Luminaris qPCR-Mastermix
- 2µl DNA

Each sample is prepared including a technical replicate which enables to calculate accuracy during the experimental setup.

Table 5: qRT-PCR program for amplification of *Gapdh*

Step	Duration	Temperature	Cycles
Initial Denaturation	2min.	50°C	1
	10min.	95°C	
Denaturation	15s	95°C	50
Annealing	30s	60°C	
Elongation	30s	72°C	
4 th segment	5s	80°C	
Melting	0s	95°C	1
	15s	65°C	
	0s	95°C	
Cooling phase	40s	40°C	1

After qRT-PCR, the PCR tubes are inverted and content is centrifuged into a 1,5ml tube to obtain the amplified product (20µl in total). This DNA is mixed with 5µl 5x loading dye and applied to a 3% agarose gel with EtBr, together with 8µl 100bp DNA ladder. The gel run is performed at U=100-110V for ~45min in order to confirm correct band size. Data obtained from the lightcycler are exported to an excel file, for further statistical analysis with GraphPad Prism software.

4.2.9.7 qRT-PCR for *Gfp*

Expected band size: ~175bp

- Q-PCR approach:**
- 2µl GFP primer (10µM each)
 - 6µl H₂O
 - 10µl Luminaris qPCR-Mastermix
 - 2µl DNA

Table 6: qRT-PCR program for amplification of *Gfp*

Step	Duration	Temperature	Cycles
Initial Denaturation	2min.	50°C	1
	10min.	95°C	
Denaturation	15s	95°C	50
Annealing	30s	60°C	
Elongation	30s	72°C	
4 th segment	5s	77°C	
Melting	0s	95°C	1
	15s	65°C	
	0s	95°C	
Cooling phase	40s	40°C	1

After qRT-PCR, the PCR tubes are inverted and content is centrifuged into a 1,5ml tube to obtain the amplified product (20µl in total). This DNA is mixed with 5µl 5x loading dye and applied to a 3% agarose gel with EtBr, together with 8µl 100bp DNA ladder. The gel run is performed at U=100-110V for ~45min in order to confirm correct band size. Data obtained from the lightcycler are exported to an excel file for further statistical analysis with GraphPad Prism software.

4.2.9.8 qRT-PCR for mouse *TrkB* Full Length

Expected band size: ~134 bp

- Q-PCR approach:**
- 2µl TrkB1940U21 & TrkBkin2074L21 primer (10µM each)
 - 6µl H₂O
 - 10µl Luminaris qPCR-Mastermix
 - 2µl DNA

Table 7: qRT-PCR program for amplification of mouse *TrkB*

Step	Duration	Temperature	Cycles
Initial Denaturation	2min.	50°C	1
	10min.	95°C	
Denaturation	15s	95°C	50
Annealing	30s	60°C	
Elongation	30s	72°C	
4 th segment	5s	80°C	
Melting	0s	95°C	1
	15s	65°C	
	0s	95°C	
Cooling phase	40s	40°C	1

After qRT-PCR, the PCR tubes are inverted and content is centrifuged into a 1,5ml tube to obtain the amplified product (20µl in total). This DNA is mixed with 5µl 5x loading dye and applied to a 3% agarose gel with EtBr, together with 8µl 100bp DNA ladder. The gel run is performed at U=100-110V for ~45min in order to confirm correct band size. Data obtained from the lightcycler are exported to an excel file for further statistical analysis with GraphPad Prism software.

4.2.9.9 qRT-PCR for mouse *TrkB T1*

Expected band size: ~187 bp

Q-PCR approach: - 2µl T1-1907U19 & T1-2094L19 primer (10µM each)

- 6µl H₂O

- 10µl Luminaris qPCR-Mastermix

- 2µl DNA

Table 8: qRT-PCR program for amplification of mouse *TrkB T1*

Step	Duration	Temperature	Cycles
Initial Denaturation	2min.	50°C	1
	10min.	95°C	
Denaturation	15s	95°C	50
Annealing	30s	60°C	
Elongation	30s	72°C	
4 th segment	5s	79°C	
Melting	0s	95°C	1
	15s	65°C	
	0s	95°C	
Cooling phase	40s	40°C	1

After qRT-PCR, the PCR tubes are inverted and content is centrifuged into a 1,5ml tube to obtain the amplified product (20µl in total). This DNA is mixed with 5µl 5x loading dye and applied to a 3% agarose gel with EtBr, together with 8µl 100bp DNA ladder. The gel run is performed at U=100-110V for ~45min in order to confirm correct band size. Data obtained from the lightcycler are exported to an excel file for further statistical analysis with GraphPad Prism software.

4.2.9.10 qRT-PCR for rat *TrkB*

Expected band size: ~178 bp

Q-PCR approach: - 2µl TrkB2026_for & TrkBkin2204rev primer (10µM each)

- 6µl H₂O

- 10µl Luminaris qPCR-Mastermix

- 2µl DNA

Table 9: qRT-PCR program for amplification of rat *TrkB*

Step	Duration	Temperature	Cycles
Initial Denaturation	2min.	50°C	1
	10min.	95°C	
Denaturation	15s	95°C	50
Annealing	30s	60°C	
Elongation	30s	72°C	
4 th segment	5s	83°C	
Melting	0s	95°C	1
	15s	65°C	
	0s	95°C	
Cooling phase	40s	40°C	1

After qRT-PCR, the PCR tubes are inverted and content is centrifuged into a 1,5ml tube to obtain the amplified product (20µl in total). This DNA is mixed with 5µl 5x loading dye and applied to a 3% agarose gel with EtBr, together with 8µl 100bp DNA ladder. The gel run is performed at U=100-110V for ~45min in order to confirm correct band size. Data obtained from the lightcycler are exported to an excel file for further statistical analysis with GraphPad Prism software.

4.2.10 Genotyping

4.2.10.1 PCR for NFL-Cre BDNF^{fl/ko}

For the genotyping and identification of NFL-Cre - BDNF^{fl/ko} mice, four independent PCRs have to be performed, in order to identify the presence of the Cre transgene, the neomycin cassette for the "knock out allele", the loxP sites flanking BDNF exon V and the remaining loxP site after successful recombination.

A) NFL-Cre PCR

Expected band size: ~250 bp

Reaction conditions:

- 1µl DNA
- 3µl 10x PCR buffer
- 3µl enhancer (5 Prime)
- 1µl dNTPs (10mM)
- 0.1µl forward primer (100pmol stock - NFL-SEQ (19mer))
- 0.1µl reverse primer (100pmol stock - pMC-Cre)19mer))
- 0.3µl Taq Polymerase (5 Prime)
- 21.5µl dH₂O

Cycle Conditions:

Table 10: PCR program for verification of Cre transgene

Step	Duration	Temperature	Cycles
Initial denaturation	5min.	94°C	1
Denaturation	1min.	94°C	29
Annealing	30s	59°C	
Elongation	1min.	72°C	
Termination	7min.	72°C	1
Hold	∞	4°C	

After the PCR is finished, all samples are mixed with 5µl 6x loading dye. The samples are applied to a 3% agarose gel (with EtBr) in 1xTAE buffer, in which a gel run at U=120V is performed for ~35min. The PCR products are identified using a photo-chamber provided with a UV light source.

B) BDNF k.o. PCR

Expected band size: ~450 bp (WT) (BD2A + BKO-1)

~420 bp (k.o.) (BD2A + 3'NEO)

- Reaction conditions:**
- 1µl DNA
 - 3µl 10x PCR buffer
 - 6µl Betaine (5M)
 - 3µl dNTPs (2mM)
 - 0.1µl forward primer (100pmol stock - BD2A)
 - 0.1µl reverse primer (100pmol stock - BKO-1 or 3'NEO)
 - 0.3µl Taq Polymerase (5 Prime)
 - 13.5µl dH₂O

Cycle Conditions:

Table 11: PCR program for verification of BDNF k.o. knock in

Step	Duration	Temperature	Cycles
Initial denaturation	2min.	95°C	1
Denaturation	30s	95°C	35
Annealing	45s	60°C	
Elongation	2min.	72°C	
Termination	10min.	72°C	1
Hold	∞	4°C	

After the PCR is finished, all samples are mixed with 5µl 6x loading dye. The samples are applied to a 2% agarose gel (with EtBr) in 1xTAE buffer, in which a gel run at U=120V is performed for ~35min. The PCR products are identified using a photo-chamber provided with a UV light source.

C) BDNF loxP PCR

- Expected band size:**
- ~620 bp (BDNF^{wt/wt})
 - ~790 bp (BDNF^{fl/fl})
 - ~ 700bp (BDNF^{fl/wt})

- Reaction conditions:**
- 1µl DNA
 - 5µl 10x PCR buffer
 - 5µl enhancer (Eppendorf)
 - 5µl dNTPs (2mM)
 - 0.5µl forward primer (20pmol stock - bdnf13)
 - 0.5µl reverse primer (20pmol stock - bdnf14)

- 0.5µl Taq Polymerase (5 Prime)

- 32.5µl dH₂O

Cycle Conditions:

Table 12: PCR program for verification of floxed BDNF

Step	Duration	Temperature	Cycles
Initial denaturation	5min.	94°C	1
Denaturation	30s	94°C	40
Annealing	45s	63°C	
Elongation	45s	72°C	
Termination	7min.	72°C	1
Hold	∞	4°C	

After the PCR is finished, all samples are mixed with 5µl 6x loading dye. The samples are applied to a 1.5% agarose gel (with EtBr) in 1xTAE buffer, in which a gel run at U=120V is performed for ~35min. The PCR products are identified using a photo-chamber provided with a UV light source.

D) BDNF - remaining loxP site after Cre - recombination

Expected band size: ~2417 bp (WT)

~2600 bp (fl/fl)

~ 600bp (recombined)

Reaction conditions:

- 1µl DNA

- 5µl 10x PCR buffer

- 5µl enhancer (Eppendorf)

- 5µl dNTPs (2mM)

- 0.5µl forward primer (20pmol stock - BDNF_499for)

- 0.5µl reverse primer (20pmol stock - BDNF_935rev)

- 0.4µl Taq Polymerase (5 Prime)

- 32.6µl dH₂O

Cycle Conditions:

Table 13: PCR program for verification of Cre mediated recombination

Step	Duration	Temperature	Cycles
Initial denaturation	5min.	94°C	1
Denaturation	30s	94°C	40
Annealing	45s	56°C	
Elongation	90s	72°C	
Termination	7min.	72°C	1
Hold	∞	4°C	

After the PCR is finished, all samples are mixed with 5µl 6x loading dye. The samples are applied to a 2% agarose gel (with EtBr) in 1xTAE buffer, in which a gel run at U=120V is performed for ~35min. The PCR products are identified using a photo-chamber provided with a UV light source.

4.2.10.2 *BDNF-myc* PCR

Expected band size: ~420 bp (WT)
~440bp (*BDNF-myc*)

Reaction conditions:

- 1µl DNA
- 3µl 10x PCR buffer
- 6µl Betaine (5M)
- 3µl dNTPs (2mM)
- 0.3µl forward primer (20pmol stock - Myc_for)
- 0.3µl reverse primer (20pmol stock - Myc_rev)
- 0.3µl Taq Polymerase (5 Prime)
- 16.1µl dH₂O

Cycle Conditions:

Table 14: PCR program for verification of *BDNF-myc*

Step	Duration	Temperature	Cycles
Initial denaturation	3min.	95°C	1
Denaturation	30s	95°C	40
Annealing	40s	54°C	
Elongation	50s	72°C	
Termination	7min.	72°C	1
Hold	∞	4°C	

After the PCR is finished, all samples are mixed with 5µl 6x loading dye. The samples are applied to a 3.5% agarose gel (with EtBr) in 1xTAE buffer, in which a gel run at U=120V is performed for at least ~60min. The PCR products are identified using a photo-chamber provided with a UV light source.

4.2.10.3 *Ntrk Rohrer (TrkB^{-/-})* PCR

Expected band size: ~ 369bp (WT)
~ 179bp (*TrkB^{-/-}*)

Reaction conditions: - 1µl DNA

- 2.5µl 10x PCR buffer
- 5µl Betaine (5M)
- 0.5µl dNTPs (10mM)
- 0.05µl forward primer (100µM stock - Trkb-c8)
- 0.05µl reverse primer (100µM stock - Trkb-n2)
- 0.05µl reverse primer (100µM stock - Pgk3-1)
- 0.3µl Taq Polymerase
- 15.55µl dH₂O

Cycle Conditions:

Table 15: PCR program for verification of *TrkB*^{-/-}

Step	Duration	Temperature	Cycles
Initial denaturation	3min.	94°C	1
Denaturation	30s	94°C	30
Annealing	30s	59°C	
Elongation	30s	68°C	
Termination	5min.	68°C	1
Hold	∞	4°C	

After the PCR is finished, all samples are mixed with 5µl 6x loading dye. The samples are applied to a 2% agarose gel (with EtBr) in 1xTAE buffer, in which a gel run at U=120V is performed for ~35min. The PCR products are identified using a photo-chamber provided with a UV light source.

4.2.10.4 *Drd1-EGFP* PCR

Expected band size: none (WT)
~250bp (*DRD1-EGFP*^{wt/tg})

Reaction conditions:

- 1µl DNA
- 2µl 10x PCR buffer
- 3.2µl dNTPs (1.25mM)
- 0.3µl forward primer (20pmol stock - DRD1_for)
- 0.3µl reverse primer (20pmol stock - GFP_rev)
- 0.2µl Taq Polymerase (5 Prime)
- 13.0µl dH₂O

Cycle Conditions:

Table 16: PCR program for verification of *Drd1-EGFP*

Step	Duration	Temperature	Cycles
Initial denaturation	5min.	95°C	1
Denaturation	1min.	94°C	35
Annealing	1min.	65°C	
Elongation	1min.	72°C	
Termination	7min.	72°C	1
Hold	∞	4°C	

After the PCR is finished, all samples are mixed with 5µl 6x loading dye. The samples are applied to a 3 % agarose gel (with EtBr) in 1xTAE buffer, in which a gel run at U=120V is performed for ~35min. The PCR products are identified using a photo-chamber provided with a UV light source.

4.2.10.5 *Drd1-Td-Tomato* PCR

Expected band size: ~324bp (WT)
~750bp (DRD1-Td-Tomato^{wt/tg})

Reaction conditions:

- 1µl DNA
- 2.5µl 10x PCR buffer (VWR)
- 1µl dNTPs (10mM)
- 2.6µl MgCl₂ (25mM)
- 1.25µl forward primer (10µM stock - 12153 & 7338)
- 1.25µl reverse primer (10µM stock - 12154 & 7339)
- 0.4µl Taq Polymerase (VWR)
- 11.5µl dH₂O

Cycle Conditions:

Table 17: PCR program for verification of *Drd1-Td-Tomato*

Step	Duration	Temperature	Cycles
Initial denaturation	2min.	94°C	1
Touchdown	20s	94°C	10
	15s -0.5s per cycle decrease	65°C	
	10s	68°C	
Denaturation	15s	94°C	28
Annealing	15s	60°C	
Elongation	10s	72°C	
Termination	2min.	72°C	1
Hold	∞	10°C	

After the PCR is finished, all samples are mixed with 5µl 6x loading dye. The samples are applied to a 3 % agarose gel (with EtBr) in 1xTAE buffer, in which a gel run at U=120V is

performed for ~35min. The PCR products are identified using a photo-chamber provided with a UV light source.

4.2.10.6 *Drd2-EGFP* PCR

Expected band size: none (WT)
~300bp (*DRD2-EGFP^{wt/tg}*)

Reaction conditions:

- 1µl DNA
- 2.5µl 10x PCR buffer
- 1µl dNTPs (10mM)
- 1µl forward primer (20pmol stock - DRD2F)
- 1µl reverse primer (20pmol stock - DRD2R)
- 0.5µl Taq Polymerase (5 Prime)
- 18.0µl dH₂O

Cycle Conditions:

Table 18: PCR program for verification of *Drd2-EGFP*

Step	Duration	Temperature	Cycles
Initial denaturation	5min.	94°C	1
Denaturation	45s	94°C	35
Annealing	45s	62°C	
Elongation	1min.	72°C	
Termination	10min.	72°C	1
Hold	∞	4°C	

After the PCR is finished, all samples are mixed with 5µl 6x loading dye. The samples are applied to a 3 % agarose gel (with EtBr) in 1xTAE buffer, in which a gel run at U=120V is performed for ~35min. The PCR products are identified using a photo-chamber provided with a UV light source.

4.2.11 Imaging and image preparation

All samples were analyzed and scanned, using either fluorescent or confocal laser microscopes (4.1.2). The obtained data were further processed using ImageJ and projected as maximum intensity images. Changes regarding brightness and contrast were made according to the rules and conditions of good scientific practice, without changing gamma-correction or the general statement of the raw data. All changes were documented and images were finally arranged with GIMP2.8.

5. Results

5.1 Optimization of BDNF Detection

The visualization of endogenous BDNF protein by immunofluorescence has remained a challenging task, on the basis of the low expression of the neurotrophic factor in rodent brain. (Altar et al., 1997; Conner et al., 1997; Yan et al., 1997b; Baquet et al., 2005; Dieni et al., 2012; Zhang et al., 2016). Another challenging task was to validate available antibodies to verify the specificity of BDNF staining on appropriate negative controls. Since conventional BDNF k.o. animals die early after birth (Jones et al., 1994; Ernfors et al., 1995; Erickson et al., 1996; Conover and Yancopoulos, 1997; Liebl et al., 1997; Brady et al., 1999), before BDNF levels reach the expression levels observed in the adult rodent brain, the only possible method is the use of conditional knock out animals (Rios et al., 2001; Gorski et al., 2003; Baquet et al., 2004; He et al., 2004; Chan et al., 2006; Monteggia et al., 2007; Unger et al., 2007; Chan et al., 2008; Rauskolb et al., 2010). We used NFL-Cre BDNF^{fl/ko} conditional BDNF k.o. mice, in which CRE mediated recombination is controlled by the neurofilament light chain (NF-L) promoter (Schweizer et al., 2002). In these mice, Cre expression and Cre mediated recombination mostly occurs in pyramidal cells of the neocortex and motor-neurons within the spinal cord. Thus, this mouse appeared useful for studying BDNF expression in the striatum which receives BDNF input from the neocortex, via corticostriatal afferences. In order to optimize the immunohistochemical detection of endogenous BDNF, we tested a total of four monoclonal BDNF antibodies which are further referred to as mAb #9 (Kolbeck et al., 1999), 4C8, 3C11, and 3B2. We also used transgenic mice expressing BDNF-myc as an independent positive control for BDNF expression, via detection of the myc tag (Matsumoto et al., 2008). By optimizing the PFA fixation, as one of the most critical steps for BDNF detection, including antigen retrieval and extensive washing procedures, we were able to

develop a highly sensitive BDNF IHC protocol and subsequently detected endogenous BDNF in brain areas other than the hippocampus.

To test the efficacy of the Cre recombination and the extent of BDNF ablation in NFL-Cre BDNF^{fl/ko} mice, we used a sandwich ELISA, following a protocol described before (Kolbeck et al., 1999). We found a reduction in BDNF protein levels of up to 80% in cortex, hippocampus, striatum, and cerebellum (**Fig.10A**) in NFL-Cre BDNF^{fl/ko} conditional BDNF k.o. Confirming previous studies (Kolbeck et al., 1999; Rauskolb et al., 2010), BDNF levels in the hippocampus ranged between 65-110ng/g wet weight, while cortical levels were found to be ~35ng/g and ~55ng/g wet weight in the striatum. In order to test the specificity of our BDNF IHC protocol and to compare our findings with previous studies (Danzer and McNamara, 2004; Dieni et al., 2012), hippocampus staining was always included as an internal control (**Fig.10B**). 3 of the 4 tested monoclonal BDNF antibodies produced positive BDNF immunoreactivity (IR) in the mossy fiber projections and their terminals in the CA3 region. In some cases, we observed severe staining of blood vessels by the monoclonal BDNF antibodies (**Fig. 10B**). Normally animals are anesthetized with CO₂ before transcardial perfusion which causes vasodilatation within the brain, increase in blood flow and diameter of blood vessels (Kitazono et al., 1995; Nelson and Quayle, 1995). For that reason, it should facilitate the perfusion process. With further improvement of the protocol, we found the temperature of the media to be a critical feature. Keeping PBS with 0,4% heparin at 4°C significantly improved the flushing process of blood vessels, while perfusion with 4% PFA (with or without 0,1% Glutaraldehyde) at 37°C turned out to be optimal conditions for BDNF-IHC (**Fig. 11**). In this way, we were able to prevent non-specific blood vessel staining by monoclonal mouse antibodies. Furthermore, we could observe single BDNF positive cells within CA3 pyramidal projection neurons (**Fig. 12**) as well as in the dentate gyrus (**Fig. 13**), as described before (Danzer and McNamara, 2004; Dieni et al., 2012).

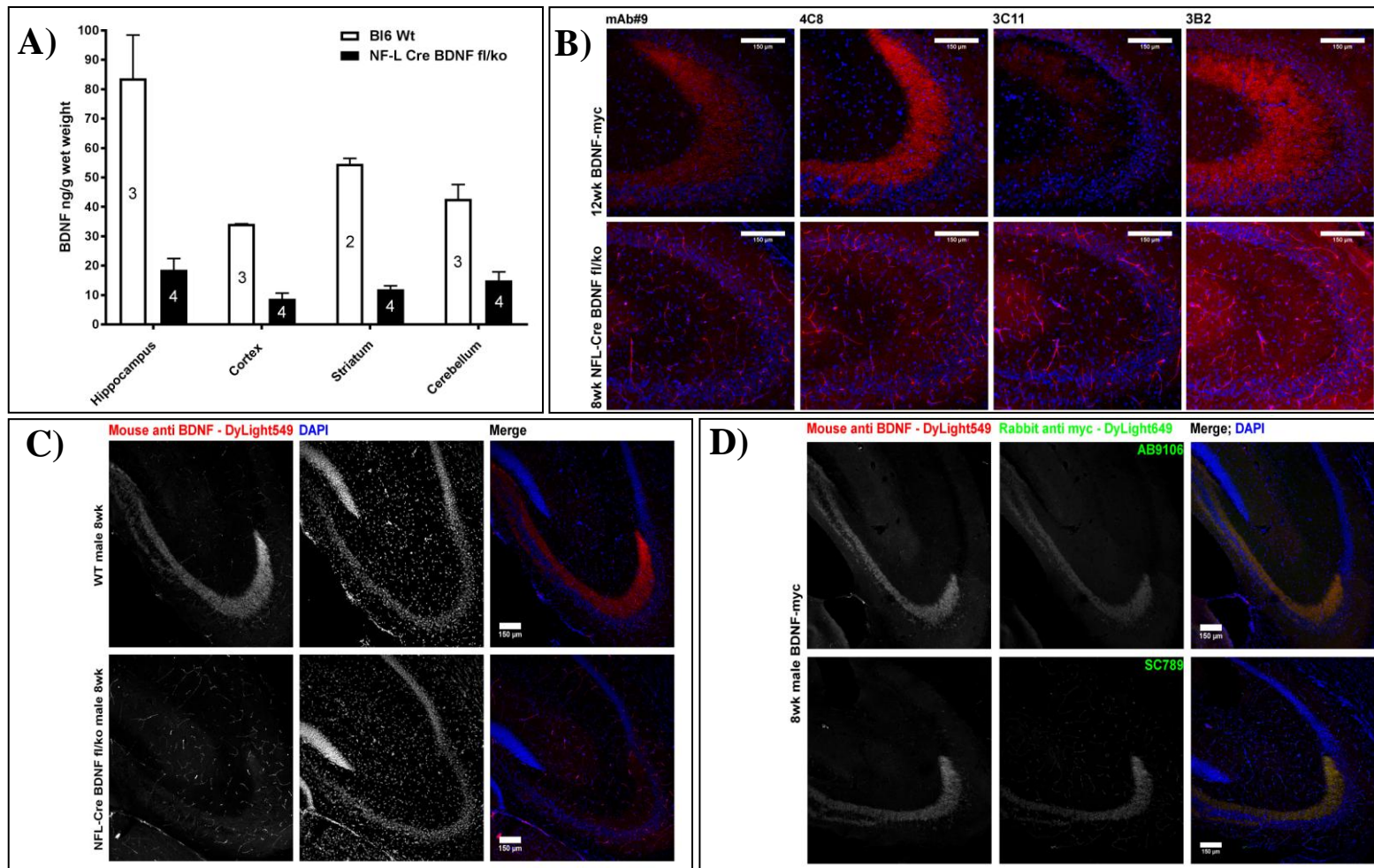


Fig. 10) BDNF antibody specificity verification: **A)** ELISA analysis of BDNF protein levels in CNS, comparing 8wk male WT C57Bl6/J (white bars) versus NFL-Cre BDNF^{fl/ko} mice (black bars) using mouse monoclonal anti BDNF antibody (mAb#9). Results are presented as a mean determined from the analysis of at least two mice per genotype (n number is indicated in the bars). **B)** Immunohistological analysis of BDNF antibody specificity in CA3 mossy fiber terminals of male WT C57Bl6/J (upper lane) or NFL-Cre BDNF^{fl/ko} hippocampus (lower lane). MAb#9, 4C8 and 3B2 showed BDNF-IR on WT tissue, while 3C11 failed to detect endogenous BDNF. 3B2 produced high background noise as seen outside the hippocampus. This background noise was most obvious on cBDNF k.o. tissue, even though the antibody did not show any specific BDNF-IR (lower lane right image). MAb#9 and 4C8 revealed no obvious BDNF-IR on cBDNF k.o. MAb#9 showed the best overall signal to noise ratio, while 4C8 showed very intense BDNF-IR, even at low antibody concentrations. All antibodies produced a blood-vessel staining, which occurs, when the perfusion and cross linking was less efficient. **C)** BDNF-IR in mossy fiber projections of 8wk male WT C57Bl6/J versus NFL-Cre BDNF^{fl/ko} hippocampus, using mAb#9. **D)** BDNF versus Myc-IR in hippocampus of 8wk male BDNF-myc mice. Myc was co-stained with two independent Rabbit polyclonal myc antibodies (Abcam AB9106; Santa Cruz SC789).

BDNF-IR was completely absent in sections derived from NFL-Cre BDNF^{fl/ko} conditional BDNF k.o mice (**Fig. 10B, C**). The mAbs #9 and 4C8 were used for further experiments, on the basis of their high affinity to BDNF and low background levels in cBDNF k.o. brain (**Fig. 10B, C**). To further evaluate the specificity of our protocol and the BDNF antibodies, we used BDNF-myc mice (Matsumoto et al., 2008), enabling the visualization of endogenous BDNF via Myc tag (**Fig. 10D**).

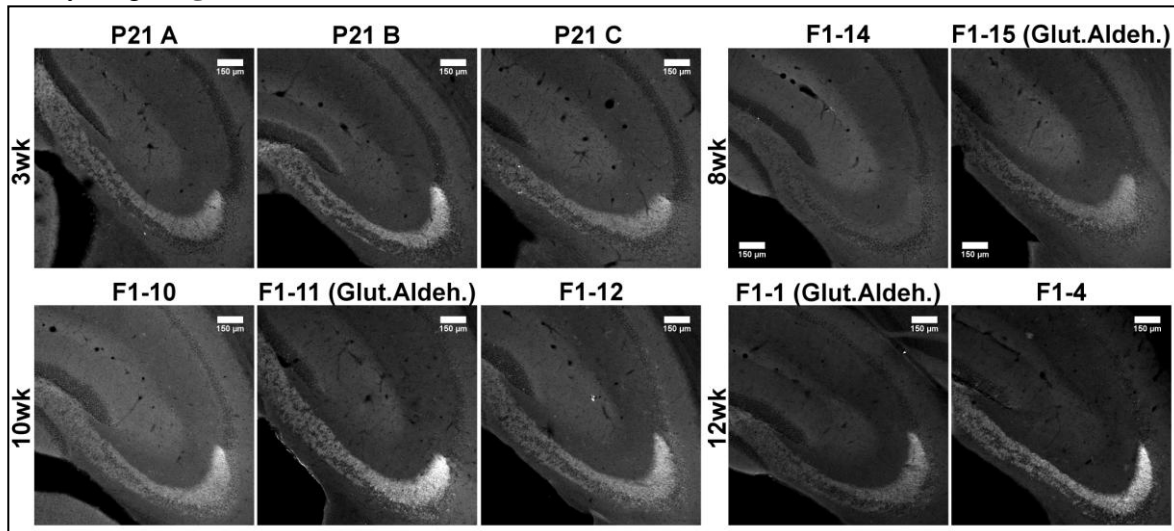


Fig. 11) Optimization of BDNF-IR in hippocampus at different ages: A) Immunohistochemical analysis of BDNF-IR in hippocampal mossy fibers at different ages ranging from 3wk to 12wk. Data show confocal images obtained with a 10x objective using the monoclonal BDNF mAb#9 antibody. In none of the cases unspecific blood vessel staining was obvious. To increase the fixation potency 0,1% Glutaraldehyde (Glut.Aldeh.) were added to the 4% PFA for perfusion of animals F1-15 (8wk), F1-11 (10wk) and F1-1 (12wk). Scale bar: 150µm

We used a total of 3 independent anti myc antibodies (SC789, AB9106, AB9132), of which SC789 also tended to bind to blood vessels (**Fig. 10D, Fig. 12, Fig. 13**). In hippocampal neurons of either CA3 (**Fig. 12**) or Dentate Gyrus (**Fig. 13**) all Myc-antibodies showed a high degree of signal overlap with the BDNF-IR of mAb#9. Taken together we developed and optimized an immunohistochemistry protocol which enables the detection of endogenous BDNF. We used monoclonal BDNF antibodies which we found to be specific since no BDNF-IR was detected in cBDNF k.o. animals. Furthermore, BDNF-IR was confirmed by co-staining with myc antibodies of tissue derived from BDNF-myc mice. Using this BDNF-IHC protocol, we then aimed to identify BDNF producing cells in cortical areas projecting afferent inputs towards the striatum.

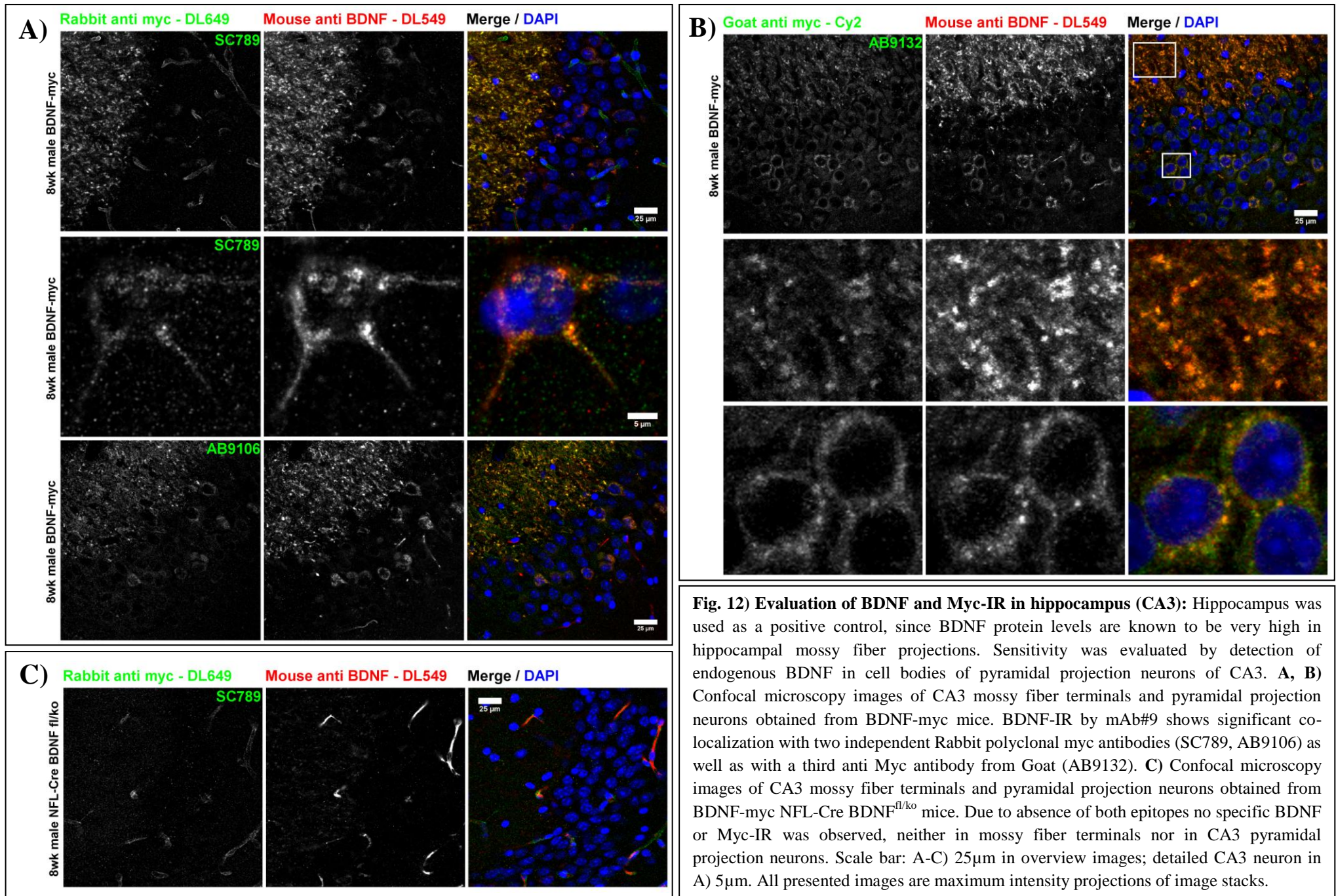


Fig. 12) Evaluation of BDNF and Myc-IR in hippocampus (CA3): Hippocampus was used as a positive control, since BDNF protein levels are known to be very high in hippocampal mossy fiber projections. Sensitivity was evaluated by detection of endogenous BDNF in cell bodies of pyramidal projection neurons of CA3. **A, B)** Confocal microscopy images of CA3 mossy fiber terminals and pyramidal projection neurons obtained from BDNF-myc mice. BDNF-IR by mAb#9 shows significant colocalization with two independent Rabbit polyclonal myc antibodies (SC789, AB9106) as well as with a third anti Myc antibody from Goat (AB9132). **C)** Confocal microscopy images of CA3 mossy fiber terminals and pyramidal projection neurons obtained from BDNF-myc NFL-Cre BDNF^{fl/ko} mice. Due to absence of both epitopes no specific BDNF or Myc-IR was observed, neither in mossy fiber terminals nor in CA3 pyramidal projection neurons. Scale bar: A-C) 25µm in overview images; detailed CA3 neuron in A) 5µm. All presented images are maximum intensity projections of image stacks.

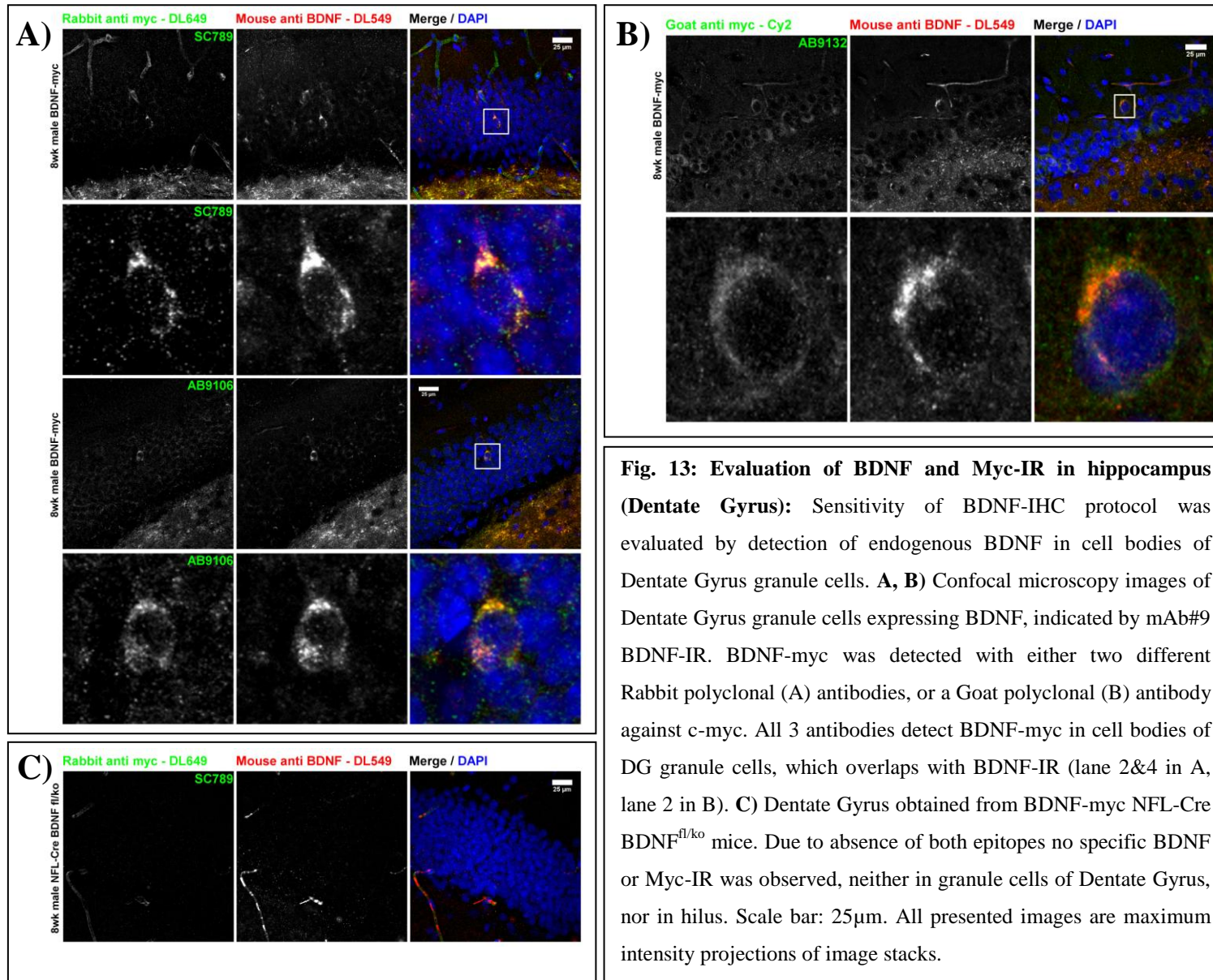


Fig. 13: Evaluation of BDNF and Myc-IR in hippocampus (Dentate Gyrus): Sensitivity of BDNF-IHC protocol was evaluated by detection of endogenous BDNF in cell bodies of Dentate Gyrus granule cells. **A, B)** Confocal microscopy images of Dentate Gyrus granule cells expressing BDNF, indicated by mAb#9 BDNF-IR. BDNF-myc was detected with either two different Rabbit polyclonal (A) antibodies, or a Goat polyclonal (B) antibody against c-myc. All 3 antibodies detect BDNF-myc in cell bodies of DG granule cells, which overlaps with BDNF-IR (lane 2&4 in A, lane 2 in B). **C)** Dentate Gyrus obtained from BDNF-myc NFL-Cre BDNF^{fl/ko} mice. Due to absence of both epitopes no specific BDNF or Myc-IR was observed, neither in granule cells of Dentate Gyrus, nor in hilus. Scale bar: 25μm. All presented images are maximum intensity projections of image stacks.

5.2 BDNF expression in Cortex and Midbrain

It was shown that striatal neurons do not express BDNF by their own, but seem to be critically dependent upon BDNF supply from external sources (Altar et al., 1997; Conner et al., 1997; Yan et al., 1997b; Rauskolb et al., 2010; Li et al., 2012). In conditional BDNF k.o. animals, the structure which is morphologically and functionally most severely affected by the absence of BDNF is the striatum, indicated by reduced dendrite volume and length, as well as significant spine loss (Rauskolb et al., 2010). This clearly indicates striatal dependence upon BDNF import from external sources. The Striatum receives glutamatergic input from the cerebral cortex and the thalamus, as well as dopaminergic afferences from the midbrain. It was shown that BDNF is present in midbrain dopaminergic neurons, at least during development and also appears to be necessary for the proper development of dopaminergic neurons (Baquet et al., 2005). Nevertheless, the cortex appears to be the predominant source of striatal BDNF which is transported along glutamatergic projections from subcortical projection neurons (Altar et al., 1997; Conner et al., 1997; Yan et al., 1997b; Gorski et al., 2003; Baquet et al., 2004; Li et al., 2012). This assumption was confirmed by the presence of BDNF mRNA and protein in cortical layers II-III, V and VI (Altar et al., 1997; Conner et al., 1997; Yan et al., 1997b; Gorski et al., 2003; Kalivas, 2009; Li et al., 2012; Park et al., 2014). For that reason, cortical layers II-III and upper layer V subcortical projection neurons are good candidates to govern the source of anterogradely transported striatal BDNF, since they send dense projection fibers towards the striatum (Kitai et al., 1976; Hedreen, 1977; Hedreen and McGrath, 1977; Schwab et al., 1977; Wise and Jones, 1977; Veening et al., 1980; Arikuni and Kubota, 1986; Voelker et al., 2004; Molnar and Cheung, 2006). This innervation of the striatum, by cortical neurons, follows a functional pattern. While projections of the pre- and infralimbic cortex target ventromedial regions of the striatum, close to the Nucleus Accumbens (NAc) (**Fig. 14A, C**), associational cortical areas innervate the dorsomedial part of the striatum (Reep et al., 2003; Yin and Knowlton, 2006). In contrast, the dorsolateral part

of the striatum receives dense afferent inputs from the motor and somatosensory cortex (**Fig. 14A-C**). This region of the striatum is critically involved in the coordination and initiation of voluntary limb movement and thus, seems to be of higher importance, for processing information about voluntary movement, through the basal ganglia circuit (Webster, 1961; Wise and Jones, 1977; Cospito and Kultas-Ilinsky, 1981; Kelley et al., 1982; Donoghue and Herkenham, 1986; McGeorge and Faull, 1989; West et al., 1990; Kanazawa et al., 1993; Kimura et al., 1993; Yin and Knowlton, 2006). Similar observations about the topographic arrangement of cortico-striatal innervation were not only made in rodents but also monkeys (Crutcher and DeLong, 1984; Alexander and DeLong, 1985).

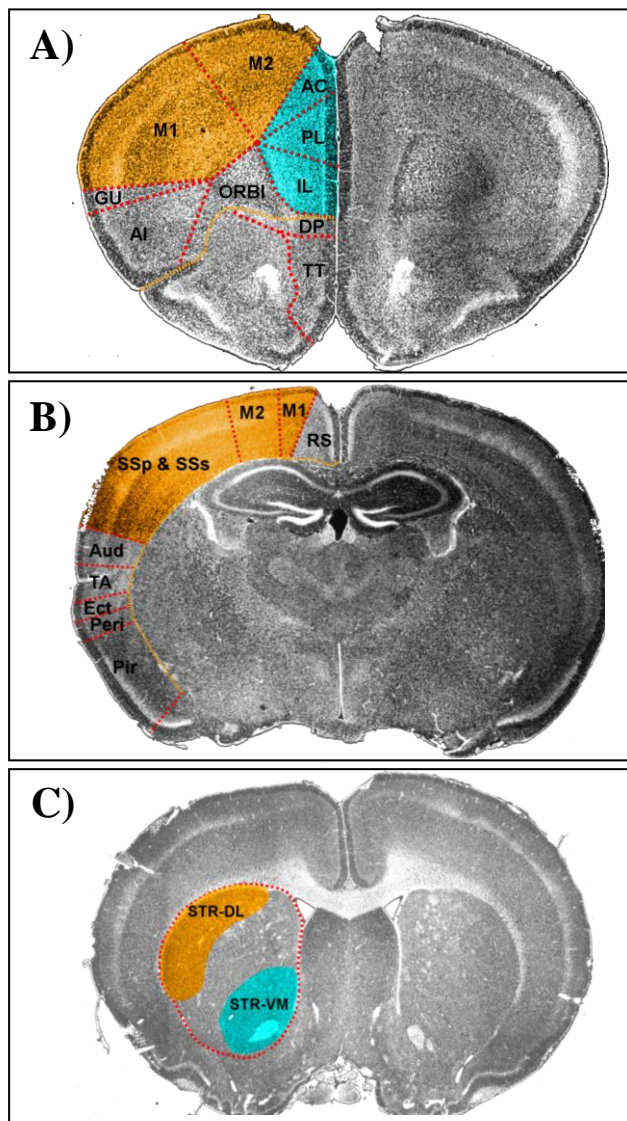


Fig. 14) Cortico-Striatal projections:

Immunohistochemistry stainings of coronal brain slices showing DAPI fluorescence (black & white) in stained nuclei. Afferent cortical projections involved in the control of voluntary movement are shown in orange in A), B) and C). Projections from cortical areas towards the striatum, involved in motivational regulation are shown in cyan in A) and C). **A)** Medial prefrontal cortex (mPFC) showing M1 and M2, which send afferent projections towards the STR-DL while AC, PL and IL send projections towards the STR-VM. **B)** Coronal brain slice showing hippocampus - posterior to mPFC in A). Posterior portions of the M1 and M2 are still evident. Additionally the SSp and SSs are also involved in movement control and send afferent projections towards STR-DL. **C)** Target regions of cortical afferent input in the striatum. Abbreviations: M1-prim. motor cortex; M2 - sec. motor cortex; AC - anterior cingulate cortex, PL - prelimbic cortex; IL - infralimbic cortex; DP - dorsal peduncular area; TT - taenia tecta; ORBI - orbital area; AI - agranular insular area; GU - gustatory areas; SSp - primary somatosensory cortex; SSs - supplementary somatosensory cortex; Aud - ventral auditory area; TA - temporal association area; Ect - ecto-rhinal cortex; Peri - perirhinal cortex; Pir - piriform cortex; STR-DL - dorsolateral striatum; STR-VM - ventromedial striatum.

In summary, cortical areas involved in the control of movement, consolidated as the somato- or senso-motoric-cortex, send their afferences towards the dorsolateral part of the striatum, in which motoric fields involved in the control of limb movements, are located. The cortical neurons, which are the origin of the afferent inputs, reside within layers II-III and V and can be identified by either Cux-1 or CTIP2 proteins (**Fig. 15A, B**). Additionally, we used FOXO-1 antibody as a marker for upper layer V neurons which were negative for CTIP2 (**Fig. 15D**) (Molyneaux et al., 2007). Layer VI neurons which usually represent cortico-thalamic projection neurons were identified by the expression of DARPP-32 and CTIP-2 (Ouimet et al., 1984; Molyneaux et al., 2007) (**Fig. 15C**). Within the same cortical layers II-III, V & VI, neuronal populations that express BDNF mRNA were shown before (Altar et al., 1997; Conner et al., 1997; Yan et al., 1997b; Gorski et al., 2003; Kalivas, 2009; Li et al., 2012; Park et al., 2014). If these discrete cortico-striatal projection neurons also express BDNF protein, in significant amounts, remains largely elusive. For that reason, we hypothesized that subcortical projection neurons of layer II-III and V, targeting either the dorsolateral or ventromedial portion of the striatum, depending on the cortical area, express BDNF protein. This cortical BDNF might get transported anterogradely, along cortico-striatal afferences, towards their presynaptic terminals within the striatum. Furthermore, we were interested to see, if there was a difference in BDNF expression levels within cortical areas involved in the control of voluntary movement, during the first postnatal weeks until 12wk. We had a special focus on the somatomotor cortical areas, since mice at 3wk of age are in a developmental stage, characterized by the onset and increase in locomotion. We were wondering, if this increase in locomotive behavior is reflected by higher neuronal activity in somatomotor-cortical areas and subsequently by BDNF expression, in order to establish functional network connectivity in the motor pathway. To test this idea, we analyzed BDNF-IR in subcortical projection neurons in 3wk and 12wk old mice, using our BDNF-IHC protocol. BDNF staining in the hippocampus was always included, to ensure functionality, sensitivity, and quality

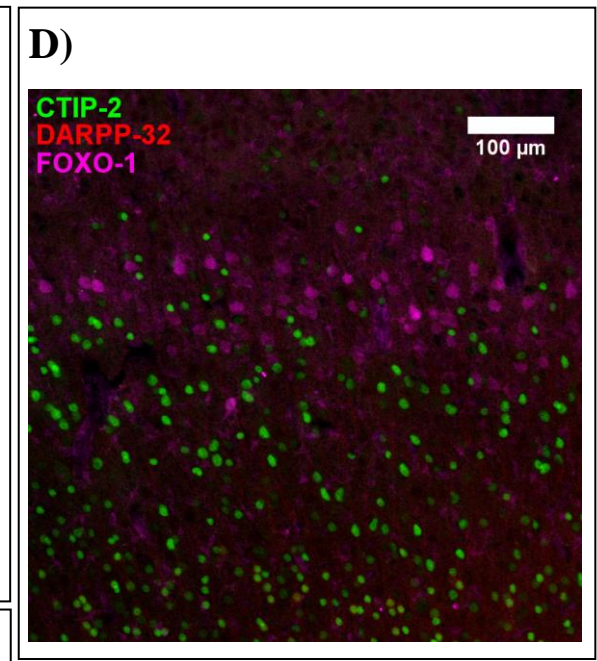
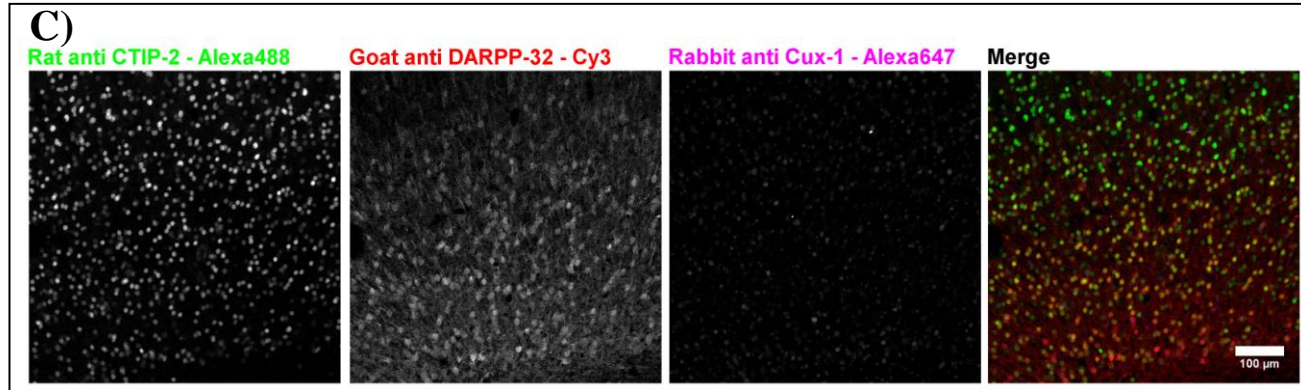
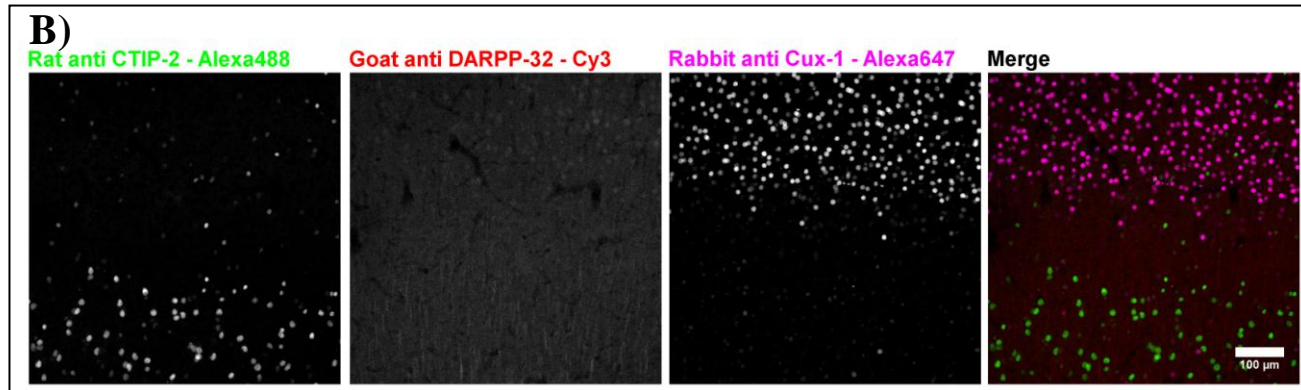
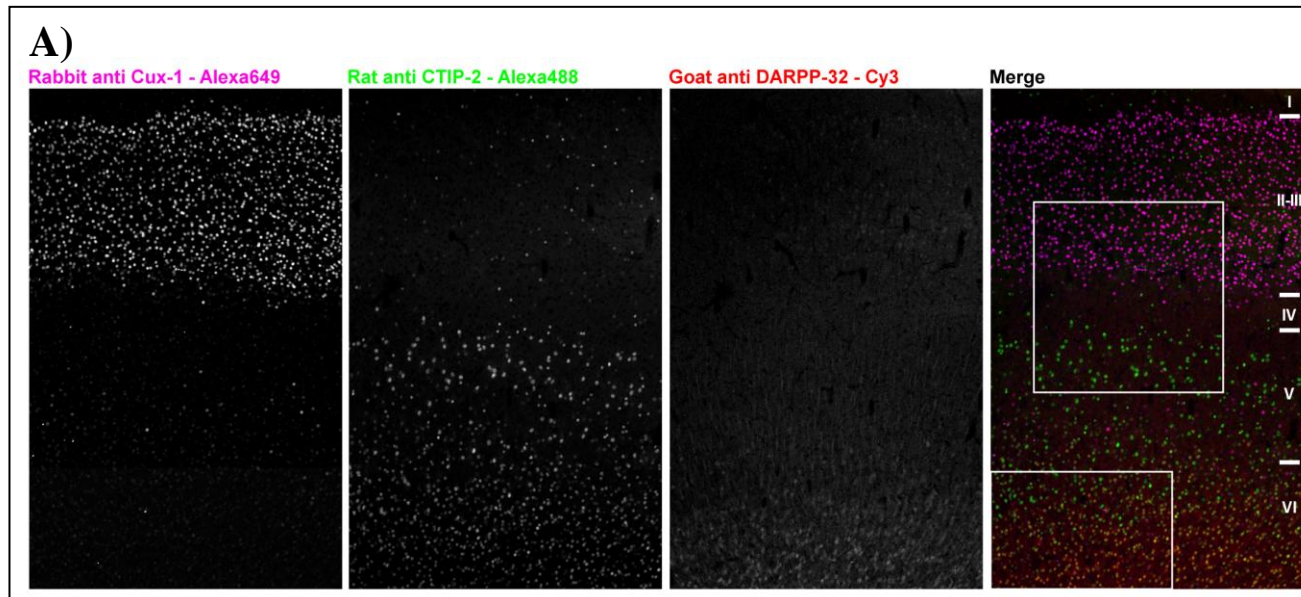


Fig. 15) Identification of cortical layers: Immunohistochemistry stainings of coronal brain slices showing the transitional area between primary (M1) and secondary (M2) motor cortex. **A)** Low magnification overview images showing cortical layering indicated by marker expression of Cux1-IR, CTIP-2-IR and DARPP-32-IR in layers II-III, V and VI respectively. An approximation of the borders between cortical layers is indicated in the merged image. **B)** High magnification image of the upper inlay in A) showing the lower edge of layer III by Cux-1-IR and the upper edge of layer V by CTIP-2-IR. **C)** High magnification image of lower inlay in A) showing DARPP-32 expression in layer VI neurons. **D)** FOXO-1 was described as a marker of a subpopulation of layer V neurons, which was found to be negative for CTIP-2. This population is located at the upper border of layer V indicated by CTIP-2 expression. Scale bar: 100µm (B-D)

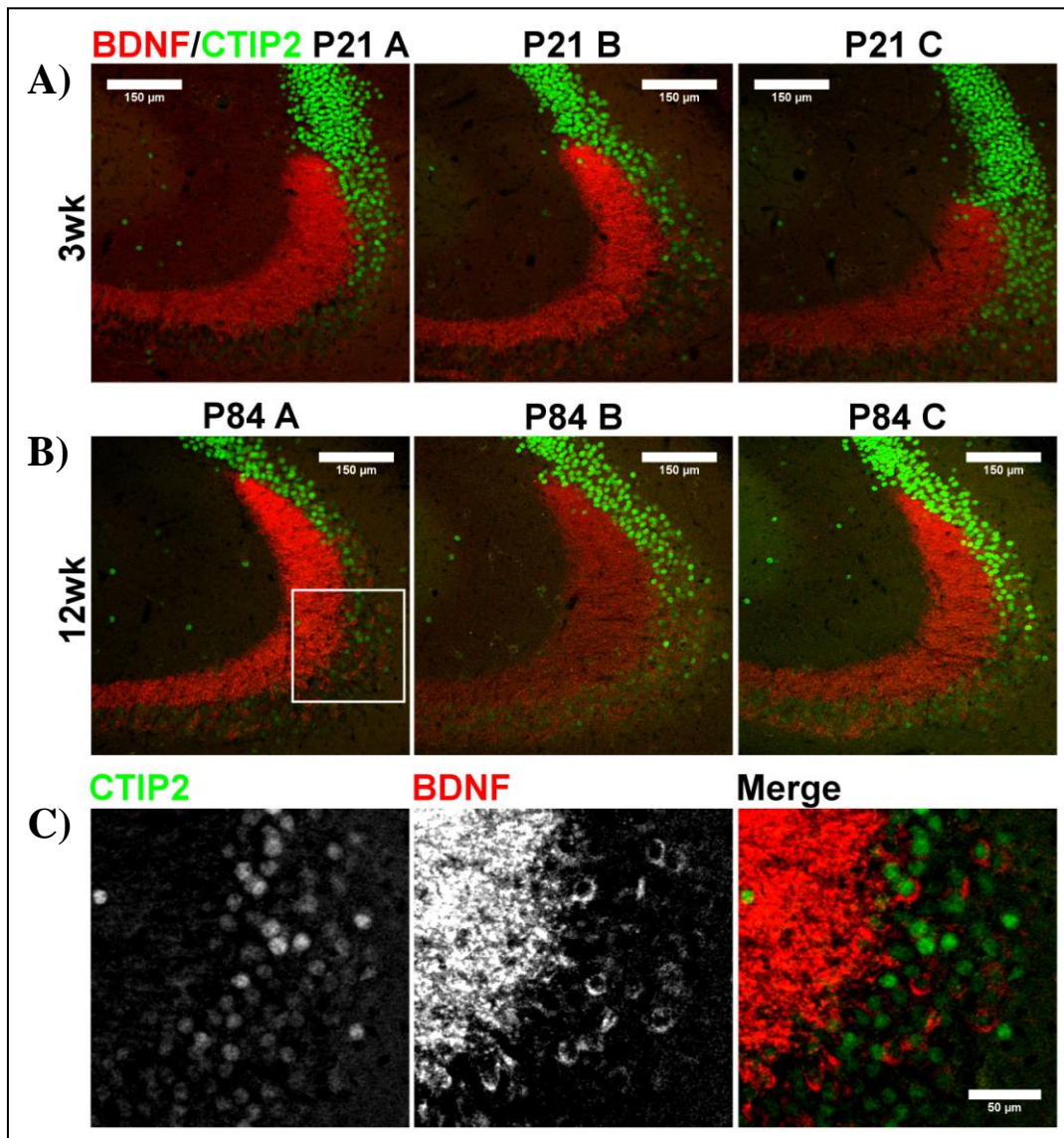


Fig. 16) Verification of BDNF-IR in hippocampal mossy fibers of 3wk & 12wk old mice: Immunohistochemical analysis of BDNF-IR in hippocampal mossy fibers at 3wk (A) and 12wk (B). Data show confocal images obtained with a 20x objective using the monoclonal BDNF mAb#9 antibody. In parallel CTIP2 was stained as marker for subcortical layer V & VI projection neurons, which also stains cells in the hippocampus. In all cases the fixation and IHC protocol lead to clear BDNF-IR, without evidence for unspecific blood vessel staining. C) Higher magnification image of the inlay in B). Single CA3 pyramidal neurons are positive for BDNF-IR. Scale bar: 150μm, 50μm (Inlay)

of the BDNF-IR (Fig. 16, P21A, B, C & F1-4 (P84 A) are depicted in Fig. 11). BDNF-IR was clearly evident in the mossy fiber projections of all 6 animals used for the analysis. Furthermore, single BDNF expressing pyramidal neurons in CA3 were found positive for BDNF expression which turned out to be a good indicator of high staining sensitivity (Fig. 16 Inlay).

5.3 BDNF expression in somatomotor cortical areas involved in the control of voluntary movement

Next, we analyzed cortical BDNF expression in the same animals, focusing on subcortical projection neurons. Layer III and V of the motor cortices, as well as layer V of the somatosensory cortex, were shown before to target the dorsolateral striatum. These regions are critically involved in the control of voluntary movement. By analyzing BDNF-IR in these cortical areas, we found that BDNF is expressed in cortical neurons, projecting towards the dorsolateral striatum. Thus BDNF-IR was evident in upper layers II-III of primary and secondary motor cortex (**Fig. 17**) and in layer V subcortical projection neurons of primary (**Fig. 18A, B**) and secondary motor cortex (**Fig. 19A, B**) as well as in primary somatosensory cortex (**Fig. 20A, B**), indicated by CTIP2 expression. BDNF expression does not seem to be restricted to CTIP-2 positive neurons since especially in the somatosensory cortex we also observed BDNF-IR in CTIP-2 negative cells (**Fig. 20A, yellow arrows**). We found BDNF-IR in upper layer V (**Fig. 18-20A**), for which we used CTIP-2 and FOXO-1-IR, to clearly identify the dorsal border of layer V (**compare Fig. 15D**). BDNF expression was also evident within deep layer V projection neurons of primary and secondary motor cortex (**in Fig. 18, 19B**). Next, we quantified first the density of BDNF as well as CTIP-2 positive cells alone (**Fig.18 - 20B, E**) and second the number of BDNF / CTIP-2 double positive, subcortical projection neurons (**Fig. 18 - 20C, F**). We compared these values in the according cortical areas between mice at 3wk and 12wk (BDNF-IR functionality for all animals shown in **Fig. 16**). We observed a significant decrease in the total number of BDNF positive cells in both, primary and secondary motor cortex in 12wk old mice (**Fig. 18, 19B, E**). In comparison we found no difference in the number of CTIP-2 expressing neurons (**Fig.18, 19B, E**). The reduction in the total number of BDNF expressing cells was also reflected by a significant decrease in the number of subcortical projection neurons which express BDNF.

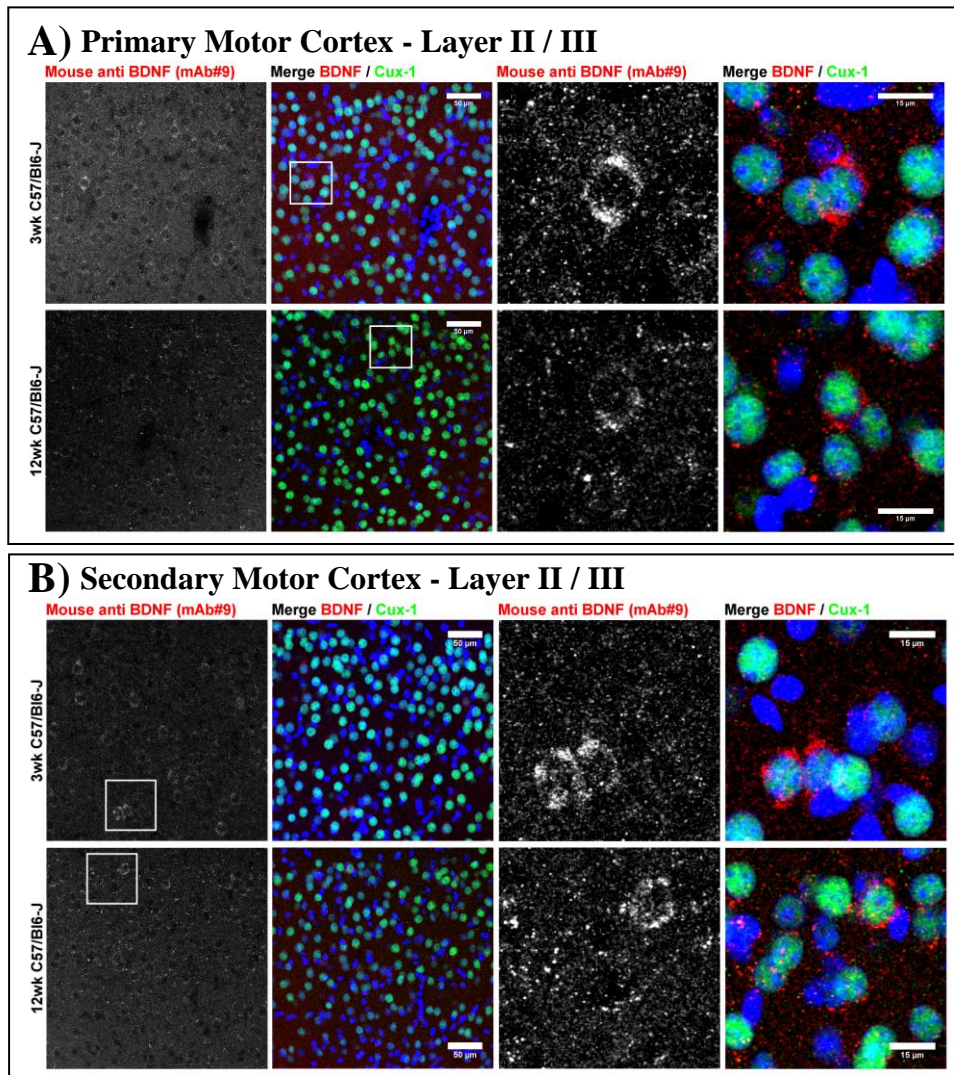


Fig. 17 BDNF-IR in layer II/III neurons of primary (M1) and secondary (M2) motor cortex: **(A)** Representative immunohistochemical images of BDNF-IR in primary motor cortex layer II / III of 3wk and 12wk old WT mice. BDNF-IR is evident in single Cux-1 positive layer II / III neurons. BDNF-IR appears stronger and in more cells at 3wk compared to 12wk. **(B)** Representative immunohistochemical images of BDNF-IR in secondary motor cortex layer II / III of 3wk and 12wk old WT mice. BDNF-IR is evident in single Cux-1 positive layer II / III neurons. Compared to primary motor cortex, BDNF expressing cells appear evenly distributed and more numerous. Nevertheless, the overall number of BDNF expressing neurons appear less at 12wk compared to 3wk. Scale bar: 50µm, 15µm (Inlay)

These neurons were identified by CTIP-2 expression (**Fig. 18, 19C, F**). We conclude that subcortical projection neurons show a BDNF downregulation at 12wk compared to 3wk in both motor cortices. This effect was found to be more severe in upper layer V neurons, compared to deep layer V neurons (**Fig. 18, 19C, F**). Interestingly, we observed the complete opposite case, namely a slight increase in the number of BDNF expressing projection neurons in layer V neurons of the somatosensory cortex (**Fig. 20B, C**). Additionally, we observed very strong BDNF-IR in deep layer VI cells, directly above the corpus callosum (**Fig. 20B,**

compare to **Fig. 14B**). This population of BDNF expressing cells was different, compared to all other cortical regions. First of all, somatosensory layer VI shows the highest density of BDNF expressing cells throughout all cortical regions analyzed (**Fig. 23**). These cells also show a much higher intensity for BDNF-IR than the motor cortices. We did not observe any difference in neither BDNF nor CTIP-2 expression during postnatal development (**Fig. 20E, F**). Second, it was the only cortical region, in which the majority of BDNF positive cells did not or only very weakly show CTIP-2-IR. Normally, layer VI somatosensory cortex governs cortico-cortical, cortico-thalamic and claustrum projecting neurons (Katz, 1987; Thomson, 2010). To which population these very strong BDNF expressing cells belong should be addressed by retrograde tracing experiments in order to identify the neuronal population by their innervated target structure. In case of upper layer VI neurons, these are the primary sensory ventral posteromedial nucleus of the thalamus (VPm) and the nucleus reticularis thalami (nRT) (Bourassa and Deschenes, 1995; Bourassa et al., 1995; Thomson, 2010; Kim et al., 2014). Deep layer VI neurons also innervate the VPm nucleus, the posterior thalamic group (Pom) and the primary sensory thalamic nuclei (Deschenes et al., 1998; Llano and Sherman, 2008; Thomson, 2010; Kim et al., 2014). A third population are layer VI cortico-cortical neurons, whose projections do not leave the cortex but instead connect the somatosensory cortex with the motor cortices (Thomson, 2010).

In summary, we found clear evidence for BDNF expression in layer II / III and layer V subcortical projections neurons of somatomotor cortical areas, identified by either Cux-1 or CTIP-2 expression. These cortical areas are known to innervate the dorsolateral striatum and are critically involved in the control of limb movement. Furthermore, strong BDNF-IR was identified in a CTIP-2 negative population of cells in deep layer VI of the primary somatosensory cortex. This cortical layer is known to densely innervate several thalamic

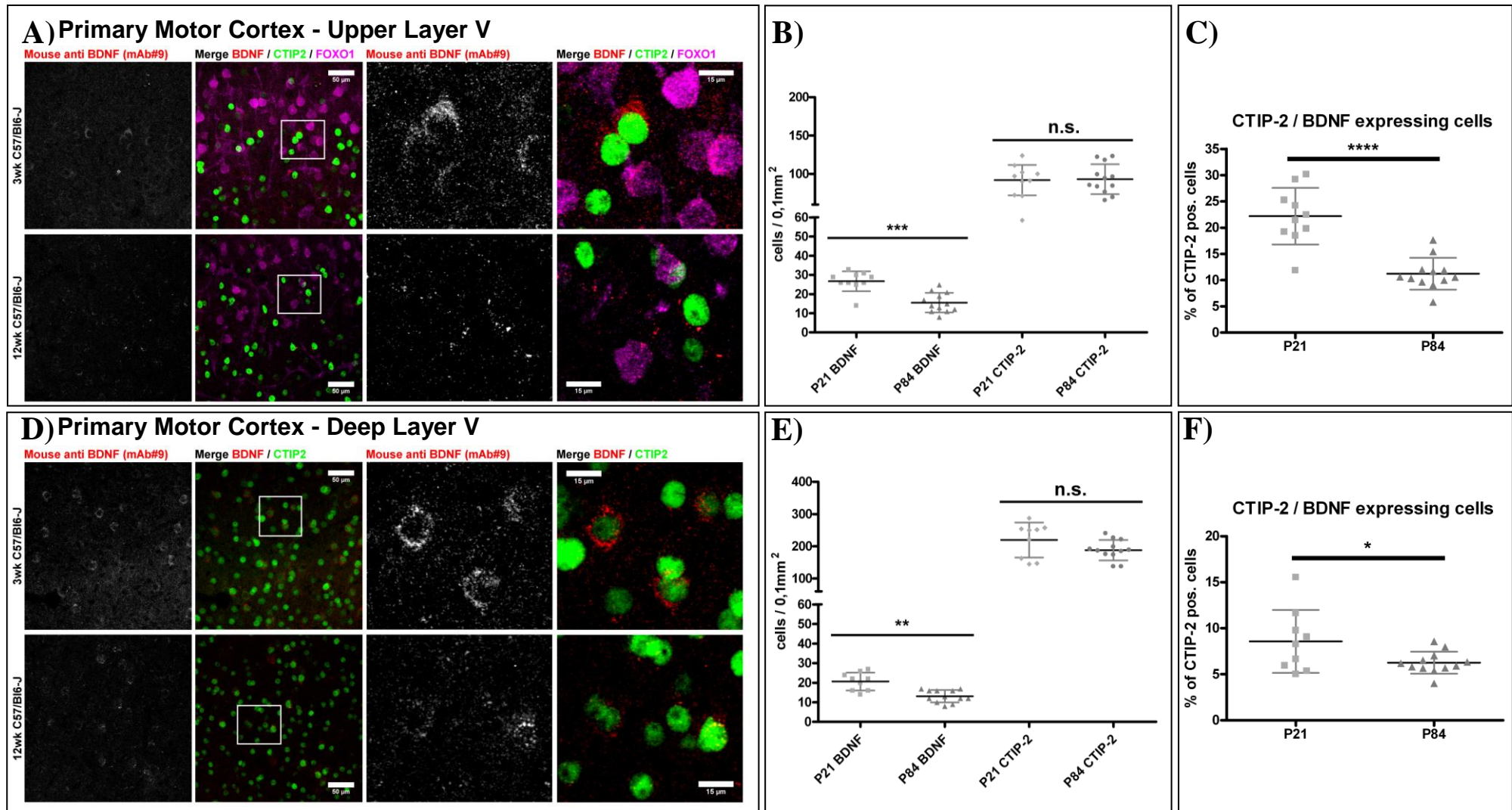


Fig. 18) Quantification of BDNF-IR in layer V subcortical projection neurons of primary motor cortex (M1): **A)** Representative immunohistochemical images of BDNF-IR in upper layer V subcortical projection neurons of primary motor cortex of 3wk and 12wk old WT mice. **B)** Quantification of cell-density with either BDNF or CTIP-2 expression in upper layer V neurons. **C)** Difference in the number of BDNF positive upper layer V subcortical projection neurons between 3wk and 12wk old mice. **D)** Representative immunohistochemical images of BDNF-IR in deep layer V subcortical projection neurons of primary motor cortex of 3wk and 12wk old WT mice. **E)** Quantification of cell-density with either BDNF or CTIP-2 expression in deep layer V neurons. **F)** Difference in the number of BDNF positive deep layer V subcortical projection neurons between 3wk and 12wk old mice. Inlays in lane 2 of A and D are depicted in lane 3 and 4. Scale bar: 50µm, 15µm (Inlay). (B; E - Mann-Whitney test; C; F - Unpaired t - test: n.s. P > 0.05; * P = 0.01-0.05; ** P = 0.001-0.01; *** P = 0.0001-0.001; **** P < 0.0001)

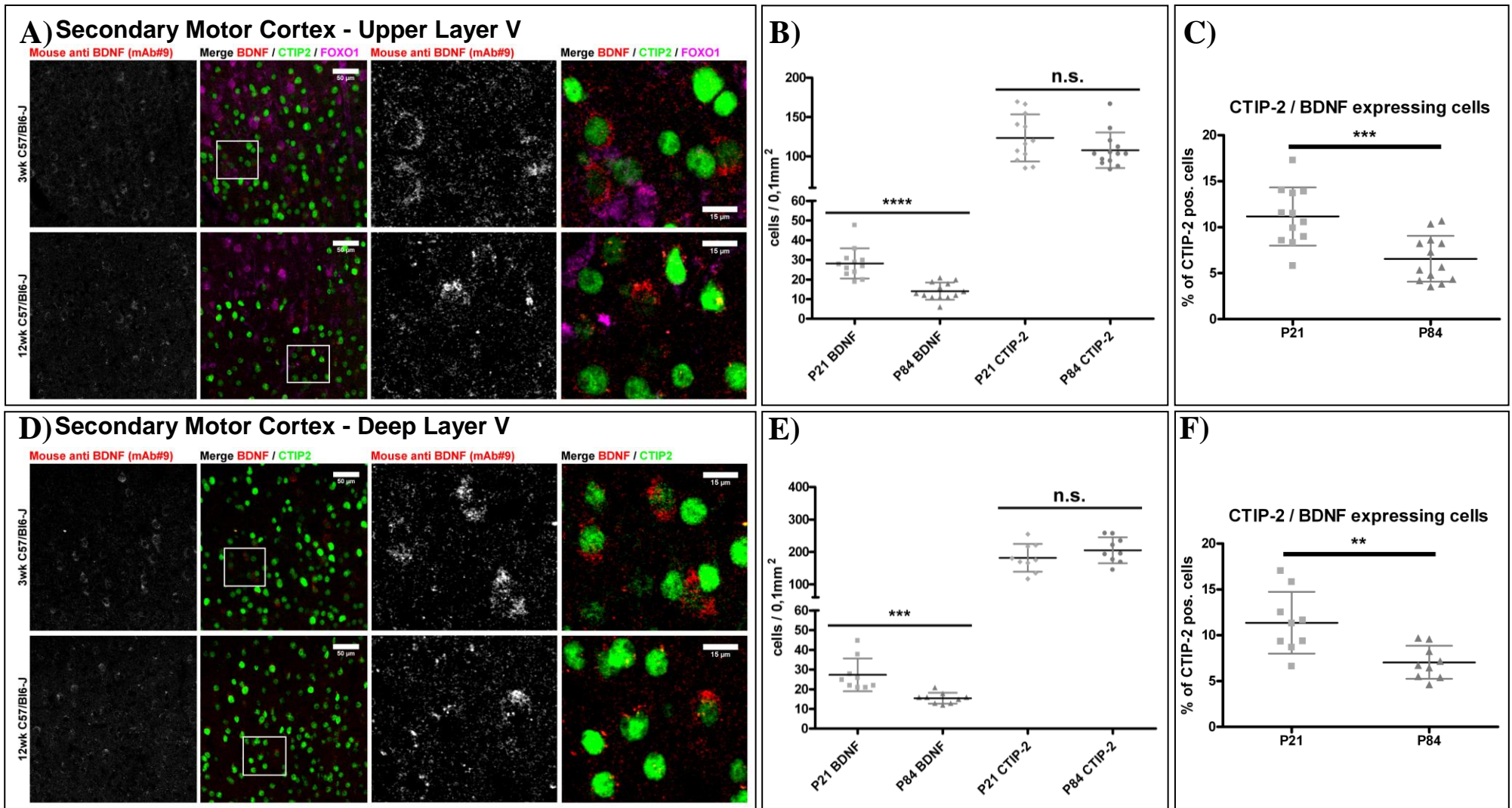


Fig. 19) Quantification of BDNF-IR in layer V subcortical projection neurons of secondary motor cortex (M2): **A)** Representative immunohistochemical images of BDNF-IR in upper layer V subcortical projection neurons of secondary motor cortex of 3wk and 12wk old WT mice. **B)** Quantification of cell-density with either BDNF or CTIP-2 expression in upper layer V neurons. **C)** Difference in the number of BDNF positive upper layer V subcortical projection neurons between 3wk and 12wk old mice. **D)** Representative immunohistochemical images of BDNF-IR in deep layer V subcortical projection neurons of secondary motor cortex of 3wk and 12wk old WT mice. **E)** Quantification of cell-density with either BDNF or CTIP-2 expression in deep layer V neurons. **F)** Difference in the number of BDNF positive deep layer V subcortical projection neurons between 3wk and 12wk old mice. Inlays in lane 2 of A and D are depicted in lane 3 and 4. Scale bar: 50µm, 15µm (Inlay). (B; E - Mann-Whitney test; C; F - Unpaired t - test: n.s. P > 0.05; * P = 0.01-0.05; ** P = 0.001-0.01; *** P = 0.0001-0.001; **** P < 0.0001)

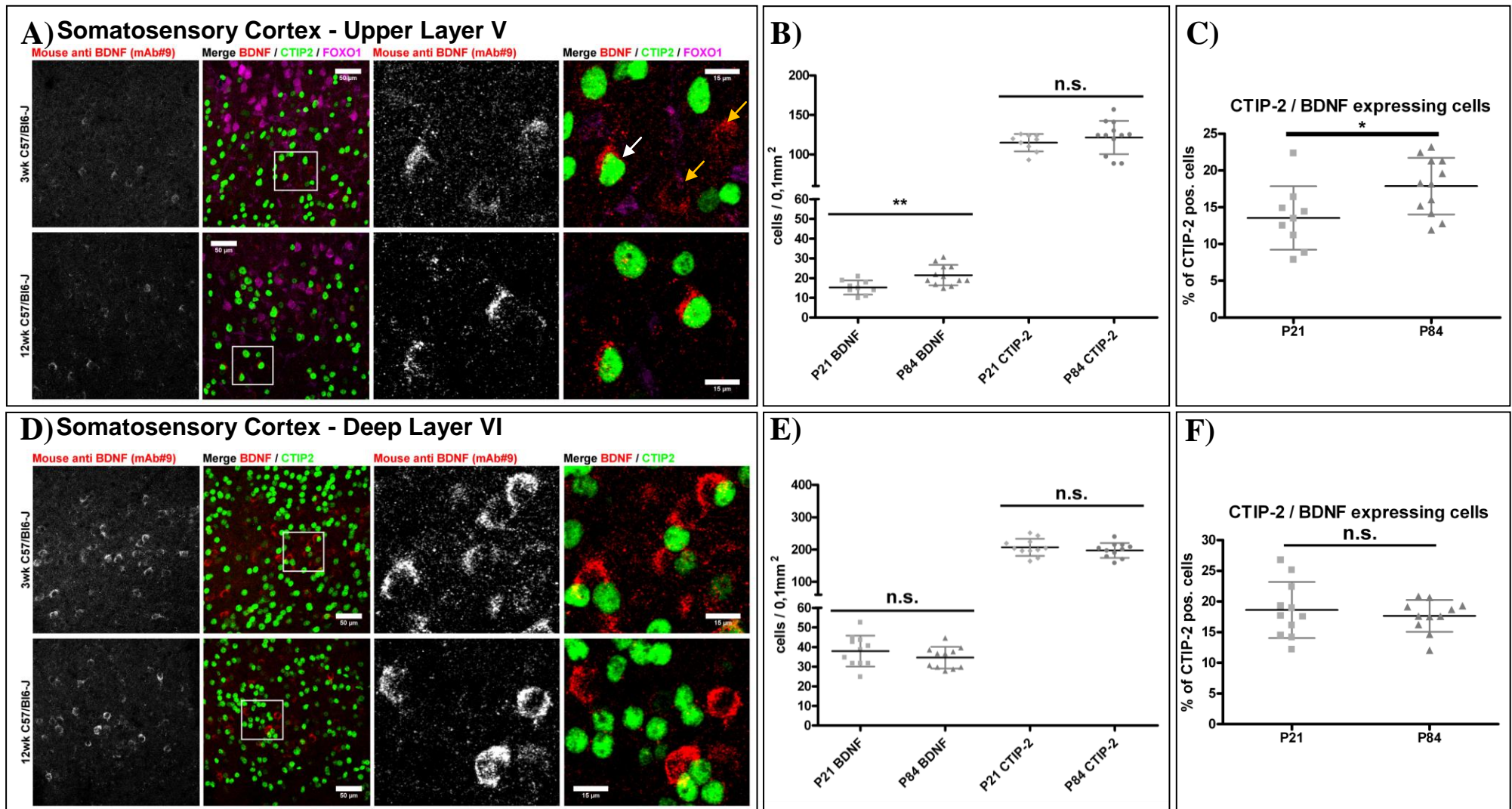


Fig. 20) Quantification of BDNF-IR in layer V and VI subcortical projection neurons of primary (SSp) and secondary somatosensory cortex (SSs): **A)** Representative immunohistochemical images of BDNF-IR in upper layer V subcortical projection neurons of somatosensory cortex of 3wk and 12wk old WT mice. BDNF expression is evident in CTIP-2 positive (white arrows) and CTIP-2 negative (yellow arrows) cells. **(B)** Quantification of cell-density with either BDNF or CTIP-2 expression in upper layer V neurons. **(C)** Difference in the number of BDNF positive layer V subcortical projection neurons between 3wk and 12wk old mice. **(D)** Representative immunohistochemical images of BDNF-IR in deep layer VI subcortical projection neurons of somatosensory cortex of 3wk and 12wk old WT mice. **(E)** Quantification of cell-density with either BDNF or CTIP-2 expression in deep layer VI neurons. **(F)** Difference in the number of BDNF positive deep layer VI subcortical projection neurons between 3wk and 12wk old mice. Inlays in lane 2 of A and D are depicted in lane 3 and 4. Scale bar: 50µm, 15µm (Inlay). (B; E - Mann-Whitney test; C; F - Unpaired t - test: n.s. P > 0.05; * P = 0.01-0.05; ** P = 0.001-0.01; *** P = 0.0001-0.001; **** P < 0.0001)

nuclei, but the identity of the BDNF expressing population remains elusive unless retrograde tracing is used to identify the projections. Nevertheless, these neurons showed very strong BDNF-IR, indicating high levels of BDNF in these neurons. Finally, we found a significant decrease in the number of BDNF expressing subcortical projection neurons at 12wk compared to 3wk in layer V of both motor cortices. This decrease was more severe in upper layer V neurons, compared to deep layer V neurons. In contrast, layer V somatosensory cortical neurons seemed to show a slight increase in BDNF expression at 12wk. This clearly indicates differences in BDNF expression during early postnatal development, affecting cortical regions which are critically involved in the control of voluntary limb movement.

5.4 BDNF expression in pre- and infralimbic cortex involved in motivational regulation

In the next attempt, we wanted to address the question whether BDNF expression profiles in pre- and infralimbic cortex, projecting towards the ventromedial striatum (**Fig. 14A, C**) also change during early postnatal development. We found BDNF-IR in CTIP-2 positive subcortical projection neurons in both cortical areas, similar to what we observed before for layer V somatomotor cortex (**Fig. 21A, D**). Nevertheless, BDNF expression was not exclusively restricted to CTIP-2 positive neurons, since single BDNF expressing cells lack a CTIP-2 signal. Similarly, we observed a slight decrease in the total number of BDNF expressing cells in the prelimbic cortex of 12wk old animals (**Fig. 21B**), while the amount of BDNF/CTIP-2 positive projection neurons did not change (**Fig. 21C**). In contrast, we observed an obvious decrease of BDNF expressing cells in the infralimbic cortex (**Fig. 21E**) which was reflected by a similar decrease in the number of BDNF/CTIP-2 double positive cells.

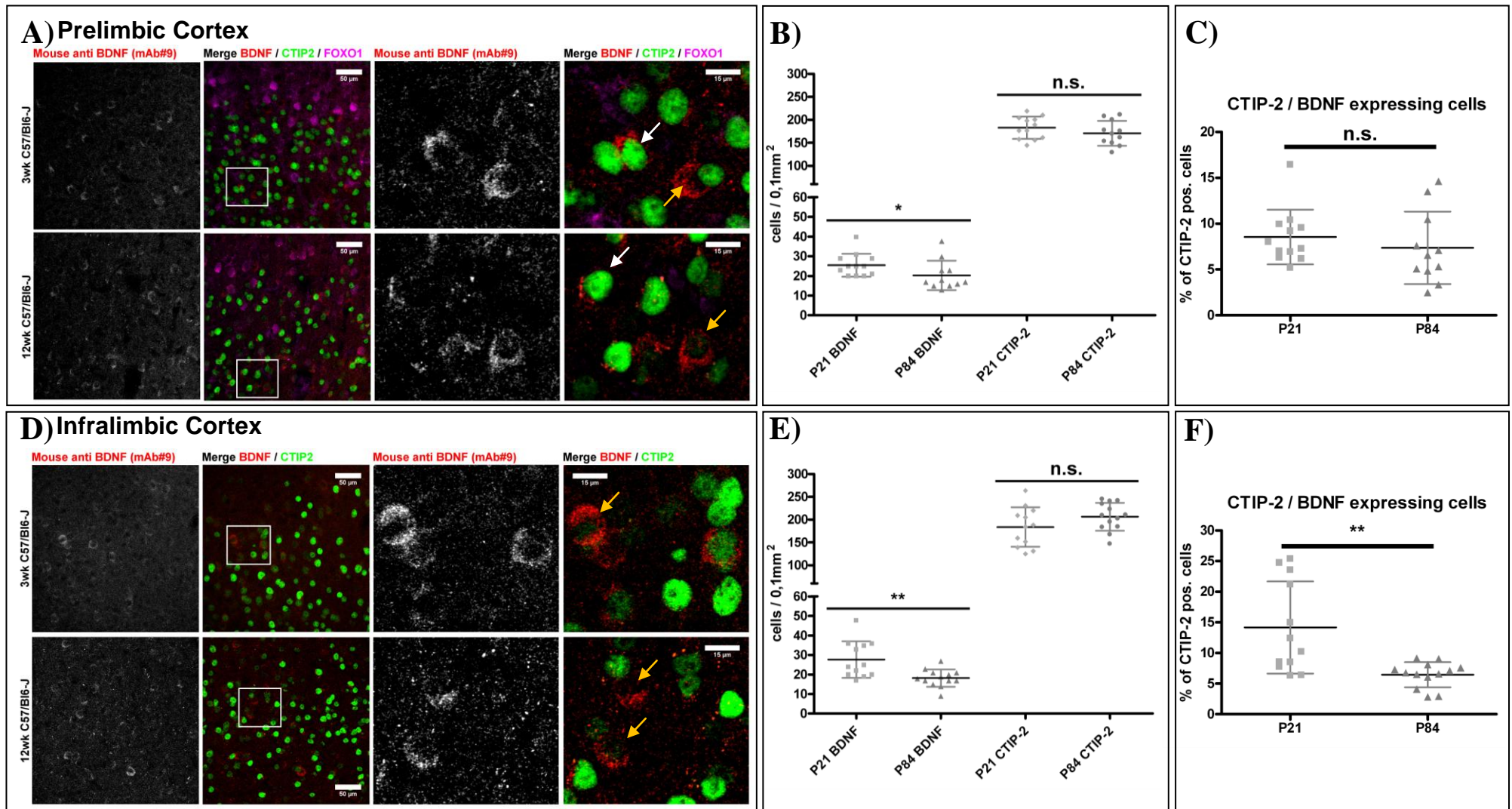


Fig. 21) Quantification of BDNF-IR in subcortical projection neurons of prelimbic (PL) and infralimbic cortex (IL): A) Representative immunohistochemical images of BDNF-IR in layer V subcortical projection neurons of prelimbic cortex of 3wk and 12wk old WT mice. BDNF expression is evident in CTIP-2 positive (white arrows) and CTIP-2 negative (yellow arrows) cells (B) Quantification of cell-density with either BDNF or CTIP-2 expression in layer V neurons. (C) Difference in the number of BDNF positive layer V subcortical projection neurons between 3wk and 12wk old mice. D) Representative immunohistochemical images of BDNF-IR in layer V subcortical projection neurons of infralimbic cortex of 3wk and 12wk old WT mice. (E) Quantification of cell-density with either BDNF or CTIP-2 expression in layer V neurons. (F) Difference in the number of BDNF positive layer V subcortical projection neurons between 3wk and 12wk old mice. Inlays in lane 2 of A and D are depicted in lane 3 and 4. Scale bar: 50µm, 15µm (Inlay). (B; E - Mann-Whitney test; C; F - Unpaired t - test: n.s. $P > 0.05$; * $P = 0.01-0.05$; ** $P = 0.001-0.01$; *** $P = 0.0001-0.001$; **** $P < 0.0001$)

Thus a decrease of BDNF expression during early postnatal development seems to affect CTIP-2 positive subcortical projection neurons in infralimbic, but not prelimbic cortex.

We made a further interesting observation in another cortical region which is located directly ventral to the infralimbic cortex and is referred to as Taenia Tecta (**Fig. 22A**). This region is known to innervate the medial central nucleus of the amygdaloid complex (Ottersen, 1982; Cassell and Wright, 1986). Within the Taenia Tecta, a slight increase in the number of BDNF expressing cells and a slight decrease in the number of CTIP-2 expressing cells was observed in 12wk old animals compared to 3wk (**Fig. 22B, C**), although none was significant. Interestingly, the combined percentage of BDNF expressing CTIP-2 positive subcortical projection neurons was significantly increased in older animals, even though this effect was weak (**Fig. 22D**). Compared to the pre- or infralimbic cortex, the BDNF expression in Taenia Tecta seems to be restricted exclusively to CTIP-2 positive neurons (compare **Fig. 22 B to Fig. 21A, D**). Another interesting observation was that the density of BDNF expressing cells in this brain region was comparable to somatosensory cortex layer VI and thus, much higher than in any other cortical brain region investigated here (**Fig. 23**). This observation is interesting in the means of emotional and fear related habits, on which BDNF expression may have an influence. In summary, we verified BDNF expression in subcortical CTIP-2 positive projection neurons in cortical regions that innervate the ventromedial striatum, namely pre- and infralimbic cortex. We did not see a significant effect on BDNF expression in the prelimbic cortex during early postnatal development. In contrast, we found evidence for a downregulation of BDNF expression in CTIP-2 positive neurons in the infralimbic cortex. Additionally, the Taenia Tecta, a region ventral to the infralimbic cortex innervating the amygdala, was drawing our attention. BDNF expression in the Taenia Tecta, like in somatosensory cortex layer VI, seems to be special. Both regions show the highest density of BDNF expressing cells and within these particular cells, BDNF-IR showed the highest intensity compared to all other cortical regions analyzed

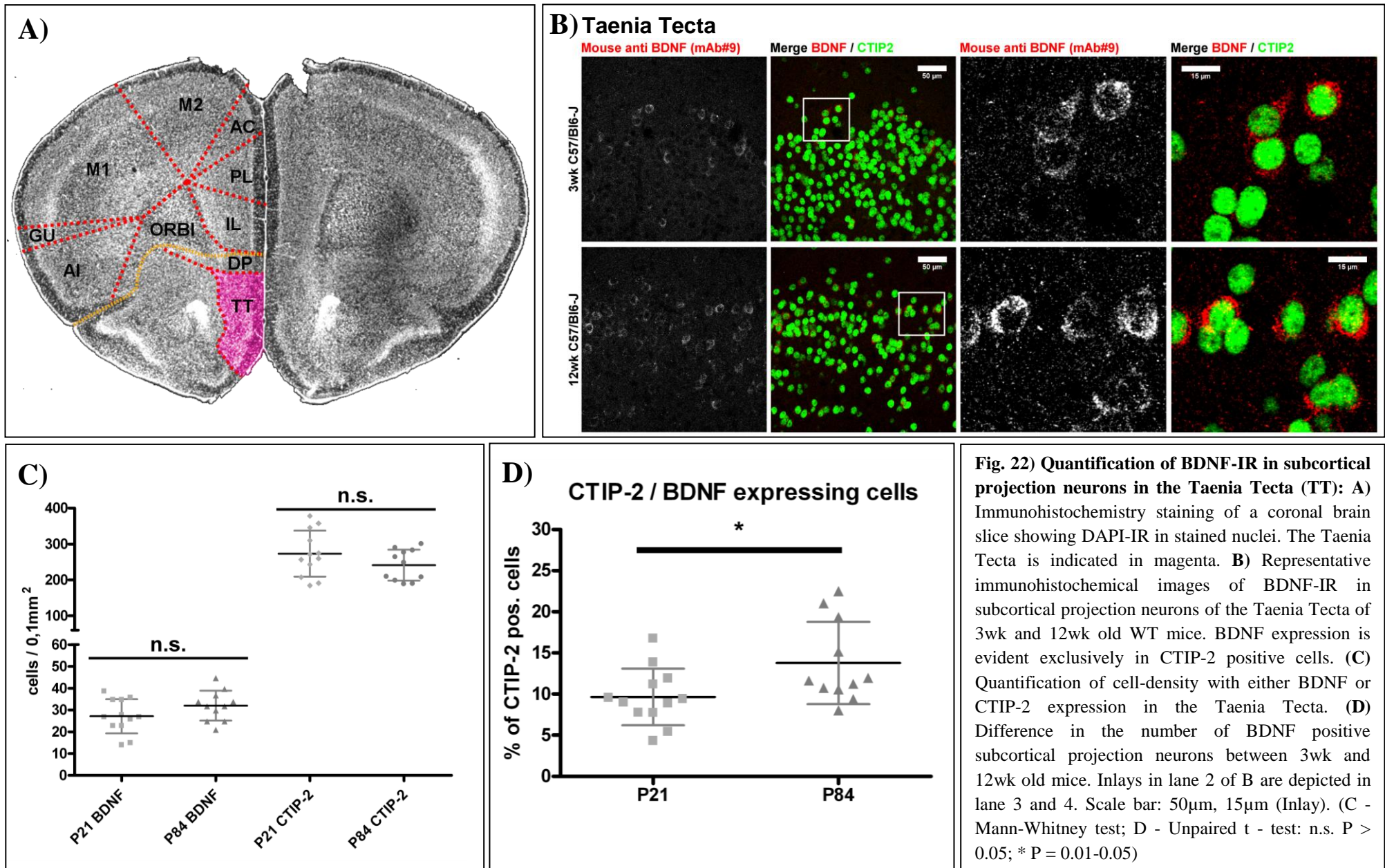


Fig. 22) Quantification of BDNF-IR in subcortical projection neurons in the Taenia Tecta (TT): **A)** Immunohistochemistry staining of a coronal brain slice showing DAPI-IR in stained nuclei. The Taenia Tecta is indicated in magenta. **B)** Representative immunohistochemical images of BDNF-IR in subcortical projection neurons of the Taenia Tecta of 3wk and 12wk old WT mice. BDNF expression is evident exclusively in CTIP-2 positive cells. **(C)** Quantification of cell-density with either BDNF or CTIP-2 expression in the Taenia Tecta. **(D)** Difference in the number of BDNF positive subcortical projection neurons between 3wk and 12wk old mice. Inlays in lane 2 of B are depicted in lane 3 and 4. Scale bar: 50µm, 15µm (Inlay). (C - Mann-Whitney test; D - Unpaired t - test: n.s. $P > 0.05$; * $P = 0.01-0.05$)

Finally, BDNF expression appears to be restricted to CTIP-2 positive cells in the Taenia Tecta, while it seems to be excluded from CTIP-2 positive cells in the somatosensory cortex.

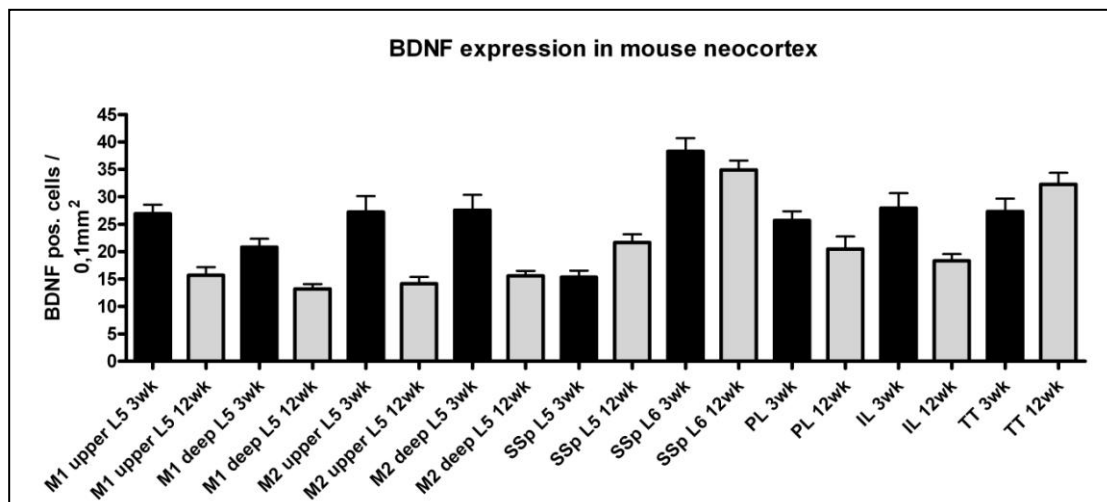


Fig. 23) Overview about the number of BDNF expressing cells in mouse neocortex: Indicated are the density values of BDNF expressing cells in denoted cortical areas comparing 3wk with 12wk old mice. Abbreviations: M1 - primary motor cortex; M2 - secondary motor cortex; SSp - primary somatosensory cortex; PL - prelimbic cortex; IL - infralimbic cortex; TT - Taenia Tecta

From these findings, we conclude that subcortical projection neurons of layer V in cortical regions which are known to innervate the striatum clearly express BDNF protein. This BDNF expression underlies developmental changes during early postnatal life. In this regard, BDNF expression gets downregulated in upper layer V subcortical projection neurons of the motor cortices, as well as the infralimbic cortex, while it gets upregulated in layer V somatosensory cortex. No difference was observed in the prelimbic cortex. Additionally, to this long-term developmental effect, we also found that individual BDNF expressing neurons differ in their BDNF-IR intensity. This could reflect protein expression levels since we observed "BDNF-strong" and "BDNF-weak" neurons. If these neurons are one source of striatal BDNF, then we would expect that BDNF expression in corticostriatal terminals is not equal as well, but it also reflects this "BDNF-strong" and "BDNF-weak" pattern. If this is true, then this pattern of BDNF expression might reflect an activity-dependent regulation of transcription and protein secretion in cortical neurons. To address this question we aimed to analyze BDNF expression in cortico-striatal terminals in the next experiment.

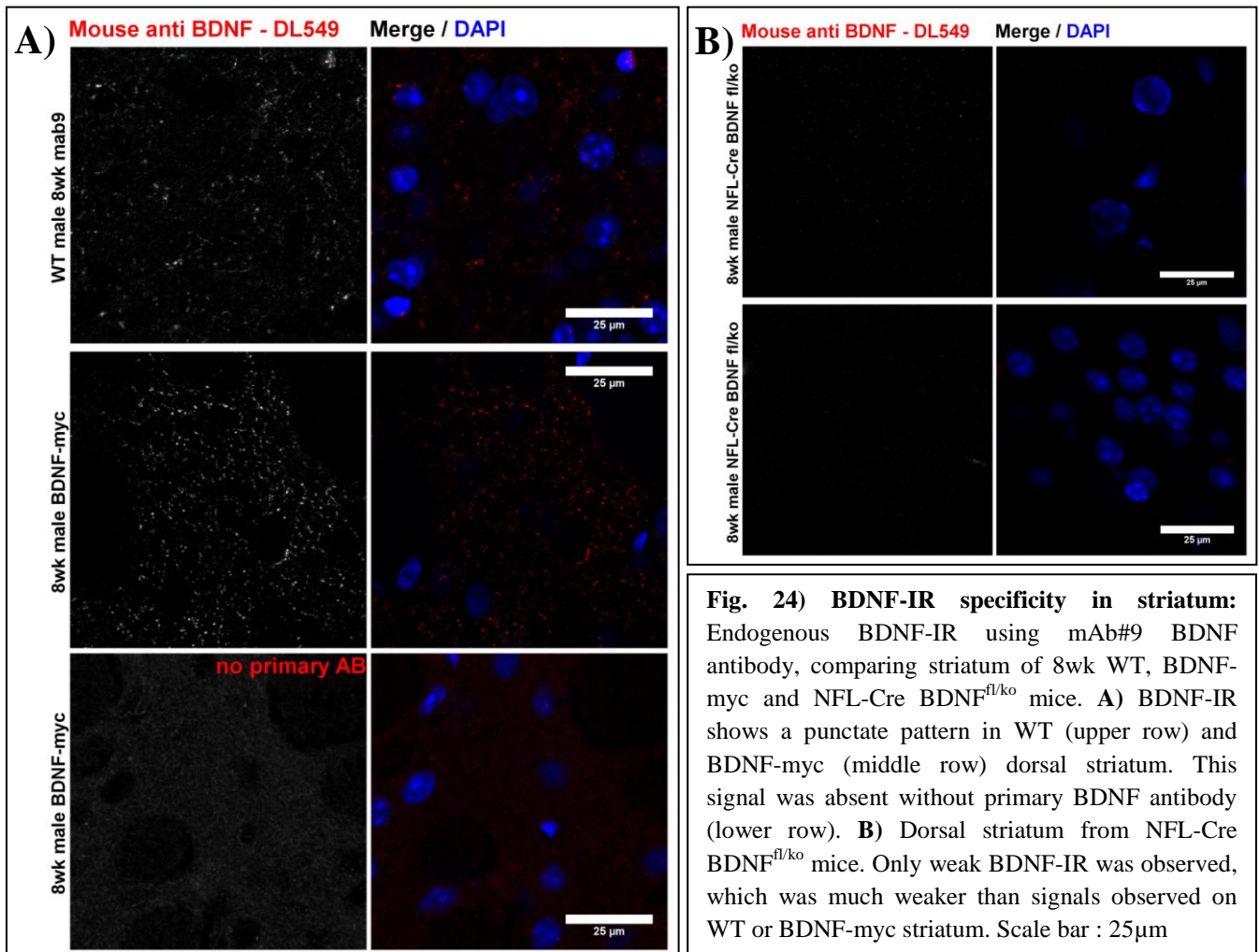
5.5 Verification of BDNF-IR in the striatum

Neuronal populations in the striatum are well known to lack any kind of autonomous BDNF expression (Conner et al., 1997; Yan et al., 1997b). Anyway, BDNF is critically involved in striatal development and function (Jia et al., 2010; Rauskolb et al., 2010; Baydyuk et al., 2011) which leads to the conclusion that BDNF is actively transported towards the striatum. Three afferent inputs target this structure which originates from the cortex, the thalamus, and the midbrain. We already found clear evidence for presence of endogenous BDNF expression in subcortical projection neurons and in the cortex, confirming observations other groups made before (Altar et al., 1997; Conner et al., 1997; Gorski et al., 2003; Baquet et al., 2004; Kalivas, 2009; Rauskolb et al., 2010; Li et al., 2012; Park et al., 2014). Next, we aimed to identify endogenous BDNF in corticostriatal terminals and to compare these to nigrostriatal terminals which are also thought to contain BDNF (Baquet et al., 2005). In order to distinguish the two different excitatory afferent inputs from the cortex and the thalamus, we had to use specific markers which also indicate presynaptic terminals. We did so by using vesicular glutamate transporter 1 (VGluT1) which is enriched in glutamatergic presynaptic terminals of neurons from cerebral cortex and hippocampus (Fremeau et al., 2001; Herzog et al., 2001; De Gois et al., 2005; Hur and Zaborszky, 2005; Wilson et al., 2005; Oda et al., 2014). In contrast, thalamic excitatory neurons, especially those located in the dorsal thalamus which innervate the striatum, predominantly express VGluT2 (Fremeau et al., 2001; Herzog et al., 2001; Hur and Zaborszky, 2005; Oda et al., 2014). VGluT1 is furthermore a preferential marker for glutamatergic terminals from the cortex, since the expression of VGluT1 and VGluT2 is rather exclusive, though it was shown that only very few regions in the CNS express both markers at the same time (Hisano et al., 2002; Li et al., 2003; Todd et al., 2003; Boulland et al., 2004; Nakamura et al., 2007; Graziano et al., 2008; Oda et al., 2014). It was also shown that only a very minor fraction of thalamic neurons express VGluT1 (Barroso-Chinea et al., 2007). Finally, recent studies using optogenetically evoked responses, have shed

more light on the modes of cortical and thalamic afferent modulation of dMSNs or iMSNs (Fieblinger et al., 2014). Both striatal MSN subtypes receive ~75% of their excitatory glutamatergic afferent inputs from the cortex and 30% from thalamus (Fieblinger et al., 2014). Taken together, VGluT1 is a robust marker for glutamatergic, cortico-striatal terminals for three reasons. First, it is expressed in a specific manner in neocortical projection neurons. Second, thalamic nuclei predominantly express VGluT2. Third, the majority of afferent inputs on both striatal medium spiny neuron subtypes originate from the cortex. For these reasons, VGluT1 was used to identify glutamatergic cortico-striatal terminals.

Generally, the detection of BDNF in the striatum remained a challenging task, due to very low levels and lack of specific and sensitive antibodies. So far it was assumed that the detection of endogenous BDNF in the striatum is not possible (Park et al., 2014). For this reason and in order to confirm the specificity of our BDNF-IHC approach, we first compared BDNF-IR in the striatum of WT, BDNF-myc and NFL-Cre BDNF^{fl/ko} mice (**Fig. 24**). We observed BDNF-IR in a punctate pattern in the dorsal striatum of either WT or BDNF-myc mice (**Fig. 24A lanes 1, 2**). This signal was clearly distinguishable from non-specific background noise which was evident when the staining was performed without primary BDNF antibody (**Fig. 24A lane 3**). In NFL-Cre BDNF^{fl/ko} dorsal striatum, we observed a very weak punctate pattern for BDNF-IR which was much less intense than the signal we found on WT or BDNF-myc (**Fig. 24B**). Since the NFL-Cre promoter causes a conditional but not complete BDNF k.o. (**Fig. 10A**), it is possible that our approach is able to detect residual BDNF-IR even in cBDNF k.o. which is indistinguishable from background, due to very minor signal intensity.

From these experiments, we conclude that the monoclonal antibody, whose specificity was shown in the hippocampus and cortical neurons before, confirmed its high sensitivity and enables the detection of endogenous BDNF in the striatum.



5.6 Detection of BDNF in presynaptic VGluT1 positive cortico-striatal terminals

For the detection of endogenous BDNF in cortico-striatal terminals, we combined BDNF with VGluT1 staining. To further increase the reliability of our approach, we conducted these experiments on BDNF-myc derived striatal tissue and included staining for the myc tag, in order to confirm the signal of endogenous BDNF. We observed BDNF-IR that was overlapping with VGluT1-IR and Myc-IR in both, the dorsolateral striatum, as well as the ventromedial striatum (**Fig. 25A, B**). In both regions, we observed the same punctate pattern for BDNF-IR, as we found before. This pattern was resembled by Myc-IR, even though the polyclonal antibody used, produced some non-specific background signal. As expected, VGluT1 produced a synapse-like punctate signal which indicates glutamatergic presynaptic terminals. These terminals might represent innervating structures from the

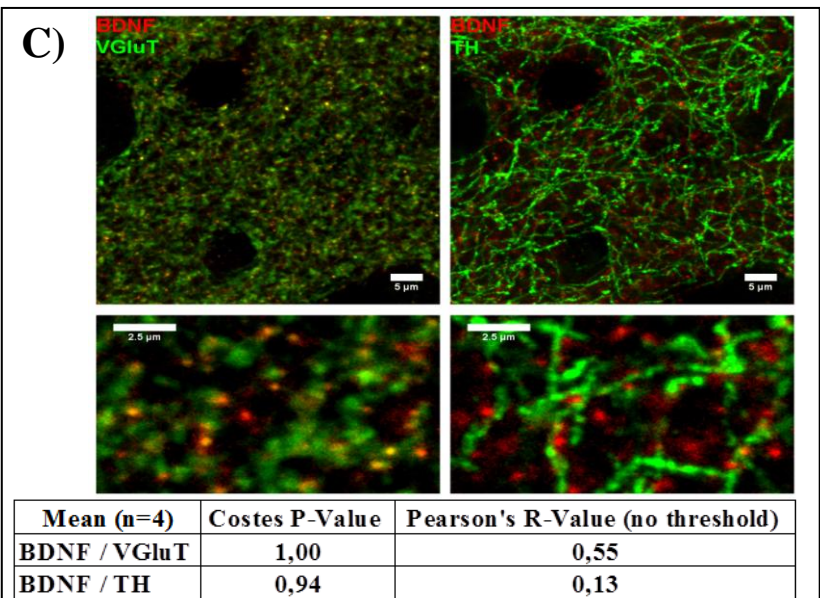
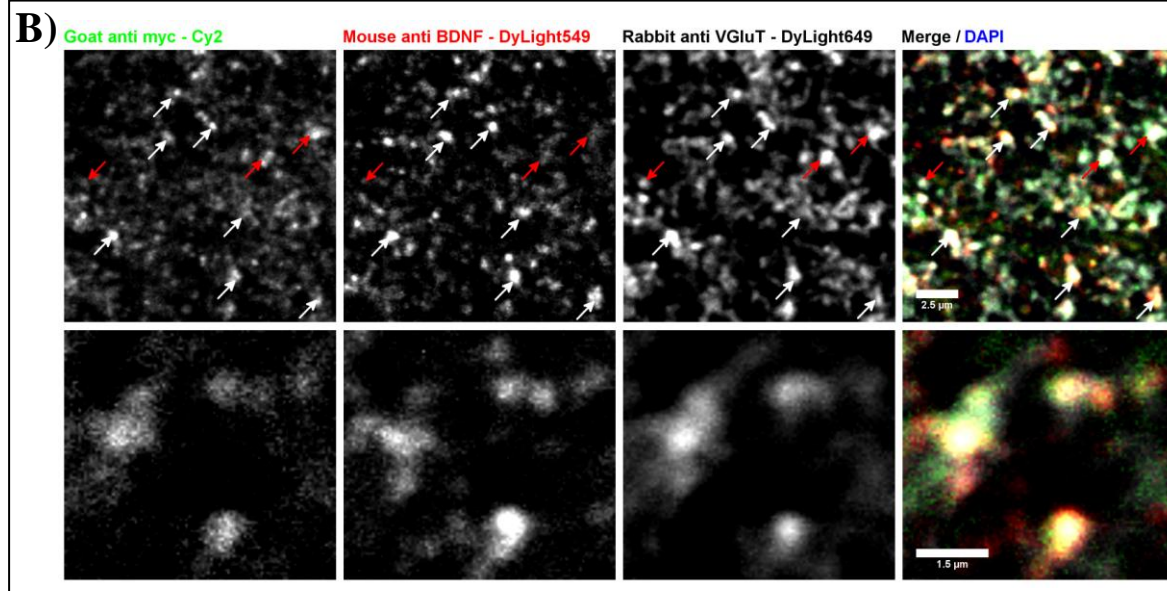
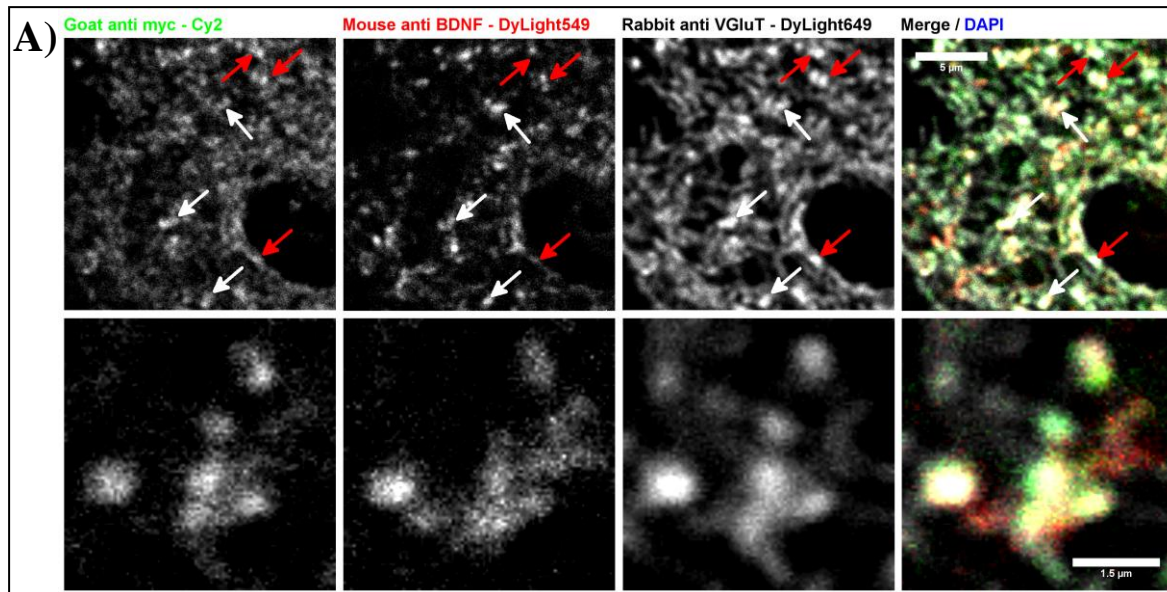


Fig. 25) Confocal analysis of BDNF expression in glutamatergic corticostriatal afferences: Triple IHC staining comparing BDNF-IR with Myc and VGluT1 in dorsal **A)** or ventral **B)** striatum of 8wk male BDNF-myc mouse. Upper row shows overview while lower row shows detail images of glutamatergic synapses at maximum resolution. Overlap between BDNF and VGluT1 forms two populations, "BDNF-strong" (white arrows) and "BDNF-weak" (red arrows). **C)** BDNF-IR within glutamatergic (VGluT1) versus dopaminergic (TH) terminals in dorsal striatum. Both images show the same region with BDNF / VGluT1 (left) or BDNF / TH (right). Table in **C)** shows statistical outcome of "Coloc2" analysis (mean values of n=4). Costes P-Value revealed true co-localization of BDNF and VGluT1. Pearson's R-Value revealed 55% co-localization of BDNF with VGluT1 and 13% co-localization between BDNF and TH. Scale bars **A)** upper row - 5μm; lower row - 1,5μm, **B)** upper row - 2,5μm; lower row - 1,5μm, **C)** upper row - 5μm; lower row 2,5μm

somatomotor cortex in the dorsolateral and from the pre- and infralimbic cortex in the ventromedial striatum. Similar to the observation that subcortical projection neurons in the named areas were found positive for BDNF-IR, we found endogenous BDNF protein in the terminals as well (**Fig. 25A and B**, lower row). Interestingly, we observed two types of VGluT1 positive terminals with regard to BDNF expression. One population showed strong BDNF-IR (**Fig. 25A, B**, upper row white arrows and lower row). Another population showed clear and strong VGluT1-IR but seemed to contain only very weak BDNF-IR (**Fig. 25A, B**, upper row red arrows). We suggest that in these terminals BDNF was either released or the BDNF content is lower, due to lower protein segregation and reduced anterograde transport from cortical neurons. This would confirm our observation that the BDNF production is not equal among cortical neurons but rather represented as "BDNF-strong" and "BDNF-weak" subcortical projection neurons. This observation might be reflected by "BDNF-strong" and "BDNF-weak" corticostriatal terminals as well.

Next, we wanted to address the question about the contribution of midbrain dopaminergic neurons in striatal BDNF supply. For this reason, we directly investigated BDNF expression in dopaminergic terminals which were labeled with tyrosine hydroxylase (TH), an enzyme required for dopamine synthesis, enriched in dopaminergic neurons. In triple staining approaches using BDNF, VGluT1, and TH, we were able to directly visualize glutamatergic corticostriatal and dopaminergic nigrostriatal afferences in the same image (**Fig. 25C**). We could confirm the previous observations of BDNF expression in VGluT1positive, presynaptic terminals (**Fig. 25C lane 2 left**). When comparing the same BDNF signal to TH-IR, we found that both markers are rather exclusive, with no obvious overlap being observed (**Fig. 25C lower row right**). This observation was confirmed by quantitative analysis of signal overlap using the Costes-P value (Costes et al., 2004) in order to calculate the significance of co-localization. This algorithm is recommended for biological systems instead of the Pearson's

R-value and can detect true co-localization of minimal 3%. A threshold value for Costes-P > 0,95 indicates true localization, while $P < 0,95$ indicates random overlap. In our case we obtained a Costes-P = 1,0 for BDNF/VGluT1 and $P = 0,94$ for BDNF/TH (**Fig. 25C**). This indicates true co-localization between BDNF and glutamatergic terminals and random overlap with dopaminergic synapses. In parallel, we calculated the Pearson's R-value which indicated that ~55% of all glutamatergic terminals, but only 13% of dopaminergic terminals contain a BDNF signal (**Fig. 25C**).

These findings confirm BDNF presence in VGluT1 positive cortico-striatal terminals and complement our observation of BDNF expression in subcortical projection neurons, targeting the dorsolateral and the ventromedial striatum. Nevertheless, confocal microscopes have an optical resolution limit of 200nm, thus presynaptic inputs from midbrain and cortex, targeting the same spine cannot be distinguished. These discrete structures are smaller than 200nm and cannot be resolved with a confocal microscope. For this reason, it is actually hard to tell if a BDNF-IR signal is located in a glutamatergic or rather a dopaminergic terminal. To circumvent this problem, we repeated the experiments using structured illumination microscopy (SIM) with a resolution of ~100-120nm. Again, we observed an overlap between BDNF-IR and VGluT1-IR (**Fig. 26A, B** yellow arrows). In contrast, TH-IR overlapped with only very few and much smaller BDNF signals (**Fig. 26A, B** blue arrows). The resolution of the setup was enough to distinguish glutamatergic from dopaminergic terminals which were found in direct neighborhood in some cases (**Fig. 26B** white arrows). In summary, this indicates that glutamatergic corticostriatal and dopaminergic nigrostriatal terminals reside in close proximity to their target structures which are spines of striatal MSNs. Significant BDNF expression was only found in VGluT1 glutamatergic synapses, while signals in dopaminergic synapses were much weaker in strength and smaller in size. We found that 49,48% of all VGluT1 positive terminals contained a BDNF signal, while only 14,03% of the dopaminergic

synapses were positive for BDNF (**Fig. 16C-F**). Interestingly, these values are very close to the Pearson's R-Value co-localization coefficient for the data obtained with the confocal microscope (**Fig. 25C**). We also obtained a Costes P-Value of 1,0 for BDNF/VGluT1 and 0,71 for BDNF/TH which confirms true co-localization between BDNF and VGluT1 and random overlap with TH. These findings support the confocal observations, but with a much higher degree in reliability.

Taken together, these data indicate that BDNF is expressed in glutamatergic cortico-striatal terminals, rather than dopaminergic nigrostriatal afferences. These terminals were evident in both, the dorsolateral and the ventromedial striatum. Both of which receive broad innervation from the cerebral cortex (**Fig. 14**). At the same time, we observed "BDNF-strong" and "BDNF-weak" terminals which reflects the situation of BDNF expression in "BDNF-strong" and "BDNF-weak" subcortical projection neurons. According to this idea, we have shown that ~50% of the glutamatergic terminals originating from the cortex contain a BDNF signal. We thus conclude that BDNF is produced by subcortical projection neurons and actively transported along cortico-striatal afferences, towards the striatum. The glutamatergic terminals which express BDNF are in the direct neighborhood to dopaminergic afferences. The presence of BDNF in those structures is striking and might be below the limit of sensitivity which we can reach with our approach. This would in turn also mean that midbrain dopaminergic neurons, if at all, produce much less BDNF than cortical neurons. For that reason, we investigated BDNF-IR presence in dopaminergic neurons of the substantia nigra pars compacta which is known to innervate the striatum.

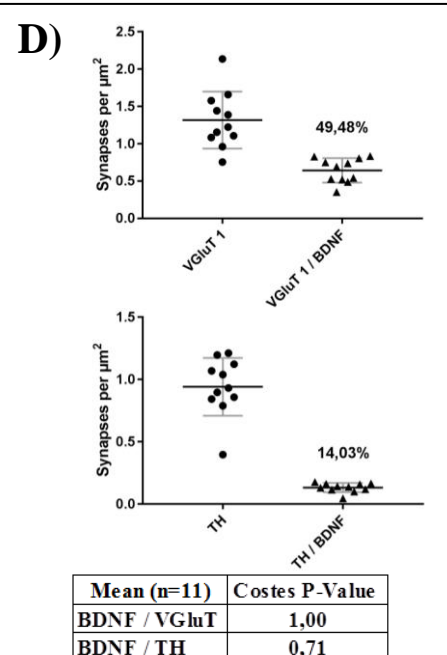
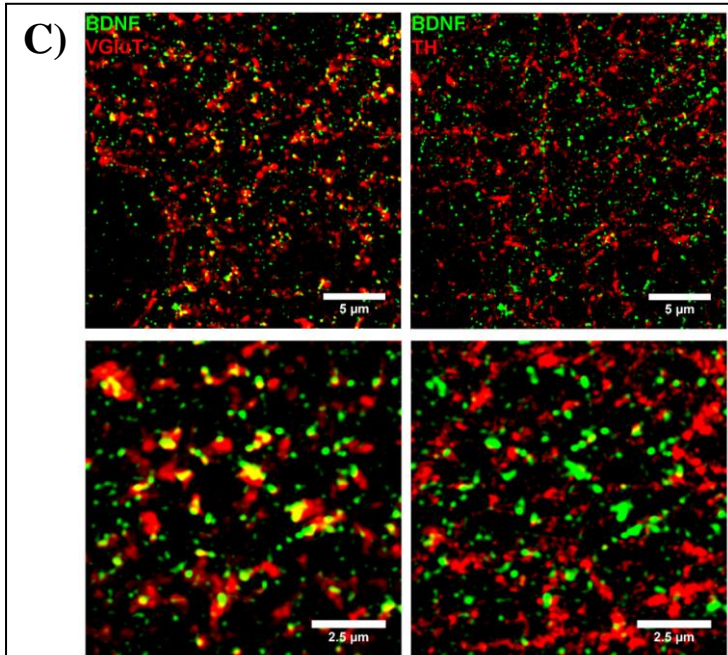
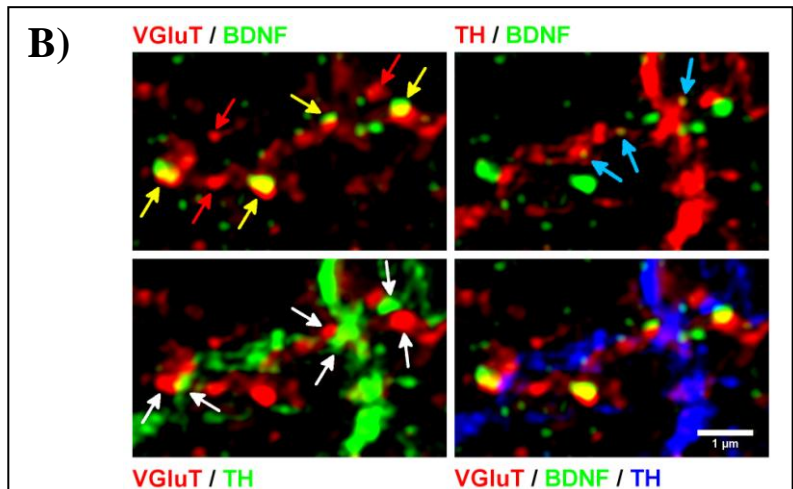
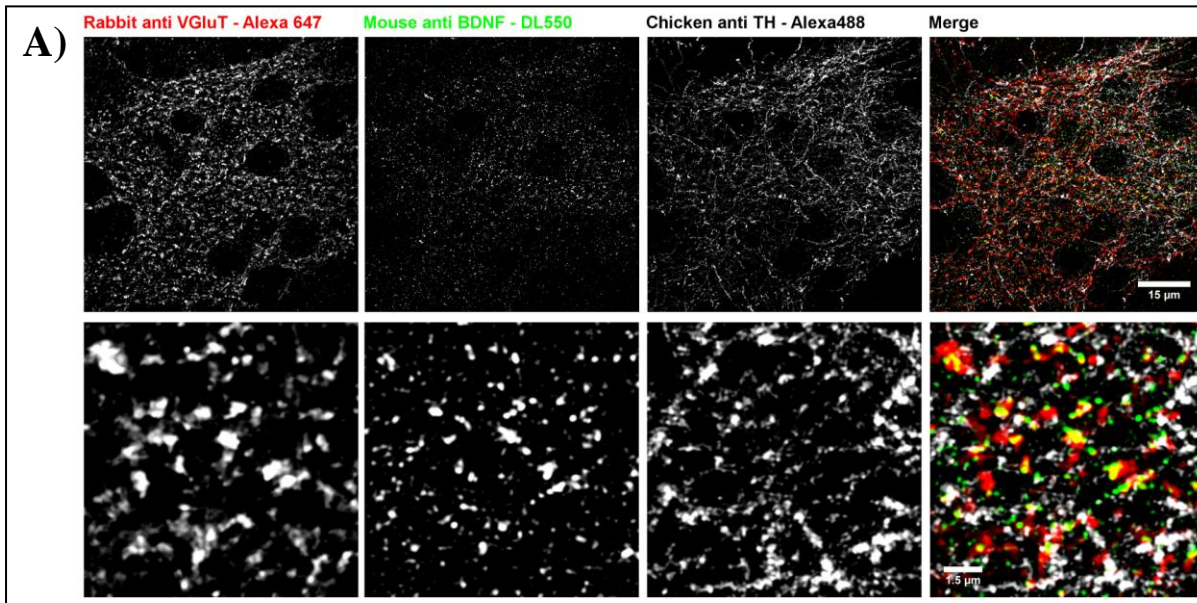
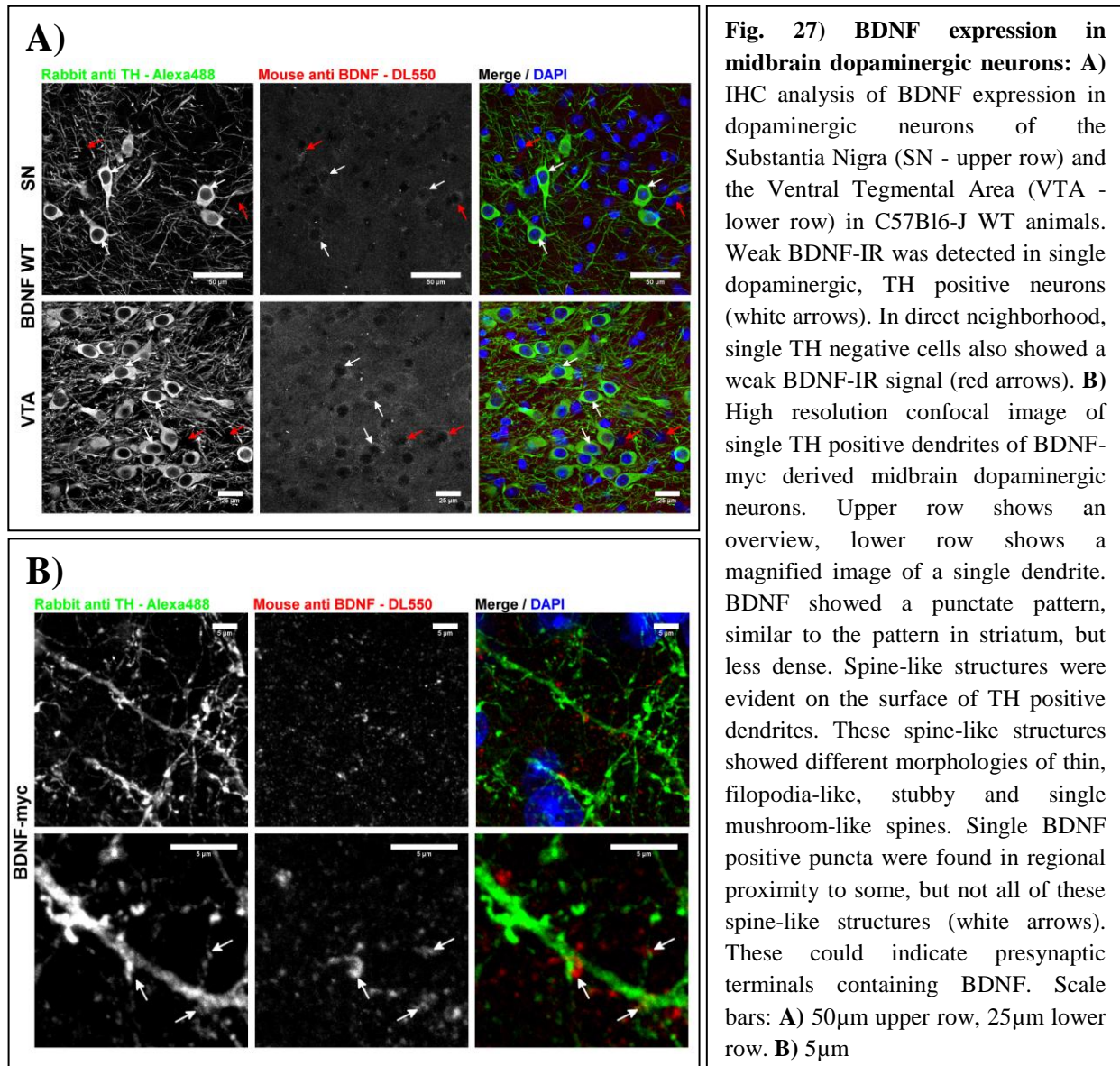


Fig. 26) Structural Illumination (SIM) analysis of BDNF expression in glutamatergic vs dopaminergic afferences: **A)** IHC staining comparing BDNF-IR in VGlut1 and TH terminals in dorsal striatum of 7wk male WT CD1 mouse. Upper row shows an overview of dorsal striatum, the lower row shows a magnified area of BDNF positive glutamatergic synapses. **B)** High magnification SIM image. Upper left: BDNF/VGlut1 double positive synapses (yellow arrows) next to BDNF negative glutamatergic synapses (red arrows). Upper right: Weak BDNF-IR signals in TH positive structures (blue arrows). Lower left: VGlut1 terminals next to TH fibers and terminals (white arrows). Lower right: merged image - BDNF (green), VGlut1 (red) and TH (blue). **C)** Representative SIM images for co-localization analysis between BDNF and VGlut1 or TH respectively. The lower row shows a magnified detail, the same as depicted in **A)** lower row. Left: BDNF vs VGlut1; right: BDNF vs TH in the same image. **D)** Statistical analysis revealed that ~50% of VGlut1 positive synapses contained BDNF. Co-localization was confirmed to be significant by a Costes P-Value >95%. Only ~14% TH positive structures contained BDNF-IR, which was no significant co-localization (Costes P<<95%). Scale bars **A)** upper row - 15μm; lower row - 1,5μm; **B)** 1μm; **C)** upper row - 5μm; lower row - 2,5μm

5.7 BDNF expression in midbrain dopaminergic neurons

For the investigation of BDNF expression in the midbrain, we analyzed both main regions which contain dopaminergic neurons, the substantia nigra (SN) and the ventral tegmental area (VTA). Both regions densely innervate the striatum (Voorn et al., 2004; Tritsch et al., 2012). We were able to detect BDNF-IR in a granular manner in the cell body of single dopaminergic neurons, in both regions (**Fig. 27A**, white arrows). Notably, there were other cells lacking TH-IR in the direct neighborhood which showed a similar BDNF-IR (**Fig. 27A**, red arrows). In comparison, the BDNF-IR in these midbrain neurons is much weaker than any signal observed in cortical neurons and may thus be arguable since our protocol might not be sensitive enough to detect these low levels.



In parallel, we made another interesting observation, namely, a punctate BDNF-IR, similar to that observed in the striatum, but with somehow lower density (**Fig. 27B**). Interestingly, this punctate pattern of BDNF-IR does not seem to be randomly distributed but rather follows TH positive neurites. At higher magnification, we even found that some of these BDNF-IR puncta are located close to spine-like structures on these dopaminergic neurons (**Fig. 27B** white arrows). If these BDNF-IR puncta represent presynaptic structures remains elusive. Nevertheless, one possibility is that afferent inputs from subcortical projections, carrying BDNF, innervate these dopaminergic neurons in the midbrain. This idea is not new and direct connections between cortical areas in the mPFC and midbrain have been demonstrated (Rinvik, 1966; Afifi et al., 1974; Bunney and Aghajanian, 1976; Beckstead, 1979; Carter, 1982; Kornhuber et al., 1984; Sesack et al., 1989; Naito and Kita, 1994; Jasmin et al., 2004; Zakiewicz et al., 2014; Hoglinger et al., 2015).

Even though we observed weak BDNF-IR in the midbrain which was not restricted to dopaminergic neurons, the signal intensity was far below any BDNF signal we found in the cortex. It could well be that dopaminergic neurons produce BDNF like suggested by others (Okazawa et al., 1992; Nishio et al., 1998; Numan and Seroogy, 1999; Venero et al., 2000; Baquet et al., 2005), but the levels appear much lower compared to cortical neurons. This would also explain, why we observed presynaptic BDNF-IR in the striatum, mainly in cortical glutamatergic terminals, rather than in midbrain dopaminergic terminals.

5.8 BDNF/TrkB mediated plasticity in rodent striatum

After we were able to identify BDNF in corticostriatal afferences which may represent a major afferent supply of this neurotrophic factor for striatal neurons, we aimed to focus on modes of TrkB expression and signaling in postsynaptic target cells, the striatal medium spiny neurons (MSNs). We were wondering, how BDNF / TrkB signaling might be mediated and integrated together with glutamate and dopamine transmission, in order to functionally integrate synaptic communication and enable modalities of plasticity on the receiving structure, the MSN spine? In other words, we were wondering how glutamatergic and dopaminergic signaling can be integrated in a functional, spatiotemporal manner to enable BDNF / TrkB interaction in this neuronal network?

By using bacterial artificial chromosome (BAC) transgenic DRD1-EGFP or DRD2-EGFP expressing mice, it was possible to show that iMSNs show a significant degeneration of spines in Parkinson's disease models, thus in the absence of dopamine (Gerfen et al., 1990; Day et al., 2006; Gerfen, 2006). This effect was found to be linked to a central role of the L-type calcium channel $Ca_v1.3\alpha1$, expressed in indirect pathway MSNs (Day et al., 2006). Similar degeneration of spines and dendrites in the striatum was also observed in cBDNF k.o. and cTrkB k.o. animals (Rauskolb et al., 2010; Baydyuk et al., 2011). Interestingly the pathological effects of presynaptic BDNF or TrkB ablation in striatal neurons are very similar and to some extent also reflect effects of dopamine ablation. Normally, BDNF is released in a Ca^{2+} dependent manner from presynaptic corticostriatal terminals which requires the activity-dependent release of glutamate and binding to presynaptic NMDA-Rs which trigger BDNF release (Park et al., 2014). BDNF then binds to TrkB that is expressed in both striatal medium spiny neuron subtypes (Costantini et al., 1999; Baydyuk et al., 2011; Li et al., 2012), but overall it was found to be enriched in DRD2 expressing iMSNs (Costantini et al., 1999; Baydyuk et al., 2011; Li et al., 2012). Somehow, these iMSNs are degenerating in patients suffering from Huntington's disease (HD) (Reiner et al., 1988). In parallel, striatal BDNF

levels are decreased in HD patients due to inhibition of *bdnf* gene expression in cortical neurons and reduction of axonal transport (Zuccato et al., 2001; Gauthier et al., 2004). Conditional TrkB k.o. on the other hand also leads to a reduction of striatal volume during embryonic development, mainly due to a significant underrepresentation of DRD2 expressing iMSNs which fail to develop correctly (Baydyuk et al., 2011). All these information point to a putative role for TrkB in striatal MSNs. For this reason, we were focusing on the expression of TrkB in striatal medium spiny neurons in this part of the project. Furthermore, we wanted to investigate a possible contribution of postsynaptic dopamine receptors in regulating TrkB expression and subsequently, BDNF / TrkB mediated signal transduction.

5.9 Verification of TrkB antibody specificity

In order to specifically detect TrkB in either immunohistochemical or quantitative approaches, like Western Blot analysis, we had to utilize antibodies which detect TrkB rather than other tyrosine kinase receptors. To address this issue, we made use of two different polyclonal antibodies against the N-terminus of mature TrkB. In addition and in order to differentiate full-length TrkB (TrkB-FL) from the truncated TrkB-T1 version, lacking a functional c-terminus, we further included an antibody directed against this truncated TrkB variant. All antibodies were tested *in vivo* and *in vitro* (**Fig. 28, 29**). To test the antibody specificity, we used mice lacking all isoforms of TrkB (Rohrer et al., 1999). These mice lack the first coding exon which both isoforms, the full-length and the truncated version, have in common and which encodes the signal peptide, as well as the start codon for TrkB (Rohrer et al., 1999). This results in complete absence of TrkB protein expression and a massive reduction in viability which ranges from 48h up to 21d in very few cases (Rohrer et al., 1999). For that reason, we analyzed newborn Ntrk Rohrer mice at P1 up to P5 and compared these mice to age-matched WT animals. IHC staining of TrkB revealed a broad and strong TrkB-IR throughout CNS (**Fig. 28A**) which was absent in TrkB ^{-/-} mice. In the striatum, we observed a perinuclear-like pattern in individual cells, but at the same time found the absence of TrkB-IR in striosomes (**Fig. 28B** left). Furthermore, we observed TrkB expression throughout the cortex with very intense staining at the most superficial cortical layer I (**Fig. 28C** left) which reflects observations about TrkB expression in developing mouse cortex (Puehringer et al., 2013). Compared to WT, we were not able to detect any significant TrkB-IR in TrkB ^{-/-} animals, neither in the striatum (**Fig. 28B** left) nor in the cortex (**Fig. 28C** left). As a further control and in order to estimate non-specific background staining from secondary antibodies, we also stained striatum and cortex without primary antibodies (**Fig. 28B, C** right). The observations we made were almost indistinguishable from immunoreactivity on TrkB ^{-/-} mice, for which reason we concluded that non-specific background is negligible.

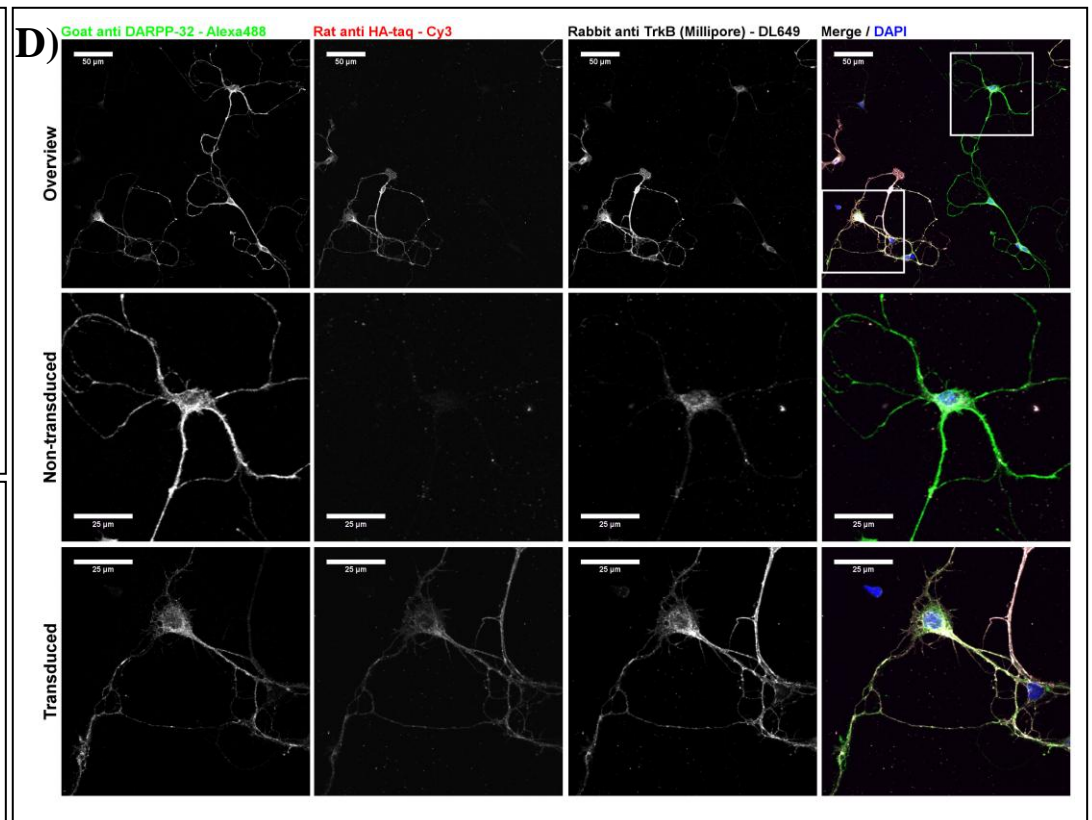
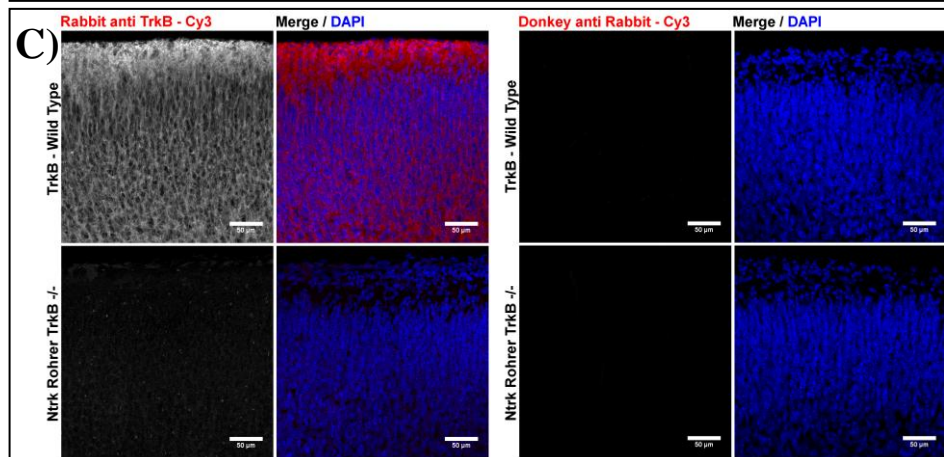
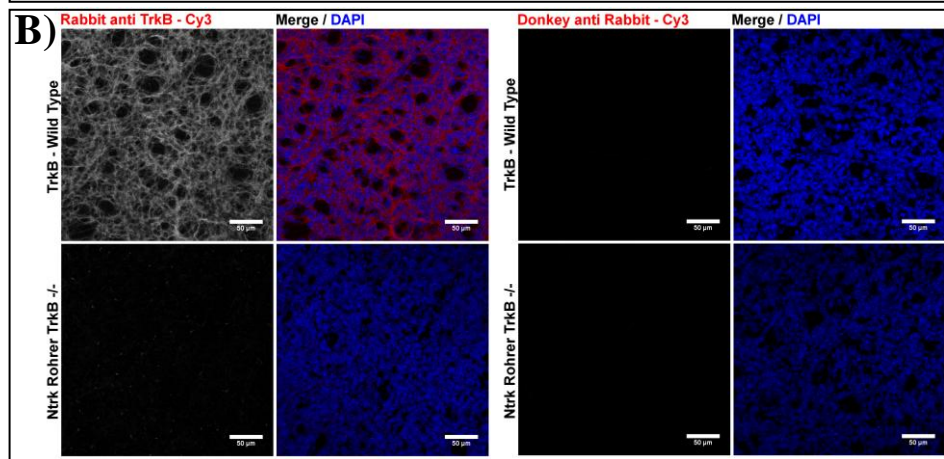
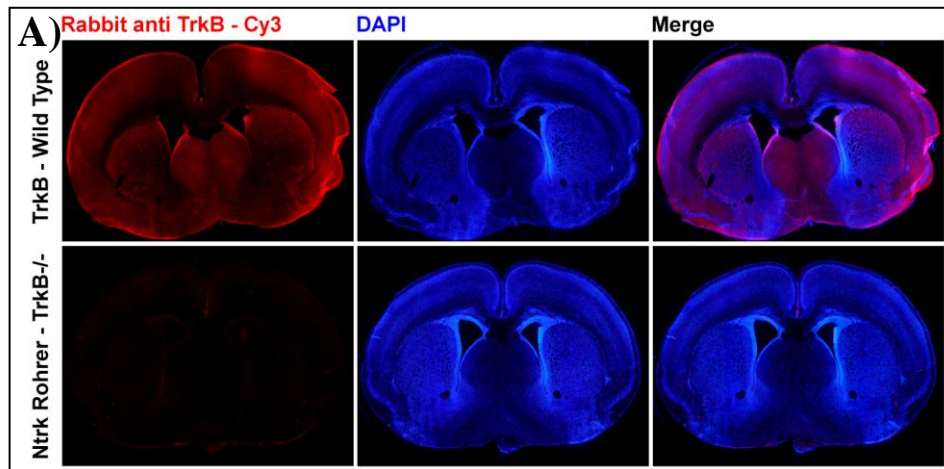


Fig.28: Verification of TrkB antibody specificity I: **A)** Postnatal PFA fixed 30µm coronal brain slices comparing TrkB-IR in P1 WT and Ntrk Rohrer TrkB $-/-$ littermates. TrkB-IR is evident in CNS of WT animals, while no significant TrkB-IR was evident in mice lacking TrkB. **B,C)** Higher resolution confocal images of brains in **A)** indicating absence of TrkB-IR in striatum (**left side in B**) and cortex (**left side in C**) of TrkB $-/-$ mice. Strong TrkB-IR was evident in striatum, excluding striosomes and cortex (**left side in B, C**), especially superficial cortical layers. **Right side in B, C**) shows negative controls without primary antibody to evaluate non-specific binding of secondary antibodies used. No significant background was evident in either case. **D)** Primary striatal MSNs obtained from TrkB $-/-$ mice at 8DIV, lacking all forms of TrkB. DARPP-32 positive MSNs of both the direct and indirect pathway show very weak TrkB-IR in the cell body of non-transduced cells (**D – middle row**). After transduction with TrkB-HA virus, TrkB-IR is massively elevated and localized to cells showing also HA-IR (**D - lower row**). In comparison, cells that were not transduced by the virus, lacking any HA-IR still show very weak TrkB-IR in the cell body which is identified as non-specific antibody related signal. Scale bar: 50µm in B, C, D (upper row); 25µm in D (middle and lower row).

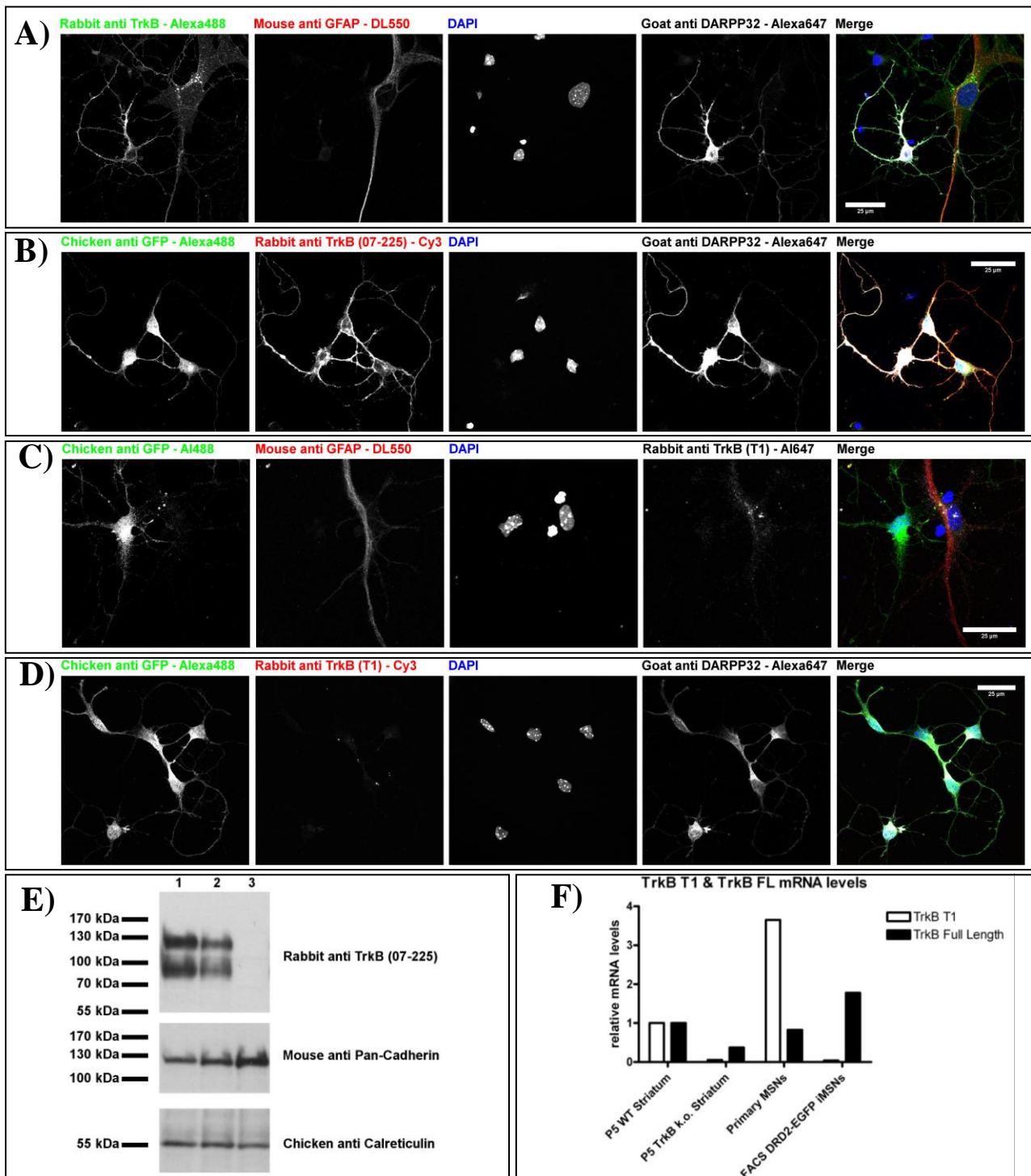


Fig.29: Verification of TrkB antibody specificity II: **A)** Primary MSN culture derived from P1 WT striatum at 8DIV. Image shows TrkB(FL)-IR in both striatal MSNs (DARPP-32) and neighboring astrocytes (GFAP). In this way, using TrkB-FL antibody it is not possible to distinguish between TrkB-FL and TrkB-T1 since the antibody binding site (N-terminus) is identical in both receptors. **B)** FACS purified iMSNs derived from striatum of DRD2-EGFP mice at 7DIV. Massive TrkB-IR is evident in DARPP-32 / GFP positive iMSNs. **C)** Primary MSN culture derived from striatum of DRD2-EGFP mice, but not FACS purified to keep astrocytes in culture at 8DIV. GFP expression was used to identify iMSNs. TrkB(T1)-IR is exclusively evident in GFAP positive astrocytes, but not in neighboring iMSNs (GFP). **D)** FACS purified iMSNs derived from striatum of DRD2-EGFP mice at 7DIV, stained for TrkB(T1) expression. No significant TrkB-T1-IR was evident in any of the DARPP-32 / GFP positive iMSNs. In comparison, these cells show strong TrkB-FL-IR (**B**). **E)** Western Blot analysis of P5 WT (1), TrkB +/- (2) and TrkB -/- (3) striatal tissue. In WT and TrkB +/- mice Full length TrkB was detected at ~130kDa (TrkB-FL) and another band at ~90kDa, even though both forms are significantly reduced in TrkB +/- mice. Full knock out TrkB -/- completely lack both forms of TrkB. **F)** Q-PCR analysis comparing P5 WT striatum with P5 TrkB -/- striatum and standard primary MSNs at 5DIV and FACS sorted iMSNs at 5DIV. Relative mRNA levels of TrkB T1 and TrkB-FL were compared in relation to the ratio of mRNA in intact P5 WT striatum. Primary MSNs express high amounts of T1, due to high density of astrocytes, while T1 mRNA is absent in pure FACS sorted iMSN cultures which show enriched TrkB FL expression (compare ICC for TrkB FL (C) and T1 (D)). Scale bar: 25µm in A-D)

In parallel, we prepared striatal tissue of TrkB^{wt}, TrkB^{+/-} and TrkB^{-/-} for Western Blot analysis (**Fig. 29E**). The Rabbit polyclonal TrkB antibody identified two major bands in WT animals at ~130kDa which might represent TrkB-FL and another band at ~90kDa which might be the truncated receptor variant. While both bands were significantly reduced in TrkB^{+/-} mice (**Fig. 29E lane 2**), no specific band was detected in TrkB^{-/-} striatum (**Fig. 29E lane 3**). Loading of equal amounts of protein was confirmed by the evidence of Calreticulin, an ER-chaperone. As an additional loading control, Pan-Cadherin, a surface associated protein was used. Interestingly, the intensity of the Pan-Cadherin band was progressively increasing with the absence of TrkB. While the protein amounts were normal in TrkB^{wt}, Pan-Cadherin levels were massively elevated in TrkB^{-/-} littermates. The absence of TrkB protein gains further support by the absence or massive reduction of TrkB mRNA in TrkB^{-/-} compared to TrkB^{wt} animals in the Q-PCR analysis (**Fig. 29F**). Even though we failed to detect TrkB-T1 mRNA, we found transcripts of TrkB-FL which do not seem to be translated into functional protein (compare **Fig. 29E lane 3** with **29F P5 TrkB ko. Striatum**). In the next experiment, we dissected the striatum of newborn P1 TrkB^{-/-} mice and dissociated the tissue to obtain a primary culture of striatal MSNs. These striatal neurons were identified by staining for DARPP-32, (**Fig. 28D**). Even though these cultures lack any form of TrkB protein, the polyclonal TrkB antibody used here still detects a weak cytoplasmic signal which is considered to be non-specific (**Fig 28D middle row**). As an internal positive control, the same culture was transduced with a virus resulting in the expression of an HA-tagged TrkB which can be independently identified. In this way, we found that TrkB-IR is significantly elevated in cells which are positive for HA-IR, thus expressing TrkB (**Fig. 28D lower row**). This strong TrkB-IR cannot only be distinguished from the non-specific background by its intensity, but also by its distribution since it highlights MSN neurites similar to the HA signal. In the next experiment, we aimed to discriminate TrkB-FL from one of the two known truncated versions of the receptor, namely TrkB-T1 (Middlemas et al., 1991), by using an

antibody which specifically detects epitopes in the C-terminus of TrkB-T1. The truncated receptor is enriched in glial cells and lacks the C-terminus including the kinase domain (Middlemas et al., 1991; Rose et al., 2003). Nevertheless, the N-terminus is equally present in both subtypes which leads to the difficulty that antibodies against the N-terminus will detect both proteins without distinguishing them. Indeed, we observed TrkB-IR in both striatal MSN subtypes, expressing DARPP-32 and neighboring GFAP positive astrocytes (**Fig. 29A**). Interestingly, the signal appearance was different in both cell types. While neurons display an almost equal distribution throughout the cell body and neurites, the signal appears in a punctuate shape in the soma of astrocytes. A similar signal was observed when primary MSN cultures, derived from DRD2-EGFP mice, were stained for TrkB-T1 which revealed a punctuate signal exclusively in astrocytes (**Fig. 29C**). The neighboring iMSNs which were identified by their GFP expression (Gong et al., 2003) completely lack any TrkB T1-IR (**Fig. 29C**). This would suggest that TrkB-T1 is expressed in striatal astrocytes rather than neurons. To test this, we performed Q-PCR analysis of purified mRNA from primary MSN cultures. We found a massive elevation of TrkB-T1 in these cultures relative to the levels in P5-WT striatum which was used as a point of reference. This may be due to progressive astrocytosis which results in the massive outnumbering of the non-dividing neurons in these cultures (**Fig. 29F**). In contrast, when striatal iMSNs known to strongly express TrkB (Baydyuk et al., 2011) were purified by FACS sorting from DRD2-EGFP mice and analyzed for TrkB mRNA expression we failed to detect TrkB-T1 (**Fig. 29F**). In contrast, TrkB-FL mRNA appeared significantly enriched compared to P5 WT striatum. These results suggest that striatal MSNs tend to express TrkB-FL, while TrkB-T1 is enriched in glial cells within the striatum. Indeed, we failed to detect any TrkB-T1-IR in FACS purified iMSNs which were further identified by DARPP-32 and GFP expression (**Fig. 29D**). Instead, the same cells show strong TrkB FL-IR using the antibody directed against the N-terminus (**Fig. 29B**). To confirm these results, we tested an independent TrkB polyclonal antibody derived from Goat which is also directed

against the TrkB N-terminus. In IHC approaches, this antibody reflected the observations we made before. It produced a strong TrkB-IR throughout the CNS in WT animals while no signal was evident in $TrkB^{-/-}$ individuals (**Fig. 30A**). These results were confirmed by immunoprecipitation of TrkB from striatal tissue, using the rabbit polyclonal antibody against TrkB. The precipitated receptor was then detected on Western Blot, using the goat anti TrkB antibody which revealed two well-defined bands at ~130kDa and ~100kDa (**Fig. 30B**). In contrast, no signal was detected in $TrkB^{-/-}$ derived striatal tissue.

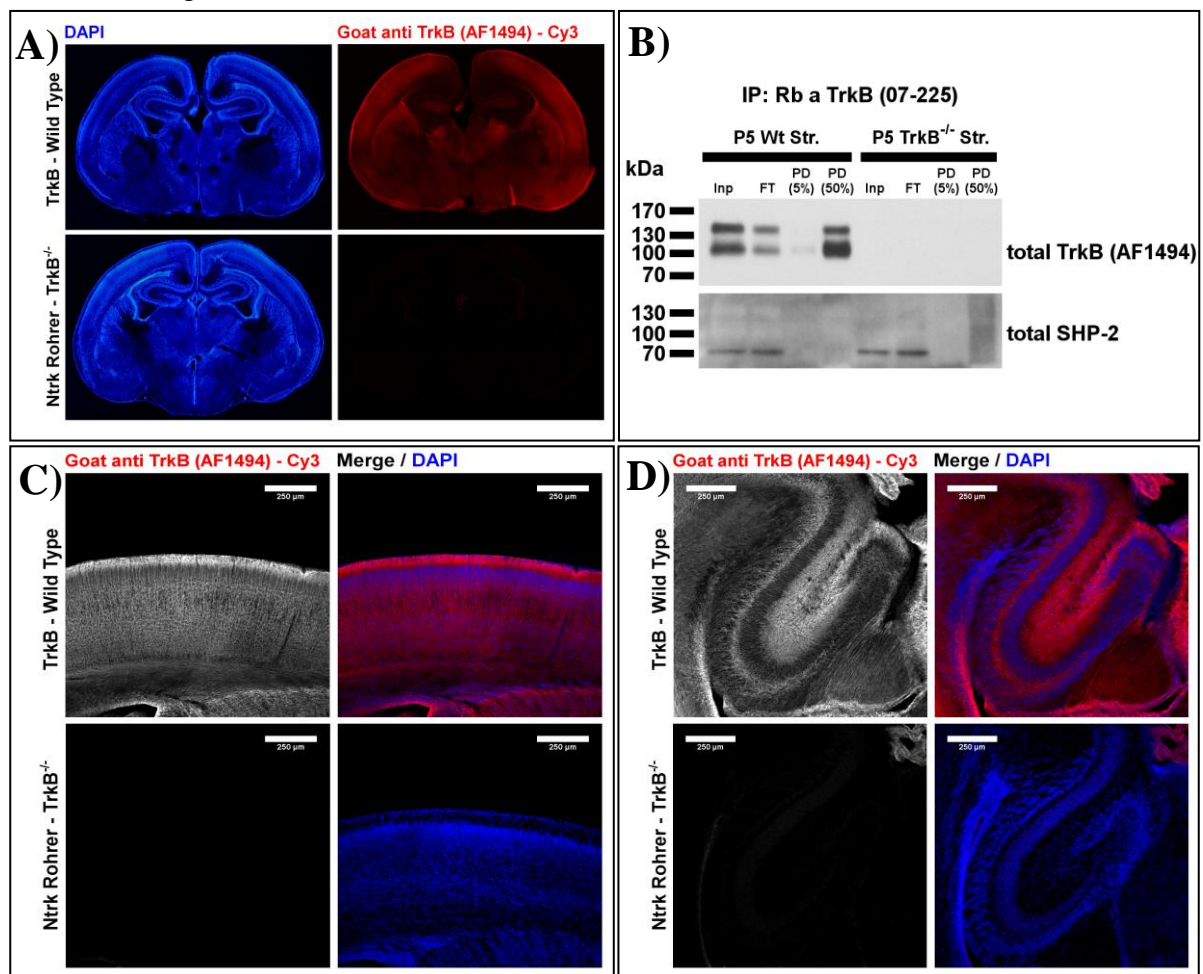


Fig.30: Verification of TrkB antibody specificity III: A) Postnatal PFA fixed 30 μ m coronal brain slices comparing TrkB-IR produced by a Goat polyclonal anti TrkB antibody in P1 WT and Ntrk Rohrer $TrkB^{-/-}$ littermates. The brain slice is more posterior compared to the one presented in Fig. 26, displaying the hippocampus in this case. TrkB-IR is evident in CNS of WT animals while no significant TrkB-IR was evident in mice lacking TrkB. B) TrkB IP confirming absence of TrkB protein in $TrkB^{-/-}$ striatum (Str.). Pull down was performed with a Rabbit polyclonal antibody against TrkB (**Fig. 26-27**) and Goat polyclonal anti TrkB was used for detection. Tyrosine-protein phosphatase non-receptor type 11 (SHP-2) was used as internal control. Abbreviations: Input (Inp), Flow Through (FT), Pull-Down (PD). C, D) Higher resolution confocal images of brains in A) indicating absence of TrkB-IR in cortex (C) and hippocampus (D) of $TrkB^{-/-}$ mice. Strong TrkB-IR was evident in superficial cortical layers and stratum lacunosum-moleculare and CA3-CA1 in hippocampus, (D). Scale bar: 250 μ m in B) and C)

Higher resolution confocal microscopy of the cortex revealed an identical staining pattern to that one produced by the rabbit anti TrkB with most intense TrkB-IR in superficial cortical layer I (**Fig. 30C, compare to Fig. 28C**). This time we also included hippocampus in the analysis since this structure is known to contain high levels of BDNF and also TrkB receptor (Conner et al., 1997; Yan et al., 1997a; Drake et al., 1999; Minichiello et al., 1999). Indeed, we observed strong TrkB-IR in CA3-CA1 and in the stratum lacunosum-moleculare (**Fig. 30D**). Both signals in the cortex and hippocampus were completely absent in TrkB^{-/-} derived tissue which confirms the antibody specificity.

In summary, these results show that both polyclonal antibodies against TrkB are suitable for detection of TrkB in immunohistochemical, as well as quantitative approaches like IP and WB analysis. Furthermore, we found that striatal MSNs, in particular, those of the indirect pathway express TrkB-FL rather than TrkB-T1, for which reason all further experiments concerning TrkB detection in MSNs reflect the presence of the full-length receptor version. We also found strong expression of TrkB-T1 in striatum derived astrocytes which confirm earlier studies, suggesting TrkB-T1 expression in glial cells (Rose et al., 2003). By using these tools, we next aimed to investigate TrkB expression within striatal neurons *in vivo* and a possible effect of dopamine on TrkB surface expression.

5.10 6-OHDA induced ablation of dopamine in nigrostriatal projections

To investigate a possible role of dopamine in the regulation of TrkB surface expression in either DRD1 expressing dMSNs or DRD2 positive iMSNs, we used unilateral 6-OHDA lesioned rats which are a well-established model system for the induction of a PD phenotype. Rats are generally preferred due to the size of target structures which are for that reason more suitable for injecting toxins into considerable brain areas (Tieu, 2011). 6-OHDA is a hydroxylated version of dopamine which has a selective toxic degenerative effect on sympathetic adrenergic neurons (Tranzer and Thoenen, 1968, 1973). This, in turn, leads to the progressive rapid loss of the nigrostriatal dopaminergic system which is highly sensitive to 6-OHDA (Jonsson, 1980) by destroying noradrenergic and dopaminergic neurons in the CNS (Ungerstedt, 1968). On the cellular level, the reason for selectively affecting these two populations is the high affinity of 6-OHDA towards dopamine and noradrenaline reuptake transporters in the plasma membrane (Luthman et al., 1989; Tieu, 2011). Once entered into the cell, the molecule is rapidly oxidized and becomes a donor for reactive oxygen species. This, in turn, causes oxidative stress-related cytotoxicity and induced cell death of the affected neurons (Saner and Thoenen, 1971; Graham, 1978; Blum et al., 2001; Tieu, 2011). In our case, 6-OHDA was unilaterally injected into the medial forebrain bundle which is one of the standard procedures and most effective in the delivery of 6-OHDA as well as induction of dopaminergic cell death. The advantage of unilateral lesions is the ability to directly compare the lesioned dopamine-depleted hemisphere with the intact hemisphere which still contains functional dopaminergic signaling (**Fig. 31A lower row, B**). The functionality of the lesion can be easily addressed by injecting dopamine receptor agonists which was apomorphine in our case. This results in the induction of a rotational motor behavior towards the ipsilateral side of the lesion which increases with the severity of the lesion itself (Ungerstedt, 1968; Ungerstedt and Arbuthnott, 1970; Hefti et al., 1980; Przedborski et al., 1995; Tieu, 2011). To visualize the ablation of dopaminergic nigrostriatal afferences, Tyrosine Hydroxylase (TH)

was immunohistochemically stained in the striatum (**Fig. 31**). TH is an enzyme which catalyzes the transition of L-tyrosine into L-Dopa, the direct precursor of dopamine (Kaufman, 1995; Nagatsu, 1995). For that reason, TH is enriched in all dopaminergic neurons and suitable for their visualization. By including TH staining, we found that TH-IR is completely absent on the striatal hemisphere that was affected by 6-OHDA lesion (**Fig. 31A lower row, B**). We also co-stained DARPP-32 in order to identify striatal MSNs and observed a somatic staining which highlights a dense network of neurites, surrounded by TH positive fibers on the intact hemisphere (**Fig. 31B**). For the reason that BDNF expression was observed in cortico-striatal neurons, projecting to the dorsolateral striatum, involved in the control of limb-related muscle coordination, we focused our investigation of dopamine-dependent, TrkB surface expression on this region (**line-point-line in Fig. 31A lower row**) and included the medial striatum (**dashed line in Fig. 31A lower row**) as well.

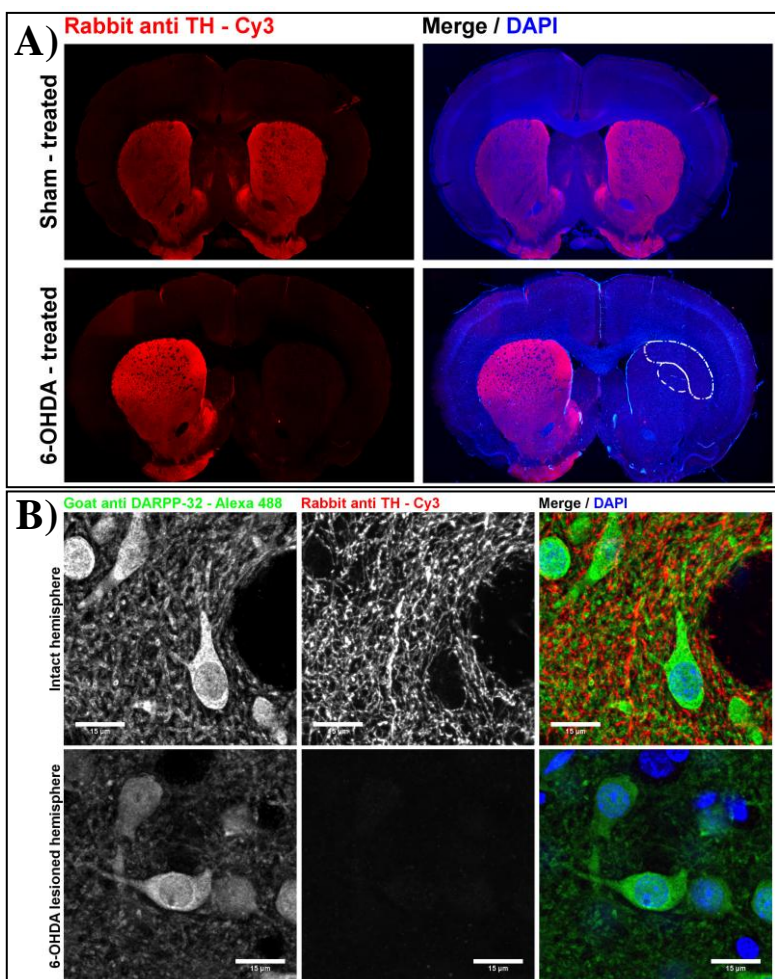


Fig.31: Unilateral 6-OHDA lesion in adult rats: Images show 30 μ m PFA fixed IHC-stainings of coronal brain slices derived from rat brain. Tyrosine-hydroxylase (TH) immunoreactivity was used to identify the lesioned hemisphere and to test the functionality of the 6-OHDA lesion. Sham treated rats, receiving injections of saline instead of 6-OHDA, were used as control (**A-upper row**). TH-IR reveals completely intact dopaminergic innervation of both striatal hemispheres. In contrast, animals that received 6-OHDA injections completely lack TH-IR on the affected hemisphere, indicating loss of dopaminergic innervation (**A-lower row**). Highlighted areas in the dorsolateral striatum (line-point-line) and medial part of the striatum (dashed line) were investigated with special focus on TrkB expression. **B**) High resolution confocal images comparing intact and lesioned hemisphere. No TH-IR was detectable after inducing the 6-OHDA lesion. DARPP-32 was stained to identify striatal MSNs. Scale bar: 15 μ m

5.11 TrkB forms intracellular aggregates in striatal MSNs in the absence of dopamine

In this experiment, we wanted to know whether TrkB staining pattern might change in IHC approaches, depending on the presence or absence of dopaminergic input to the striatum. Furthermore, we wanted to know if both striatal MSNs might be equally affected. To address this question, we stained TrkB on brain slices derived from unilaterally lesioned rats and compared the intact hemisphere to the lesioned hemisphere. The absence of dopamine was again confirmed by complete lack of TH-IR on the lesioned hemisphere (**Fig. 32A**). While TrkB-IR appeared in an equally distributed staining pattern on the intact hemisphere, we observed relatively huge, punctuate-like signals on the lesioned hemisphere of all rats analyzed (**Fig. 32A**). To rule out that this is non-specific autofluorescence which can be intense at green wavelengths, we labeled TrkB indirectly with both, green and red fluorescent secondary antibodies (**Fig. 32A**). There was no change in pattern or general appearance of these punctuate TrkB-IR signals. At higher resolution, we found that these TrkB puncta are located intracellular and within these cells in the direct periphery to the nucleus (**Fig. 32B**). For that reason, we further considered these TrkB puncta as kind of an aggregate of TrkB, formed in striatal cells in the absence of dopamine. In some very rare cases, similar aggregate-like structures were also evident on the intact hemisphere (**Fig. 32A white arrow**), but due to the infrequent observation of these events, we doubt that these structures are equivalents to the aggregates of TrkB on the lesioned hemisphere.

In order to confirm the observations we made using the rabbit polyclonal antibody against TrkB, we further included an antibody recognizing the C-terminus of TrkA, TrkB, and TrkC, as well as the Goat anti-TrkB (**Fig. 30**) and the antibody against the truncated receptor version (**Fig. 29C, D**). In the absence of dopamine, the panTrk antibody revealed a similar staining pattern as we observed before (**Fig. 31A, B**).

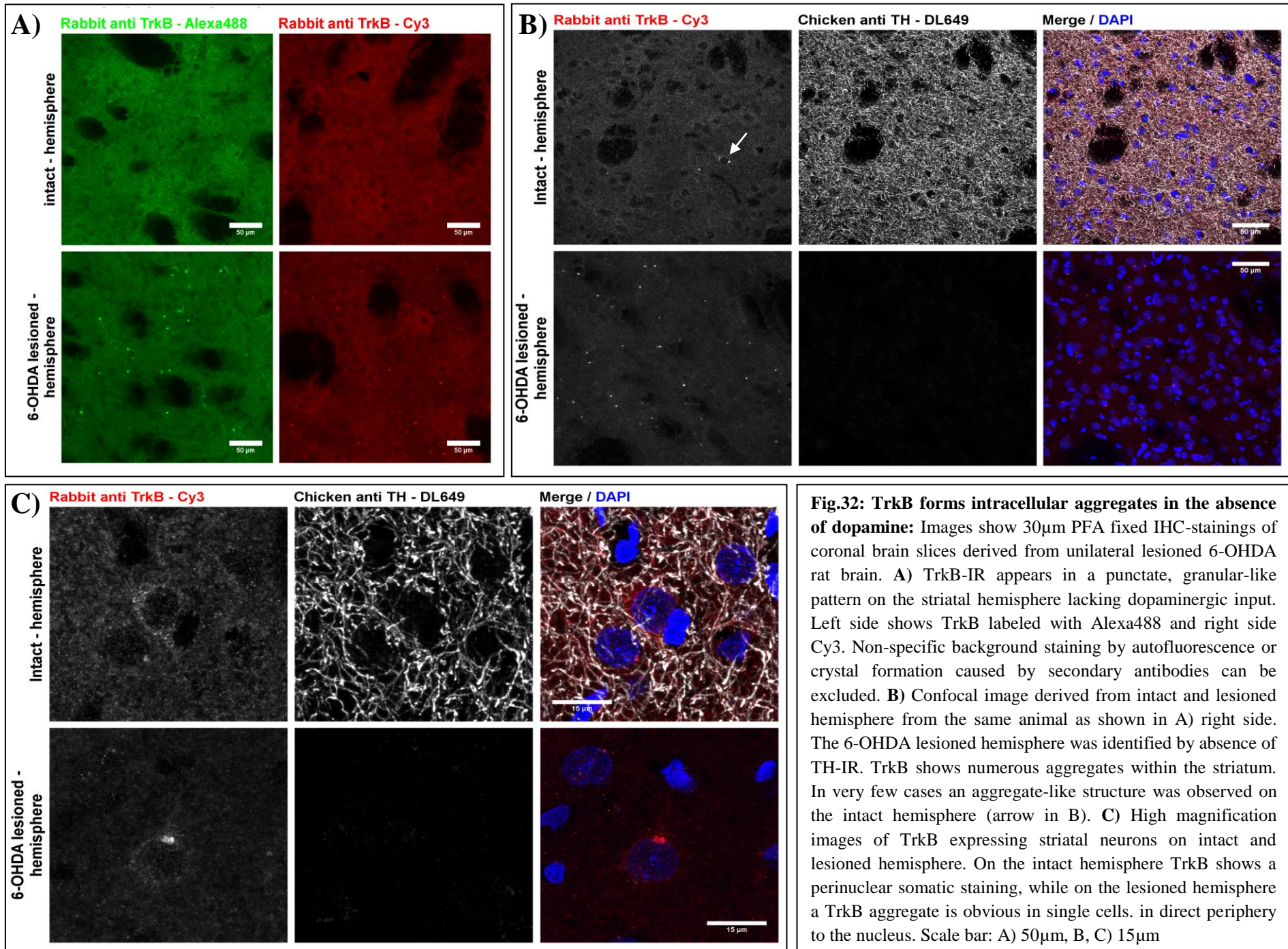


Fig.32: TrkB forms intracellular aggregates in the absence of dopamine: Images show 30µm PFA fixed IHC-stainings of coronal brain slices derived from unilateral lesioned 6-OHDA rat brain. **A)** TrkB-IR appears in a punctate, granular-like pattern on the striatal hemisphere lacking dopaminergic input. Left side shows TrkB labeled with Alexa488 and right side Cy3. Non-specific background staining by autofluorescence or crystal formation caused by secondary antibodies can be excluded. **B)** Confocal image derived from intact and lesioned hemisphere from the same animal as shown in A) right side. The 6-OHDA lesioned hemisphere was identified by absence of TH-IR. TrkB shows numerous aggregates within the striatum. In very few cases an aggregate-like structure was observed on the intact hemisphere (arrow in B). **C)** High magnification images of TrkB expressing striatal neurons on intact and lesioned hemisphere. On the intact hemisphere TrkB shows a perinuclear somatic staining, while on the lesioned hemisphere a TrkB aggregate is obvious in single cells. in direct periphery to the nucleus. Scale bar: A) 50µm, B, C) 15µm

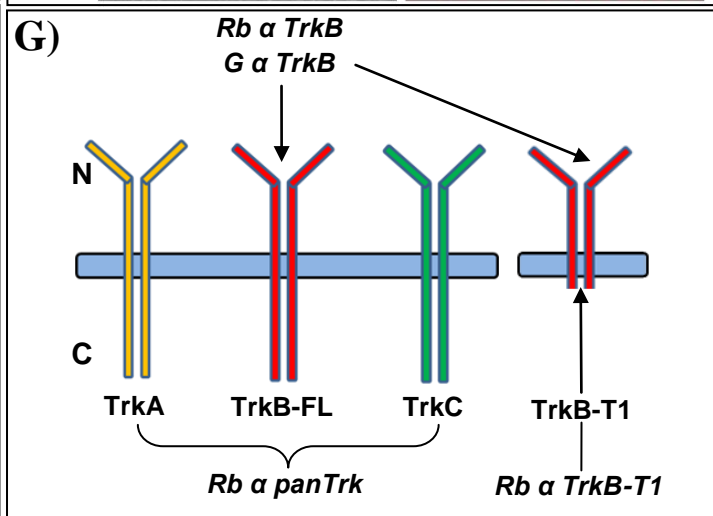
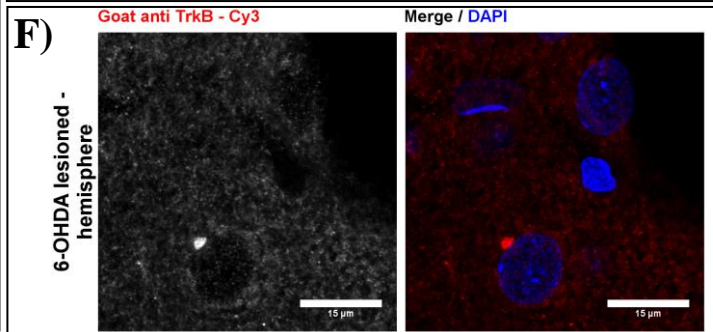
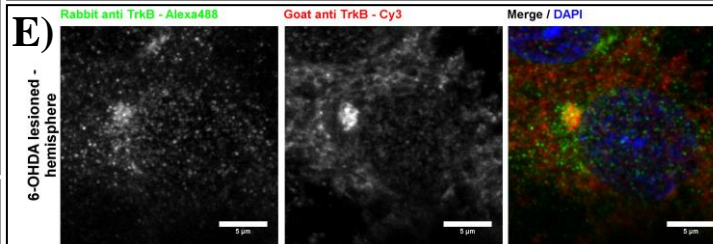
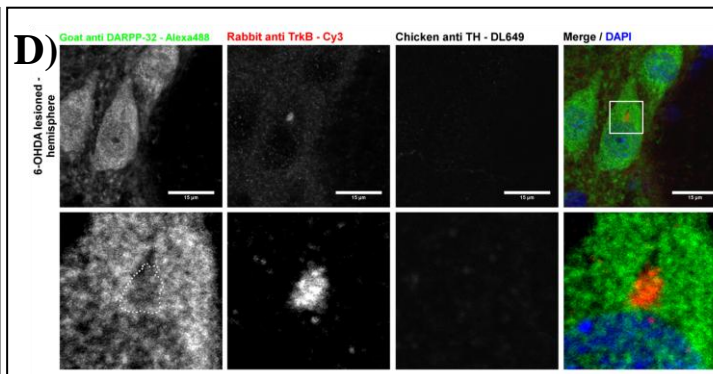
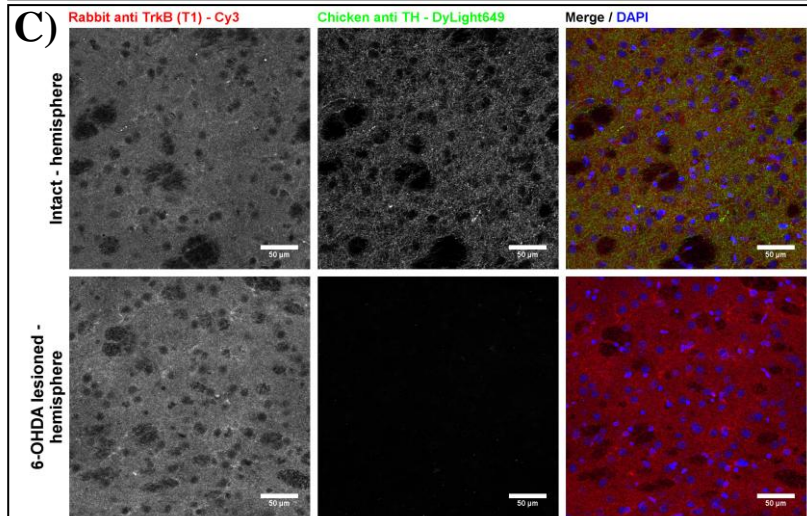
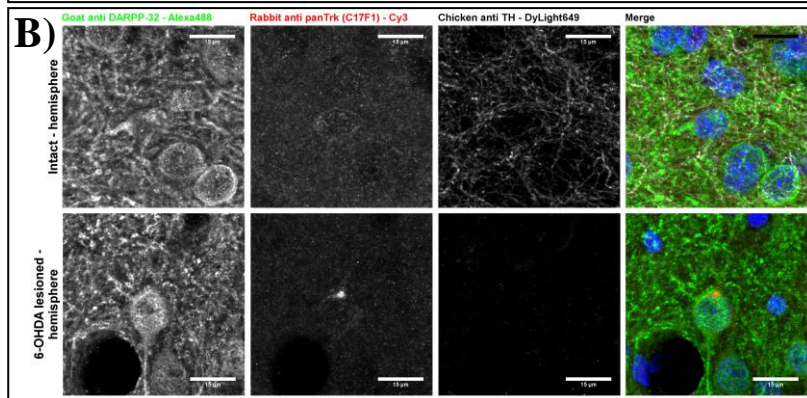
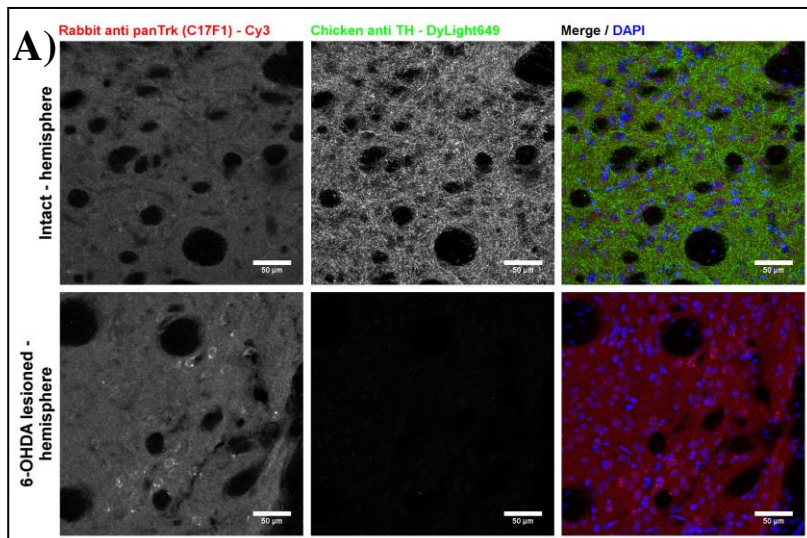


Fig.33: TrkB-FL is the main component of intracellular aggregates: Images show 30μm PFA fixed IHC-stainings of coronal brain slices derived from rat brain. **A)** Confocal image of panTrk-IR on both intact and lesioned hemisphere. Pan-Trk-IR reveals aggregate formation in the absence of dopamine (lower row). **B)** High resolution confocal image from the same animals as shown in A), indicating that panTrk aggregates form in DARPP-32 positive MSNs. On intact hemisphere, panTrk shows weak perinuclear like staining pattern in single DARPP-32 positive MSNs. On the dopamine depleted hemisphere, single MSNs show a strong pan-Trk aggregate which was exclusively found in DARPP-32 positive MSNs. **C)** TrkB-T1-IR reveals no obvious difference between intact and dopamine depleted hemisphere and no formation of aggregate-like structures. **D)** The Rabbit polyclonal antibody against the N-terminus of TrkB identifies significant TrkB aggregates exclusively in DARPP-32 positive MSNs. Note that not all MSNs are affected. **E)** Combined application of Rabbit and Goat polyclonal antibody against the N-terminus of TrkB. Both antibodies detect the TrkB aggregate. TrkB-IR by the Rabbit antibody appears weaker in this combined staining approach. **F)** Goat polyclonal anti TrkB identifies a clear intracellular aggregate, when applied alone. **G)** Schematic drawing of Trk receptors and antibodies used including their binding epitopes. Rabbit and Goat anti TrkB target the N-terminus of TrkB-FL and TrkB-T1. Pan-Trk binds to C-terminus of TrkA, B and TrkC. Rabbit anti TrkB-T1 recognizes the C-terminus of the truncated TrkB receptor. N-terminus (N), C-termini (C) Scale bar: A, C) 50μm; B, D, F) 15μm; E) 5μm

At higher resolution and by including DARPP-32-IR, we found that these aggregates occur in some but not all striatal MSNs, regardless of using TrkB antibodies against C-terminus (**Fig. 33B**) or N-terminus (**Fig. 33D**). The aggregate seems to form a gap in the cytoplasm, offering the possibility that the structure is surrounded by a membrane within an intracellular compartment (**dashed line in Fig. 33D**). Furthermore, the staining pattern by the panTrk antibody perfectly reflected the observations with the rabbit polyclonal TrkB antibody (**compare Fig. 33A, B and Fig 32B, C**). This means a perinuclear somatic staining on the intact hemisphere and an aggregate formation in nuclear periphery on the lesioned hemisphere. In contrast, when we used the TrkB-T1 antibody on the intact, as well as on the lesioned hemisphere, both were indistinguishable and we did not observe any form of aggregate (**Fig. 33C**). This suggests that it is indeed TrkB-FL aggregating in striatal MSNs and confirms our *in vitro* results that TrkB-T1 is preferentially expressed in striatal astrocytes and TrkB-FL in striatal MSNs (**Fig. 29**). Finally, we also tested the goat polyclonal antibody against TrkB. We found the same aggregate as with the rabbit polyclonal antibody, even though the TrkB-IR appeared weaker for the rabbit antibody as when it is stained alone (**Fig. 33E**). We suggested that both antibodies compete for binding epitopes at the N-terminus of the receptor. Nevertheless, the goat anti TrkB antibody appeared to have a much higher affinity for TrkB compared to the rabbit equivalent. Indeed, we found strong TrkB-IR and a clear aggregate of TrkB even at much lower antibody concentration (**Fig. 33F**). The binding epitopes and target sites of the different antibodies used in this experiment are summarized in **Fig. 33G**. Altogether, we found that TrkB forms intracellular aggregates in striatal MSNs in the absence of dopaminergic innervation. The same aggregate was identified by two TrkB antibodies against the N-terminus and by a pan-Trk antibody which targets the C-terminus of TrkA, TrkB, and TrkC. An antibody against the truncated TrkB-T1 version failed to detect any aggregate. This suggests that it is indeed TrkB-FL which aggregates at a perinuclear position in DARPP-32 positive striatal MSNs and confirms our observations about TrkB

expression *in vitro*. Nevertheless, we cannot rule out that other Trk receptors might also be affected and accumulate in the same place. In the next experiment, we attempted to identify the type of striatal neuron which is affected by TrkB aggregate formation.

5.12 TrkB aggregates specifically form in MSNs of the direct pathway

Since striatal MSNs appear similar in shape and size, it is very hard to distinguish them, unless making use of specifically expressed marker proteins or transgenic model systems. Even though it was shown that dMSNs express DRD1, Dynorphin, and Substance P (Penney and Young, 1983; Alexander and Crutcher, 1990; Gerfen, 1992; Gerfen and Surmeier, 2011), it remains difficult to identify these cells by marker expression. The reason for this is either the absence of specific antibodies or low abundance of target proteins. DRD2 expressing iMSNs instead can be identified by the expression of Enkephalin (Chesselet and Graybiel, 1983; Beckstead and Kersey, 1985) which is an endogenous opioid peptide that can be found in dense core vesicles (Cheng et al., 1995). It produces a strong somatic immunoreactivity which reflects cell shape and enables the identification of particular cells, expressing this marker (Dieni et al., 2012). For this reason, we decided to use Met-Enk expression in order to distinguish iMSNs from dMSNs. We stained Met-Enk on DRD1-EGFP and DRD2-EGFP derived striatum in order to test the specific expression of Met-Enk in iMSNs (**Fig. 34A, B**). Indeed, we observed that Met-Enk-IR and GFP-IR on DRD1-EGFP derived striatum occurred in separated cell populations, indicating that dMSNs do not express significant amounts of Met-Enk (**Fig. 34A**). In comparison, iMSNs identified by GFP-IR on DRD2-EGFP derived striatum showed significant co-expression with Met-Enk (**Fig. 34A, B**). Thus we confirmed that Met-Enk is specifically expressed in striatal iMSNs, rather than in neighboring dMSNs, both of which expressed DARPP-32 (**Fig. 32B**). In comparison to mice which enable transgenic manipulation, rats are not amenable to induction of mutations. For that reason, the

discrimination between the direct and indirect pathway MSNs is only feasible by using marker expression like Met-Enk, rather than transgenic GFP expression. Protein expression and mRNA analysis in the past found that Met-Enk is upregulated in dopamine-depleted striatal MSNs (Gerfen et al., 1991; Levy et al., 1995; Koizumi et al., 2013). We observed the same phenomenon, namely a significant increase in Met-Enk-IR on the lesioned striatal hemisphere which enabled the clear identification of these iMSNs (**Fig. 34C**). Again we observed obvious TrkB aggregates and increased TrkB-IR in the soma of single MSNs (**Fig. 34D**). Interestingly, all MSNs containing an aggregate of TrkB failed to express Met-Enk (**Fig. 34D**). Neighboring Met-Enk positive iMSNs did not show any significant somatic TrkB-IR. For this reason, we conclude that the formation of TrkB aggregates is restricted to DRD1 expressing MSNs of the direct pathway and occurs exclusively in absence of dopaminergic input. Following our hypothesis, DRD1 activation and $G_{\alpha s}$ mediated stimulation of AC-1 leads to an increase of intracellular cAMP levels which may cause TrkB export to the cell surface. We suggested that in the absence of DRD1 activation, TrkB might either be retained in the secretory pathway or accumulates after increased import via endocytosis. For this reason, we aimed to identify the compartment in which TrkB forms these aggregates.

5.13 TrkB aggregates occur in the endocytic rather than in the secretory pathway

Following our hypothesis, we suggested that in the absence of DRD1 signaling which normally increases cAMP levels, TrkB export might be disturbed. The aggregates of TrkB that we indeed found in dMSNs might be the receptor which is either retained within the ER or forms an aggregate due to an increase in import of TrkB from the cell surface and false recycling. For this reason, we analyzed TrkB aggregate formation in either the secretory or endocytic pathway, using appropriate markers (**Fig. 35**). To first address the question of whether TrkB

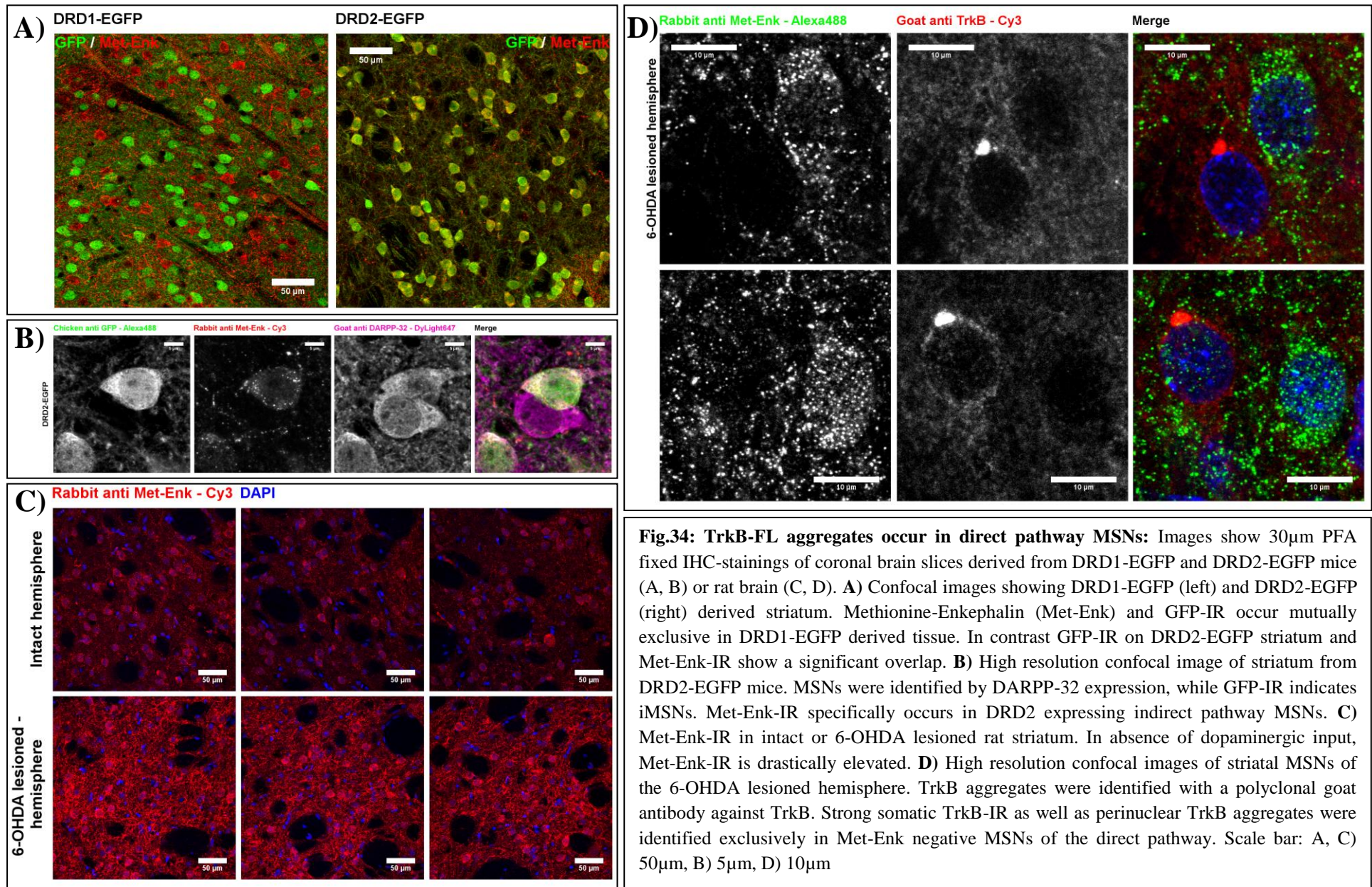


Fig.34: TrkB-FL aggregates occur in direct pathway MSNs: Images show 30 μ m PFA fixed IHC-stainings of coronal brain slices derived from DRD1-EGFP and DRD2-EGFP mice (A, B) or rat brain (C, D). **A)** Confocal images showing DRD1-EGFP (left) and DRD2-EGFP (right) derived striatum. Methionine-Enkephalin (Met-Enk) and GFP-IR occur mutually exclusive in DRD1-EGFP derived tissue. In contrast GFP-IR on DRD2-EGFP striatum and Met-Enk-IR show a significant overlap. **B)** High resolution confocal image of striatum from DRD2-EGFP mice. MSNs were identified by DARPP-32 expression, while GFP-IR indicates iMSNs. Met-Enk-IR specifically occurs in DRD2 expressing indirect pathway MSNs. **C)** Met-Enk-IR in intact or 6-OHDA lesioned rat striatum. In absence of dopaminergic input, Met-Enk-IR is drastically elevated. **D)** High resolution confocal images of striatal MSNs of the 6-OHDA lesioned hemisphere. TrkB aggregates were identified with a polyclonal goat antibody against TrkB. Strong somatic TrkB-IR as well as perinuclear TrkB aggregates were identified exclusively in Met-Enk negative MSNs of the direct pathway. Scale bar: A, C) 50 μ m, B) 5 μ m, D) 10 μ m

is retained within the ER, we co-stained with Calreticulin (ER-lumen) and Calnexin (ER-membrane). In confocal stainings, we were not able to see any co-localization between TrkB and either of the two markers (**Fig. 36A**). In contrast, especially Calreticulin-IR revealed the formation of a gap-like structure at the same position as TrkB forms an aggregate (**Fig. 36A arrow**). This observation appears like TrkB is displacing the ER which can be interpreted in two ways. First, TrkB forms a very dense aggregate within the ER which displaces the ER-

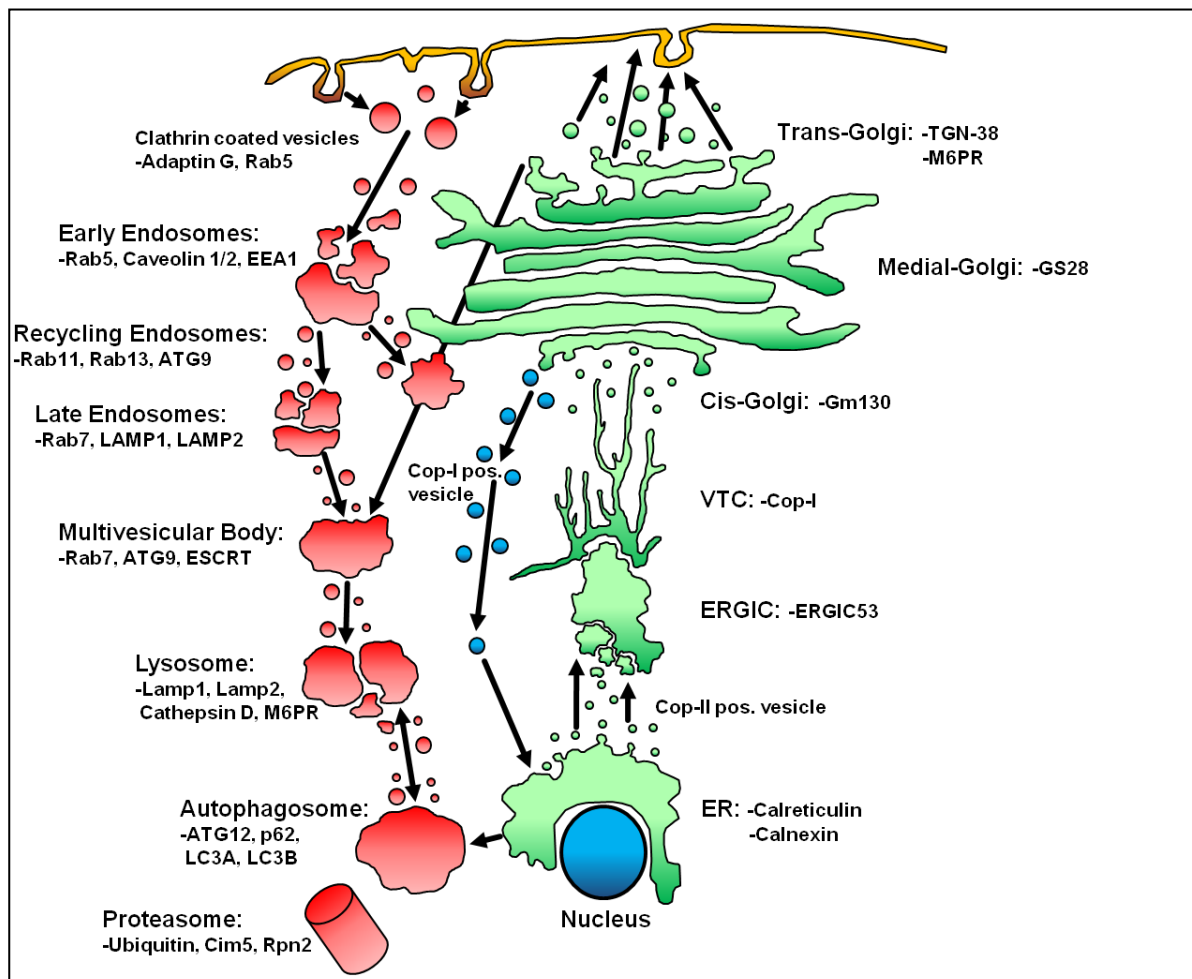


Fig.35: Simplified model of the secretory and endocytic pathways: Secretory pathway is depicted in green and endocytic pathway in red. Arrows indicate either anterograde transport to the cell surface through the secretory pathway or retrograde transport after import from the cell surface towards the soma via the endocytic pathway. Abbreviations: ER-Endoplasmatic Reticulum; Cop I / Cop II - Coat Protein I / II; ERGIC - ER-Golgi Intermediate Compartment; VTC - Vesicular Tubular Cluster; Gm130 - (cis) Golgi Matrix Protein of 130kDa; GS28 - Golgi SNARE Protein of 28kDa; TGN-38 - Trans Golgi Network Protein 38; M6PR - Mannose-6 Phosphat Receptor; Rab5, 7, 11, 13 - Ras-Associated Protein 5, 7, 11, 13; EEA1 - Early Endosome Antigen 1; ATG9, 12 - Autophagy-Related Protein 9, 12; LAMP1, 2 - Lysosomal Associated Membrane Protein 1, 2; ESCRT - Endosomal Sorting Complex Required for Transport; LC3A, B - Microtubule-associated proteins 1A/1B light chain 3A, B; Cim5 - 26S Proteasome AAA-ATPase Subunit RPT1; Rpn2 - Ribophorin-2.

luminal Calreticulin. Second, TrkB forms an accumulation outside the ER but displaces the whole ER compartment due to the size of the aggregate. Nevertheless, the resolution of a confocal microscope might be too limited to resolve these closely associated structures. To test this, we analyzed the same staining with SIM (~110-120nm) high resolution and dSTORM super-resolution (~20nm) microscopy (**Fig. 36B, C**). In both cases, the ER-gap formation was clearly evident with Calreticulin (**Fig. 36B, C**), but also with Calnexin (**Fig. 36B**). Within this gap, we observed the TrkB aggregate that does not show any overlap in immunoreactivity. Especially with dSTORM, we found that the TrkB aggregate is not contained within the ER-lumen, since it is surrounded but not associated with the Calreticulin-IR signal. Approaches visualizing membranes, like electron microscopy, are required to finally clarify this point. We next analyzed TrkB aggregate formation in the cis-Golgi-apparatus (**Fig. 36D**). Even though weak GM130-IR was observed closely associated with TrkB (**Fig. 36D arrow**), this signal appeared of unusual shape compared to the Golgi-cisternae, usually labeled by GM130. Again, we observed a gap formation in the Calreticulin-IR, surrounding TrkB. Finally, we wanted to find out if the trans-Golgi, the exit structure of proteins leaving the Golgi-apparatus and heading towards their destination, might contribute to TrkB aggregation. Even though we observed clear trans-Golgi staining by TGN-38-IR in both confocal (**Fig. 36E top**) and SIM (**Fig. 36E bottom**) staining approaches, both failed to indicate TrkB localization in the trans-Golgi network. From these results, we conclude that the formation of TrkB aggregates is rather uncertain to occur within the secretory pathway. To further support our idea that TrkB aggregation might be due to the failure of receptor recycling after endocytosis, leading to its progressive accumulation, we investigated critical steps of the endocytic recycling pathway. To check whether endocytosis and endosome formation are affected we stained the early endosome marker Rab-5, as well as the recycling endosome marker Rab-7 which is also contained within multi-vesicular bodies (**Fig. 37A, B**).

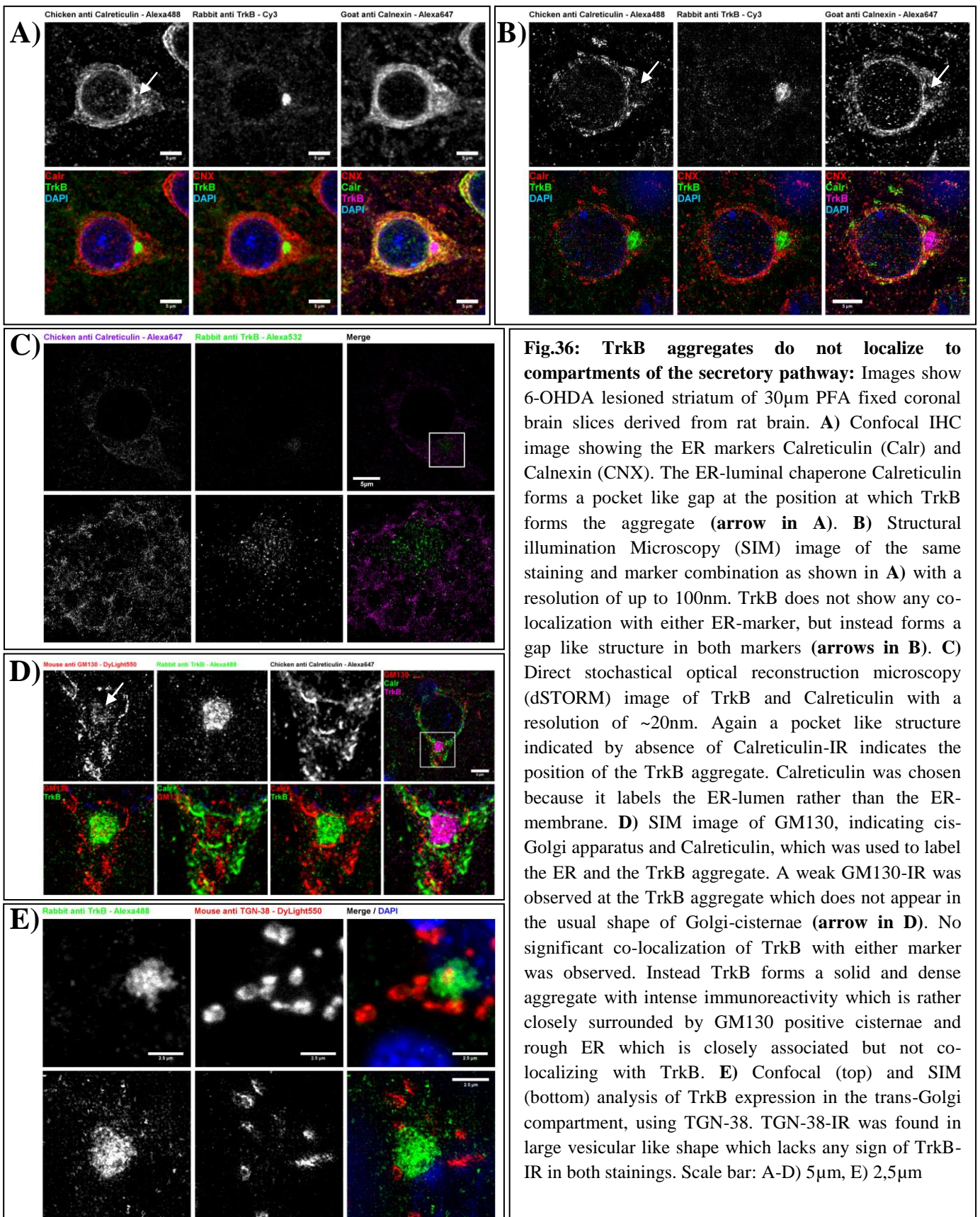


Fig.36: TrkB aggregates do not localize to compartments of the secretory pathway: Images show 6-OHDA lesioned striatum of 30µm PFA fixed coronal brain slices derived from rat brain. **A)** Confocal IHC image showing the ER markers Calreticulin (Calr) and Calnexin (CNX). The ER-luminal chaperone Calreticulin forms a pocket like gap at the position at which TrkB forms the aggregate (arrow in A). **B)** Structural illumination Microscopy (SIM) image of the same staining and marker combination as shown in A) with a resolution of up to 100nm. TrkB does not show any co-localization with either ER-marker, but instead forms a gap like structure in both markers (arrows in B). **C)** Direct stochastic optical reconstruction microscopy (dSTORM) image of TrkB and Calreticulin with a resolution of ~20nm. Again a pocket like structure indicated by absence of Calreticulin-IR indicates the position of the TrkB aggregate. Calreticulin was chosen because it labels the ER-lumen rather than the ER-membrane. **D)** SIM image of GM130, indicating cis-Golgi apparatus and Calreticulin, which was used to label the ER and the TrkB aggregate. A weak GM130-IR was observed at the TrkB aggregate which does not appear in the usual shape of Golgi-cisternae (arrow in D). No significant co-localization of TrkB with either marker was observed. Instead TrkB forms a solid and dense aggregate with intense immunoreactivity which is rather closely surrounded by GM130 positive cisternae and rough ER which is closely associated but not co-localizing with TrkB. **E)** Confocal (top) and SIM (bottom) analysis of TrkB expression in the trans-Golgi compartment, using TGN-38. TGN-38-IR was found in large vesicular like shape which lacks any sign of TrkB-IR in both stainings. Scale bar: A-D) 5µm, E) 2.5µm

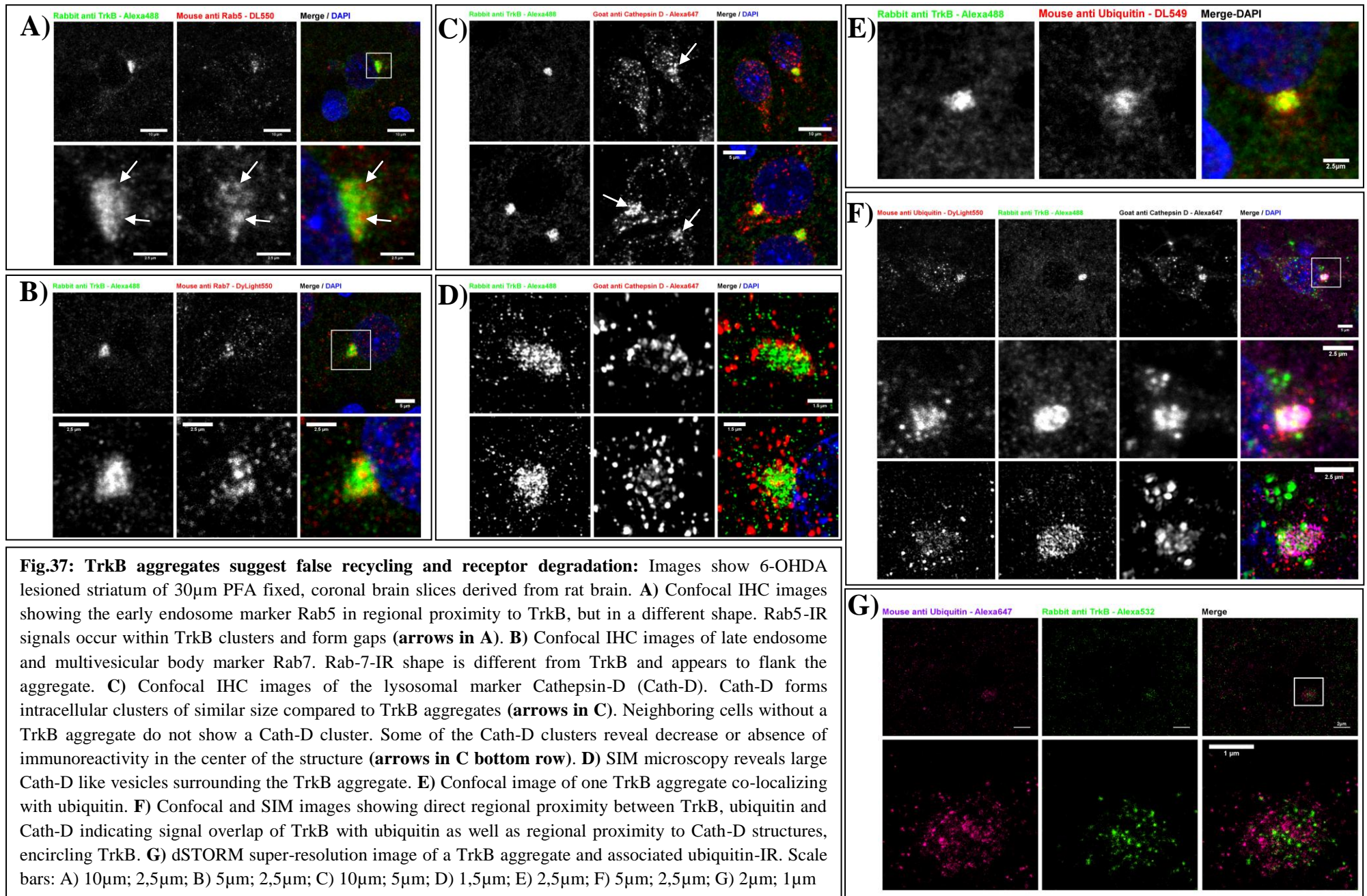


Fig.37: TrkB aggregates suggest false recycling and receptor degradation: Images show 6-OHDA lesioned striatum of 30μm PFA fixed, coronal brain slices derived from rat brain. **A)** Confocal IHC images showing the early endosome marker Rab5 in regional proximity to TrkB, but in a different shape. Rab5-IR signals occur within TrkB clusters and form gaps (arrows in A). **B)** Confocal IHC images of late endosome and multivesicular body marker Rab7. Rab-7-IR shape is different from TrkB and appears to flank the aggregate. **C)** Confocal IHC images of the lysosomal marker Cathepsin-D (Cath-D). Cath-D forms intracellular clusters of similar size compared to TrkB aggregates (arrows in C). Neighboring cells without a TrkB aggregate do not show a Cath-D cluster. Some of the Cath-D clusters reveal decrease or absence of immunoreactivity in the center of the structure (arrows in C bottom row). **D)** SIM microscopy reveals large Cath-D like vesicles surrounding the TrkB aggregate. **E)** Confocal image of one TrkB aggregate co-localizing with ubiquitin. **F)** Confocal and SIM images showing direct regional proximity between TrkB, ubiquitin and Cath-D indicating signal overlap of TrkB with ubiquitin as well as regional proximity to Cath-D structures, encircling TrkB. **G)** dSTORM super-resolution image of a TrkB aggregate and associated ubiquitin-IR. Scale bars: A) 10μm; 2,5μm; B) 5μm; 2,5μm; C) 10μm; 5μm; D) 1,5μm; E) 2,5μm; F) 5μm; 2,5μm; G) 2μm; 1μm

Even though the immunoreactivity of both markers was found to resemble the shape of the TrkB aggregate, they still differ in some aspects. First, Rab-5 appears to form smaller vesicular clusters that might indicate early endosomes. These clusters are somehow embedded within the TrkB aggregates since the Rab-5 clusters form small gaps within the TrkB signal (**Fig. 37A arrows**). We made a similar observation for Rab-7 which appears in several separate and smaller cluster-like structures in regional proximity to the solid TrkB aggregate (**Fig. 37B**). We did not observe these dense Rab-5 and Rab-7 structures in cells lacking a TrkB aggregate. We, therefore, suggest that even though there might be an unusual endosome formation and accumulation, TrkB might still be beyond this processing step of the endosomal pathway. It is possible that TrkB gets rapidly internalized, but stuck in the process of recycling or degradation. This could subsequently lead to the accumulation of TrkB instead of getting degraded or recycled. Earlier studies have shown that TrkB is preferably transported to the lysosomal degradational pathway in contrast to TrkA which is recycled at the plasma membrane (Chen et al., 2005). Similarly, it was shown that entering the degradational pathway is an efficient method to reduce receptor surface expression and subsequent reduction in exposure to certain receptor ligands and induction of downstream signaling cascades (Chen et al., 2005). Contrary, the recycling of TrkA at the plasma membrane requires a signal sequence in the C-terminal juxtamembrane of the receptor which is absent in TrkB (Chen et al., 2005). Thus, it is assumable that if TrkB is entering the degradational pathway, it might be evident within lysosomal compartments. To test this theory, we used Cathepsin D (Cath-D), a lysosomal aspartyl protease, ubiquitously expressed in lysosomes and involved in protein degradation, to identify lysosomes (Barrett, 1970; Diment et al., 1989). Indeed, we were able to identify Cath-D clusters exclusively in striatal dMSNs developing an aggregate of TrkB (**Fig. 37 C upper row**). Neighboring cells, lacking any kind of TrkB accumulation did not show a Cath-D cluster. These clusters appeared similar in shape and size compared to the TrkB aggregate. The only difference was the

reduction or absence of Cath-D-IR in the center of the cluster formation (**arrows in Fig. 37C lower row**). For that reason, we suggested that Cath-D might be part of a huge lysosomal formation containing TrkB. To test this, we performed SIM microscopy to increase optical resolution (**Fig. 37D**). We found numerous large Cath-D-positive vesicular-like structures which appear to encircle TrkB (**Fig. 37D upper row**). Anyway, these structures do not appear as a large continuous structure, but rather as an assembly of multiple sub-compartments flanking the TrkB aggregate, while only some of the Cath-D signals appear to co-localize with TrkB in the center of the aggregate (**Fig. 37D lower row, Fig. 37F**). These data suggest a defect in correct TrkB degradation in the lysosomal pathway after endocytosis. From our observations, we conclude that TrkB is not able to correctly enter the lysosome for degradation and forms an aggregate instead. This raises the question if there are alternative ways for TrkB degradation in order to prevent cytotoxicity of the aggregate formation. Alternative TrkB degradation was shown to be mediated by the proteasome which was still evident after inhibition of lysosomal degradation (Sommerfeld et al., 2000). Similarly, inhibition of proteasomal degradation efficiently stabilized TrkB (Sommerfeld et al., 2000). Even though unusual, several other reports found evidence for the degradation of transmembrane receptors via the proteasomal pathway, including receptor tyrosine kinases (Miyazawa et al., 1994; Yee et al., 1994; Mori et al., 1995; Mimnaugh et al., 1996; Jeffers et al., 1997; Magnifico et al., 1998; Sommerfeld et al., 2000). To induce this process, the targeted proteins need to be marked for degradation by poly-ubiquitination which has been demonstrated for receptor tyrosine kinases (Mori et al., 1992; Galcheva-Gargova et al., 1995; Mori et al., 1995; Sommerfeld et al., 2000). We tested for increased TrkB ubiquitination in the aggregates (**Fig. 37E-G**) and were able to observe strong ubiquitin-IR, overlapping with TrkB-IR using confocal microscopy (**Fig. 37E, F upper & middle row**), SIM (**Fig. 37F lower row**) and dSTORM (**Fig. 37G**). This ubiquitin signal appeared at the same place and in a similar shape compared to the TrkB-IR which became evident by use of high-resolution

microscopy techniques (**Fig. 37F lower row, G**). Nevertheless, not all TrkB aggregates showed ubiquitin-IR at an equivalent level. We also were able to observe TrkB aggregates that only showed weak or no ubiquitin co-staining. This might be due to the fact that the half-life of these complexes is quite short and ubiquitin tails might get rapidly removed by isopeptidases (Sommerfeld et al., 2000). Nevertheless, ubiquitination and proteasomal degradation are interesting considerable mechanisms, especially since this process appears independent of BDNF binding and in turn represents a constitutive mode of receptor turnover (Sommerfeld et al., 2000). Anyway, TrkB receptor turnover and recycling seem to be significantly disturbed in dMSNs, thus leading to the accumulation of TrkB and formation of an intracellular aggregate. It is also possible that due to a decrease in TrkB surface expression after dopamine ablation, dMSNs try to compensate for deficient TrkB signaling by upregulation of *nrk2* transcription. To test this possibility, we next wanted to investigate TrkB mRNA levels on the intact and 6-OHDA lesioned striatum. Furthermore, we wanted to know if the number of dMSNs forming these aggregates is progressively increasing over time and tried to estimate the earliest time point when the first aggregates occur after inducing the 6-OHDA lesion.

5.14 The number of TrkB aggregates remains stable over time

To estimate the occurrence and development of the TrkB aggregates, we analyzed unilateral 6-OHDA lesioned rats at 2wk, 4wk and 16wk after induction of the lesion (**Fig. 38 A, B**). When quantifying the density of aggregates, we observed significant differences between individual animals (**Fig. 38A**). Compared to this, the average number of aggregates did not change significantly over the whole 4 months (**Fig. 38B**). This observation already indicates two things. First, the full extent of aggregates is already present 2wk after lesion-induction. This implies that the aggregates occur as early as the striatal dopamine ablation is complete or

below a threshold which was shown to be ~3wk after 6-OHDA injection into the medial forebrain bundle (Sarre et al., 2004). Still, it takes ~5wk for the substantia nigra neurons to degenerate completely (Sarre et al., 2004). Subsequently, 2wk is the earliest possible time point to investigate TrkB aggregate formation, since otherwise ablation of dopamine from the striatum cannot be guaranteed. Second, since the number of TrkB aggregates remains relatively stable over a period of 16wk, they are either not degenerated, implying constant aggregate-growth, or a permanent cycle of degradation and re-formation. It is also possible cells try to compensate for inaccurate TrkB surface expression and signaling by increasing *ntrk2* transcription to increase TrkB protein levels. This implies an increase in TrkB mRNA on the lesioned hemisphere relative to the intact striatum. To test this idea, we performed Q-PCR analysis for TrkB-FL mRNA at 4wk and 16wk after induction of the lesion (**Fig. 38C**). There was no significant difference in TrkB-FL mRNA between both hemispheres, regardless of the time point analyzed (**Fig. 38C**). Nevertheless, we observed a slight but not significant trend towards a decrease of TrkB mRNA on the lesioned hemisphere (**Fig. 38C**). Since TrkB expression is normal, an accumulation of protein may be due to false degradation. A progressive intracellular accumulation of TrkB protein by the failure of degradation might also be evident by an increase in total TrkB protein on the lesioned hemisphere. To test this, we analyzed the TrkB levels in the intact and dopamine ablated striatum at 4wk or 16wk after the lesion. We observed a slight but not significant increase in TrkB protein levels on the lesioned hemisphere at both time points (**Fig. 38D, E**). Interestingly this was true for the ~130kDa TrkB-FL variant, leaving the ~90kDa band almost unchanged. This confirms our observations that the aggregate consists of the full-length variant which is preferentially expressed in striatal MSNs (**Fig. 29, 33**). Similarly, we observed a significant increase in Cath-D at 4wk, but not 16wk. This might in part reflect the clusters of lysosomal structures, surrounding the TrkB aggregates which we found in IHC stainings (**Fig. 37C, D, F**). Furthermore, we observed a slight but not significant increase in LC-3-II, a protein which

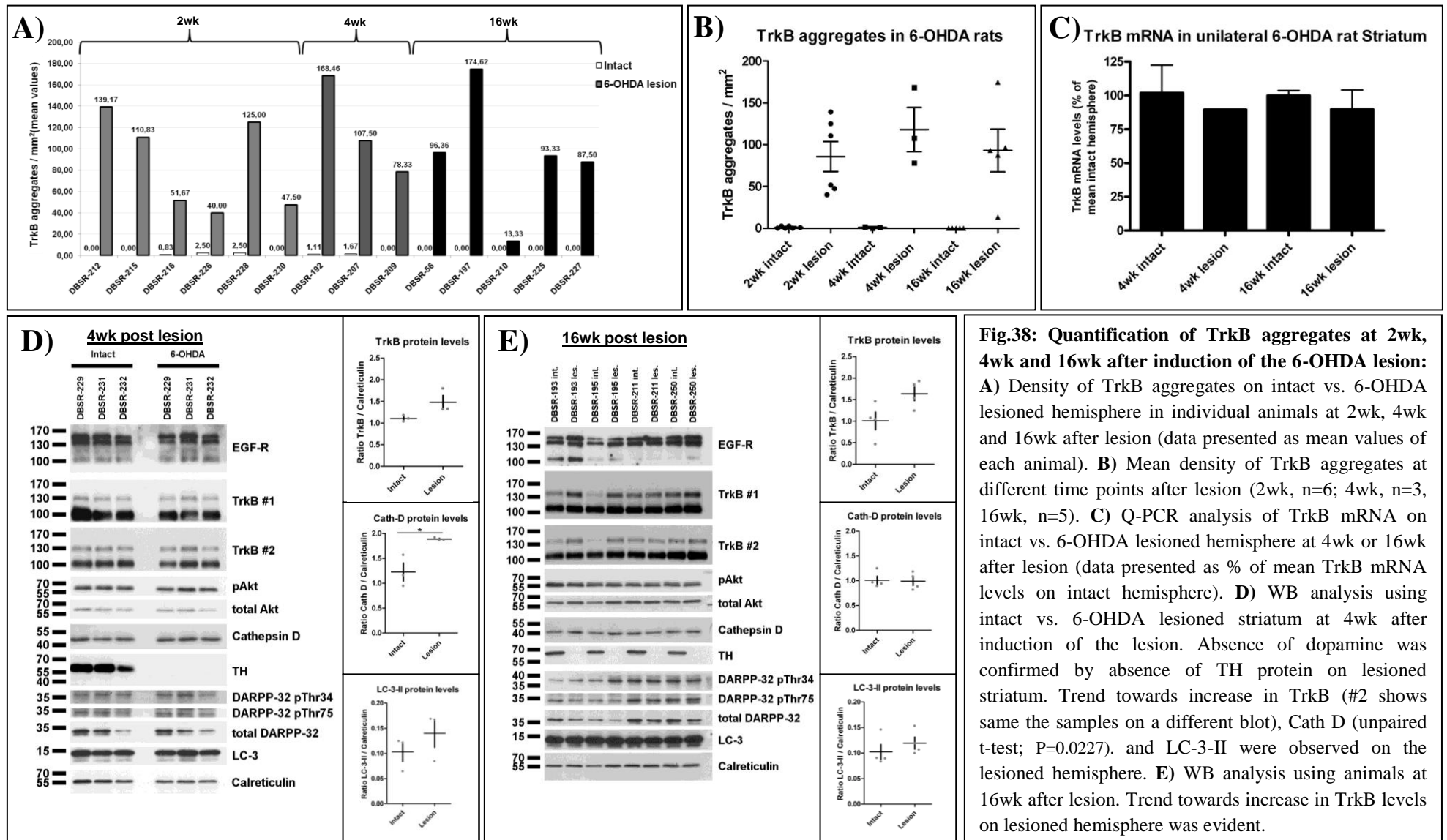


Fig.38: Quantification of TrkB aggregates at 2wk, 4wk and 16wk after induction of the 6-OHDA lesion: **A)** Density of TrkB aggregates on intact vs. 6-OHDA lesioned hemisphere in individual animals at 2wk, 4wk and 16wk after lesion (data presented as mean values of each animal). **B)** Mean density of TrkB aggregates at different time points after lesion (2wk, n=6; 4wk, n=3, 16wk, n=5). **C)** Q-PCR analysis of TrkB mRNA on intact vs. 6-OHDA lesioned hemisphere at 4wk or 16wk after lesion (data presented as % of mean TrkB mRNA levels on intact hemisphere). **D)** WB analysis using intact vs. 6-OHDA lesioned striatum at 4wk after induction of the lesion. Absence of dopamine was confirmed by absence of TH protein on lesioned striatum. Trend towards increase in TrkB (#2 shows same the samples on a different blot), Cath D (unpaired t-test; P=0.0227). and LC-3-II were observed on the lesioned hemisphere. **E)** WB analysis using animals at 16wk after lesion. Trend towards increase in TrkB levels on lesioned hemisphere was evident.

is involved in autophagosomal degradation (**Fig. 35**). We observed both, LC-3-I and LC-3-II which is the smaller version of the protein that mediates membrane fusion events (Weidberg et al., 2011). For that reason, we focused on LC-3-II rather than LC-3-I. It is still possible that a certain fraction of TrkB might be retained in the ER which is then exported to autophagosomes in order to prevent ER-stress.

In summary, these data show that even though there are individual differences in the density of TrkB aggregates between single animals, the average amount remains stable at least for 16wk. Furthermore, we found that the aggregates occur as early as the dopamine ablation is complete, leading to an increase of TrkB-FL protein on the lesioned hemisphere, while mRNA levels appear unchanged. Finally, lysosomal and autophagosomal proteins show a slight trend towards an increase in protein levels. This might indicate intensified efforts of the cellular machinery to degrade the TrkB aggregates which obviously fails or is insufficient.

5.15 Translocation of TrkB in striatal MSNs *in vitro*

By using the 6-OHDA *in vivo* model system of striatal dopamine ablation, we observed a significant effect on TrkB localization within dMSNs. We hypothesized that due to DRD1 mediated stimulation of AC-1 and subsequent increase in intracellular cAMP levels, TrkB might get recruited to the cell surface (**Fig. 6**) which was shown before, for cAMP in general (Meyer-Franke et al., 1998) and for DRD1 activation, in particular (Iwakura et al., 2008). At basal conditions, spontaneous activity in midbrain dopaminergic neurons provides a constant baseline level of dopamine in postsynaptic structures which is called "tonic" dopamine state (Grace, 1991; Floresco et al., 2003; Grace et al., 2007). In striatal MSNs, this tonic state may cause an equilibrium between TrkB export and import followed by degradation, keeping TrkB surface expression levels on an average "baseline level". In dMSNs, increase in firing rate of dopaminergic neurons could then change this equilibrium towards elevated TrkB surface expression. Such an effect was indeed described after stimulation of DRD1 expressing dMSNs with suitable agonists *in vitro*, but the exact mechanism remains elusive (Iwakura et al., 2008). If this observation is comparable to an *in vivo* system, TrkB surface expression in dMSNs would be at "baseline levels" in normal rats and might decrease in absence of dopamine. Indeed, we found evidence for the latter case in the 6-OHDA model, indicated by intracellular aggregates of TrkB in dMSNs (**Fig. 34D**). Since DRD1 mediated mechanisms are relatively well described in dMSNs, the role of DRD2 in iMSNs remains rather elusive. This is a contentious issue since it was shown that the role of TrkB in iMSNs might be even more important because the receptor is preferentially expressed in these MSNs (Baydyuk et al., 2011). Following our hypothesis, activation of DRD2 leads to a decrease in cAMP levels which would attenuate TrkB export and surface expression. In contrast, ablation of dopamine which is the case in 6-OHDA lesioned striatum would abolish DRD2 activity, including the inhibitory effect on AC-1 and subsequently increase cAMP levels which could facilitate TrkB surface expression. Nevertheless, we could not see such an effect in the striatum which might

be due to the fact that a limited number of TrkB is distributed among a huge cell-surface of an iMSN (**Fig. 34D**). To make this experiment more feasible, we wanted to address the question if DRD2 activation also contributes to TrkB translocation in an *in vitro* approach. The idea was to obtain pure cultures of iMSNs and investigate the effect of agonist-mediated DRD2 stimulation on TrkB translocation in these cells.

5.16 Fluorescence-activated cell sorting (FACS) using transgenic mice enables specific enrichment of iMSNs *in vitro*

Even though striatal MSNs comprise ~95% of striatal neurons (Kawaguchi, 1997; Bolam et al., 2000; Tepper and Bolam, 2004), the yield of MSNs in primary striatal cultures remains largely poor, ranging at around 2% (Watts et al., 1997; Penrod et al., 2011). Indeed, we were able to confirm this yield in our own primary cultures of MSNs (**Fig. 39**). Additionally, we tried to increase the amount of MSNs in these cultures by an antibody driven pull-down method called "panning" which is successfully used to enrich motor-neurons *in vitro* (Rossoll et al., 2002). Even though we combined the use of antibodies against DRD1 / DRD2, we failed to significantly increase the concentration of medium spiny neurons (**Fig. 39B**). Another problem of these primary cultures is the presence and proliferation of glial cells (Penrod et al., 2011) which is the main cause of low MSN concentration. Since glial cells keep on proliferating, the ratio of MSNs in the culture is progressively decreasing. Nevertheless, glial cells were reported to have a positive effect on MSN survival and differentiation due to trophic support (Sebben et al., 1990; Skogh and Campbell, 2003). Nevertheless, these "mixed primary cultures" have several disadvantages. First, it is not possible to distinguish dMSNs from iMSNs since there are no morphological cues to discriminate them. Second, due to their low concentration, quantitative analysis is not feasible and will be masked by an excess of glial cells. Third, trophic effects mediated by non-MSN cells might already influence effects on TrkB translocation or transactivation

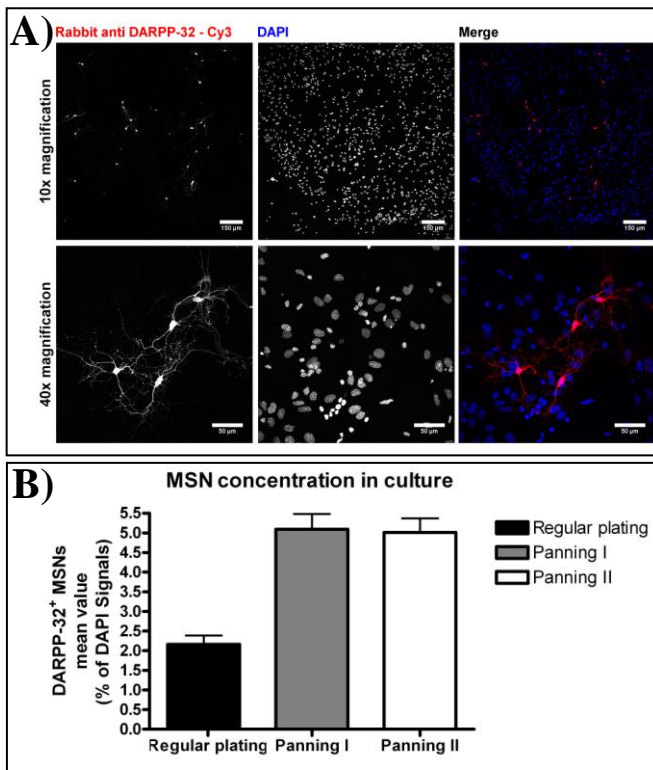


Fig.39: Concentration of striatal MSNs in primary cell culture: **A)** Primary culture of P3 striatal MSNs without panning procedure at 6DIV. Striatal MSNs of either pathway (dMSNs, iMSNs) were identified by expression of DARPP-32. DAPI was stained in order to estimate the total cell count for quantification. **B)** Quantitative analysis of DARPP-32 positive MSNs in cultures derived from regular plating (shown in A). Average concentration of medium spiny neurons in culture is approximately 2%. Additionally cell culture dishes pre-incubated with antibodies against surface epitopes like DRD2 were used, enabling a "pull-down" of MSNs which increases the concentration to 5% (Panning I). Cells that were not washed off during first run were washed again and plated (Panning II). 2 of each culture were obtained from 1 preparation and compared by analysis of confocal ICC images. Scale bar: A) upper row - 150 μ m; lower row - 50 μ m.

which we want to correlate to dopamine receptor activation. Thus, a completely non-stimulated basal state is a preconditioned starting point for the analysis of dopamine-mediated effects on TrkB. One way of achieving this is to obtain pure cultures of either dMSNs or iMSNs by FACS sorting featuring the side-effect of the complete absence of glial cells in primary cultures. For this reason, we used transgenic mice expressing GFP under control of DRD1 or DRD2 (Gong et al., 2003), in order to obtain FACS sorted MSNs. In these mice, GFP is expressed specifically in dMSNs or iMSNs respectively which enables the identification of the certain subtype *in vivo*. Before obtaining cell cultures, we confirmed specific GFP expression *in vivo* at P1 which is the time point used for cell culture preparation and compared this pattern to adult mice (**Fig. 40**). Since all transgenic mice were kept in a FVB genetic background, WT FVB mice were used as a negative control indicating the absence of GFP-IR from striatum at both time points, P1 and P77 (**Fig. 40A**). In contrast, strong GFP-IR was evident in striatum and Globus Pallidus of DRD2-EGFP mice (**Fig. 40C**). The projections of iMSNs terminate in the external segment of the globus pallidus (GPe) which was also evident in IHC stainings (**Fig. 40C row 2, 4**, for morphology compare **Fig.**

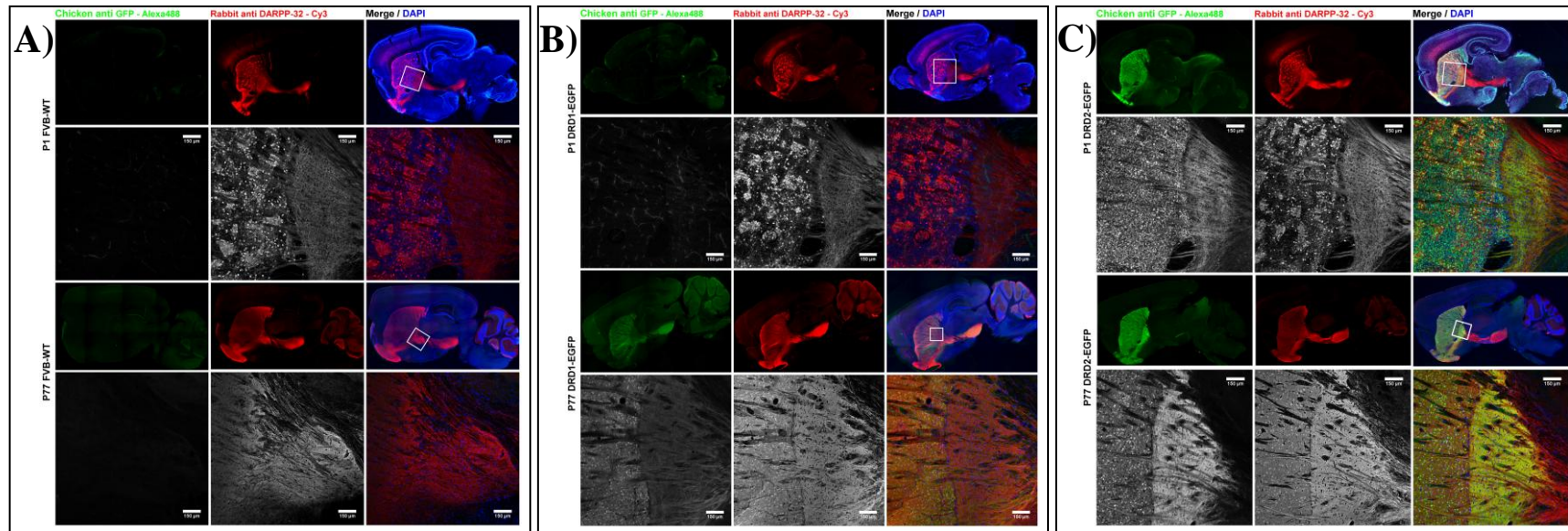
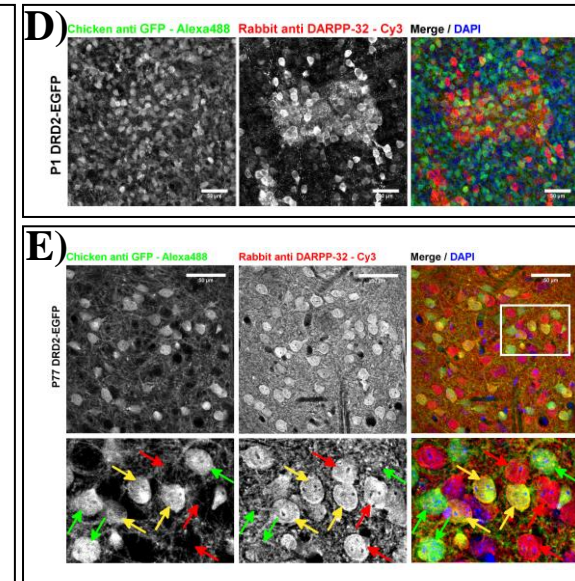


Fig.40: DRD1-EGFP and DRD2-EGFP mice *in vivo* expression analysis: A-C) Overview and confocal images showing IHC for GFP and DARPP-32 on sagittal brain slices of FVB-WT (A), DRD1-EGFP (B) and DRD2-EGFP (C). No GFP-IR was evident in P1 or P77 brain of FVB-WT, while DARPP-32-IR was evident in striatum and striato-nigral projections (A). In DRD1-EGFP mice no GFP-IR was evident at P1, while in P77 striatum GFP-IR labeled the direct pathway MSNs (B). Projections of the direct pathway bypass the external segment of the globus pallidus, indicated by absence of GFP-IR (B-lower row). C) Strong GFP-IR was detected in indirect pathway MSNs in both postnatal stages, P1 and P77. Projections from iMSNs end in the lateral globus pallidus, indicated by strong GFP-IR (C-lower row). D) High resolution image of P1 DRD2-EGFP striatum. GFP-IR is evident in a dense pattern, equally distributed throughout the striatum. In contrast DARPP-32 shows a patch like pattern at that stage with positive cells arranged in dense spots. E) P77 striatum of a DRD-EGFP mouse. Single GFP positive cells are evident, as well as DARPP-32-IR which is equally distributed in MSNs within the striatum. Three distinct populations of cells were identified. 1.) DARPP-32 positive, which represent dMSNs (red arrows). 2.) DARPP-32 / GFP positive which represent iMSNs (yellow arrows). 3.) GFP positive but DARPP-32 negative cells (green arrows), which might indicate DRD2 expressing interneurons. Scale bar: A, B, C) 150 μ m; D, E) 50 μ m



2). Compared to iMSNs, dMSNs bypass the GPe and directly target the internal segment of the Globus Pallidus (GPi) as well as the substantia nigra in the midbrain. Similarly, GFP-IR was absent in the GPe, while strong staining was evident in striatonigral projections in adult mice (**Fig. 40B row 3, 4**). Interestingly no GFP-IR was evident in P1 newborn DRD1-EGFP mice (**Fig. 40B row 1, 2**). Anyway, correct genetic and transgenic background was confirmed by PCR for each individual animal displayed (**Fig. 41A**). Thus, there might be an insufficient transcription of GFP from the locus of insertion. To test this, we dissected the striatum of FVB-WT, DRD1-EGFP as well as DRD2-EGFP mice at P1 and assessed GFP mRNA levels by Q-PCR (**Fig. 41B**). Compared to DRD2-EGFP mice, there was almost no GFP mRNA evident in DRD1-EGFP animals. In contrast, the mRNA levels were only slightly above the WT negative control which confirmed our suggestion that the transcription of GFP at P1 is too low in DRD1-EGFP mice to detect GFP protein. Nevertheless, GFP expression appeared normal in adult DRD1-EGFP animals at P77, even though the GFP-IR appeared weaker compared to DRD2-EGFP mice (**Fig. 40B, C row 3, 4**). Higher resolution of P1 striatum also revealed a patchy pattern of DARPP-32 expressing cells, independent of the genetic background (**Fig. 40D**). These patches which represent a conglomerate of DARPP-32 positive cells were originally identified to be striosomal

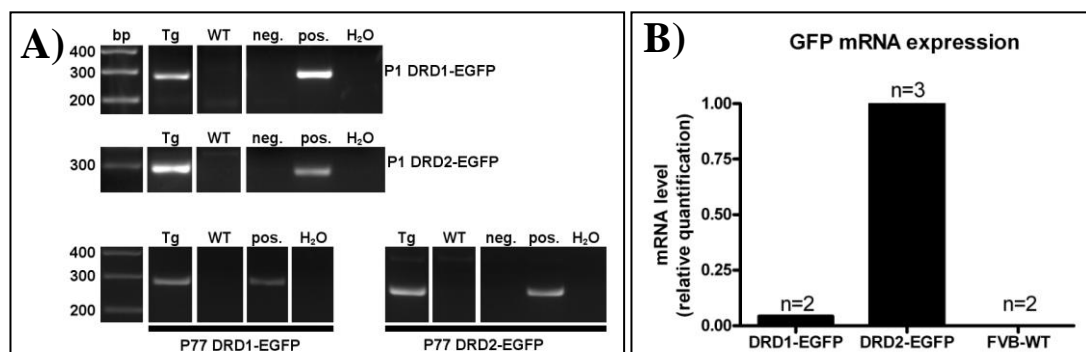
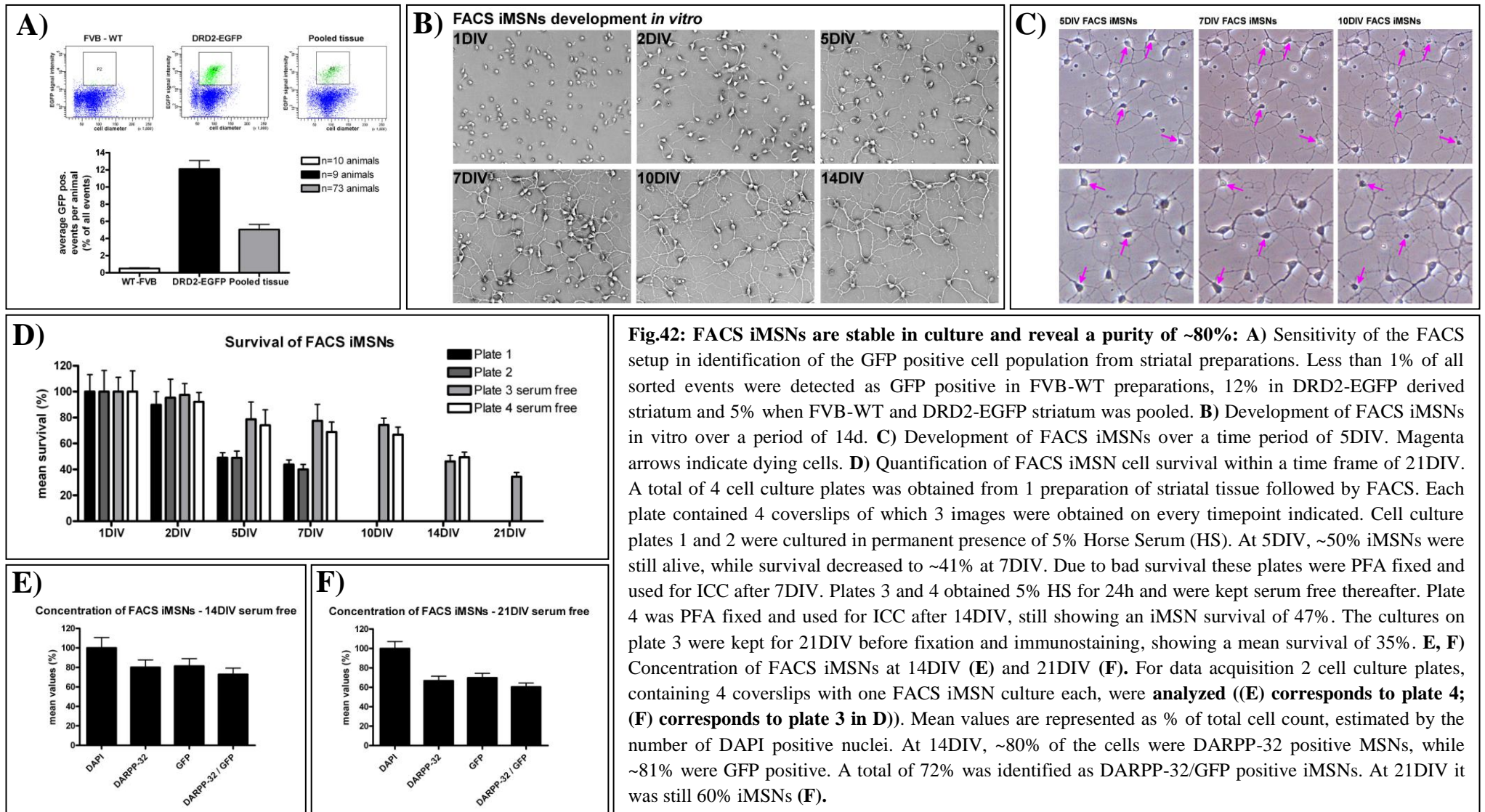


Fig.41: Newborn DRD1-EGFP mice fail to express GFP mRNA: **A)** Genotyping PCR indicating correct identification of genetic background. PCR corresponds to animals represented in Fig. 38. bp - base-pairs; Tg - transgenic animal; WT - Wild Type control animal; neg. - Wild Type PCR control; pos. - transgenic PCR control; H₂O - DNA free negative control. **B)** Q-PCR analysis of striatal GFP mRNA levels. P1 DRD1-EGFP mice show very low GFP-mRNA compared to DRD2-EGFP striatum, which was used as reference. No GFP mRNA was evident in FVB-WT control animals.

formations occurring during embryogenesis and early postnatal life (Anderson et al., 1997; Passante et al., 2008). These patches were not evident in adult animals at P77 anymore (**Fig. 40E**). Anyway, in DRD2-EGFP mice we observed three distinct cellular populations within the striatum when co-stained with DARPP-32 (**Fig. 40E**). The first population expressed only DARPP-32 lacking GFP-IR which identifies these cells as medium spiny neurons of the direct pathway (dMSNs) since these cells lack DRD2 (**Fig. 40E red arrows**). The second population is DRD2 expressing iMSNs indicated by GFP and DARPP-32-IR within the same cell (**Fig. 40E yellow arrows**). Finally, we observed a third population which lacks any DARPP-32-IR but still shows GFP-IR (**Fig. 40E green arrows**). This could be due to tissue penetration issues resulting from the DARPP-32 antibody failing to stain MSNs that were actually positive for this marker. Nevertheless, we cannot exclude that these GFP expressing cells which lack DARPP-32 represent DRD2 expressing, large cholinergic interneurons as described before (Bertran-Gonzalez et al., 2008; Matamales et al., 2009).

In summary, these data show that GFP expression in DRD2-EGFP animals is suitable to enable FACS sorting of iMSNs from striatal tissue of newborn mice. We may not prevent contamination by GFP expressing cholinergic interneurons which express DRD2 similar to iMSNs. Nevertheless, this contamination should be tolerable, as 95% of striatal neurons are MSNs, of which ~50% are iMSNs, while interneurons comprise only 5% of the neuronal population including NPY, Parvalbumin and cholinergic interneurons (Kawaguchi, 1997; Bolam et al., 2000; Tepper and Bolam, 2004). This relation is still more preferable than a mixed primary culture with only 2% total MSN concentration, of which only ~1% represents iMSNs. DRD2-EGFP mice are thus suitable for FACS sorting, in order to address the question of whether DRD2 activation causes changes in TrkB translocation *in vitro*.

In order to estimate the sensitivity of the FACS sorter regarding detection of GFP, we compared cell suspensions obtained from FVB-WT striatum, with DRD2-EGFP striatum. In



WT controls, less than 1% of all signals were accounted as "positive" which might be due to autofluorescence (**Fig. 42A**). In comparison, an average of ~12% GFP positive events was detected during the sorting process of striatal cell suspension from DRD2-EGFP mice (**Fig. 42 lane 2**). The disadvantage of these single preparations of DRD2-EGFP striatum is that even though the specificity and outcome are quite high, the time cost is enormous since the genotype of individual pups needs to be determined before preparation. For that reason we tested if it is possible to pool the tissue, making the genotyping procedure unnecessary and speeding up the work-pace. This had the advantage that sorted cells reach a viable environment on a cell culture dish much earlier. Indeed, we found convincing outcome of the sorting process, even though it was on the expense of efficacy which was reduced naturally by ~50% compared to pure DRD2-EGFP derived tissue (**Fig. 42 row 3**). After plating the FACS iMSNs, we investigated cell survival over a time period of up to 21DIV (**Fig. 42B-D**). Usually, neurons are not prone for FACS sorting due to their electro-sensitivity and general vulnerability towards physical stress as well as exposure to lasers. Nevertheless, we observed that FACS iMSNs develop normal and form neurites and protrusions already at 2DIV (**Fig. 42B**). After 14-21DIV, FACS iMSNs developed a dense network of fibers and connections between each other (**Fig. 42B 14DIV**). Even though we observed cell death in some cases (**Fig. 42C magenta arrows**), the overall quality of the cultures was in a vital shape showing ~47% survival after 14DIV and still 35% after 21DIV (**Fig. 42D**). We further observed a critical effect of the presence of serum within these FACS iMSN cultures. Since these cultures lack any presence of glial cells and trophic support required for cell survival and development (Sebben et al., 1990; Skogh and Campbell, 2003), it must be provided either way. For that reason, 5% horse serum (HS) was added to the cell culture medium, either permanently or only for 24h. We found that permanent presence of serum has a negative effect on FACS iMSN survival since ~41% of the cells were still alive after 7DIV, while it was ~73% when the serum-containing medium was replaced with serum-free medium after 24h (**Fig. 42D**).

These findings indicate that FACS of striatal MSNs is indeed feasible and that these cultures develop normal and survive long enough to enable *in vitro* approaches for biochemical and immunocytochemical analysis. In the next step, we aimed to clearly identify the sorted cells as iMSNs. Even though the morphology of these cells appears "neuron-like", we cannot exclude certain contamination by other cells than iMSNs, due to the fact that DRD2 promoter activity and resulting GFP expression is not restricted to striatal iMSNs in DRD2-EGFP mice (Mengod et al., 1989). In order to identify the FACS sorted cells as striatal medium spiny neurons, we tested for DARPP-32 expression. The vast majority of cells expressed DARPP-32 together with GFP at 7, 13, and 21 DIV (**Fig. 43**). In addition, we observed single cells that lacked DARPP-32-IR but showed strong GFP expression (**magenta arrows in Fig. 43A, B, C**). Due to the low frequency of their appearance compared to DARPP-32 expressing MSNs, it is possible that these GFP expressing DARPP-32 negative cells represent large cholinergic interneurons which were described in these DRD2-EGFP mice (Bertran-Gonzalez et al., 2008; Matamales et al., 2009). Furthermore, we observed some very few cells that showed DARPP-32 signal, but only very weak GFP-IR (**cyan arrows in Fig. 43A, B, C**). These became obvious starting from ~10-13DIV onwards (**Fig. 43B, C**). It is possible that iMSNs down-regulate their DRD2 promoter activity in these cultures, followed by a decrease of GFP even though it was reported that DRD2 mRNA increases in iMSNs in the absence of dopamine signaling *in vivo* (Gerfen et al., 1990). Nevertheless, it is also possible that single GFP negative dMSNs are integrated into these cultures caused by contamination during the FACS sorting process.

In summary, we found that the vast majority of FACS sorted cells are indeed DARPP-32 positive MSNs (**Fig. 43D row 3**). Compared to regular primary cultures obtained from WT animals (**Fig. 43D lane 1**) which do not allow the discrimination between dMSNs and iMSNs, primary cultures obtained from DRD2-EGFP mice, are already a major improvement, in order

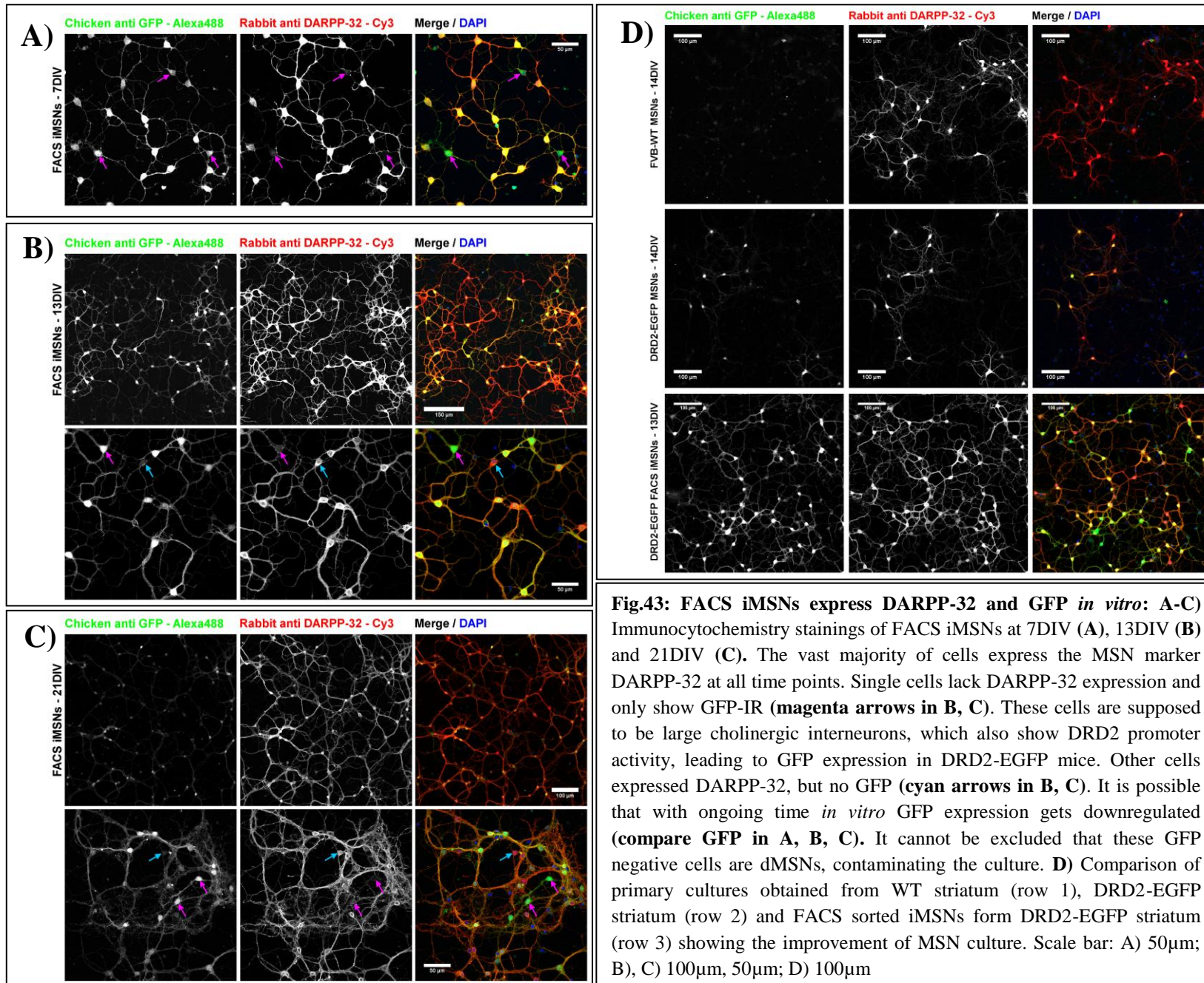
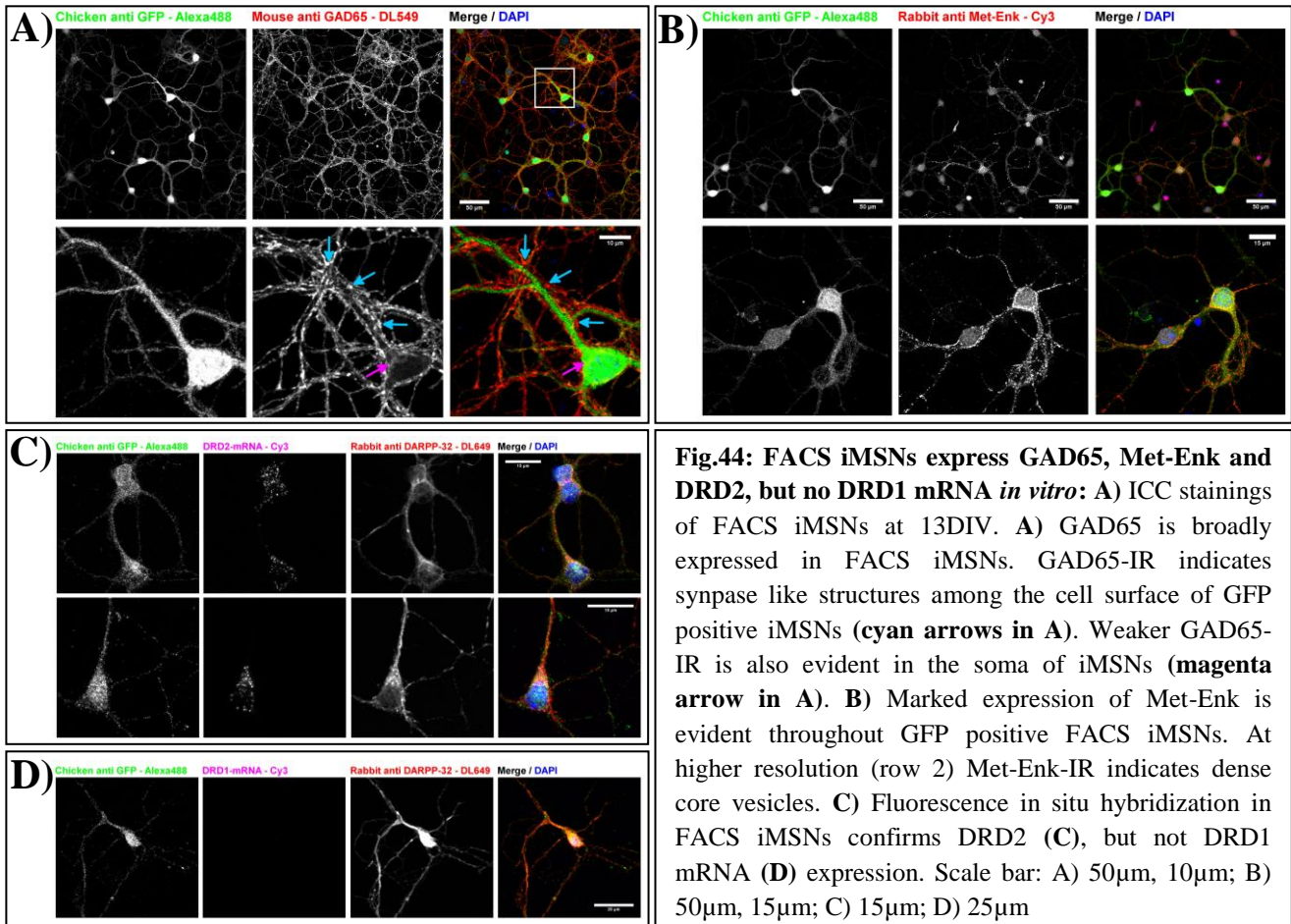


Fig.43: FACS iMSNs express DARPP-32 and GFP *in vitro*: A-C) Immunocytochemistry stainings of FACS iMSNs at 7DIV (A), 13DIV (B) and 21DIV (C). The vast majority of cells express the MSN marker DARPP-32 at all time points. Single cells lack DARPP-32 expression and only show GFP-IR (magenta arrows in B, C). These cells are supposed to be large cholinergic interneurons, which also show DRD2 promoter activity, leading to GFP expression in DRD2-EGFP mice. Other cells expressed DARPP-32, but no GFP (cyan arrows in B, C). It is possible that with ongoing time *in vitro* GFP expression gets downregulated (compare GFP in A, B, C). It cannot be excluded that these GFP negative cells are dMSNs, contaminating the culture. **D)** Comparison of primary cultures obtained from WT striatum (row 1), DRD2-EGFP striatum (row 2) and FACS sorted iMSNs from DRD2-EGFP striatum (row 3) showing the improvement of MSN culture. Scale bar: A) 50 μ m; B), C) 100 μ m, 50 μ m; D) 100 μ m

to identify iMSNs (**Fig. 43D row 2**). Anyway, glial contamination and low yield of MSNs which is ~2% complicates the investigation of specific properties of striatal MSNs. By FACS of DRD2-GFP striatal tissue, we were able to increase the yield of iMSNs to ~80% at 13-14DIV (**Fig. 42E, Fig. 43D row 3**). Another critical property of striatal MSNs is the expression of γ -butyric acid (GABA). To identify GABAergic neurons, L-glutamic acid decarboxylase (GAD) can be used as a prominent marker, an enzyme which converts glutamate into GABA. GAD exists in two isoforms GAD65 which is enriched in synaptic vesicle pools (Kaufman et al., 1991; Jin et al., 2003) and GAD67 which is spread evenly throughout the cell (Kaufman et al., 1991). Thus, we next examined the GABAergic character of these FACS sorted cultures by focusing on GAD65, the isoform associated with synaptic vesicles which might provide evidence for synapse formation in these cultures. In fact, we observed dense GAD65-IR throughout the FACS iMSNs (**Fig. 44A row 1**). At higher resolution, we also confirmed GAD65-IR in the soma of GFP positive iMSNs which provides evidence for direct expression from these neurons (**magenta arrow in Fig. 44A row 2**). Since GAD65 is an enzyme associated with GABAergic synaptic vesicles, we finally identified numerous GAD65 positive synaptic-like structures among the surface of GFP positive iMSNs (**cyan arrows in Fig. 44A row 2**). As one of the most important endogenous marker proteins for iMSNs, we sequentially used Met-Enk expression to verify iMSN identity (Chesselet and Graybiel, 1983; Beckstead and Kersey, 1985). We already showed specific expression of Met-Enk in iMSNs *in vivo* (**Fig. 34**) and were now able to corroborate this observation in FACS iMSNs *in vitro*. Met-Enk was significantly expressed in the vast majority of cells within these cultures (**Fig. 44 B**). Nevertheless, we observed that the density of Met-Enk positive dense core vesicles within FACS iMSNs was pronounced at different degrees throughout the cultures, with overall quiet high expression (**Fig. 44 B row 2**). The appearance of Met-Enk-IR in FACS iMSNs very much resembled the one observed in iMSNs in the 6-OHDA lesioned striatal hemisphere in rats lacking dopamine and thus



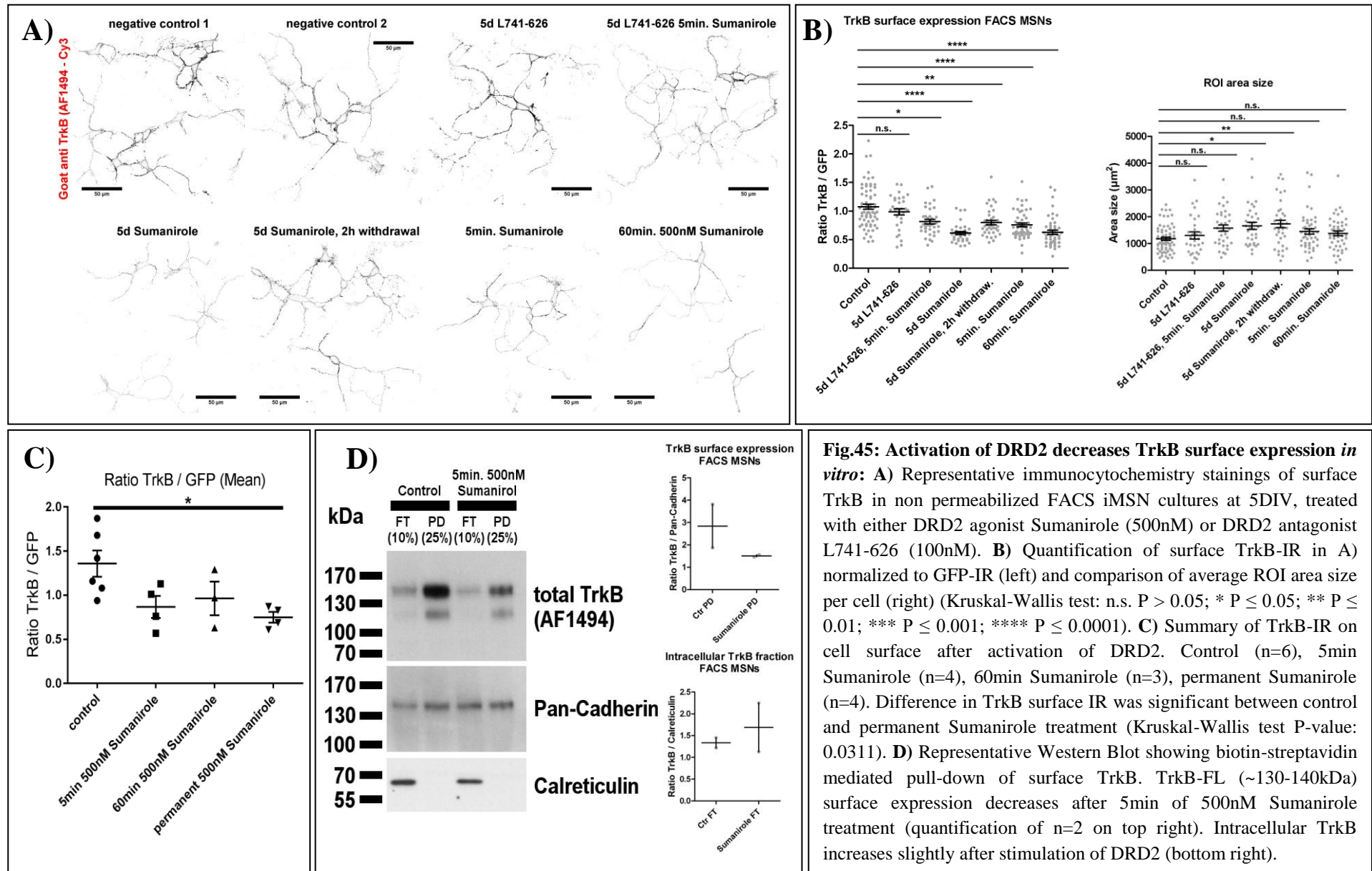
showed an upregulation of Met-Enk (Fig. 34C, D) (Gerfen et al., 1991; Levy et al., 1995; Koizumi et al., 2013). Similarly, the FACS iMSN cultures also lacked dopamine agonists and related activation of dopaminergic signaling cascades which might induce an excess of Met-Enk expression. As a final proof for the verification of iMSN identity, we confirmed the presence of DRD2 mRNA which is specific for the majority of iMSNs. We did so, by using appropriate RNA probes for *in situ* hybridization which was combined with immunofluorescence staining (Fig. 44C). Thus, we clearly identified DRD2 mRNA within the soma of FACS iMSNs. In contrast, we failed to detect DRD1 mRNA for which the expression should be restricted mainly to dMSNs in the striatum (Fig. 44D).

Altogether, we have shown that FACS of iMSNs from DRD2-EGFP striatum is a feasible way to increase the yield of iMSNs *in vitro*, from 1-2% in primary culture to ~80% at 14DIV. The identity of iMSNs was clearly confirmed by expression of DARPP-32, GAD65, Met-Enk protein and DRD2 mRNA. These cells form dense networks showing indications of synapse

formation and confirm a survival of up to 21DIV. Especially the significant enrichment of iMSNs makes this cell culture system a preferential way for *in vitro* studies of MSN modalities. Nevertheless, we also found cells that were of presumably another origin than MSN fate, as they lack DARPP-32 expression but express GFP at the same time. These cells might be large cholinergic aspiny interneurons which were described as GFP positive, due to DRD2 expression in the DRD2-EGFP transgenic mouse model system (Bertran-Gonzalez et al., 2008; Matamales et al., 2009). In the next experiment, we used these FACS iMSNs for the investigation of DRD2 mediated effects on the translocation of TrkB.

5.17 Activation of DRD2 by the high-affinity agonist Sumanitrole prevents TrkB surface expression

According to our hypothesis, we assumed that because of the GPCR family member DRD2, AC-1 gets inhibited via receptor-mediated $G_{\alpha i}$ signaling which subsequently causes a decrease in cAMP levels (De Camilli et al., 1979; Onali et al., 1981; Enjalbert and Bockaert, 1983; McDonald et al., 1984; Onali et al., 1985) (**compare Fig. 3**). Since TrkB surface expression was identified to be depending on cAMP (Meyer-Franke et al., 1998), a decrease might lead to reduced TrkB expression on the cell surface. To test this, we obtained FACS iMSNs and investigated TrkB surface expression after activating or inhibiting DRD2. To rule out transient activity of DRD2 at steady state conditions, we kept control cultures in the presence of the potent selective DRD2 antagonist L741-626 (Bowery et al., 1996; Costanza et al., 2001; Grundt et al., 2007). For TrkB visualization, we used the antibody against TrkB N-terminus derived from goat (**Fig. 30**). We did not observe a change in TrkB surface expression levels compared to non-stimulated controls which indicates that DRD2 is presumably inactive under serum-free, steady state, cell culture conditions (**Fig. 45A, B**). For induction of DRD2 signaling, we used Sumanitrole, a highly selective, potent DRD2 agonist (McCall et al., 2005; Weber et al., 2010). After stimulation of DRD2, we observed a marked



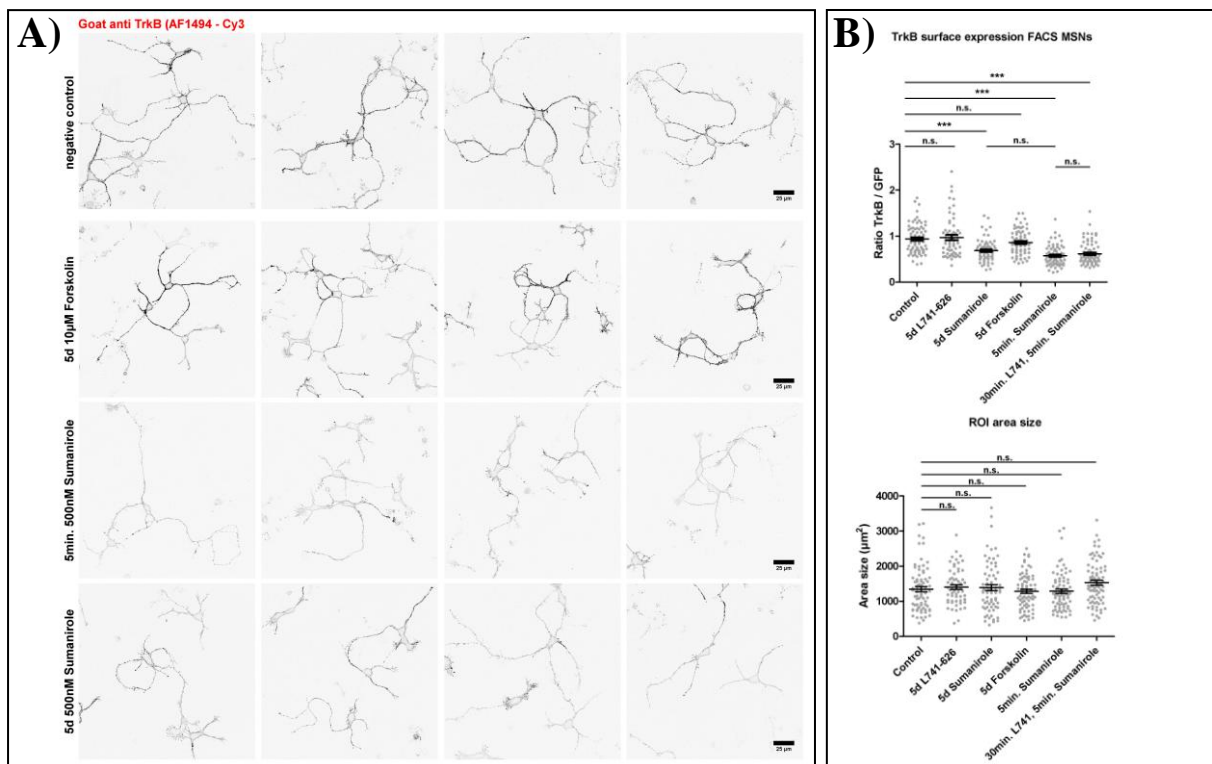


Fig.46: Maximum TrkB surface expression is already acquired under steady state conditions *in vitro*:

A) Representative immunocytochemistry stainings of surface TrkB in non permeabilized FACS iMSNs cultures at 5DIV, treated with either 10µM Forskolin or 500nM DRD2 agonist Sumanirole. **B)** Quantification of surface TrkB-IR in A) normalized to GFP-IR (negative control). Neither inhibition of DRD2 by L741-626 nor stimulation of AC-1 by Forskolin has a positive effect on TrkB surface expression. In contrast Sumanirole decreases TrkB surface expression within 5min to a level which stays the same even after 5d permanent presence of Sumanirole. 100nM L741-626 cannot inhibit the negative effect of 500nM Sumanirole on TrkB surface expression. Mean ROI area size per analyzed cell is indistinguishable in all conditions. An average number of 72 cells was analyzed for each condition (Kruskal-Wallis test: n.s. $P > 0.05$; * $P \leq 0.05$; ** $P \leq 0.01$; *** $P \leq 0.001$; **** $P \leq 0.0001$).

the decrease in TrkB surface IR as early as 5min of incubation, even after pre-treatment with L741-626 (**Fig. 45A, B, C; Fig. 46**). This might be due to the fact that even though the affinity of L741-626 ($K_i=2.4\text{nM}$) is higher than that of Sumanirole ($K_i=9,0\text{nM}$), the effect of the latter was predominant since used at a slight excess over the inhibitor. Nevertheless, the activation of DRD2 by Sumanirole caused a significant decrease of TrkB surface-IR which reached its maximum extent after 5min of incubation and remained at low levels for up to 5d in the presence of Sumanirole (**Fig. 45C**). In comparison, when FACS iMSNs were kept in the presence of 500nM Sumanirole for 5d followed by washing and replacement with agonist free cell culture medium, the TrkB surface IR levels showed signs of recovery towards control levels within 2h (**Fig. 45A, B lane 4, 5**). To test if TrkB surface expression can be facilitated, compared to steady state controls, by elevated cAMP levels, we treated FACS iMSNs with

100 μ M Forskolin which is a potent stimulator of adenylyl-cyclases, able to increase cAMP levels (Seamon et al., 1981). Anyway, we did not observe a significant difference in TrkB surface IR levels compared to non-stimulated controls (**Fig. 46A, lane 1, 2, B**). This suggests AC(-1) activity and cAMP levels at steady state conditions are sufficient to already induce maximum TrkB surface expression within iMSNs. To ensure comparability of the data not only TrkB and GFP-IR levels were obtained, but also the ROI area size per cell which critically influences IR intensity values. The mean ROI values were not significantly different from each other under most of the conditions (**Fig. 45 B, Fig. 46 B**). Nevertheless, in one experiment we observed increased cellular ROI areas, indicating larger cell size when FACS iMSNs were kept in Sumanitrole presence for 5d (**Fig. 45B**) which we did not observe, when these experiments were repeated (**Fig. 46B**). For this reason, we cannot completely exclude the trophic and morphological effects of permanent DRD2 activation on the affected iMSN development *in vitro*. In order to overcome this issue, we aimed to reproduce these data independently via TrkB surface biotinylation and WB analysis. Indeed, we found the same effect of reduced surface expression after FACS iMSNs were treated with 500nM Sumanitrole for 5min. (**Fig. 45D**). We observed a clear trend towards a decrease in TrkB surface expression, while the intracellular TrkB levels were increasing (**Fig. 45D**). As a control, we used Pan-Cadherin which identifies several isoforms of this cell surface protein which was unaffected by DRD2 activation. In summary, these data point towards a rapid effect of DRD2 activation on the decrease in TrkB surface expression levels. This effect was evident at its full extent as early as 5min and persisted for up to 5d in the presence of DRD2 agonist Sumanitrole. In contrast, there was no effect of DRD2 antagonist L741-626 which confirmed the absence of DRD2 signaling under steady state cell culture conditions, used for FACS iMSN cultures. Furthermore, we did not find evidence for a positive effect of the AC activator Forskolin on the increase in TrkB surface expression which indicates the full capacity of surface TrkB in FACS iMSNs under steady state conditions. These findings subsequently

support the idea that DRD2 signaling via $G_{\alpha i}$ attenuates AC-1 activity, causing a decrease in cAMP levels, followed by a decrease in TrkB surface expression (**compare Fig. 6**). We were wondering, if the activation of DRD2 may not only have an effect on the localization but also on the indirect activation of TrkB. For this reason, we investigated the induction of DRD2 downstream signaling cascades and induction of TrkB phosphorylation in the next experiment.

5.18 Stimulation of DRD2 with Sumanrole causes induction of pTrkB

In previous studies, evidence was found that besides activation by BDNF, TrkB can also be transactivated by other receptor tyrosine kinases like EGFR (Puehringer et al., 2013) and GPCRs like DRD1 in dMSNs (Iwakura et al., 2008) or Adenosine receptor 2α (A2a-R) in motor-neurons (Wiese et al., 2007). Similarly, GPCRs were shown to transactivate other tyrosine receptor kinases like TrkA (Lee and Chao, 2001; Lee et al., 2002; Rajagopal et al., 2004). This kind of transactivation does not occur on the cell surface, but rather on intracellular membranes and was originally described as a rather slow process occurring over hours (Lee and Chao, 2001; Rajagopal et al., 2004). For this reason, we were wondering if TrkB might get transactivated intracellular after stimulation of DRD2. FACS iMSNs were exposed to 500nM Sumanrole, as performed before, for the analysis of TrkB translocation. Successful activation of DRD2 was confirmed by induction of pMAPK downstream of $G_{\beta\gamma}$ mediated PLC- β and subsequent PKC activation (**compare Fig. 4**) which was reported to follow activation of several GPCRs including DRD2 (Berg et al., 1992; Yan et al., 1999; Lee and Chao, 2001). Indeed, we found significant induction of pMAPK as early as 30s after application of Sumanrole which returned to levels indistinguishable from the negative control after 60min. (**Fig. 47A**). This exactly reflects observations obtained by another DRD2 agonist Quinpirole ((Yan et al., 1999). Even though we were able to reproduce these findings, using

Quinpirole on FACS iMSNs as well, the effect on pMAPK induction appeared much less intense than observed with Sumaniprole (**compare pMAPK in Fig. 47 E, F, G**). Since phosphorylation of MAPK occurs within seconds to minutes, as described for GPCRs, the effect was described as not being related to Trk transactivation which is much slower (Lee and Chao, 2001). As another indicator for successful and specific activation of DRD2, we used the induction of pDARPP-32 Thr75, as a result of $G_{\alpha i}$ mediated inhibition of AC-1 and decrease in cAMP levels (**compare Fig. 3**) (Nishi et al., 1997; Fienberg and Greengard, 2000; Bateup et al., 2008). In FACS iMSNs treated with Sumaniprole, we observed a significant increase in pDARPP-32-Thr75 levels which became significant after 15min and remained elevated until 60min, when pMAPK levels already returned to basal conditions (**Fig. 47B, lanes 5-8 in E, lanes 5-7 in F**). Finally, we attempted to screen for pTrk induction, using an antibody against the intracellular kinase domain which is not specific to TrkB, but rather present in several tyrosine kinase receptors, due to the nature of the receptor composition. In fact, we repeatedly observed induction of pTrk (**Fig. 47 E, F**) which was significant after 60min exposure to Sumaniprole (**Fig. 47C,**). Interestingly, pTrk induction occurred together with a slight, but not significant increase in pSrc (**Fig. 47D, E, F**), a member of a family of kinases which was reported to be an important requirement for ligand-independent neurotrophin receptor transactivation (Rajagopal and Chao, 2006; Puehringer et al., 2013). As a positive control, to confirm the specificity of pTrk induction, we incubated FACS iMSN cultures with 10ng/ml BDNF and observed strong pTrk induction, as well as an increase in pMAPK after 5min incubation (**Fig. 47F lane 9**). Interestingly, we did not see any of the described effects when we used non-FACS, primary MSN cultures (**left side in Fig. 47 E, F**). In these cultures, we also observed a prominent TrkB band at ~90kDa (**Fig. 47E, F**) which might represent the truncated receptor version mainly found in glial cells, as we confirmed before by ICC (**Fig. 29C, D**) and Q-PCR (**Fig. 29F**). In contrast, the prominent band in FACS iMSNs was the TrkB-FL version at ~130kDa (**Fig. 47E, F**) which also confirms findings from

Q-PCR (**Fig. 29F**) and ICC (**Fig. 29B, D**). In summary, these results indicate a ligand-independent activation of TrkB after stimulation of DRD2 in FACS iMSNs which becomes significant after 60min and occurred together with a slight increase in pSrc. The slow time course of pTrk induction correlates with transactivation mechanisms described for other GPCRs (Lee and Chao, 2001; Wiese et al., 2007; Iwakura et al., 2008). Anyway, we failed to reproduce these results by using the less potent DRD2 agonist Quinpirole, even though we observed a slight induction of pTrk on WB (**Fig. 47G lane 3**), but not in ICC (**Fig. 47H**) which may be due to incubation times being too short. Furthermore, we also failed to detect c-FOS expression which is an early response gene transcribed after pCREB induction, downstream of Trk receptor signaling (**Fig. 47I**). In contrast, BDNF exposure significantly induced both pTrk and c-FOS in ICC stainings of FACS iMSNs (**Fig. 47H, I**). These observations, using Quinpirole, also reflects findings made by other groups, with the same agonist on the investigation of pTrk induction, who also failed to find TrkB transactivation in MSN cultures using this agonist (Iwakura et al., 2008). The evidence for pTrk induction after stimulation of DRD2 in our experiments might be due to three important facts. First, we are using highly enriched cultures of iMSNs without major glial cell contamination. Second, by this feature, we prevent trophic effects that might interfere with GPCR and Trk receptor signaling otherwise masking weak effects, especially since our cells were kept in a serum-free environment without neurotrophic factors. Third, we observed a much stronger effect of the highly potent and specific agonist Sumanriole compared to Quinpirole which let us prefer this agonist for our applications. In summary, TrkB transactivation seems to occur in parallel to decrease TrkB surface expression, even though slower. Decrease in TrkB surface expression after DRD2 stimulation was observed at its full extent after 5min, while pTrk induction became significant after 60min. This might indicate a possible transactivation of TrkB on intracellular sites rather than on the cell surface, similar to a mechanism observed for TrkA activation, after GPCR stimulation in primary neurons (Rajagopal et al., 2004).

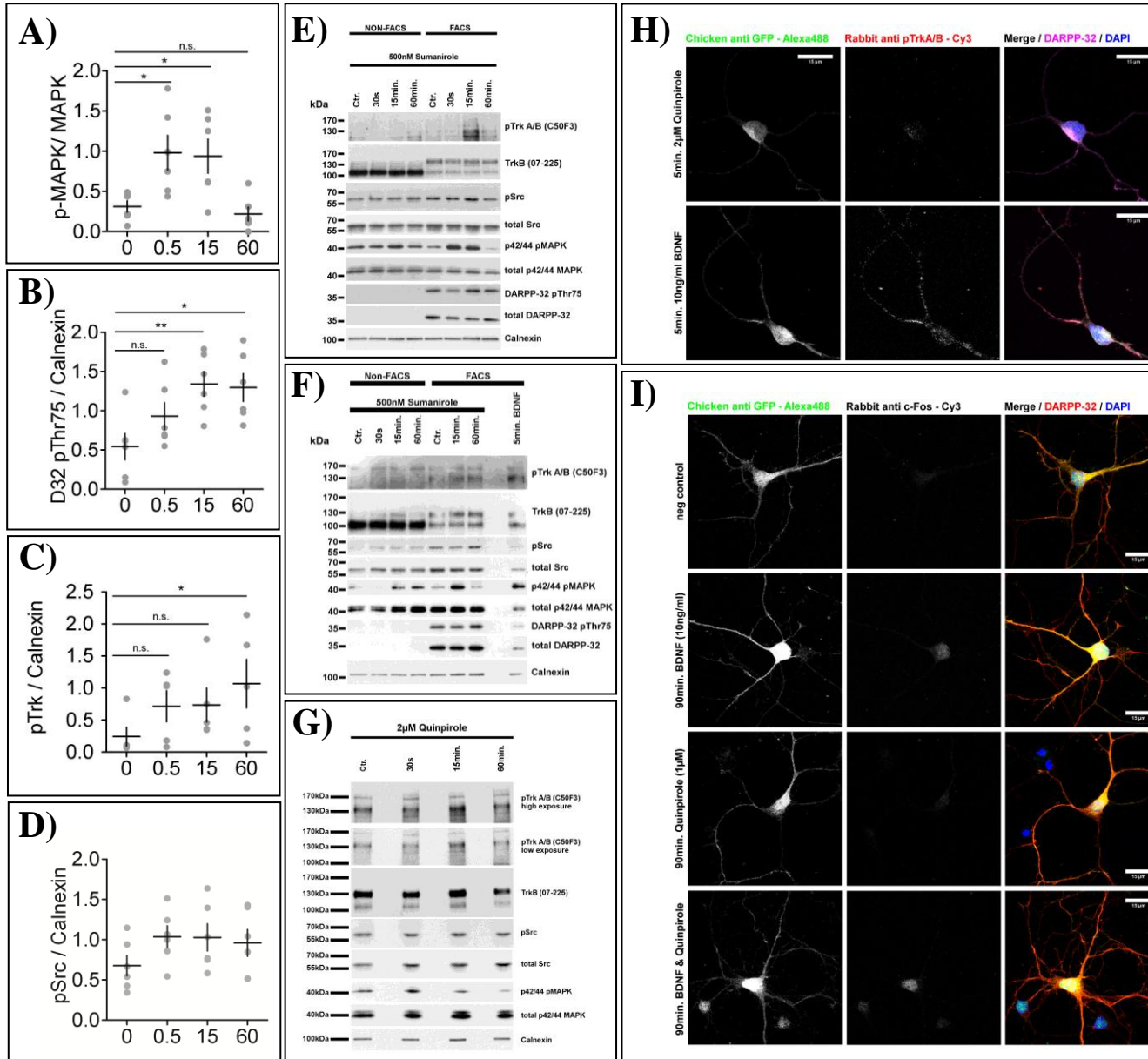


Fig.47: Transactivation of TrkB after stimulation of DRD2 in iMSNs *in vitro*: A) Quantification of pMAPK induction after DRD2 stimulation with 500nM Sumanriole in FACS iMSNs after 0.5min, 15min and 60min. (n=6). Significant pMAPK induction is evident after 0.5min and 15min and returns to control levels after 60min. B) Progressive induction of pDARPP-32 Thr75 after DRD2 activation (n=6). C) Quantification of pTrk induction in FACS iMSNs after DRD2 stimulation (n=6). D) Slight, but not significant increase in pSrc levels after Sumanriole treatment (A-D Bonferroni's multiple comparison test - significance threshold $\alpha = 0.05$; n.s. $P > 0.05$; * $P \leq 0.05$; ** $P \leq 0.01$). E, F) Representative Western Blots used for quantification in A-D). Evidence for induction of pTrk, pSrc, pMAPK and pDARPP-32 Thr75 are obvious only in Sumanriole treated FACS iMSNs (lanes 5-8 in E, lanes 5-7 in F). In contrast only weak induction of pMAPK and no evidence for pTrk, pSrc and pDARPP-32 Thr75 were observed in non-FACS MSN mixed cultures (lanes 1-4 in E, F). In these cultures the prominent band detected with TrkB antibodies were ~90-100kDa (lanes 1-4 in E, F), while the 130kDa TrkB-FL variant was much more evident in FACS iMSNs (lanes 5-8 in E, lanes 5-7 in F). 10ng/ml BDNF was used as positive control for pTrk and rapid pMAPK induction, evident after 5min (lane 9 in F). G) FACS iMSNs stimulated with 2 μ M Quinpirole for 0.5min, 15min and 60min. Weak induction of pMAPK and pTrkB were evident, but overall much weaker compared to Sumanriole mediated effects. H, I) Representative ICC stainings of pTrk and c-FOS induction by 10ng/ml BDNF each. In contrast 2 μ M Quinpirole failed to induce pTrk at 5min and c-FOS after 90min in FACS iMSNs. Scale bar: H, I) 15 μ m.

6. Discussion

Current models of neurotrophin function have emerged from observations in the peripheral nervous system, where these proteins act as target-derived survival factors for developing neurons (Levi-Montalcini and Hamburger, 1951). In the CNS, BDNF plays a crucial role in differentiation and synaptic maturation of neurons and is involved in regulating synaptic plasticity (Lewin and Barde, 1996; Kaplan and Miller, 2000; Huang and Reichardt, 2001; Poo, 2001; Minichiello, 2009). In this context, it has initially been thought, and it is still believed by many researchers, that BDNF is derived from postsynaptic spines and dendrites (Kolarow et al., 2007; Kuczewski et al., 2008; Kuczewski et al., 2009; Edelman et al., 2015). Most of the modes of BDNF action, especially the finding that BDNF expression is activity-dependent (Isackson et al., 1991; Boatell et al., 1992; Castren et al., 1992; Gall, 1993; Gwag and Springer, 1993; Ghosh et al., 1994) have been based on findings in the hippocampus, which turned out to contain high levels of this factor (Conner et al., 1997). In contrast, still little is known about BDNF expression and function in cortical neurons.

The aim of this work was to optimize techniques for detection of BDNF in cortical neurons and to characterize its function in cortico-striatal projections, as well as to characterize its role in structures for the central control of motor function.

6.1 Developmental expression of BDNF in layer V subcortical projection neurons of the motor cortex

Inhibitory neurons within the Corpus striatum that account for approximately ~95% of the striatal neuronal population (Gerfen et al., 1990; Kawaguchi, 1997; Bolam et al., 2000) are crucial elements for controlling voluntary movements within the CNS (Penney and Young, 1983; Graybiel et al., 1994; Mink, 1996) and are directly or indirectly affected by neurodegenerative diseases such as Parkinson's or Huntington's disease (Freund et al., 1984; Albin et al., 1989; Bergman et al., 1990; DeLong, 1990; Gerfen et al., 1990). A major source

of striatal BDNF supply arises from cortical projection neurons. Previous studies found significant BDNF mRNA in cortical layers II, III, V and VI (Conner et al., 1997; Yan et al., 1997). The absence of striatal BDNF mRNA leads to the assumption that cortical layer V pyramidal neurons could be a potential source of striatal BDNF, based on morphological properties of their subcortical projections. Indeed earlier reports found evidence for BDNF mRNA in cortical layers II/III, V and VI, thus supporting the idea of anterograde delivery of BDNF towards target structures (Altar et al., 1997; Conner et al., 1997; Yan et al., 1997; Gorski et al., 2003; Kalivas, 2009; Li et al., 2012; Park et al., 2014). Anyway, the identity of these cortical neurons remains elusive, as do their innervated target structures. Furthermore, the presence of endogenous BDNF in cortico-striatal terminals has not been directly confirmed, but by over-expression of transgenic modified variants of BDNF (Park et al., 2014). This is problematic since over-expression initially leads or led to the observation of BDNF on postsynaptic spines and the idea of autocrine mechanisms of BDNF release on postsynaptic sites. Anyway, this model would not explain modes of BDNF activity on striatal neurons which lack expression of this factor, but rather favor the idea of anterograde transport from cortical neurons. Our aim was to identify BDNF expressing cortical neurons and to define its function in cortico-striatal projections as a central element of voluntary movement control. Therefore, we developed a highly sensitive BDNF IHC protocol which enables the reliable detection of endogenous BDNF protein up to the single synapse level. Based on this, we identified BDNF not only in the hippocampus, confirming earlier reports (Dieni et al., 2012), but also in the cerebral cortex and striatum. We clearly identified BDNF in CTIP-2 positive neurons of layer V, which are known to innervate subcortical target structures, especially the striatum. Furthermore, these neurons govern a small population of corticospinal motor neurons (CSMNs), which are crucial elements of motor function (Arlotta et al., 2005). For that reason, these findings support the idea of anterograde BDNF transport from layer V pyramidal neurons towards the striatum. In addition, we provide new insights into BDNF

expression in other cortical layers, also innervating the striatum, namely Cux-1 positive neurons of layer II/III. This observation leads to the suggestion that striatal BDNF may be supplied from neurons of different cortical subpopulations other than just layer V. Finally we found strong BDNF expression in layer VI of somatosensory cortex, leading to the suggestion that targets, other than the striatum also obtain trophic support from cortical neurons. One might argue that the BDNF immunoreactivity observed in cortical neurons in our experiments originates from presynaptic uptake and retrograde transport towards the cell body, as suggested by others (DiStefano et al., 1992; Curtis et al., 1995; Mufson et al., 1999). This can be excluded by the fact, that the target region of these neurons, the striatum, does not govern BDNF expressing cells. For this reason, BDNF uptake and retrograde transport appear rather unlikely.

After we identified BDNF expression in these cortical neurons, we aimed to investigate aspects of the regulation of BDNF expression within these cells. Thus, we identified regional differences in the density of BDNF expressing cells between cortical areas that seemed to depend on postnatal development. The most significant effect was observed in upper layer V primary (M1) and secondary (M2) motor cortex which showed a severe down-regulation of BDNF in CTIP-2 positive subcortical projection neurons. In this background, it is important to note that age-related changes in brain activity between young and old individuals were observed in human as well. This includes cortical areas which are involved in movement control, also affecting even simple motor functions (Mattay et al., 2002). Other groups have related these age-dependent changes in activity to a reduction in the ability to modulate inhibitory signaling in the aging motor cortex (Opie et al., 2015). This, in turn, affects changes in pre- and post-synaptic motor cortex inhibition (Opie et al., 2015), which critically involves inhibitory cortical interneurons (Wonders and Anderson, 2006). Thus postnatal changes in modes of inhibitory cortical signaling might also influence activity-dependent

BDNF expression in cortical neurons. In this regard, it is noteworthy that even though inhibitory cortical interneurons are born between E12.5-E16.5 in mice, their postnatal maturation can last for several weeks (Wonders and Anderson, 2006). This could also cause changes in early postnatal activity and subsequently BDNF expression in cortical neurons which are involved in motor function. Both regions, in which we observed reduced BDNF expression, are involved in the control of voluntary movement and target the dorsolateral striatum, as does the primary somatosensory cortex (SSp). In contrast, BDNF was expressed in slightly more CTIP-2 positive neurons in layer V of the SSp at 12wk compared to 3wk. Interestingly, there is intense muscle growth in mice during the first 3 postnatal weeks (Gokhin et al., 2008). Young mice also show increased activity from P10³, followed by opening their eyes between P14-P16⁴ and also start exploring their environment. This suggests two things. First, BDNF expression might be upregulated at an early postnatal age, when mice start to move and explore their environment, in order to set up and fine-tune neuronal networks required for voluntary movement. Once the network is established, BDNF levels might decrease again in affected cortical neurons. There is also upcoming evidence, that the motor cortex is required for learning but not carrying out motor skills (Kawai et al., 2015). This supports the idea of temporal BDNF upregulation required for learning new motor skills. Once established, BDNF levels may decrease to basal condition again. Second, since this decrease seems to affect some regions more than others, it may differentially contribute to the network function and output. Meaning that motor cortices down-regulate their BDNF expression once the functional network is established, while BDNF expressing cells in SSp stay mostly unaffected, possibly due to a higher requirement for plasticity and variability in their projections. Independent of age-related changes in BDNF expression, it was shown that physical activity is able to increase BDNF expression in Hippocampus and cortex (Neeper et

³ <https://oacu.oir.nih.gov/sites/default/files/uploads/training-resources/jaxpupposter.pdf>

⁴ <http://www.informatics.jax.org/silver/chapters/4-4.shtml>

al., 1995; Neeper et al., 1996; Griesbach et al., 2004; Ding et al., 2006; Rasmussen et al., 2009) which is suggested to be due to an increase in neuronal activity (Isackson et al., 1991; Boatell et al., 1992; Castren et al., 1992; Gall, 1993; Gwag and Springer, 1993; Ghosh et al., 1994) and causes an improvement of cognitive functions (van Praag et al., 1999; Adlard et al., 2004; Gomez-Pinilla et al., 2008). Significant induction of BDNF mRNA expression was also observed in the frontal cortex of rats and mice after accessing a running wheel for a period between 2d and 7d (Neeper et al., 1995; Neeper et al., 1996; Hall et al., 2014). But in contrast to the hippocampus, in which the BDNF mRNA levels remain high for longer periods, BDNF mRNA levels in mPFC decrease after 2d (Neeper et al., 1996). Similarly, no significant difference in BDNF protein levels was observed in the motor cortex of mice after accessing a running wheel for 7d (Takahashi et al., 2017). This might indicate a time-window in which new motor skills are established in the network. Even though these mice are used to normal locomotion, running wheel performance might require a certain degree of coordination and adaption, which in turn requires BDNF and adaptive, activity-dependent changes in the cortico-striatal system. On the other hand, the increase in BDNF expression might also reflect a higher degree of neuronal activity, not necessarily involve learning-related processes. Interestingly this activity-dependent BDNF expression is critically linked to BDNF exon III in rats and exon IV promoter activity in mice (Tao et al., 1998). Promoter IV activity was described as a critical mediator of neuronal circuit development and synaptic plasticity in prefrontal cortex neurons (Sakata et al., 2009), which also contains the motor cortices. In order to provide a better basis to distinguish these two possibilities, we optimized techniques for identifying those neurons that are responsible for the up-regulation of BDNF expression after initiation of physical exercise in the running wheel. So far the identity of neurons, reacting to physical activity by upregulating BDNF expression, remains elusive. Thus the identification of those cortical neurons is a crucial question to address in future experiments.

We identified subcortical projection neurons of layer V by the expression of CTIP-2. CTIP-2 itself, a zinc finger transcription factor, is required for the correct development of subcortical axonal projections to the striatum and spinal cord, both of which are central elements of voluntary movement (Arlotta et al., 2005). We furthermore used another transcription factor, Cux-1 as a marker for layer II/III cortical neurons which are known to innervate the striatum and to be involved in movement control (Gerfen, 1989; Nieto et al., 2004). We identified BDNF expression in neurons of both populations and furthermore observed a down-regulation of BDNF during postnatal life. So far it remains largely elusive if these neurons show changes in their activity during postnatal periods and if this correlates with BDNF expression. Anyway, changes in cortical neuron activity at different ages were suggested at least in human (Mattay et al., 2002; Opie et al., 2015). Our observations so far raise several questions. First, do BDNF expressing neurons belong to a functional subpopulation in M1 and M2, involved in movement control and what are their subcortical target structures? Second, does physical activity indeed increase BDNF levels in these neurons? Third, does an increase in BDNF expression also lead to an increased release from presynaptic terminals? To address these questions it is critical to clarify the neuronal identity, function and the subcortical target structures. This could be achieved by tracing these cortical neurons, using retrograde tracers and investigate BDNF upregulation in labeled cortical neurons after physical exercise. If BDNF is indeed a crucial element of motor skill learning in cortico-striatal projections from motor cortices, then conditional k.o. of BDNF in these neurons should prevent or deteriorate motor skill learning. This could be achieved by injection of retro-AAV-CRE viruses into the dorsolateral striatum of BDNF^{fl/fl} mice. In this case, BDNF is abolished from subcortical projection neurons involved in the control of voluntary movement, even though this includes neurons from other regions than only motor cortices. These mice should perform much worse in learning new motor skills, like "single pellet reaching task" or "lever pull task". Additionally, retrograde tracing, combined with optogenetic stimulation turned out to be a

very useful tool for studying network structure, function and dynamics *in vivo* (Kim et al., 2014; Tovote et al., 2016). By injecting retrograde tracers, combined with vectors triggering expression of channel-rhodopsins, it would not only be possible to trace BDNF positive neurons in M1 and M2 and investigate BDNF expression after physical exercise. Instead, it could be possible to optogenetically stimulate these cells and "induce" neuronal activity, possibly resulting in BDNF expression. If it is possible to induce BDNF expression and stimulate activity in the affected subcortical projection neurons, this could be an "induced" therapeutic strategy to improve pathological traits of patients suffering from movement disorders. At the same time, it covers many risks. Stimulation of subcortical projection neurons, involved in higher order control of movement initiation, might cause spasticity, seizures, dystonia, and dyskinesia.

6.2 BDNF expression in cortical neurons is reflected by BDNF expression in cortico-striatal terminals

Besides the observation of differential BDNF expression throughout distinct brain areas, we also found layer specific differences between single BDNF expressing cells. We identified "BDNF-strong" and "BDNF-weak" cortical neurons throughout all areas analyzed, showing more or less intense somatic BDNF-IR. This suggests that BDNF expression in the presynaptic terminals of those neurons might reflect the status of the somatic BDNF expression. Indeed, we observed "BDNF-strong" and "BDNF-weak" glutamatergic terminals in both, the dorsal and ventral striatum which are innervation targets of the somatomotor cortex as well as limbic cortices. This also might correlate with differential network activity, not only within the striatal projections but in BDNF expressing, subcortical projection neurons in other parts of the cortex, described here. This, in turn, could possibly involve BDNF-exon IV promoter. For the identification of cortico-striatal terminals, we used VGluT1, since its expression is restricted to glutamatergic neurons of the cortex rather than the thalamus which expresses VGluT2 and also innervates the striatum (Freneau et al., 2001;

Herzog et al., 2001; De Gois et al., 2005; Hur and Zaborszky, 2005; Wilson et al., 2005; Oda et al., 2014). We found that ~50% of all VGluT1 positive presynapses, but only ~14% of the dopaminergic terminals showed BDNF-IR. True co-localization of up to 3% sensitivity was calculated in an unbiased way, using the Costes-P-Value algorithm which is recommended for biological systems, rather than the Pearsons R-Value (Costes et al., 2004). This algorithm was used to distinguish true co-localization from random signal overlap. In this way we could show that significant colocalization was revealed only for VGluT1, but not for TH which confirms observations made by others using genetically modified BDNF (Park et al., 2014). This does not necessarily mean that dopaminergic nigrostriatal neurons do not express BDNF. First of all, we observed weak BDNF-IR in some dopaminergic neurons in the midbrain. Anyway, it was much less intense than any cortical BDNF signal confirming earlier observations (Altar et al., 1997). It is possible that the levels of BDNF produced by midbrain neurons are too low for our IHC protocol to be detectable. Indirect evidence for BDNF expression in midbrain dopaminergic neurons comes from studies using LacZ / β -Gal reporter, which indicates BDNF expression but provides no information about the protein itself (Baquet et al., 2005). Even though LacZ staining was evident during postnatal life this does not necessarily imply strong BDNF expression at that time (Baquet et al., 2005). While detection of BDNF mRNA does not necessarily represent BDNF protein content in these cells (Seroogy et al., 1994; Howells et al., 2000). We suggest that, if there is BDNF expression in midbrain dopaminergic neurons, it is much less compared to cortical neurons. Similarly, BDNF was sparse in dopaminergic terminals in the striatum. We used TH as a marker for dopaminergic terminals, which is actually not restricted to presynapses but is rather expressed throughout the cell body and neurites of dopaminergic neurons, while VGluT1 is restricted to glutamatergic presynapses. In turn, the co-localization between BDNF and TH is lower due to stochastic means of the signal distribution. In summary, we cannot exclude BDNF expression from nigrostriatal neurons since our protocol might not be sensitive enough.

6.3 BDNF expression in the limbic cortex

We also observed BDNF expression in neurons of the prelimbic and infralimbic cortex. Similar to neurons of the motor cortex, BDNF was found to be expressed by CTIP-2 positive neurons. In case of the infralimbic cortex, we observed a decrease in the number of BDNF expressing CTIP-2 positive neurons during postnatal life, while the prelimbic cortex did not show a significant change. Nevertheless, BDNF expression was also observed in CTIP-2 negative cells in both regions. Both brain areas are known to innervate ventromedial to dorsomedial parts of the striatum, especially areas close to the Nucleus accumbens (NAc) (Balleine and Dickinson, 1998; Corbit and Balleine, 2003; Reep et al., 2003; Yin and Knowlton, 2006). Furthermore, the prelimbic as well as the infralimbic cortex play crucial roles in goal-directed behavior, instrumental learning, especially in appetitive Pavlovian learning and also can mediate activity in associative and sensorimotor networks (Balleine and Dickinson, 1998; Leon and Shadlen, 1999; Tsujimoto and Sawaguchi, 2002; Corbit and Balleine, 2003; Tsujimoto and Sawaguchi, 2004a, b). Suitable observations were made in rats with lesions of the prelimbic area losing sensitivity to devaluation and degradation (Balleine and Dickinson, 1998; Corbit and Balleine, 2003). In contrast lesions or inactivation of the infralimbic cortex which is involved in the inhibitory control of Pavlovian conditioned reactions (Rhodes and Killcross, 2004; Yin and Knowlton, 2006) resulted in sensitivity to devaluation even in overtrained rats who already developed a habit (Coutureau and Killcross, 2003; Killcross and Coutureau, 2003). Finally, both cortical areas are suggested to play a central role in modalities of addiction which critically involves synaptic plasticity (Peters et al., 2008; West et al., 2014) (Kauer and Malenka, 2007; Luscher and Malenka, 2011). Nevertheless, a role for BDNF in facilitating these mechanisms of goal-directed behavior and learning remain largely elusive. We observed BDNF expression in subcortical projection neurons that express CTIP-2 of both, the prelimbic and infralimbic cortex. It is possible that the projections of those neurons terminate in the striatum and may play a role in the modes of

plasticity described above. Accordingly, we observed BDNF in presynaptic, glutamatergic terminals close to the NAc, an area which receives dense input from both limbic cortices. Interestingly the prelimbic cortex did not show any change in BDNF expression during postnatal life, while BDNF seems to be downregulated in CTIP-2 positive neurons of the infralimbic cortex. It is, therefore, a crucial question if down-regulation of BDNF expression in these subcortical projection neurons correlates with a specific cortical participation in goal-directed behavior? Finally, this and the fact that the development of addiction involves synaptic plasticity, it is also possible that BDNF expressing neurons of the pre- and infralimbic cortex contribute to these modes of learning. One way to address this issue would be the selective optogenetic stimulation of neuronal populations which were found to down-regulate BDNF, in order to induce BDNF expression. It would be furthermore crucial to address the question of whether and how neurons of the pre- and infralimbic cortex change BDNF expression in paradigms of self-administration and in condition to addictive drugs like cocaine in rodents? This might provide insight into the development and manifestation of habits in general and drug addiction in particular.

6.4 BDNF expression in cortical areas of the ventral mPFC

We made another intriguing observation in a region referred to as Taenia Tecta (TT) which showed very intense BDNF expression, exclusively in CTIP-2 positive subcortical projection neurons. Overall the density of BDNF expressing neurons was one of the highest among all cortical areas investigated. This fits well with earlier observations on mRNA levels (Conner et al., 1997; Yan et al., 1997). The TT is part of the most ventral mPFC and not much is known about its function. So far it was shown that the TT densely innervates the central nucleus of the Amygdala (CEA), but not the basolateral Amygdala (BLA) (Ottersen, 1982; Cassell and Wright, 1986). The CEA, in turn, is supposed to be involved in attentional processes and associative learning, for which reason a similar function was also implemented for the TT as a higher order cortical structure (Gallagher and Schoenbaum, 1999; Holland and Gallagher,

1999; Maddux and Holland, 2011). This view is also supported by experiments about lesions of the ventral part of the mPFC, including the TT (Maddux and Holland, 2011) In our experiments, the TT did not show major differences in BDNF expression during postnatal life which might be interpreted as indication for high network activity and the requirement for a high level of plasticity, variability and adaptability within this network. This idea would match the suggestion that the TT is involved in attentional processes and associative learning (Maddux and Holland, 2011), especially since BDNF is well known to be involved in learning and memory. In this case, it would make sense that in order to manifest learning and synaptic plasticity, BDNF could be provided by higher order cortical neurons. Even though our data are preliminary, BDNF expression has never been described in this part of the brain so far and our observations about the density and intensity of BDNF-IR in neurons of the TT suggest a particular role for BDNF in these projection neurons. Nevertheless, not much is known about the ventral parts of the mPFC and tracing the subcortical projections from those cortical areas is a crucial step in order to understand network connectivity and functionality. It would also be interesting to investigate the role of BDNF in the TT for associative learning tasks, especially how individuals perform when BDNF is knocked out especially in this part of the cortex?

6.5 BDNF expression in layer VI somatosensory cortex

Another region which showed high density in BDNF expressing cells with, at the same time, very high BDNF levels, was found in layer VI of the primary somatosensory cortex (SSp). Even though these results fit RNA based observations on BDNF expression (Conner et al., 1997), endogenous BDNF has not been described in that detail so far. Especially one observation was surprising and unexpected to us. While BDNF expression was highly restricted to CTIP-2 positive neurons in the Taenia Tecta, it is the exact opposite case in SSp layer VI. Indeed SSp layer VI was the only cortical region observed in which the majority of BDNF was expressed in CTIP-2 negative cells. CTIP-2 is normally found in layer V

subcortical projection neurons and to a lesser extent in layer VI cortico-thalamic, but not in cortico-cortical projections (Arlotta et al., 2005; Molyneaux et al., 2007). Layer VI SSp is known to densely innervate several thalamic nuclei but also governs intracortical projection neurons that target motor areas and projections to the claustrum (Katz, 1987; Thomson, 2010). It is possible that the population of BDNF expressing CTIP-2 negative neurons reflects cortico-thalamic or cortico-cortical projection neurons. With special regard to our preliminary observations about BDNF expression in this part of the cortex, it is absolutely important to clearly identify these neurons. Marker protein expression might not be feasible since many markers lack the specificity for distinct cell types. An adequate way would be, to identify these neurons via retrograde tracing. Transcranial injection of tracer molecules or viruses into the target regions would help, not only to clarify the cortico-cortical or cortico-thalamic identity of BDNF positive neurons in layer VI SSp. It also might help to obtain more detailed information about subpopulations, with regard to the innervation of distinct target nuclei within a common target region, like the thalamus. Therefore it is possible that BDNF positive layer VI SSp neurons innervate different thalamic nuclei and therefore belong to several functional subpopulations.

In summary, these results show for the first time the direct visualization of endogenous BDNF in cortico-striatal, rather than nigrostriatal terminals. We also describe BDNF expression and changes in the expression pattern in cortical areas during postnatal development. Our observations of BDNF down-regulation in motor cortices during postnatal development point to the possibility that BDNF is critically involved in learning motor skills, rather than execution of learned motor tasks. Our observations of cortical BDNF distribution and the possibility to reliably visualize lowest amounts of endogenous BDNF may have major implications on the development of new therapeutic strategies for neurodegenerative diseases.

6.6 Translocation and transactivation of TrkB in striatal medium spiny neurons

BDNF release from presynaptic terminals in the striatum appears as a highly regulated process. This includes BDNF expression in cortical neurons, active anterograde transport and NMDAR-dependent and Ca^{2+} -mediated BDNF release from presynaptic cortico-striatal terminals (Park et al., 2014; Lopez-Benito et al., 2018). Induction of plasticity between two distinct presynaptic inputs targeting the same spine, which is the case for cortico-striatal and nigrostriatal projections, would imply a high degree of synchronicity. Meaning a spatiotemporal control between dopaminergic and glutamatergic signaling in which BDNF / TrkB interaction is a key mediator for plasticity. Interestingly it has been shown that dopamine is a critical mediator of plasticity on cortico-striatal axospineous connections, even though not on all of them (Day et al., 2006; Gerfen, 2006; Shen et al., 2008; Villalba and Smith, 2013; Plotkin et al., 2014; Shen et al., 2016). Dopamine is involved in striatal LTP and LTD (Shen et al., 2008; Plotkin et al., 2014; Shen et al., 2016), controls MSN spine density (McNeill et al., 1988; Ingham et al., 1989; Anglade et al., 1996; Ingham et al., 1998; Zaja-Milatovic et al., 2005; Day et al., 2006; Deutch, 2006; Gerfen, 2006; Deutch et al., 2007; Villalba et al., 2009; Villalba and Smith, 2010) and also stability of presynaptic cortico-striatal terminals (Stephens et al., 2005; Day et al., 2006). It was also suggested that some synaptic connections stimulate molecular pathways for plasticity regulation, while others do not (Plotkin et al., 2014; Zhai et al., 2018). Similarly, we found that ~50% of VGluT1 positive synapses in the striatum contain BDNF. It may be possible that BDNF / TrkB interaction plays a critical role in this scenario. For this reason, these connections might also be a target for dopamine-dependent plasticity regulation. It would make sense in this regard if postsynaptic TrkB activation is also a highly regulated process, in which the binding of BDNF is only the final step for receptor activation and subsequent LTP induction. For this reason, we propose a model, in which TrkB surface expression is bidirectional controlled by GPCRs

(Fig. 48). Even though this idea is not completely new (Fino et al., 2005; Yin and Knowlton, 2006; Calabresi et al., 2007; Shen et al., 2008; Shen et al., 2016; Zhai et al., 2018), a specific mechanism that modulates plasticity through regulation of TrkB cell surface expression, was not considered so far.

The preferred activation of $G_{\alpha s/olf}$ receptors like DRD1 in dMSNs or A2aR in iMSNs (Calabresi et al., 2007; Shen et al., 2008; Jia et al., 2010) could facilitate TrkB surface expression and would thus act as a prerequisite for induction of LTP. In contrast, predominant activation of $G_{\alpha i/o}$ GPCRs, like M4R in dMSNs or DRD2 in iMSNs, would decrease TrkB surface expression and facilitate LTD (Shen et al., 2008; Shen et al., 2016). We were able to observe a decrease in TrkB surface expression after stimulation of DRD2 *in vitro*. The same was true for dMSNs in the absence of DRD1 activity *in vivo*, which turned out to accumulate TrkB in intracellular compartments. This can be explained by the absence of DRD1 activity, which would otherwise trigger TrkB surface expression. The striatum underlies constant changes in terms of movement control and motivation and thus should govern a high degree of plasticity. A restriction of LTP and LTD to either of the two MSN subtypes would massively limit striatal flexibility, for which reason bidirectional synaptic plasticity has long been suggested (Yin and Knowlton, 2006; Shen et al., 2008; Zhai et al., 2018). Both forms of plasticity are indeed expressed on glutamatergic cortico-striatal synapses and are crucial elements for motor skill learning and cognitive functions (Calabresi et al., 1996; Wickens et al., 2003; Mahon et al., 2004; Calabresi et al., 2007). The induction of LTP on striatal neurons itself seems to require the simultaneous activation of postsynaptic NMDARs, GPCRs and TrkB (Calabresi et al., 2007; Kreitzer and Malenka, 2008; Shen et al., 2008; Plotkin et al., 2014). Interestingly, the required GPCRs belong to the same family of $G_{\alpha s}$ coupled receptors, able to stimulate adenylyl cyclase activity (Shen et al., 2008; Plotkin et al., 2014) and increase in cAMP levels. This was shown to trigger TrkB surface expression (Meyer-Franke et al.,

1998). Parallel secretion of glutamate and BDNF from cortico-striatal afferences would result in the simultaneous activation of postsynaptic NMDARs, TrkB and G_{os} coupled GPCRs, causing LTP induction (Plotkin et al., 2014). Indeed there is evidence showing that activation of DRD1 in dMSNs increases TrkB surface expression (Iwakura et al., 2008) and leads to the induction of LTP (Reynolds et al., 2001; Calabresi et al., 2007; Shen et al., 2008). Similarly, activation of A2aR, in the presence of DRD2 antagonists, contributes to LTP induction in iMSNs (Shen et al., 2008; Plotkin et al., 2014). In contrast GPCRs coupled to G_{ai} subunits, like DRD2, CB-1 or M4R, inhibit AC-1 activity and decrease cAMP levels (De Camilli et al., 1979; Onali et al., 1981; Enjalbert and Bockaert, 1983; McDonald et al., 1984; Onali et al., 1985; Shen et al., 2016) leading to a decrease in TrkB surface expression. This, in turn, might prevent LTP. In fact, stimulation of DRD2 in iMSNs, using the agonist quinpirole leads to robust induction of LTD (Kreitzer and Malenka, 2005; Shen et al., 2008). Similarly, we observed a rapid decrease in TrkB surface expression after DRD2 stimulation *in vitro*, which would prevent LTP in favor of LTD (**Fig. 45, 46, 48**). If DRD2 signaling in iMSNs is either pharmacologically antagonized, prevented by 6-OHDA lesion or by genetic k.o. from iMSNs, then these cells switch from inducing LTD to induction of LTP instead (Calabresi et al., 1997; Shen et al., 2008). Likewise, we observed a progressive recovery of TrkB surface expression after DRD2 agonists were washed off. Similarly, DRD1 inhibition in dMSNs induces LTD, depending on presynaptic CB1 or postsynaptic M4R receptor activation (Shen et al., 2008; Shen et al., 2016; Zhai et al., 2018). We, therefore, suggest a hypothetic model in order to explain these observations. We hypothesize that activation of different GPCRs balances TrkB surface expression in dMSNs and iMSNs (**Fig. 48**). In turn, this might contribute to LTP or LTD induction in striatal neurons. This model predicts a cAMP-dependent regulation of TrkB surface expression by the stimulation or inhibition of AC-1 by either G_{os} or G_{ai} coupled GPCRs. In dMSNs, these might be DRD1 (G_{os}) and M4R (G_{ai}) (Iwakura et al., 2008; Shen et al., 2008; Plotkin et al., 2014; Shen et al., 2016) (**Fig. 48A**).

It is furthermore possible that a basic condition without stimulation of GPCRs results in a baseline activity of AC-1 and subsequent cAMP levels. These baseline cAMP levels might be sufficient to induce TrkB surface expression. The activity of G_{oi} GPCRs might be required to drop cAMP levels below this threshold in order to remove TrkB from the cell surface. This hypothesis is supported by our observation that TrkB surface expression is detectable also under non-stimulated, serum-free conditions in both FACS iMSNs (**Fig. 45, 46**) and FACS dMSNs (**preliminary results**) and that the cell surface expression can be decreased after stimulation of DRD2 receptors. The absence of Dopamine can be remodeled *in vivo* by 6-OHDA induced lesions. In difference to the *in vitro* situation, activity of G_{oi} GPCRs like M4R in dMSNs might persist in the network and decrease cAMP levels in dMSNs. This might cause a decrease in TrkB surface expression in these dMSNs. Indeed we observed intracellular TrkB aggregates exclusively in dMSNs on the lesioned hemisphere as early as 14d after lesion. It is possible that these aggregates occur much earlier than 14d, possibly when dopamine (and cAMP) levels are decreasing below a certain threshold. Interestingly, these aggregates were not caused by increased TrkB expression, but rather seem to result in deficient TrkB degradation in lysosomes and proteasomes (**Fig. 37C-G, 38C-E**). Evidence for the latter case might be the observation of an increase in total TrkB protein levels on the lesioned hemisphere. If our predicted model is true, then either activation of DRD1 or the inhibition of G_{oi} GPCRs like M4R might restore TrkB surface expression and prevent cluster formation. It will be a crucial experiment to isolate dMSNs by FACS and perform *in vitro* analysis of GPCR mediated TrkB surface expression. In preliminary results we failed to see a further increase in TrkB surface expression after stimulation of DRD1, neither in primary, nor in FACS dMSNs (**data not shown**). This might be due to the baseline AC-1 activity which is sufficient to drive TrkB surface expression. Thus it is possible that activation of G_{oi} GPCRs (M4R) will decrease surface TrkB like DRD2 does in iMSNs.

Similar to the idea of baseline AC-1 activity under non-stimulated conditions, we found intense TrkB surface expression in FACS enriched iMSNs in the absence of specific GPCR stimulation. Stimulation of DRD2 (G_{ai}) led to a rapid decrease in TrkB surface expression, in both ICC and WB, within 5min. Stimulation of DRD2 could, therefore, abolish the basal activity of adenylyl-cyclase 1 below the critical threshold level. Evidence for this assumption comes from two observations. First, washing off the DRD2 agonist causes an increase in TrkB surface expression after 2h, indicating a recovery towards basal levels. Second, we did not see a further increase in TrkB surface expression after treatment with the AC-1 activator Forskolin (**Fig. 46**). This could explain why iMSNs usually induce LTD (Shen et al., 2008). Such iMSNs can switch to LTP in the absence of DRD2 activity, in case A2aR (G_{as}) is stimulated (Shen et al., 2008; Plotkin et al., 2014). These observations support our model, and they would predict increased TrkB surface expression as a trigger for LTP induction (**Fig. 48**). Nevertheless, in the 6-OHDA striatum, we did not see significant differences in subcellular TrkB localization in iMSNs between intact and lesioned hemisphere. One explanation might be the limitation in resolution of confocal microscopy. It is possible that in the absence of dopamine and DRD2 activation, TrkB surface expression will increase in iMSNs. The visualization of this effect might require high-resolution techniques to visualize the distribution of TrkB among a large MSN surface. Compared to this, an accumulation of TrkB in the soma of dMSNs is more feasible for visualization.

However, there are several open questions related to this proposed model. The mechanisms by which LTP and LTD are regulated might be more complex, also including regulatory mechanisms from presynaptic inputs. Other groups have shown, that MSNs, especially iMSNs lose their spines in PD (McNeill et al., 1988; Ingham et al., 1989; Anglade et al., 1996; Ingham et al., 1998; Zaja-Milatovic et al., 2005; Day et al., 2006; Deutch, 2006; Gerfen, 2006; Deutch et al., 2007; Villalba et al., 2009; Villalba and Smith, 2010). This effect

was in part due to increased postsynaptic $Ca_v1.3$ opening when DRD2 activation is lost. (Day et al., 2006; Gerfen, 2006). Nevertheless, presynaptic cortico-striatal terminals are also affected in PD and show increased degeneration (Stephens et al., 2005; Day et al., 2006). These observations provide valuable evidence for an important role in cortico-striatal plasticity. It is, therefore, possible that not only postsynaptic effects are mediated by dopamine but that this neurotransmitter has direct or indirect effects on presynaptic terminals as well.

It is important to note that the modes of signal transduction between DRD1 and DRD2 are critically different. While DRD2 inhibits AC-1 activity, causing a decrease in cAMP levels (De Camilli et al., 1979; Onali et al., 1981; Enjalbert and Bockaert, 1983; McDonald et al., 1984; Onali et al., 1985; Memo et al., 1986), DRD1 promotes an increase of cAMP by stimulating AC-1 (Memo et al., 1986; Dearry et al., 1990; Monsma et al., 1990; Zhou et al., 1990; Sugamori et al., 1994; Demchyshyn et al., 1995). Similarly, postsynaptic L-type Ca^{2+} currents are regulated bidirectional by DRD1 and DRD2. DRD2 inhibits the opening of L-type Ca^{2+} channels, as mentioned above (Day et al., 2006). In contrast, DRD1 was shown to increase L-type Ca^{2+} currents in a cAMP-PKA-PP-1 dependent manner (Surmeier et al., 1995). Neuronal activity and Ca^{2+} signaling were also shown to play an essential role in TrkB surface expression in hippocampal neurons (Du et al., 2000). Nevertheless, when extracellular Ca^{2+} was removed, or postsynaptic Ca^{2+} channels or NMDARs were blocked, the effect on TrkB surface expression was attenuated but not abolished (Du et al., 2000). Thus it is possible that Ca^{2+} signaling and regulation of cAMP levels together influence TrkB surface expression (Meyer-Franke et al., 1998; Du et al., 2000). In this regard, DRD1 facilitates L-type Ca^{2+} currents and cAMP levels, which both promote TrkB surface expression. On the other hand inhibition of L-type Ca^{2+} currents and cAMP production are achieved by DRD2 in iMSNs. Interestingly, the surface expression of AMPA receptors is influenced by DRD1 and DRD2

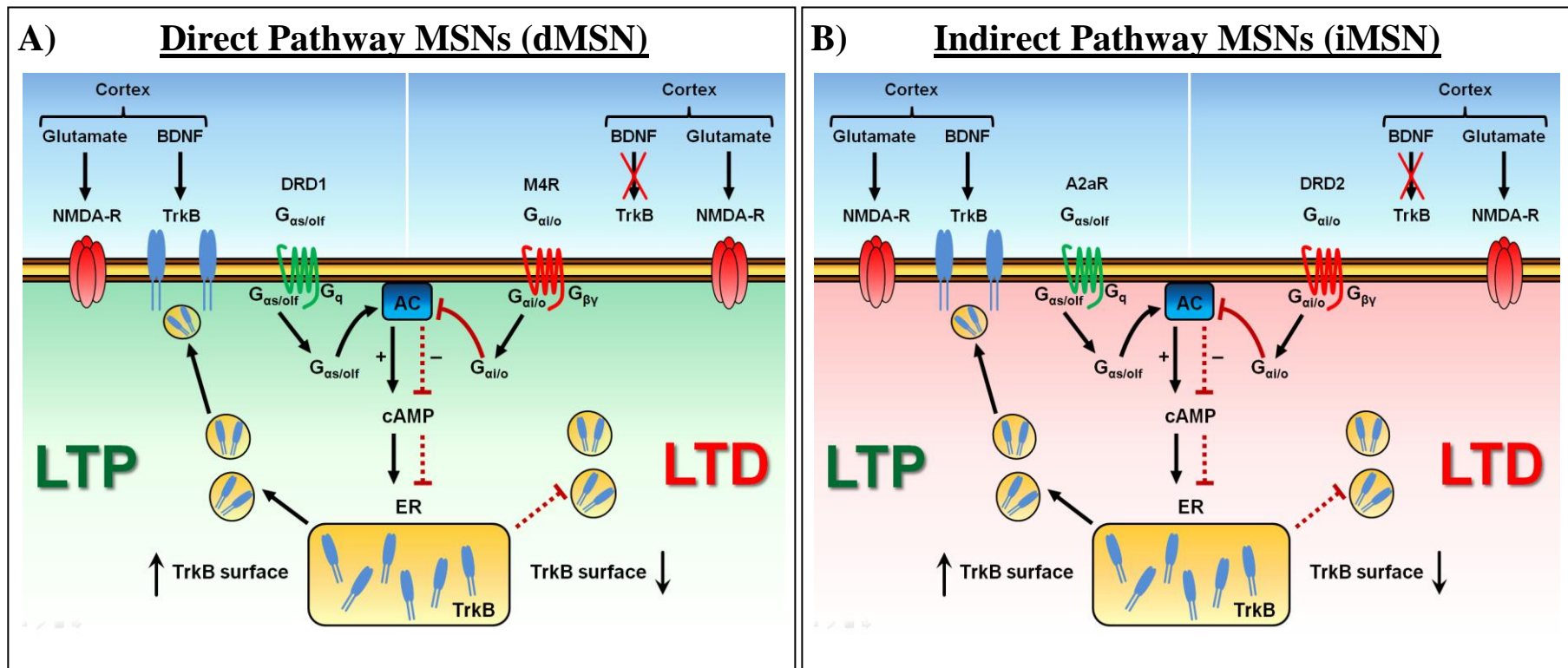


Fig.48: Hypothetic model of GPCR-mediated TrkB surface expression in striatal MSNs: **A)** In direct pathway MSNs, activation of DRD1 triggers increased activation of AC-1, resulting in increase of cAMP levels. This in turn might cause an increase in TrkB surface expression and would favor a model of plasticity towards LTP induction (**left side in A**). G_{ai} GPCRs like M4R would act antagonistically in this system. Activation of M4R in the absence of DRD1 stimulation (6-OHDA model of PD) would cause inhibition of AC-1 and decrease of cAMP below a critical threshold, which would be required for TrkB surface expression. This would cause a decrease of TrkB surface expression, preventing LTP induction in favor of LTD (**right side in A**). It is possible that AC-1 shows a certain baseline activity in the absence of both G_{as/olf} or G_{ai} activation, which is sufficient for TrkB surface expression. **B)** In indirect pathway MSNs activation of DRD2 (in the absence of A2aR activity) will cause a decrease in TrkB surface expression by AC-1 inhibition, leading to LTD induction. Nevertheless, iMSNs are also able to induce LTP, which requires the stimulation of A2aR and simultaneous inhibition of DRD2 in order to increase cAMP levels by AC-1 stimulation and to increase TrkB surface expression. In case of PD, activity of DRD1 in dMSNs (A), as well as DRD2 in iMSNs (B) would be abolished. If the counteracting GPCR in each MSNs subtype is still active, then dMSNs should induce LTD, while iMSNs should induce LTP.

activity in an opposite manner (Sun et al., 2005; Sun et al., 2008). Furthermore, DRD1 was suggested to act on membrane trafficking of NMDARs (Flores-Hernandez et al., 2002; Braithwaite et al., 2006; Hallett et al., 2006; Gao and Wolf, 2008).

Finally, there is substantial evidence, that dopamine might not only affect translocation of TrkB in postsynaptic MSNs but also cause a ligand-independent receptor transactivation which was shown for DRD1 activation in dMSNs (Iwakura et al., 2008). Anyway, TrkB transactivation has not been shown for DRD2 stimulation in iMSNs before (Iwakura et al., 2008). We, therefore, developed a cell culture system, in which we enriched dMSNs or iMSNs by FACS. This system helped us to overcome the major limitations of low MSN yield and the presence of both subtypes in the same culture. By obtaining pure subtype specific MSN cultures, we found evidence for a slow but progressive induction of pTrkB after stimulation of DRD2 *in vitro*. In contrast, similar to others (Iwakura et al., 2008), we failed to detect pTrkB induction after DRD2 stimulation in primary MSN cultures which reveal only ~2-5% MSNs. Stochastically only 50% of these MSNs are iMSNs, meaning ~1-2,5% of all cells in these cultures. Furthermore, trophic effects might be masked by the presence of glial cells and secreted factors. Indeed the predominant band for TrkB was TrkB-T1, lacking the C-terminus with phosphorylation sites (**Fig. 47E, F**).

Stimulation of FACS iMSNs with DRD2 agonist Sumanitrole induced significant TrkB phosphorylation on its kinase domain after 60min. It is possible that the mechanism is related to TrkB transactivation by EGFR (Puehringer et al., 2013) or DRD1 (Iwakura et al., 2008) activity and might include the activity of Src kinases. Transactivation of TrkB could thus represent a modulatory system for fine adaption on synaptic connections which is independent of BDNF release from corticostriatal terminals.

In summary, our results provide evidence for the crucial involvement of BDNF / TrkB signaling in striatal plasticity and activity-dependent BDNF secretion especially in the motor

cortex. The idea of bidirectional regulation of cAMP levels by either G_{α_s} or G_{α_i} GPCRs in both MSN subtypes enables the possibility of controlled TrkB surface expression, depending on the mode of activation of the MSN itself. This in turn might represent a switch between LTP and LTD and supports the idea of "*bidirectional plasticity at glutamatergic synapses on striatal MSNs*" (Fino et al., 2005; Calabresi et al., 2007; Shen et al., 2008; Shen et al., 2016; Zhai et al., 2018). This makes sense in the means of plasticity and adaptability which would be much more limited if LTP or LTD was cell type dependent. Furthermore, these findings support the idea of the simultaneous activity of postsynaptic NMDARs, GPCRs and TrkB in order to induce LTP. For this reason, our findings might provide new insights into the modes of plasticity and for the development of therapeutic strategies against neurodegenerative diseases, directly or indirectly affecting the striatum and basal ganglia.

7. References

- Adlard PA, Perreau VM, Engesser-Cesar C, Cotman CW (2004) The timecourse of induction of brain-derived neurotrophic factor mRNA and protein in the rat hippocampus following voluntary exercise. *Neuroscience letters* 363:43-48.
- Afifi AK, Bahuth NB, Kaelber WW, Mikhael E, Nassar S (1974) The cortico-nigral fibre tract. An experimental Fink-Heimer study in cats. *J Anat* 118:469-476.
- Albin RL, Young AB, Penney JB (1989) The functional anatomy of basal ganglia disorders. *Trends Neurosci* 12:366-375.
- Alexander GE, DeLong MR (1985) Microstimulation of the primate neostriatum. II. Somatotopic organization of striatal microexcitable zones and their relation to neuronal response properties. *J Neurophysiol* 53:1417-1430.
- Alexander GE, Crutcher MD (1990) Functional architecture of basal ganglia circuits: neural substrates of parallel processing. *Trends Neurosci* 13:266-271.
- Alexander GE, DeLong MR, Strick PL (1986) Parallel organization of functionally segregated circuits linking basal ganglia and cortex. *Annual review of neuroscience* 9:357-381.
- Altar CA, Cai N, Bliven T, Juhasz M, Conner JM, Acheson AL, Lindsay RM, Wiegand SJ (1997) Anterograde transport of brain-derived neurotrophic factor and its role in the brain. *Nature* 389:856-860.
- Anden NE, Carlsson A, Dahlstroem A, Fuxe K, Hillarp NA, Larsson K (1964) Demonstration and Mapping out of Nigro-Neostriatal Dopamine Neurons. *Life Sci* (1962) 3:523-530.
- Anderson SA, Qiu M, Bulfone A, Eisenstat DD, Meneses J, Pedersen R, Rubenstein JL (1997) Mutations of the homeobox genes *Dlx-1* and *Dlx-2* disrupt the striatal subventricular zone and differentiation of late born striatal neurons. *Neuron* 19:27-37.
- Arikuni T, Kubota K (1986) The organization of prefrontocaudate projections and their laminar origin in the macaque monkey: a retrograde study using HRP-gel. *The Journal of comparative neurology* 244:492-510.
- Arlotta P, Molyneaux BJ, Chen J, Inoue J, Kominami R, Macklis JD (2005) Neuronal subtype-specific genes that control corticospinal motor neuron development in vivo. *Neuron* 45:207-221.
- Bamford NS, Zhang H, Schmitz Y, Wu NP, Cepeda C, Levine MS, Schmauss C, Zakharenko SS, Zablow L, Sulzer D (2004) Heterosynaptic dopamine neurotransmission selects sets of corticostriatal terminals. *Neuron* 42:653-663.
- Baquet ZC, Gorski JA, Jones KR (2004) Early striatal dendrite deficits followed by neuron loss with advanced age in the absence of anterograde cortical brain-derived neurotrophic factor. *The Journal of neuroscience : the official journal of the Society for Neuroscience* 24:4250-4258.
- Baquet ZC, Bickford PC, Jones KR (2005) Brain-derived neurotrophic factor is required for the establishment of the proper number of dopaminergic neurons in the substantia nigra pars compacta. *The Journal of neuroscience : the official journal of the Society for Neuroscience* 25:6251-6259.
- Barbacid M (1994) The Trk family of neurotrophin receptors. *Journal of neurobiology* 25:1386-1403.
- Barde YA, Edgar D, Thoenen H (1982) Purification of a new neurotrophic factor from mammalian brain. *The EMBO journal* 1:549-553.
- Barrett AJ (1970) Cathepsin D. Purification of isoenzymes from human and chicken liver. *Biochem J* 117:601-607.
- Barroso-Chinea P, Castle M, Aymerich MS, Perez-Manso M, Erro E, Tunon T, Lanciego JL (2007) Expression of the mRNAs encoding for the vesicular glutamate transporters 1 and 2 in the rat thalamus. *The Journal of comparative neurology* 501:703-715.
- Bateup HS, Svenningsson P, Kuroiwa M, Gong S, Nishi A, Heintz N, Greengard P (2008) Cell type-specific regulation of DARPP-32 phosphorylation by psychostimulant and antipsychotic drugs. *Nature neuroscience* 11:932-939.
- Baydyuk M, Russell T, Liao GY, Zang K, An JJ, Reichardt LF, Xu B (2011) TrkB receptor controls striatal formation by regulating the number of newborn striatal neurons. *Proceedings of the National Academy of Sciences of the United States of America* 108:1669-1674.

- Beaulieu JM, Gainetdinov RR (2011) The physiology, signaling, and pharmacology of dopamine receptors. *Pharmacol Rev* 63:182-217.
- Beckstead RM (1979) An autoradiographic examination of corticocortical and subcortical projections of the mediodorsal-projection (prefrontal) cortex in the rat. *The Journal of comparative neurology* 184:43-62.
- Beckstead RM (1988) Association of dopamine D1 and D2 receptors with specific cellular elements in the basal ganglia of the cat: the uneven topography of dopamine receptors in the striatum is determined by intrinsic striatal cells, not nigrostriatal axons. *Neuroscience* 27:851-863.
- Beckstead RM, Kersey KS (1985) Immunohistochemical demonstration of differential substance P-, met-enkephalin-, and glutamic-acid-decarboxylase-containing cell body and axon distributions in the corpus striatum of the cat. *The Journal of comparative neurology* 232:481-498.
- Beckstead RM, Domesick VB, Nauta WJ (1979) Efferent connections of the substantia nigra and ventral tegmental area in the rat. *Brain Res* 175:191-217.
- Belin D, Jonkman S, Dickinson A, Robbins TW, Everitt BJ (2009) Parallel and interactive learning processes within the basal ganglia: relevance for the understanding of addiction. *Behavioural brain research* 199:89-102.
- Benabid AL, Chabardes S, Mitrofanis J, Pollak P (2009) Deep brain stimulation of the subthalamic nucleus for the treatment of Parkinson's disease. *Lancet Neurol* 8:67-81.
- Berg MM, Sternberg DW, Parada LF, Chao MV (1992) K-252a inhibits nerve growth factor-induced trk proto-oncogene tyrosine phosphorylation and kinase activity. *The Journal of biological chemistry* 267:13-16.
- Bergman H, Wichmann T, DeLong MR (1990) Reversal of experimental parkinsonism by lesions of the subthalamic nucleus. *Science* 249:1436-1438.
- Bertran-Gonzalez J, Herve D, Girault JA, Valjent E (2010) What is the Degree of Segregation between Striatonigral and Striatopallidal Projections? *Front Neuroanat* 4.
- Bertran-Gonzalez J, Bosch C, Maroteaux M, Matamales M, Herve D, Valjent E, Girault JA (2008) Opposing patterns of signaling activation in dopamine D1 and D2 receptor-expressing striatal neurons in response to cocaine and haloperidol. *The Journal of neuroscience : the official journal of the Society for Neuroscience* 28:5671-5685.
- Biber MP, Kneisley LW, LaVail JH (1978) Cortical neurons projecting to the cervical and lumbar enlargements of the spinal cord in young and adult rhesus monkeys. *Experimental neurology* 59:492-508.
- Blum D, Torch S, Lambeng N, Nissou M, Benabid AL, Sadoul R, Verna JM (2001) Molecular pathways involved in the neurotoxicity of 6-OHDA, dopamine and MPTP: contribution to the apoptotic theory in Parkinson's disease. *Prog Neurobiol* 65:135-172.
- Boatell LL, Lindfors N, Ballarin M, Ernfors P, Mahy N, Persson H (1992) Activation of basal forebrain cholinergic neurons differentially regulates brain-derived neurotrophic factor mRNA expression in different projection areas. *Neuroscience letters* 136:203-208.
- Bolam JP, Hanley JJ, Booth PA, Bevan MD (2000) Synaptic organisation of the basal ganglia. *J Anat* 196 (Pt 4):527-542.
- Boulland JL, Qureshi T, Seal RP, Rafiki A, Gundersen V, Bergersen LH, Fremereau RT, Jr., Edwards RH, Storm-Mathisen J, Chaudhry FA (2004) Expression of the vesicular glutamate transporters during development indicates the widespread corelease of multiple neurotransmitters. *The Journal of comparative neurology* 480:264-280.
- Bourassa J, Deschenes M (1995) Corticothalamic projections from the primary visual cortex in rats: a single fiber study using biocytin as an anterograde tracer. *Neuroscience* 66:253-263.
- Bourassa J, Pinault D, Deschenes M (1995) Corticothalamic projections from the cortical barrel field to the somatosensory thalamus in rats: a single-fibre study using biocytin as an anterograde tracer. *The European journal of neuroscience* 7:19-30.

- Bowery BJ, Razzaque Z, Emms F, Patel S, Freedman S, Bristow L, Kulagowski J, Seabrook GR (1996) Antagonism of the effects of (+)-PD 128907 on midbrain dopamine neurones in rat brain slices by a selective D2 receptor antagonist L-741,626. *Br J Pharmacol* 119:1491-1497.
- Brady R, Zaidi SI, Mayer C, Katz DM (1999) BDNF is a target-derived survival factor for arterial baroreceptor and chemoafferent primary sensory neurons. *The Journal of neuroscience : the official journal of the Society for Neuroscience* 19:2131-2142.
- Braithwaite SP, Adkisson M, Leung J, Nava A, Masterson B, Urfer R, Oksenberg D, Nikolich K (2006) Regulation of NMDA receptor trafficking and function by striatal-enriched tyrosine phosphatase (STEP). *The European journal of neuroscience* 23:2847-2856.
- Bunney BS, Aghajanian GK (1976) The precise localization of nigral afferents in the rat as determined by a retrograde tracing technique. *Brain Res* 117:423-435.
- Calabresi P, Pisani A, Mercuri NB, Bernardi G (1996) The corticostriatal projection: from synaptic plasticity to dysfunctions of the basal ganglia. *Trends Neurosci* 19:19-24.
- Calabresi P, Picconi B, Tozzi A, Di Filippo M (2007) Dopamine-mediated regulation of corticostriatal synaptic plasticity. *Trends Neurosci* 30:211-219.
- Calabresi P, Saiardi A, Pisani A, Baik JH, Centonze D, Mercuri NB, Bernardi G, Borrelli E (1997) Abnormal synaptic plasticity in the striatum of mice lacking dopamine D2 receptors. *The Journal of neuroscience : the official journal of the Society for Neuroscience* 17:4536-4544.
- Calabresi P, Gubellini P, Centonze D, Picconi B, Bernardi G, Chergui K, Svenningsson P, Fienberg AA, Greengard P (2000) Dopamine and cAMP-regulated phosphoprotein 32 kDa controls both striatal long-term depression and long-term potentiation, opposing forms of synaptic plasticity. *The Journal of neuroscience : the official journal of the Society for Neuroscience* 20:8443-8451.
- Carter CJ (1982) Topographical distribution of possible glutamatergic pathways from the frontal cortex to the striatum and substantia nigra in rats. *Neuropharmacology* 21:379-383.
- Cassell MD, Wright DJ (1986) Topography of projections from the medial prefrontal cortex to the amygdala in the rat. *Brain Res Bull* 17:321-333.
- Castren E, Zafra F, Thoenen H, Lindholm D (1992) Light regulates expression of brain-derived neurotrophic factor mRNA in rat visual cortex. *Proceedings of the National Academy of Sciences of the United States of America* 89:9444-9448.
- Cepeda C, Colwell CS, Itri JN, Chandler SH, Levine MS (1998) Dopaminergic modulation of NMDA-induced whole cell currents in neostriatal neurons in slices: contribution of calcium conductances. *J Neurophysiol* 79:82-94.
- Chalifoux JR, Carter AG (2010) GABAB receptors modulate NMDA receptor calcium signals in dendritic spines. *Neuron* 66:101-113.
- Chan JP, Unger TJ, Byrnes J, Rios M (2006) Examination of behavioral deficits triggered by targeting Bdnf in fetal or postnatal brains of mice. *Neuroscience* 142:49-58.
- Chan JP, Cordeira J, Calderon GA, Iyer LK, Rios M (2008) Depletion of central BDNF in mice impedes terminal differentiation of new granule neurons in the adult hippocampus. *Mol Cell Neurosci* 39:372-383.
- Chen ZY, Ieraci A, Tanowitz M, Lee FS (2005) A novel endocytic recycling signal distinguishes biological responses of Trk neurotrophin receptors. *Mol Biol Cell* 16:5761-5772.
- Cheng PY, Svingos AL, Wang H, Clarke CL, Jenab S, Beczkowska IW, Inturrisi CE, Pickel VM (1995) Ultrastructural immunolabeling shows prominent presynaptic vesicular localization of delta-opioid receptor within both enkephalin- and nonenkephalin-containing axon terminals in the superficial layers of the rat cervical spinal cord. *The Journal of neuroscience : the official journal of the Society for Neuroscience* 15:5976-5988.
- Chesselet MF, Graybiel AM (1983) Met-enkephalin-like and dynorphin-like immunoreactivities of the basal ganglia of the cat. *Life Sci* 33 Suppl 1:37-40.
- Chomczynski P, Sacchi N (1987) Single-step method of RNA isolation by acid guanidinium thiocyanate-phenol-chloroform extraction. *Anal Biochem* 162:156-159.

- Cohen S, Levi-Montalcini R, Hamburger V (1954) A Nerve Growth-Stimulating Factor Isolated from Sarcom as 37 and 180. *Proceedings of the National Academy of Sciences of the United States of America* 40:1014-1018.
- Conner JM, Lauterborn JC, Yan Q, Gall CM, Varon S (1997) Distribution of brain-derived neurotrophic factor (BDNF) protein and mRNA in the normal adult rat CNS: evidence for anterograde axonal transport. *The Journal of neuroscience : the official journal of the Society for Neuroscience* 17:2295-2313.
- Conover JC, Yancopoulos GD (1997) Neurotrophin regulation of the developing nervous system: analyses of knockout mice. *Rev Neurosci* 8:13-27.
- Conover JC, Erickson JT, Katz DM, Bianchi LM, Poueymirou WT, McClain J, Pan L, Helgren M, Ip NY, Boland P, et al. (1995) Neuronal deficits, not involving motor neurons, in mice lacking BDNF and/or NT4. *Nature* 375:235-238.
- Cospito JA, Kultas-Illinsky K (1981) Synaptic organization of motor corticostriatal projections in the rat. *Experimental neurology* 72:257-266.
- Costantini LC, Feinstein SC, Radeke MJ, Snyder-Keller A (1999) Compartmental expression of trkB receptor protein in the developing striatum. *Neuroscience* 89:505-513.
- Costanza RM, Barber DJ, Terry P (2001) Antagonism of the discriminative stimulus effects of cocaine at two training doses by dopamine D2-like receptor antagonists. *Psychopharmacology (Berl)* 158:146-153.
- Costes SV, Daelemans D, Cho EH, Dobbin Z, Pavlakis G, Lockett S (2004) Automatic and quantitative measurement of protein-protein colocalization in live cells. *Biophys J* 86:3993-4003.
- Cowan WM, Powell TP (1966) Strio-pallidal projection in the monkey. *J Neurol Neurosurg Psychiatry* 29:426-439.
- Crutcher MD, DeLong MR (1984) Single cell studies of the primate putamen. II. Relations to direction of movement and pattern of muscular activity. *Exp Brain Res* 53:244-258.
- Curtis R, Adryan KM, Stark JL, Park JS, Compton DL, Weskamp G, Huber LJ, Chao MV, Jaenisch R, Lee KF, et al. (1995) Differential role of the low affinity neurotrophin receptor (p75) in retrograde axonal transport of the neurotrophins. *Neuron* 14:1201-1211.
- Danzer SC, McNamara JO (2004) Localization of brain-derived neurotrophic factor to distinct terminals of mossy fiber axons implies regulation of both excitation and feedforward inhibition of CA3 pyramidal cells. *The Journal of neuroscience : the official journal of the Society for Neuroscience* 24:11346-11355.
- Day M, Wang Z, Ding J, An X, Ingham CA, Shering AF, Wokosin D, Ilijic E, Sun Z, Sampson AR, Mugnaini E, Deutch AY, Sesack SR, Arbuthnott GW, Surmeier DJ (2006) Selective elimination of glutamatergic synapses on striatopallidal neurons in Parkinson disease models. *Nature neuroscience* 9:251-259.
- De Camilli P, Macconi D, Spada A (1979) Dopamine inhibits adenylate cyclase in human prolactin-secreting pituitary adenomas. *Nature* 278:252-254.
- De Gois S, Schafer MK, Defamie N, Chen C, Ricci A, Weihe E, Varoqui H, Erickson JD (2005) Homeostatic scaling of vesicular glutamate and GABA transporter expression in rat neocortical circuits. *The Journal of neuroscience : the official journal of the Society for Neuroscience* 25:7121-7133.
- de Lau LM, Breteler MM (2006) Epidemiology of Parkinson's disease. *Lancet Neurol* 5:525-535.
- Dearry A, Gingrich JA, Falardeau P, Fremeau RT, Jr., Bates MD, Caron MG (1990) Molecular cloning and expression of the gene for a human D1 dopamine receptor. *Nature* 347:72-76.
- Deep-Brain Stimulation for Parkinson's Disease Study G, Obeso JA, Olanow CW, Rodriguez-Oroz MC, Krack P, Kumar R, Lang AE (2001) Deep-brain stimulation of the subthalamic nucleus or the pars interna of the globus pallidus in Parkinson's disease. *N Engl J Med* 345:956-963.
- DeLong MR (1990) Primate models of movement disorders of basal ganglia origin. *Trends Neurosci* 13:281-285.
- DeLong MR, Crutcher MD, Georgopoulos AP (1985) Primate globus pallidus and subthalamic nucleus: functional organization. *J Neurophysiol* 53:530-543.

- DeLong MR, Alexander GE, Georgopoulos AP, Crutcher MD, Mitchell SJ, Richardson RT (1984) Role of basal ganglia in limb movements. *Hum Neurobiol* 2:235-244.
- Demchyshyn LL, Sugamori KS, Lee FJ, Hamadanizadeh SA, Niznik HB (1995) The dopamine D1D receptor. Cloning and characterization of three pharmacologically distinct D1-like receptors from *Gallus domesticus*. *The Journal of biological chemistry* 270:4005-4012.
- Deschenes M, Veinante P, Zhang ZW (1998) The organization of corticothalamic projections: reciprocity versus parity. *Brain Res Brain Res Rev* 28:286-308.
- DeVito JL, Anderson ME (1982) An autoradiographic study of efferent connections of the globus pallidus in *Macaca mulatta*. *Exp Brain Res* 46:107-117.
- DeVito JL, Anderson ME, Walsh KE (1980) A horseradish peroxidase study of afferent connections of the globus pallidus in *Macaca mulatta*. *Exp Brain Res* 38:65-73.
- Dieni S, Matsumoto T, Dekkers M, Rauskolb S, Ionescu MS, Deogracias R, Gundelfinger ED, Kojima M, Nestel S, Frotscher M, Barde YA (2012) BDNF and its pro-peptide are stored in presynaptic dense core vesicles in brain neurons. *The Journal of cell biology* 196:775-788.
- Diment S, Martin KJ, Stahl PD (1989) Cleavage of parathyroid hormone in macrophage endosomes illustrates a novel pathway for intracellular processing of proteins. *The Journal of biological chemistry* 264:13403-13406.
- Ding YH, Mrizek M, Lai Q, Wu Y, Reyes R, Jr., Li J, Davis WW, Ding Y (2006) Exercise preconditioning reduces brain damage and inhibits TNF-alpha receptor expression after hypoxia/reoxygenation: an in vivo and in vitro study. *Curr Neurovasc Res* 3:263-271.
- DiStefano PS, Friedman B, Radziejewski C, Alexander C, Boland P, Schick CM, Lindsay RM, Wiegand SJ (1992) The neurotrophins BDNF, NT-3, and NGF display distinct patterns of retrograde axonal transport in peripheral and central neurons. *Neuron* 8:983-993.
- Donoghue JP, Herkenham M (1986) Neostriatal projections from individual cortical fields conform to histochemically distinct striatal compartments in the rat. *Brain Res* 365:397-403.
- Drake CT, Milner TA, Patterson SL (1999) Ultrastructural localization of full-length trkB immunoreactivity in rat hippocampus suggests multiple roles in modulating activity-dependent synaptic plasticity. *The Journal of neuroscience : the official journal of the Society for Neuroscience* 19:8009-8026.
- Du J, Feng L, Yang F, Lu B (2000) Activity- and Ca(2+)-dependent modulation of surface expression of brain-derived neurotrophic factor receptors in hippocampal neurons. *The Journal of cell biology* 150:1423-1434.
- Enjalbert A, Bockaert J (1983) Pharmacological characterization of the D2 dopamine receptor negatively coupled with adenylate cyclase in rat anterior pituitary. *Mol Pharmacol* 23:576-584.
- Erickson JT, Conover JC, Borday V, Champagnat J, Barbacid M, Yancopoulos G, Katz DM (1996) Mice lacking brain-derived neurotrophic factor exhibit visceral sensory neuron losses distinct from mice lacking NT4 and display a severe developmental deficit in control of breathing. *The Journal of neuroscience : the official journal of the Society for Neuroscience* 16:5361-5371.
- Ernfors P, Lee KF, Jaenisch R (1994) Mice lacking brain-derived neurotrophic factor develop with sensory deficits. *Nature* 368:147-150.
- Ernfors P, Wetmore C, Olson L, Persson H (1990a) Identification of cells in rat brain and peripheral tissues expressing mRNA for members of the nerve growth factor family. *Neuron* 5:511-526.
- Ernfors P, Ibanez CF, Ebendal T, Olson L, Persson H (1990b) Molecular cloning and neurotrophic activities of a protein with structural similarities to nerve growth factor: developmental and topographical expression in the brain. *Proceedings of the National Academy of Sciences of the United States of America* 87:5454-5458.
- Ernfors P, Kucera J, Lee KF, Loring J, Jaenisch R (1995) Studies on the physiological role of brain-derived neurotrophic factor and neurotrophin-3 in knockout mice. *Int J Dev Biol* 39:799-807.
- Fieblinger T, Graves SM, Sebel LE, Alcacer C, Plotkin JL, Gertler TS, Chan CS, Heiman M, Greengard P, Cenci MA, Surmeier DJ (2014) Cell type-specific plasticity of striatal projection neurons in parkinsonism and L-DOPA-induced dyskinesia. *Nature communications* 5:5316.

- Fienberg AA, Greengard P (2000) The DARPP-32 knockout mouse. *Brain Res Brain Res Rev* 31:313-319.
- Fino E, Glowinski J, Venance L (2005) Bidirectional activity-dependent plasticity at corticostriatal synapses. *The Journal of neuroscience : the official journal of the Society for Neuroscience* 25:11279-11287.
- Flores-Hernandez J, Cepeda C, Hernandez-Echeagaray E, Calvert CR, Jokel ES, Fienberg AA, Greengard P, Levine MS (2002) Dopamine enhancement of NMDA currents in dissociated medium-sized striatal neurons: role of D1 receptors and DARPP-32. *J Neurophysiol* 88:3010-3020.
- Floresco SB, West AR, Ash B, Moore H, Grace AA (2003) Afferent modulation of dopamine neuron firing differentially regulates tonic and phasic dopamine transmission. *Nature neuroscience* 6:968-973.
- Fremeau RT, Jr., Troyer MD, Pahner I, Nygaard GO, Tran CH, Reimer RJ, Bellocchio EE, Fortin D, Storm-Mathisen J, Edwards RH (2001) The expression of vesicular glutamate transporters defines two classes of excitatory synapse. *Neuron* 31:247-260.
- Freund TF, Powell JF, Smith AD (1984) Tyrosine hydroxylase-immunoreactive boutons in synaptic contact with identified striatonigral neurons, with particular reference to dendritic spines. *Neuroscience* 13:1189-1215.
- Galcheva-Gargova Z, Theroux SJ, Davis RJ (1995) The epidermal growth factor receptor is covalently linked to ubiquitin. *Oncogene* 11:2649-2655.
- Gall CM (1993) Seizure-induced changes in neurotrophin expression: implications for epilepsy. *Experimental neurology* 124:150-166.
- Gao C, Wolf ME (2008) Dopamine receptors regulate NMDA receptor surface expression in prefrontal cortex neurons. *Journal of neurochemistry* 106:2489-2501.
- Gauthier LR, Charrin BC, Borrell-Pages M, Dompierre JP, Rangone H, Cordelieres FP, De Mey J, MacDonald ME, Lessmann V, Humbert S, Saudou F (2004) Huntingtin controls neurotrophic support and survival of neurons by enhancing BDNF vesicular transport along microtubules. *Cell* 118:127-138.
- Georgopoulos AP, DeLong MR, Crutcher MD (1983) Relations between parameters of step-tracking movements and single cell discharge in the globus pallidus and subthalamic nucleus of the behaving monkey. *The Journal of neuroscience : the official journal of the Society for Neuroscience* 3:1586-1598.
- Gerfen CR (1992) The neostriatal mosaic: multiple levels of compartmental organization in the basal ganglia. *Annual review of neuroscience* 15:285-320.
- Gerfen CR (2006) Indirect-pathway neurons lose their spines in Parkinson disease. *Nature neuroscience* 9:157-158.
- Gerfen CR, Surmeier DJ (2011) Modulation of striatal projection systems by dopamine. *Annual review of neuroscience* 34:441-466.
- Gerfen CR, McGinty JF, Young WS, 3rd (1991) Dopamine differentially regulates dynorphin, substance P, and enkephalin expression in striatal neurons: in situ hybridization histochemical analysis. *The Journal of neuroscience : the official journal of the Society for Neuroscience* 11:1016-1031.
- Gerfen CR, Engber TM, Mahan LC, Susel Z, Chase TN, Monsma FJ, Jr., Sibley DR (1990) D1 and D2 dopamine receptor-regulated gene expression of striatonigral and striatopallidal neurons. *Science* 250:1429-1432.
- Ghosh A, Carnahan J, Greenberg ME (1994) Requirement for BDNF in activity-dependent survival of cortical neurons. *Science* 263:1618-1623.
- Gomez-Pinilla F, Vaynman S, Ying Z (2008) Brain-derived neurotrophic factor functions as a metabotrophin to mediate the effects of exercise on cognition. *The European journal of neuroscience* 28:2278-2287.
- Gong S, Zheng C, Doughty ML, Losos K, Didkovsky N, Schambra UB, Nowak NJ, Joyner A, Leblanc G, Hatten ME, Heintz N (2003) A gene expression atlas of the central nervous system based on bacterial artificial chromosomes. *Nature* 425:917-925.

- Gorski JA, Zeiler SR, Tamowski S, Jones KR (2003) Brain-derived neurotrophic factor is required for the maintenance of cortical dendrites. *The Journal of neuroscience : the official journal of the Society for Neuroscience* 23:6856-6865.
- Grace AA (1991) Phasic versus tonic dopamine release and the modulation of dopamine system responsivity: a hypothesis for the etiology of schizophrenia. *Neuroscience* 41:1-24.
- Grace AA, Floresco SB, Goto Y, Lodge DJ (2007) Regulation of firing of dopaminergic neurons and control of goal-directed behaviors. *Trends Neurosci* 30:220-227.
- Graham DG (1978) Oxidative pathways for catecholamines in the genesis of neuromelanin and cytotoxic quinones. *Mol Pharmacol* 14:633-643.
- Graybiel AM, Aosaki T, Flaherty AW, Kimura M (1994) The basal ganglia and adaptive motor control. *Science* 265:1826-1831.
- Graziano A, Liu XB, Murray KD, Jones EG (2008) Vesicular glutamate transporters define two sets of glutamatergic afferents to the somatosensory thalamus and two thalamocortical projections in the mouse. *The Journal of comparative neurology* 507:1258-1276.
- Griesbach GS, Hovda DA, Molteni R, Wu A, Gomez-Pinilla F (2004) Voluntary exercise following traumatic brain injury: brain-derived neurotrophic factor upregulation and recovery of function. *Neuroscience* 125:129-139.
- Grundt P, Husband SL, Luedtke RR, Taylor M, Newman AH (2007) Analogues of the dopamine D2 receptor antagonist L741,626: Binding, function, and SAR. *Bioorg Med Chem Lett* 17:745-749.
- Gwag BJ, Springer JE (1993) Activation of NMDA receptors increases brain-derived neurotrophic factor (BDNF) mRNA expression in the hippocampal formation. *Neuroreport* 5:125-128.
- Hall JM, Vetreno RP, Savage LM (2014) Differential cortical neurotrophin and cytogetic adaptation after voluntary exercise in normal and amnesic rats. *Neuroscience* 258:131-146.
- Hallett M, Khoshbin S (1980) A physiological mechanism of bradykinesia. *Brain* 103:301-314.
- Hallett PJ, Spoelgen R, Hyman BT, Standaert DG, Dunah AW (2006) Dopamine D1 activation potentiates striatal NMDA receptors by tyrosine phosphorylation-dependent subunit trafficking. *The Journal of neuroscience : the official journal of the Society for Neuroscience* 26:4690-4700.
- He XP, Kotloski R, Nef S, Luikart BW, Parada LF, McNamara JO (2004) Conditional deletion of TrkB but not BDNF prevents epileptogenesis in the kindling model. *Neuron* 43:31-42.
- Hedreen JC (1977) Corticostriatal cells identified by the peroxidase method. *Neuroscience letters* 4:1-7.
- Hedreen JC, McGrath S (1977) Observations on labeling of neuronal cell bodies, axons, and terminals after injection of horseradish peroxidase into rat brain. *The Journal of comparative neurology* 176:225-246.
- Hefti F, Melamed E, Wurtman RJ (1980) Partial lesions of the dopaminergic nigrostriatal system in rat brain: biochemical characterization. *Brain Res* 195:123-137.
- Heiman M, Schaefer A, Gong S, Peterson JD, Day M, Ramsey KE, Suarez-Farinas M, Schwarz C, Stephan DA, Surmeier DJ, Greengard P, Heintz N (2008) A translational profiling approach for the molecular characterization of CNS cell types. *Cell* 135:738-748.
- Hemmings HC, Jr., Nairn AC, Greengard P (1984a) DARPP-32, a dopamine- and adenosine 3':5'-monophosphate-regulated neuronal phosphoprotein. II. Comparison of the kinetics of phosphorylation of DARPP-32 and phosphatase inhibitor 1. *The Journal of biological chemistry* 259:14491-14497.
- Hemmings HC, Jr., Greengard P, Tung HY, Cohen P (1984b) DARPP-32, a dopamine-regulated neuronal phosphoprotein, is a potent inhibitor of protein phosphatase-1. *Nature* 310:503-505.
- Hemmings HC, Jr., Nairn AC, Aswad DW, Greengard P (1984c) DARPP-32, a dopamine- and adenosine 3':5'-monophosphate-regulated phosphoprotein enriched in dopamine-innervated brain regions. II. Purification and characterization of the phosphoprotein from bovine caudate nucleus. *The Journal of neuroscience : the official journal of the Society for Neuroscience* 4:99-110.

- Hemmings HC, Jr., Williams KR, Konigsberg WH, Greengard P (1984d) DARPP-32, a dopamine- and adenosine 3':5'-monophosphate-regulated neuronal phosphoprotein. I. Amino acid sequence around the phosphorylated threonine. *The Journal of biological chemistry* 259:14486-14490.
- Hendry SH, Schwark HD, Jones EG, Yan J (1987) Numbers and proportions of GABA-immunoreactive neurons in different areas of monkey cerebral cortex. *The Journal of neuroscience : the official journal of the Society for Neuroscience* 7:1503-1519.
- Hersch SM, Ciliax BJ, Gutekunst CA, Rees HD, Heilman CJ, Yung KK, Bolam JP, Ince E, Yi H, Levey AI (1995) Electron microscopic analysis of D1 and D2 dopamine receptor proteins in the dorsal striatum and their synaptic relationships with motor corticostriatal afferents. *The Journal of neuroscience : the official journal of the Society for Neuroscience* 15:5222-5237.
- Herzog E, Bellenchi GC, Gras C, Bernard V, Ravassard P, Bedet C, Gasnier B, Giros B, El Mestikawy S (2001) The existence of a second vesicular glutamate transporter specifies subpopulations of glutamatergic neurons. *The Journal of neuroscience : the official journal of the Society for Neuroscience* 21:RC181.
- Higley MJ, Sabatini BL (2010) Competitive regulation of synaptic Ca²⁺ influx by D2 dopamine and A2A adenosine receptors. *Nature neuroscience* 13:958-966.
- Hisano S, Sawada K, Kawano M, Kanemoto M, Xiong G, Mogi K, Sakata-Haga H, Takeda J, Fukui Y, Nogami H (2002) Expression of inorganic phosphate/vesicular glutamate transporters (BNPI/VGLUT1 and DNPI/VGLUT2) in the cerebellum and precerebellar nuclei of the rat. *Brain Res Mol Brain Res* 107:23-31.
- Hofer M, Pagliusi SR, Hohn A, Leibrock J, Barde YA (1990) Regional distribution of brain-derived neurotrophic factor mRNA in the adult mouse brain. *The EMBO journal* 9:2459-2464.
- Hoglinger GU, Alvarez-Fischer D, Arias-Carrion O, Djufri M, Windolph A, Keber U, Borta A, Ries V, Schwarting RK, Scheller D, Oertel WH (2015) A new dopaminergic nigro-olfactory projection. *Acta Neuropathol* 130:333-348.
- Howells DW, Porritt MJ, Wong JY, Batchelor PE, Kalnins R, Hughes AJ, Donnan GA (2000) Reduced BDNF mRNA expression in the Parkinson's disease substantia nigra. *Experimental neurology* 166:127-135.
- Huang EJ, Reichardt LF (2001) Neurotrophins: roles in neuronal development and function. *Annual review of neuroscience* 24:677-736.
- Hur EE, Zaborszky L (2005) Vglut2 afferents to the medial prefrontal and primary somatosensory cortices: a combined retrograde tracing in situ hybridization study [corrected]. *The Journal of comparative neurology* 483:351-373.
- Isackson PJ, Huntsman MM, Murray KD, Gall CM (1991) BDNF mRNA expression is increased in adult rat forebrain after limbic seizures: temporal patterns of induction distinct from NGF. *Neuron* 6:937-948.
- Iwakura Y, Nawa H, Sora I, Chao MV (2008) Dopamine D1 receptor-induced signaling through TrkB receptors in striatal neurons. *The Journal of biological chemistry* 283:15799-15806.
- Jasmin L, Burkey AR, Granato A, Ohara PT (2004) Rostral agranular insular cortex and pain areas of the central nervous system: a tract-tracing study in the rat. *The Journal of comparative neurology* 468:425-440.
- Jeanblanc J, He DY, Carnicella S, Kharazia V, Janak PH, Ron D (2009) Endogenous BDNF in the dorsolateral striatum gates alcohol drinking. *The Journal of neuroscience : the official journal of the Society for Neuroscience* 29:13494-13502.
- Jeffers M, Taylor GA, Weidner KM, Omura S, Vande Woude GF (1997) Degradation of the Met tyrosine kinase receptor by the ubiquitin-proteasome pathway. *Mol Cell Biol* 17:799-808.
- Jia Y, Gall CM, Lynch G (2010) Presynaptic BDNF promotes postsynaptic long-term potentiation in the dorsal striatum. *The Journal of neuroscience : the official journal of the Society for Neuroscience* 30:14440-14445.
- Jin H, Wu H, Osterhaus G, Wei J, Davis K, Sha D, Floor E, Hsu CC, Kopke RD, Wu JY (2003) Demonstration of functional coupling between gamma -aminobutyric acid (GABA) synthesis

- and vesicular GABA transport into synaptic vesicles. *Proceedings of the National Academy of Sciences of the United States of America* 100:4293-4298.
- Johnson TN, Rosvold HE (1971) Topographic projections on the globus pallidus and the substantia nigra of selectively placed lesions in the precommissural caudate nucleus and putamen in the monkey. *Experimental neurology* 33:584-596.
- Jones KR, Farinas I, Backus C, Reichardt LF (1994) Targeted disruption of the BDNF gene perturbs brain and sensory neuron development but not motor neuron development. *Cell* 76:989-999.
- Jonsson G (1980) Chemical neurotoxins as denervation tools in neurobiology. *Annual review of neuroscience* 3:169-187.
- Kalivas PW (2009) The glutamate homeostasis hypothesis of addiction. *Nature reviews Neuroscience* 10:561-572.
- Kanazawa I, Murata M, Kimura M (1993) Roles of dopamine and its receptors in generation of choreic movements. *Advances in neurology* 60:107-112.
- Kaplan DR, Miller FD (2000) Neurotrophin signal transduction in the nervous system. *Current opinion in neurobiology* 10:381-391.
- Katz LC (1987) Local circuitry of identified projection neurons in cat visual cortex brain slices. *The Journal of neuroscience : the official journal of the Society for Neuroscience* 7:1223-1249.
- Kaufman DL, Houser CR, Tobin AJ (1991) Two forms of the gamma-aminobutyric acid synthetic enzyme glutamate decarboxylase have distinct intraneuronal distributions and cofactor interactions. *Journal of neurochemistry* 56:720-723.
- Kaufman S (1995) Tyrosine hydroxylase. *Adv Enzymol Relat Areas Mol Biol* 70:103-220.
- Kawaguchi Y (1997) Neostriatal cell subtypes and their functional roles. *Neurosci Res* 27:1-8.
- Kebabian JW, Calne DB (1979) Multiple receptors for dopamine. *Nature* 277:93-96.
- Kelley AE, Domesick VB, Nauta WJ (1982) The amygdalostriatal projection in the rat--an anatomical study by anterograde and retrograde tracing methods. *Neuroscience* 7:615-630.
- Kim J, Matney CJ, Blankenship A, Hestrin S, Brown SP (2014) Layer 6 corticothalamic neurons activate a cortical output layer, layer 5a. *The Journal of neuroscience : the official journal of the Society for Neuroscience* 34:9656-9664.
- Kim R, Nakano K, Jayaraman A, Carpenter MB (1976) Projections of the globus pallidus and adjacent structures: an autoradiographic study in the monkey. *The Journal of comparative neurology* 169:263-290.
- Kimura M, Aosaki T, Ishida A (1993) Neurophysiological aspects of the differential roles of the putamen and caudate nucleus in voluntary movement. *Advances in neurology* 60:62-70.
- Kitai ST, Kocsis JD, Wood J (1976) Origin and characteristics of the cortico-caudate afferents: an anatomical and electrophysiological study. *Brain Res* 118:137-141.
- Kitazono T, Faraci FM, Taguchi H, Heistad DD (1995) Role of potassium channels in cerebral blood vessels. *Stroke* 26:1713-1723.
- Koizumi H, Morigaki R, Okita S, Nagahiro S, Kaji R, Nakagawa M, Goto S (2013) Response of striosomal opioid signaling to dopamine depletion in 6-hydroxydopamine-lesioned rat model of Parkinson's disease: a potential compensatory role. *Front Cell Neurosci* 7:74.
- Kolbeck R, Bartke I, Eberle W, Barde YA (1999) Brain-derived neurotrophic factor levels in the nervous system of wild-type and neurotrophin gene mutant mice. *Journal of neurochemistry* 72:1930-1938.
- Kornhuber J, Kim JS, Kornhuber ME, Kornhuber HH (1984) The cortico-nigral projection: reduced glutamate content in the substantia nigra following frontal cortex ablation in the rat. *Brain Res* 322:124-126.
- Korte M, Carroll P, Wolf E, Brem G, Thoenen H, Bonhoeffer T (1995) Hippocampal long-term potentiation is impaired in mice lacking brain-derived neurotrophic factor. *Proceedings of the National Academy of Sciences of the United States of America* 92:8856-8860.
- Kramer PF, Christensen CH, Hazelwood LA, Dobi A, Bock R, Sibley DR, Mateo Y, Alvarez VA (2011) Dopamine D2 receptor overexpression alters behavior and physiology in *Drd2-EGFP* mice. *The Journal of neuroscience : the official journal of the Society for Neuroscience* 31:126-132.

- Kreitzer AC, Malenka RC (2005) Dopamine modulation of state-dependent endocannabinoid release and long-term depression in the striatum. *The Journal of neuroscience : the official journal of the Society for Neuroscience* 25:10537-10545.
- Kreitzer AC, Malenka RC (2008) Striatal plasticity and basal ganglia circuit function. *Neuron* 60:543-554.
- Kruger R, Kuhn W, Muller T, Woitalla D, Graeber M, Kosel S, Przuntek H, Epplen JT, Schols L, Riess O (1998) Ala30Pro mutation in the gene encoding alpha-synuclein in Parkinson's disease. *Nat Genet* 18:106-108.
- Kumar R, Lozano AM, Kim YJ, Hutchison WD, Sime E, Halket E, Lang AE (1998) Double-blind evaluation of subthalamic nucleus deep brain stimulation in advanced Parkinson's disease. *Neurology* 51:850-855.
- Kunzle H (1975) Bilateral projections from precentral motor cortex to the putamen and other parts of the basal ganglia. An autoradiographic study in *Macaca fascicularis*. *Brain Res* 88:195-209.
- Kunzle H (1977) Projections from the primary somatosensory cortex to basal ganglia and thalamus in the monkey. *Exp Brain Res* 30:481-492.
- Kunzle H (1978) An autoradiographic analysis of the efferent connections from premotor and adjacent prefrontal regions (areas 6 and 9) in *macaca fascicularis*. *Brain Behav Evol* 15:185-234.
- Kuo JS, Carpenter MB (1973) Organization of pallidothalamic projections in the rhesus monkey. *The Journal of comparative neurology* 151:201-236.
- Lang AE, Lozano AM (1998a) Parkinson's disease. Second of two parts. *N Engl J Med* 339:1130-1143.
- Lang AE, Lozano AM (1998b) Parkinson's disease. First of two parts. *N Engl J Med* 339:1044-1053.
- Lee FS, Chao MV (2001) Activation of Trk neurotrophin receptors in the absence of neurotrophins. *Proceedings of the National Academy of Sciences of the United States of America* 98:3555-3560.
- Lee FS, Rajagopal R, Chao MV (2002) Distinctive features of Trk neurotrophin receptor transactivation by G protein-coupled receptors. *Cytokine Growth Factor Rev* 13:11-17.
- Lesscher HM, Vanderschuren LJ (2012) Compulsive drug use and its neural substrates. *Rev Neurosci* 23:731-745.
- Levi-Montalcini R, Hamburger V (1951) Selective growth stimulating effects of mouse sarcoma on the sensory and sympathetic nervous system of the chick embryo. *J Exp Zool* 116:321-361.
- Levy R, Vila M, Herrero MT, Faucheux B, Agid Y, Hirsch EC (1995) Striatal expression of substance P and methionin-enkephalin in genes in patients with Parkinson's disease. *Neuroscience letters* 199:220-224.
- Lewin GR, Barde YA (1996) Physiology of the neurotrophins. *Annual review of neuroscience* 19:289-317.
- Li JL, Xiong KH, Dong YL, Fujiyama F, Kaneko T, Mizuno N (2003) Vesicular glutamate transporters, VGLUT1 and VGLUT2, in the trigeminal ganglion neurons of the rat, with special reference to coexpression. *The Journal of comparative neurology* 463:212-220.
- Li Y, Yui D, Luikart BW, McKay RM, Li Y, Rubenstein JL, Parada LF (2012) Conditional ablation of brain-derived neurotrophic factor-TrkB signaling impairs striatal neuron development. *Proceedings of the National Academy of Sciences of the United States of America* 109:15491-15496.
- Liebl DJ, Tessarollo L, Palko ME, Parada LF (1997) Absence of sensory neurons before target innervation in brain-derived neurotrophic factor-, neurotrophin 3-, and TrkC-deficient embryonic mice. *The Journal of neuroscience : the official journal of the Society for Neuroscience* 17:9113-9121.
- Liles SL (1985) Activity of neurons in putamen during active and passive movements of wrist. *J Neurophysiol* 53:217-236.
- Liu X, Ernfors P, Wu H, Jaenisch R (1995) Sensory but not motor neuron deficits in mice lacking NT4 and BDNF. *Nature* 375:238-241.

- Llano DA, Sherman SM (2008) Evidence for nonreciprocal organization of the mouse auditory thalamocortical-corticothalamic projection systems. *The Journal of comparative neurology* 507:1209-1227.
- Lobo MK, Covington HE, 3rd, Chaudhury D, Friedman AK, Sun H, Damez-Werno D, Dietz DM, Zaman S, Koo JW, Kennedy PJ, Mouzon E, Mogri M, Neve RL, Deisseroth K, Han MH, Nestler EJ (2010) Cell type-specific loss of BDNF signaling mimics optogenetic control of cocaine reward. *Science* 330:385-390.
- Lopez-Benito S, Sanchez-Sanchez J, Brito V, Calvo L, Lisa S, Torres-Valle M, Palko ME, Vicente-Garcia C, Fernandez-Fernandez S, Bolanos JP, Gines S, Tessarollo L, Arevalo JC (2018) Regulation of BDNF Release by ARMS/Kidins220 through Modulation of Synaptotagmin-IV Levels. *The Journal of neuroscience : the official journal of the Society for Neuroscience* 38:5415-5428.
- Luikart BW, Parada LF (2006) Receptor tyrosine kinase B-mediated excitatory synaptogenesis. *Prog Brain Res* 157:15-24.
- Luthman J, Fredriksson A, Sundstrom E, Jonsson G, Archer T (1989) Selective lesion of central dopamine or noradrenaline neuron systems in the neonatal rat: motor behavior and monoamine alterations at adult stage. *Behavioural brain research* 33:267-277.
- Macpherson JM, Marangoz C, Miles TS, Wiesendanger M (1982) Microstimulation of the supplementary motor area (SMA) in the awake monkey. *Exp Brain Res* 45:410-416.
- Magnifico A, Tagliabue E, Ardini E, Casalini P, Colnaghi MI, Menard S (1998) Heregulin beta1 induces the down regulation and the ubiquitin-proteasome degradation pathway of p185HER2 oncoprotein. *FEBS letters* 422:129-131.
- Mahon S, Deniau JM, Charpier S (2004) Corticostriatal plasticity: life after the depression. *Trends Neurosci* 27:460-467.
- Markram H, Toledo-Rodriguez M, Wang Y, Gupta A, Silberberg G, Wu C (2004) Interneurons of the neocortical inhibitory system. *Nature reviews Neuroscience* 5:793-807.
- Matamales M, Bertran-Gonzalez J, Salomon L, Degos B, Deniau JM, Valjent E, Herve D, Girault JA (2009) Striatal medium-sized spiny neurons: identification by nuclear staining and study of neuronal subpopulations in BAC transgenic mice. *PLoS One* 4:e4770.
- Matsumoto T, Rauskolb S, Polack M, Klose J, Kolbeck R, Korte M, Barde YA (2008) Biosynthesis and processing of endogenous BDNF: CNS neurons store and secrete BDNF, not pro-BDNF. *Nature neuroscience* 11:131-133.
- McCall RB, Lookingland KJ, Bedard PJ, Huff RM (2005) Sumanriole, a highly dopamine D2-selective receptor agonist: in vitro and in vivo pharmacological characterization and efficacy in animal models of Parkinson's disease. *J Pharmacol Exp Ther* 314:1248-1256.
- McDonald WM, Sibley DR, Kilpatrick BF, Caron MG (1984) Dopaminergic inhibition of adenylate cyclase correlates with high affinity agonist binding to anterior pituitary D2 dopamine receptors. *Mol Cell Endocrinol* 36:201-209.
- McGeorge AJ, Faull RL (1989) The organization of the projection from the cerebral cortex to the striatum in the rat. *Neuroscience* 29:503-537.
- Meinecke DL, Peters A (1987) GABA immunoreactive neurons in rat visual cortex. *The Journal of comparative neurology* 261:388-404.
- Memo M, Missale C, Carruba MO, Spano PF (1986) Pharmacology and biochemistry of dopamine receptors in the central nervous system and peripheral tissue. *J Neural Transm Suppl* 22:19-32.
- Mengod G, Martinez-Mir MI, Vilaro MT, Palacios JM (1989) Localization of the mRNA for the dopamine D2 receptor in the rat brain by in situ hybridization histochemistry. *Proceedings of the National Academy of Sciences of the United States of America* 86:8560-8564.
- Meyer-Franke A, Wilkinson GA, Kruttgen A, Hu M, Munro E, Hanson MG, Jr., Reichardt LF, Barres BA (1998) Depolarization and cAMP elevation rapidly recruit TrkB to the plasma membrane of CNS neurons. *Neuron* 21:681-693.
- Middlemas DS, Lindberg RA, Hunter T (1991) trkB, a neural receptor protein-tyrosine kinase: evidence for a full-length and two truncated receptors. *Mol Cell Biol* 11:143-153.

- Mimnaugh EG, Chavany C, Neckers L (1996) Polyubiquitination and proteasomal degradation of the p185c-erbB-2 receptor protein-tyrosine kinase induced by geldanamycin. *The Journal of biological chemistry* 271:22796-22801.
- Minichiello L (2009) TrkB signalling pathways in LTP and learning. *Nature reviews Neuroscience* 10:850-860.
- Minichiello L, Korte M, Wolfer D, Kuhn R, Unsicker K, Cestari V, Rossi-Arnaud C, Lipp HP, Bonhoeffer T, Klein R (1999) Essential role for TrkB receptors in hippocampus-mediated learning. *Neuron* 24:401-414.
- Mink JW (1996) The basal ganglia: focused selection and inhibition of competing motor programs. *Prog Neurobiol* 50:381-425.
- Miyata M, Sasaki K (1984) Horseradish peroxidase studies on thalamic and striatal connections of the mesial part of area 6 in the monkey. *Neuroscience letters* 49:127-133.
- Miyazawa K, Toyama K, Gotoh A, Hendrie PC, Mantel C, Broxmeyer HE (1994) Ligand-dependent polyubiquitination of c-kit gene product: a possible mechanism of receptor down modulation in M07e cells. *Blood* 83:137-145.
- Molnar Z, Cheung AF (2006) Towards the classification of subpopulations of layer V pyramidal projection neurons. *Neurosci Res* 55:105-115.
- Molyneaux BJ, Arlotta P, Menezes JR, Macklis JD (2007) Neuronal subtype specification in the cerebral cortex. *Nature reviews Neuroscience* 8:427-437.
- Monsma FJ, Jr., Mahan LC, McVittie LD, Gerfen CR, Sibley DR (1990) Molecular cloning and expression of a D1 dopamine receptor linked to adenylyl cyclase activation. *Proceedings of the National Academy of Sciences of the United States of America* 87:6723-6727.
- Monteggia LM, Luikart B, Barrot M, Theobald D, Malkovska I, Nef S, Parada LF, Nestler EJ (2007) Brain-derived neurotrophic factor conditional knockouts show gender differences in depression-related behaviors. *Biol Psychiatry* 61:187-197.
- Mori S, Heldin CH, Claesson-Welsh L (1992) Ligand-induced polyubiquitination of the platelet-derived growth factor beta-receptor. *The Journal of biological chemistry* 267:6429-6434.
- Mori S, Tanaka K, Omura S, Saito Y (1995) Degradation process of ligand-stimulated platelet-derived growth factor beta-receptor involves ubiquitin-proteasome proteolytic pathway. *The Journal of biological chemistry* 270:29447-29452.
- Muakkassa KF, Strick PL (1979) Frontal lobe inputs to primate motor cortex: evidence for four somatotopically organized 'premotor' areas. *Brain Res* 177:176-182.
- Mufson EJ, Kroin JS, Sendera TJ, Sobrevela T (1999) Distribution and retrograde transport of trophic factors in the central nervous system: functional implications for the treatment of neurodegenerative diseases. *Prog Neurobiol* 57:451-484.
- Murray EA, Coulter JD (1981) Organization of corticospinal neurons in the monkey. *The Journal of comparative neurology* 195:339-365.
- Nagatsu T (1995) Tyrosine hydroxylase: human isoforms, structure and regulation in physiology and pathology. *Essays Biochem* 30:15-35.
- Naito A, Kita H (1994) The cortico-nigral projection in the rat: an anterograde tracing study with biotinylated dextran amine. *Brain Res* 637:317-322.
- Nakamura K, Watakabe A, Hioki H, Fujiyama F, Tanaka Y, Yamamori T, Kaneko T (2007) Transiently increased colocalization of vesicular glutamate transporters 1 and 2 at single axon terminals during postnatal development of mouse neocortex: a quantitative analysis with correlation coefficient. *The European journal of neuroscience* 26:3054-3067.
- Nauta WJ, Mehler WR (1966) Projections of the lentiform nucleus in the monkey. *Brain Res* 1:3-42.
- Neeper SA, Gomez-Pinilla F, Choi J, Cotman C (1995) Exercise and brain neurotrophins. *Nature* 373:109.
- Neeper SA, Gomez-Pinilla F, Choi J, Cotman CW (1996) Physical activity increases mRNA for brain-derived neurotrophic factor and nerve growth factor in rat brain. *Brain Res* 726:49-56.
- Nelson MT, Quayle JM (1995) Physiological roles and properties of potassium channels in arterial smooth muscle. *Am J Physiol* 268:C799-822.

- Nieto M, Monuki ES, Tang H, Imitola J, Haubst N, Khoury SJ, Cunningham J, Gotz M, Walsh CA (2004) Expression of Cux-1 and Cux-2 in the subventricular zone and upper layers II-IV of the cerebral cortex. *The Journal of comparative neurology* 479:168-180.
- Nishi A, Snyder GL, Greengard P (1997) Bidirectional regulation of DARPP-32 phosphorylation by dopamine. *The Journal of neuroscience : the official journal of the Society for Neuroscience* 17:8147-8155.
- Nishio T, Furukawa S, Akiguchi I, Sunohara N (1998) Medial nigral dopamine neurons have rich neurotrophin support in humans. *Neuroreport* 9:2847-2851.
- Numan S, Seroogy KB (1999) Expression of trkB and trkC mRNAs by adult midbrain dopamine neurons: a double-label in situ hybridization study. *The Journal of comparative neurology* 403:295-308.
- Obeso JA, Olanow CW, Nutt JG (2000) Levodopa motor complications in Parkinson's disease. *Trends Neurosci* 23:S2-7.
- Oda S, Funato H, Sato F, Adachi-Akahane S, Ito M, Takase K, Kuroda M (2014) A subset of thalamocortical projections to the retrosplenial cortex possesses two vesicular glutamate transporter isoforms, VGLUT1 and VGLUT2, in axon terminals and somata. *The Journal of comparative neurology* 522:2089-2106.
- Okazawa H, Murata M, Watanabe M, Kamei M, Kanazawa I (1992) Dopaminergic stimulation up-regulates the in vivo expression of brain-derived neurotrophic factor (BDNF) in the striatum. *FEBS letters* 313:138-142.
- Onali P, Schwartz JP, Costa E (1981) Dopaminergic modulation of adenylate cyclase stimulation by vasoactive intestinal peptide in anterior pituitary. *Proceedings of the National Academy of Sciences of the United States of America* 78:6531-6534.
- Onali P, Olanow MC, Gessa GL (1985) Characterization of dopamine receptors mediating inhibition of adenylate cyclase activity in rat striatum. *Mol Pharmacol* 28:138-145.
- Ottersen OP (1982) Connections of the amygdala of the rat. IV: Corticoamygdaloid and intraamygdaloid connections as studied with axonal transport of horseradish peroxidase. *The Journal of comparative neurology* 205:30-48.
- Quimet CC, Miller PE, Hemmings HC, Jr., Walaas SI, Greengard P (1984) DARPP-32, a dopamine- and adenosine 3':5'-monophosphate-regulated phosphoprotein enriched in dopamine-innervated brain regions. III. Immunocytochemical localization. *The Journal of neuroscience : the official journal of the Society for Neuroscience* 4:111-124.
- Palmer C, Schmidt EM, McIntosh JS (1981) Corticospinal and corticorubral projections from the supplementary motor area in the monkey. *Brain Res* 209:305-314.
- Parent A, Bouchard C, Smith Y (1984) The striatopallidal and striatonigral projections: two distinct fiber systems in primate. *Brain Res* 303:385-390.
- Parent A, Mackey A, Smith Y, Boucher R (1983) The output organization of the substantia nigra in primate as revealed by a retrograde double labeling method. *Brain Res Bull* 10:529-537.
- Park H, Popescu A, Poo MM (2014) Essential role of presynaptic NMDA receptors in activity-dependent BDNF secretion and corticostriatal LTP. *Neuron* 84:1009-1022.
- Parkinson J (2002) An essay on the shaking palsy. 1817. *J Neuropsychiatry Clin Neurosci* 14:223-236; discussion 222.
- Passante L, Gaspard N, Degraeve M, Frisen J, Kullander K, De Maertelaer V, Vanderhaeghen P (2008) Temporal regulation of ephrin/Eph signalling is required for the spatial patterning of the mammalian striatum. *Development* 135:3281-3290.
- Penney JB, Jr., Young AB (1983) Speculations on the functional anatomy of basal ganglia disorders. *Annual review of neuroscience* 6:73-94.
- Penrod RD, Kourrich S, Kearney E, Thomas MJ, Lanier LM (2011) An embryonic culture system for the investigation of striatal medium spiny neuron dendritic spine development and plasticity. *Journal of neuroscience methods* 200:1-13.
- Phillips HS, Hains JM, Laramée GR, Rosenthal A, Winslow JW (1990) Widespread expression of BDNF but not NT3 by target areas of basal forebrain cholinergic neurons. *Science* 250:290-294.

- Picconi B, Centonze D, Hakansson K, Bernardi G, Greengard P, Fisone G, Cenci MA, Calabresi P (2003) Loss of bidirectional striatal synaptic plasticity in L-DOPA-induced dyskinesia. *Nature neuroscience* 6:501-506.
- Plotkin JL, Day M, Peterson JD, Xie Z, Kress GJ, Rafalovich I, Kondapalli J, Gertler TS, Flajolet M, Greengard P, Stavarache M, Kaplitt MG, Rosinski J, Chan CS, Surmeier DJ (2014) Impaired TrkB receptor signaling underlies corticostriatal dysfunction in Huntington's disease. *Neuron* 83:178-188.
- Polymeropoulos MH, Lavedan C, Leroy E, Ide SE, Dehejia A, Dutra A, Pike B, Root H, Rubenstein J, Boyer R, Stenroos ES, Chandrasekharappa S, Athanassiadou A, Papapetropoulos T, Johnson WG, Lazzarini AM, Duvoisin RC, Di Iorio G, Golbe LI, Nussbaum RL (1997) Mutation in the alpha-synuclein gene identified in families with Parkinson's disease. *Science* 276:2045-2047.
- Poo MM (2001) Neurotrophins as synaptic modulators. *Nature reviews Neuroscience* 2:24-32.
- Price JL, Drevets WC (2012) Neural circuits underlying the pathophysiology of mood disorders. *Trends Cogn Sci* 16:61-71.
- Pringsheim T, Wiltshire K, Day L, Dykeman J, Steeves T, Jette N (2012) The incidence and prevalence of Huntington's disease: a systematic review and meta-analysis. *Mov Disord* 27:1083-1091.
- Przedborski S, Levivier M, Jiang H, Ferreira M, Jackson-Lewis V, Donaldson D, Togasaki DM (1995) Dose-dependent lesions of the dopaminergic nigrostriatal pathway induced by intrastriatal injection of 6-hydroxydopamine. *Neuroscience* 67:631-647.
- Puehringer D, Orel N, Luningschror P, Subramanian N, Herrmann T, Chao MV, Sendtner M (2013) EGF transactivation of Trk receptors regulates the migration of newborn cortical neurons. *Nature neuroscience* 16:407-415.
- Rajagopal R, Chao MV (2006) A role for Fyn in Trk receptor transactivation by G-protein-coupled receptor signaling. *Mol Cell Neurosci* 33:36-46.
- Rajagopal R, Chen ZY, Lee FS, Chao MV (2004) Transactivation of Trk neurotrophin receptors by G-protein-coupled receptor ligands occurs on intracellular membranes. *The Journal of neuroscience : the official journal of the Society for Neuroscience* 24:6650-6658.
- Rasmussen P, Brassard P, Adser H, Pedersen MV, Leick L, Hart E, Secher NH, Pedersen BK, Pilegaard H (2009) Evidence for a release of brain-derived neurotrophic factor from the brain during exercise. *Exp Physiol* 94:1062-1069.
- Rauskolb S, Zagrebelsky M, Dreznjak A, Deogracias R, Matsumoto T, Wiese S, Erne B, Sendtner M, Schaeren-Wiemers N, Korte M, Barde YA (2010) Global deprivation of brain-derived neurotrophic factor in the CNS reveals an area-specific requirement for dendritic growth. *The Journal of neuroscience : the official journal of the Society for Neuroscience* 30:1739-1749.
- Reep RL, Cheatwood JL, Corwin JV (2003) The associative striatum: organization of cortical projections to the dorsocentral striatum in rats. *The Journal of comparative neurology* 467:271-292.
- Reiner A, Albin RL, Anderson KD, D'Amato CJ, Penney JB, Young AB (1988) Differential loss of striatal projection neurons in Huntington disease. *Proceedings of the National Academy of Sciences of the United States of America* 85:5733-5737.
- Reynolds JN, Hyland BI, Wickens JR (2001) A cellular mechanism of reward-related learning. *Nature* 413:67-70.
- Rinvik E (1966) The cortico-nigral projection in the cat. An experimental study with silver impregnation methods. *The Journal of comparative neurology* 126:241-254.
- Rios M, Fan G, Fekete C, Kelly J, Bates B, Kuehn R, Lechan RM, Jaenisch R (2001) Conditional deletion of brain-derived neurotrophic factor in the postnatal brain leads to obesity and hyperactivity. *Mol Endocrinol* 15:1748-1757.
- Rodriguez-Oroz MC et al. (2005) Bilateral deep brain stimulation in Parkinson's disease: a multicentre study with 4 years follow-up. *Brain* 128:2240-2249.
- Rohrer B, Korenbrot JI, LaVail MM, Reichardt LF, Xu B (1999) Role of neurotrophin receptor TrkB in the maturation of rod photoreceptors and establishment of synaptic transmission to the

- inner retina. *The Journal of neuroscience : the official journal of the Society for Neuroscience* 19:8919-8930.
- Roland PE, Larsen B, Lassen NA, Skinhoj E (1980) Supplementary motor area and other cortical areas in organization of voluntary movements in man. *J Neurophysiol* 43:118-136.
- Rose CR, Blum R, Pichler B, Lepier A, Kafitz KW, Konnerth A (2003) Truncated TrkB-T1 mediates neurotrophin-evoked calcium signalling in glia cells. *Nature* 426:74-78.
- Rossoll W, Kroning AK, Ohndorf UM, Steegborn C, Jablonka S, Sendtner M (2002) Specific interaction of Smn, the spinal muscular atrophy determining gene product, with hnRNP-R and gry-rbp/hnRNP-Q: a role for Smn in RNA processing in motor axons? *Hum Mol Genet* 11:93-105.
- Sakata K, Woo NH, Martinowich K, Greene JS, Schloesser RJ, Shen L, Lu B (2009) Critical role of promoter IV-driven BDNF transcription in GABAergic transmission and synaptic plasticity in the prefrontal cortex. *Proceedings of the National Academy of Sciences of the United States of America* 106:5942-5947.
- Salgado H, Tecuapetla F, Perez-Rosello T, Perez-Burgos A, Perez-Garci E, Galarraga E, Vargas J (2005) A reconfiguration of CaV2 Ca²⁺ channel current and its dopaminergic D2 modulation in developing neostriatal neurons. *J Neurophysiol* 94:3771-3787.
- Saner A, Thoenen H (1971) Model experiments on the molecular mechanism of action of 6-hydroxydopamine. *Mol Pharmacol* 7:147-154.
- Sarre S, Yuan H, Jonkers N, Van Hemelrijck A, Ebinger G, Michotte Y (2004) In vivo characterization of somatodendritic dopamine release in the substantia nigra of 6-hydroxydopamine-lesioned rats. *Journal of neurochemistry* 90:29-39.
- Schell GR, Strick PL (1984) The origin of thalamic inputs to the arcuate premotor and supplementary motor areas. *The Journal of neuroscience : the official journal of the Society for Neuroscience* 4:539-560.
- Schlessinger J (2000) Cell signaling by receptor tyrosine kinases. *Cell* 103:211-225.
- Schwab M, Agid Y, Glowinski J, Thoenen H (1977) Retrograde axonal transport of 125I-tetanus toxin as a tool for tracing fiber connections in the central nervous system; connections of the rostral part of the rat neostriatum. *Brain Res* 126:211-224.
- Schweizer U, Gunnarsen J, Karch C, Wiese S, Holtmann B, Takeda K, Akira S, Sendtner M (2002) Conditional gene ablation of Stat3 reveals differential signaling requirements for survival of motoneurons during development and after nerve injury in the adult. *The Journal of cell biology* 156:287-297.
- Seamon KB, Padgett W, Daly JW (1981) Forskolin: unique diterpene activator of adenylate cyclase in membranes and in intact cells. *Proceedings of the National Academy of Sciences of the United States of America* 78:3363-3367.
- Sebben M, Gabrion J, Manzoni O, Sladeczek F, Gril C, Bockaert J, Dumuis A (1990) Establishment of a long-term primary culture of striatal neurons. *Brain Res Dev Brain Res* 52:229-239.
- Selemon LD, Goldman-Rakic PS (1985) Longitudinal topography and interdigitation of corticostriatal projections in the rhesus monkey. *The Journal of neuroscience : the official journal of the Society for Neuroscience* 5:776-794.
- Seroogy KB, Lundgren KH, Tran TM, Guthrie KM, Isackson PJ, Gall CM (1994) Dopaminergic neurons in rat ventral midbrain express brain-derived neurotrophic factor and neurotrophin-3 mRNAs. *The Journal of comparative neurology* 342:321-334.
- Sesack SR, Deutch AY, Roth RH, Bunney BS (1989) Topographical organization of the efferent projections of the medial prefrontal cortex in the rat: an anterograde tract-tracing study with *Phaseolus vulgaris* leucoagglutinin. *The Journal of comparative neurology* 290:213-242.
- Shen W, Flajolet M, Greengard P, Surmeier DJ (2008) Dichotomous dopaminergic control of striatal synaptic plasticity. *Science* 321:848-851.
- Shen W, Plotkin JL, Francardo V, Ko WK, Xie Z, Li Q, Fieblinger T, Wess J, Neubig RR, Lindsley CW, Conn PJ, Greengard P, Bezard E, Cenci MA, Surmeier DJ (2016) M4 Muscarinic Receptor Signaling Ameliorates Striatal Plasticity Deficits in Models of L-DOPA-Induced Dyskinesia. *Neuron* 90:1139.

- Shepherd JD, Huganir RL (2007) The cell biology of synaptic plasticity: AMPA receptor trafficking. *Annu Rev Cell Dev Biol* 23:613-643.
- Skeberdis VA, Chevaleyre V, Lau CG, Goldberg JH, Pettit DL, Suadicani SO, Lin Y, Bennett MV, Yuste R, Castillo PE, Zukin RS (2006) Protein kinase A regulates calcium permeability of NMDA receptors. *Nature neuroscience* 9:501-510.
- Skogh C, Campbell K (2003) Homotopic glial regulation of striatal projection neuron differentiation. *Neuroreport* 14:1037-1040.
- Sommerfeld MT, Schweigreiter R, Barde YA, Hoppe E (2000) Down-regulation of the neurotrophin receptor TrkB following ligand binding. Evidence for an involvement of the proteasome and differential regulation of TrkA and TrkB. *The Journal of biological chemistry* 275:8982-8990.
- Soppet D, Escandon E, Maragos J, Middlemas DS, Reid SW, Blair J, Burton LE, Stanton BR, Kaplan DR, Hunter T, Nikolics K, Parada LF (1991) The neurotrophic factors brain-derived neurotrophic factor and neurotrophin-3 are ligands for the trkB tyrosine kinase receptor. *Cell* 65:895-903.
- Spillantini MG, Schmidt ML, Lee VM, Trojanowski JQ, Jakes R, Goedert M (1997) Alpha-synuclein in Lewy bodies. *Nature* 388:839-840.
- Stoof JC, Kebabian JW (1984) Two dopamine receptors: biochemistry, physiology and pharmacology. *Life Sci* 35:2281-2296.
- Sugamori KS, Demchyshyn LL, Chung M, Niznik HB (1994) D1A, D1B, and D1C dopamine receptors from *Xenopus laevis*. *Proceedings of the National Academy of Sciences of the United States of America* 91:10536-10540.
- Sun X, Zhao Y, Wolf ME (2005) Dopamine receptor stimulation modulates AMPA receptor synaptic insertion in prefrontal cortex neurons. *The Journal of neuroscience : the official journal of the Society for Neuroscience* 25:7342-7351.
- Sun X, Milovanovic M, Zhao Y, Wolf ME (2008) Acute and chronic dopamine receptor stimulation modulates AMPA receptor trafficking in nucleus accumbens neurons cocultured with prefrontal cortex neurons. *The Journal of neuroscience : the official journal of the Society for Neuroscience* 28:4216-4230.
- Surmeier DJ, Graves SM, Shen W (2014) Dopaminergic modulation of striatal networks in health and Parkinson's disease. *Current opinion in neurobiology* 29:109-117.
- Surmeier DJ, Bargas J, Hemmings HC, Jr., Nairn AC, Greengard P (1995) Modulation of calcium currents by a D1 dopaminergic protein kinase/phosphatase cascade in rat neostriatal neurons. *Neuron* 14:385-397.
- Svenningsson P, Nishi A, Fisone G, Girault JA, Nairn AC, Greengard P (2004) DARPP-32: an integrator of neurotransmission. *Annu Rev Pharmacol Toxicol* 44:269-296.
- Szabo J (1967) The efferent projections of the putamen in the monkey. *Experimental neurology* 19:463-476.
- Takahashi K, Maejima H, Ikuta G, Mani H, Asaka T (2017) Exercise combined with low-level GABAA receptor inhibition up-regulates the expression of neurotrophins in the motor cortex. *Neuroscience letters* 636:101-107.
- Tanji J, Evarts EV (1976) Anticipatory activity of motor cortex neurons in relation to direction of an intended movement. *J Neurophysiol* 39:1062-1068.
- Tanji J, Taniguchi K, Saga T (1980) Supplementary motor area: neuronal response to motor instructions. *J Neurophysiol* 43:60-68.
- Tao X, Finkbeiner S, Arnold DB, Shaywitz AJ, Greenberg ME (1998) Ca²⁺ influx regulates BDNF transcription by a CREB family transcription factor-dependent mechanism. *Neuron* 20:709-726.
- Tepper JM, Bolam JP (2004) Functional diversity and specificity of neostriatal interneurons. *Current opinion in neurobiology* 14:685-692.
- Thoenen H (1995) Neurotrophins and neuronal plasticity. *Science* 270:593-598.
- Thomson AM (2010) Neocortical layer 6, a review. *Front Neuroanat* 4:13.
- Tieu K (2011) A guide to neurotoxic animal models of Parkinson's disease. *Cold Spring Harb Perspect Med* 1:a009316.

- Todd AJ, Hughes DI, Polgar E, Nagy GG, Mackie M, Ottersen OP, Maxwell DJ (2003) The expression of vesicular glutamate transporters VGLUT1 and VGLUT2 in neurochemically defined axonal populations in the rat spinal cord with emphasis on the dorsal horn. *The European journal of neuroscience* 17:13-27.
- Tovote P, Esposito MS, Botta P, Chaudun F, Fadok JP, Markovic M, Wolff SB, Ramakrishnan C, Fenno L, Deisseroth K, Herry C, Arber S, Luthi A (2016) Midbrain circuits for defensive behaviour. *Nature* 534:206-212.
- Tranzer JP, Thoenen H (1968) An electron microscopic study of selective, acute degeneration of sympathetic nerve terminals after administration of 6-hydroxydopamine. *Experientia* 24:155-156.
- Tranzer JP, Thoenen H (1973) Selective destruction of adrenergic nerve terminals by chemical analogues of 6-hydroxydopamine. *Experientia* 29:314-315.
- Tritsch NX, Sabatini BL (2012) Dopaminergic modulation of synaptic transmission in cortex and striatum. *Neuron* 76:33-50.
- Tritsch NX, Ding JB, Sabatini BL (2012) Dopaminergic neurons inhibit striatal output through non-canonical release of GABA. *Nature* 490:262-266.
- Tsiola A, Hamzei-Sichani F, Peterlin Z, Yuste R (2003) Quantitative morphologic classification of layer 5 neurons from mouse primary visual cortex. *The Journal of comparative neurology* 461:415-428.
- Unger TJ, Calderon GA, Bradley LC, Sena-Esteves M, Rios M (2007) Selective deletion of Bdnf in the ventromedial and dorsomedial hypothalamus of adult mice results in hyperphagic behavior and obesity. *The Journal of neuroscience : the official journal of the Society for Neuroscience* 27:14265-14274.
- Ungerstedt U (1968) 6-Hydroxy-dopamine induced degeneration of central monoamine neurons. *Eur J Pharmacol* 5:107-110.
- Ungerstedt U, Arbuthnott GW (1970) Quantitative recording of rotational behavior in rats after 6-hydroxy-dopamine lesions of the nigrostriatal dopamine system. *Brain Res* 24:485-493.
- van Praag H, Christie BR, Sejnowski TJ, Gage FH (1999) Running enhances neurogenesis, learning, and long-term potentiation in mice. *Proceedings of the National Academy of Sciences of the United States of America* 96:13427-13431.
- Veening JG, Cornelissen FM, Lieven PA (1980) The topical organization of the afferents to the caudatoputamen of the rat. A horseradish peroxidase study. *Neuroscience* 5:1253-1268.
- Venero JL, Vizuete ML, Revuelta M, Vargas C, Cano J, Machado A (2000) Upregulation of BDNF mRNA and trkB mRNA in the nigrostriatal system and in the lesion site following unilateral transection of the medial forebrain bundle. *Experimental neurology* 161:38-48.
- Voelker CC, Garin N, Taylor JS, Gahwiler BH, Hornung JP, Molnar Z (2004) Selective neurofilament (SMI-32, FNP-7 and N200) expression in subpopulations of layer V pyramidal neurons in vivo and in vitro. *Cereb Cortex* 14:1276-1286.
- Voorn P, Vanderschuren LJ, Groenewegen HJ, Robbins TW, Pennartz CM (2004) Putting a spin on the dorsal-ventral divide of the striatum. *Trends Neurosci* 27:468-474.
- Walaas SI, Greengard P (1984) DARPP-32, a dopamine- and adenosine 3':5'-monophosphate-regulated phosphoprotein enriched in dopamine-innervated brain regions. I. Regional and cellular distribution in the rat brain. *The Journal of neuroscience : the official journal of the Society for Neuroscience* 4:84-98.
- Wang HY, Undie AS, Friedman E (1995) Evidence for the coupling of Gq protein to D1-like dopamine sites in rat striatum: possible role in dopamine-mediated inositol phosphate formation. *Mol Pharmacol* 48:988-994.
- Watts C, Dunnett SB, Rosser AE (1997) Effect of embryonic donor age and dissection on the DARPP-32 content of cell suspensions used for intrastriatal transplantation. *Experimental neurology* 148:271-280.
- Weber M, Chang WL, Breier MR, Yang A, Millan MJ, Swerdlow NR (2010) The effects of the dopamine D2 agonist sumanirole on prepulse inhibition in rats. *Eur Neuropsychopharmacol* 20:421-425.

- Webster KE (1961) Cortico-striate interrelations in the albino rat. *J Anat* 95:532-544.
- Weidberg H, Shpilka T, Shvets E, Abada A, Shimron F, Elazar Z (2011) LC3 and GATE-16 N termini mediate membrane fusion processes required for autophagosome biogenesis. *Dev Cell* 20:444-454.
- Weinrich M, Wise SP (1982) The premotor cortex of the monkey. *The Journal of neuroscience : the official journal of the Society for Neuroscience* 2:1329-1345.
- West MO, Carelli RM, Pomerantz M, Cohen SM, Gardner JP, Chapin JK, Woodward DJ (1990) A region in the dorsolateral striatum of the rat exhibiting single-unit correlations with specific locomotor limb movements. *J Neurophysiol* 64:1233-1246.
- Wetmore C, Ernfors P, Persson H, Olson L (1990) Localization of brain-derived neurotrophic factor mRNA to neurons in the brain by in situ hybridization. *Experimental neurology* 109:141-152.
- Wickens JR, Reynolds JN, Hyland BI (2003) Neural mechanisms of reward-related motor learning. *Current opinion in neurobiology* 13:685-690.
- Wiese S, Jablonka S, Holtmann B, Orel N, Rajagopal R, Chao MV, Sendtner M (2007) Adenosine receptor A2A-R contributes to motoneuron survival by transactivating the tyrosine kinase receptor TrkB. *Proceedings of the National Academy of Sciences of the United States of America* 104:17210-17215.
- Wilson NR, Kang J, Hueske EV, Leung T, Varoqui H, Murnick JG, Erickson JD, Liu G (2005) Presynaptic regulation of quantal size by the vesicular glutamate transporter VGLUT1. *The Journal of neuroscience : the official journal of the Society for Neuroscience* 25:6221-6234.
- Wise SP, Jones EG (1977) Cells of origin and terminal distribution of descending projections of the rat somatic sensory cortex. *The Journal of comparative neurology* 175:129-157.
- Yan Q, Radeke MJ, Matheson CR, Talvenheimo J, Welcher AA, Feinstein SC (1997a) Immunocytochemical localization of TrkB in the central nervous system of the adult rat. *The Journal of comparative neurology* 378:135-157.
- Yan Q, Rosenfeld RD, Matheson CR, Hawkins N, Lopez OT, Bennett L, Welcher AA (1997b) Expression of brain-derived neurotrophic factor protein in the adult rat central nervous system. *Neuroscience* 78:431-448.
- Yan Z, Feng J, Fienberg AA, Greengard P (1999) D(2) dopamine receptors induce mitogen-activated protein kinase and cAMP response element-binding protein phosphorylation in neurons. *Proceedings of the National Academy of Sciences of the United States of America* 96:11607-11612.
- Yee NS, Hsiau CW, Serve H, Vosseller K, Besmer P (1994) Mechanism of down-regulation of c-kit receptor. Roles of receptor tyrosine kinase, phosphatidylinositol 3'-kinase, and protein kinase C. *The Journal of biological chemistry* 269:31991-31998.
- Yin HH, Knowlton BJ (2006) The role of the basal ganglia in habit formation. *Nature reviews Neuroscience* 7:464-476.
- Yu PY, Eisner GM, Yamaguchi I, Mouradian MM, Felder RA, Jose PA (1996) Dopamine D1A receptor regulation of phospholipase C isoform. *The Journal of biological chemistry* 271:19503-19508.
- Yung KK, Bolam JP, Smith AD, Hersch SM, Ciliax BJ, Levey AI (1995) Immunocytochemical localization of D1 and D2 dopamine receptors in the basal ganglia of the rat: light and electron microscopy. *Neuroscience* 65:709-730.
- Zakiewicz IM, Bjaalie JG, Leergaard TB (2014) Brain-wide map of efferent projections from rat barrel cortex. *Front Neuroinform* 8:5.
- Zarranz JJ, Alegre J, Gomez-Esteban JC, Lezcano E, Ros R, Ampuero I, Vidal L, Hoenicka J, Rodriguez O, Atares B, Llorens V, Gomez Tortosa E, del Ser T, Munoz DG, de Yebenes JG (2004) The new mutation, E46K, of alpha-synuclein causes Parkinson and Lewy body dementia. *Ann Neurol* 55:164-173.
- Zhai S, Tanimura A, Graves SM, Shen W, Surmeier DJ (2018) Striatal synapses, circuits, and Parkinson's disease. *Current opinion in neurobiology* 48:9-16.
- Zhang MD, Barde S, Yang T, Lei B, Eriksson LI, Mathew JP, Andreska T, Akassoglou K, Harkany T, Hokfelt TG, Terrando N (2016) Orthopedic surgery modulates neuropeptides and BDNF

- expression at the spinal and hippocampal levels. *Proceedings of the National Academy of Sciences of the United States of America* 113:E6686-E6695.
- Zhou QY, Grandy DK, Thambi L, Kushner JA, Van Tol HH, Cone R, Pribnow D, Salon J, Bunzow JR, Civelli O (1990) Cloning and expression of human and rat D1 dopamine receptors. *Nature* 347:76-80.
- Zuccato C, Ciammola A, Rigamonti D, Leavitt BR, Goffredo D, Conti L, MacDonald ME, Friedlander RM, Silani V, Hayden MR, Timmusk T, Sipione S, Cattaneo E (2001) Loss of huntingtin-mediated BDNF gene transcription in Huntington's disease. *Science* 293:493-498.

8. Appendix

8.1 Table of figures

Fig. 1	The basal ganglia circuit	10
Fig. 2	Projections of the Direct and Indirect pathway in mouse Striatum	17
Fig. 3	DRD1 & DRD2 mediate different modes of PKA activity	19
Fig. 4	DRD1 & DRD2 mediated PLC (β) signaling cascade	21
Fig. 5	Striatal LTP induction	24
Fig. 6	Hypothetic - DRD1 & DRD2 mediated TrkB trafficking in striatal MSNs	25
Fig. 7	Hypothetic model of synaptic connectivity on striatal medium spiny neurons	27
Fig. 8	Hypothetic model of LTP induction on striatal medium spiny neurons	29
Fig. 9	Technical setup for semi-dry and wet-blotting	59
Fig. 10	BDNF antibody specificity verification	83
Fig. 11	Optimization of BDNF-IR in hippocampus at different ages	84
Fig. 12	Evaluation of BDNF and Myc-IR in hippocampus (CA3)	85
Fig. 13	Evaluation of BDNF and Myc-IR in hippocampus (Dentate Gyrus)	86
Fig. 14	Cortico-Striatal projections	88
Fig. 15	Identification of cortical layers	90
Fig. 16	Verification of BDNF-IR in hippocampal mossy fibers of 3wk & 12wk old mice	91
Fig. 17	BDNF-IR in layer II/III neurons of primary (M1) and secondary (M2) motor cortex	93
Fig. 18	Quantification of BDNF-IR in layer V subcortical projection neurons of primary motor cortex (M1)	95
Fig. 19	Quantification of BDNF-IR in layer V subcortical projection neurons of secondary motor cortex (M2)	96
Fig. 20	Quantification of BDNF-IR in layer V and VI subcortical projection neurons of primary and secondary somatosensory cortex (SSp; SSs)	97
Fig. 21	Quantification of BDNF-IR in subcortical projection neurons of pre- and infralimbic cortex (PL; IL)	99
Fig. 22	Quantification of BDNF-IR in subcortical projection neurons in the Taenia Tecta (TT)	101
Fig. 23	Overview about the number of BDNF expressing cells in mouse neocortex	102
Fig. 24	BDNF-IR specificity in striatum	105
Fig. 25	Confocal analysis of BDNF expression in glutamatergic corticostriatal afferences	106
Fig. 26	Structural Illumination (SIM) analysis of BDNF expression in glutamatergic vs dopaminergic afferences	110
Fig. 27	BDNF expression in midbrain dopaminergic neurons	111
Fig. 28	Verification of TrkB antibody specificity I	116
Fig. 29	Verification of TrkB antibody specificity II	117
Fig. 30	Verification of TrkB antibody specificity III	120
Fig. 31	Unilateral 6-OHDA lesion in adult rats	123

Fig. 32	TrkB forms intracellular aggregates in the absence of dopamine	125
Fig. 33	TrkB-FL is the main component of intracellular aggregates	126
Fig. 34	TrkB-FL aggregates occur in direct pathway MSNs	130
Fig. 35	Simplified model of the secretory and endocytic pathways	131
Fig. 36	TrkB aggregates do not localize to compartments of the secretory pathway	133
Fig. 37	TrkB aggregates suggest false recycling and receptor degradation	134
Fig. 38	Quantification of TrkB aggregates at 2wk, 4wk, and 16wk after induction of the 6-OHDA lesion	139
Fig. 39	Concentration of striatal MSNs in primary cell culture	143
Fig. 40	DRD1-EGFP and DRD2-EGFP mice <i>in vivo</i> expression analysis	144
Fig. 41	Newborn DRD1-EGFP mice fail to express GFP mRNA	145
Fig. 42	FACS iMSNs are stable in culture and reveal a purity of ~80%	147
Fig. 43	FACS iMSNs express DARPP-32 and GFP <i>in vitro</i>	150
Fig. 44	FACS iMSNs express GAD65, Met-Enk, and DRD2, but no DRD1 mRNA <i>in vitro</i>	152
Fig. 45	Activation of DRD2 decreases TrkB surface expression <i>in vitro</i>	154
Fig. 46	Maximum TrkB surface expression is already acquired under steady-state conditions <i>in vitro</i>	155
Fig. 47	Transactivation of TrkB after stimulation of DRD2 in iMSNs <i>in vitro</i>	160
Fig. 48	Hypothetic model of GPCR mediated TrkB surface expression in striatal MSNs	174

8.2 Table of tables

Tab. 1	List of genotyping primers	43
Tab. 2	List of qRT-PCR primers	44
Tab. 3	Preparation of standard-curve BSA samples	56
Tab. 4	Dilution of standard-curve BSA samples in "working reagent" for photometer analysis	57
Tab. 5	qRT-PCR program for amplification of GAPDH	70
Tab. 6	qRT-PCR program for amplification of GFP	71
Tab. 7	qRT-PCR program for amplification of mouse TrkB	72
Tab. 8	qRT-PCR program for amplification of mouse TrkB T1	72
Tab. 9	qRT-PCR program for amplification of rat TrkB	73
Tab. 10	PCR program for verification of Cre transgene	74
Tab. 11	PCR program for verification of BDNF k.o. knockin	75
Tab. 12	PCR program for verification of floxed BDNF	76
Tab. 13	PCR program for verification of Cre mediated recombination	76
Tab. 14	PCR program for verification of BDNF-myc	77
Tab. 15	PCR program for verification of TrkB ^{-/-}	78
Tab. 16	PCR program for verification of DRD1-EGFP	79
Tab. 17	PCR program for verification of DRD1-Td-Tomato	79
Tab. 18	PCR program for verification of DRD2-EGFP	80

8.3 Abbreviations

6-OHDA	6-Hydroxydopamine
A2aR	Adenosine 2a receptor
AA	Amino Acid
AC-1	Adenylyl-cyclase 1
AC	Anterior cingulate cortex
AI	Agranular insular area
Akt	Akt kinase / Protein kinase B
AMPA-R	α -amino-3-hydroxy-5-methyl-4-isoxazolepropionic acid receptor
APS	Ammonium persulfate
ATP	Adenosine-tri-phosphate
Aud	Ventral auditory area
BDNF	Brain-derived neurotrophic factor
BSA	Bovine-serum-albumin
CAMKII	Ca ²⁺ /calmodulin-dependent protein kinase II
cAMP	Cyclic adenosine monophosphate
c-Fos	Fos Proto-Oncogene, AP-1 Transcription Factor Subunit
cDNA	Complementary DNA
CNS	Central nervous system
Cre	Cre (cyclic) recombinase
CREB	cAMP response element-binding protein
CTIP-2	B-Cell CLL/Lymphoma 11B (Zinc Finger Protein)
CTX (IL)	Infralimbic cortex
CTX (M1)	Primary motor cortex
CTX (M2)	Secondary / supplementary motor cortex
CTX (PL)	Prelimbic cortex
CTX (S)	Somatosensory cortex
Cux1 / CDP	Cut Like Homeobox 1
DAG	Diacylglycerol
DARPP-32	Dopamine and cAMP-regulated phosphoprotein of 32kDa
dNTP	Nucleoside triphosphate
DP	Dorsal peduncular area
DRD1	Dopamine-receptor 1
DRD2	Dopamine-receptor 2
Ect	Ectorhinal cortex
EGF-R	Epidermal growth factor receptor
EGFP	Enhanced green fluorescent protein
ELISA	Enzyme-linked immunosorbent assay
ER	Endoplasmatic reticulum
FISH	Fluorescence <i>in situ</i> hybridization
FOXO1	Forkhead Box Protein O1A
GAD65	Glutamic acid decarboxylase (65kDa)
GAD67	Glutamic acid decarboxylase (67kDa)
GFAP	Glial fibrillary acidic protein (
GM130	Golgin subfamily A member 2
GPCR	G protein-coupled receptor
GP(e)	Globus Pallidus - external segment

GP(i)	Globus Pallidus - internal segment
GU	Gustatory areas
HA	Hemagglutinin
GFP	Green fluorescent protein
HBSS	Hanks Balanced Salt Solution
HRP / POD	Horse-raddish-peroxidase
ICC	Immunocytochemistry
IHC	Immunohistochemistry
IF	Immunofluorescence
IP	Immunoprecipitation
IP ₃	inositol 1,4,5-trisphosphate
kb	Kilo-bases
kDa	Kilo Dalton
k.o.	Knock out
l	liter
LC-3B	Microtubule-associated proteins 1A/1B light chain 3B
LTD	Long-term depression
LTP	Long-term potentiation
M	Molar
m	Milli
μ	Micro
M4R	Muscarinic acetylcholine receptor M4
Map2	Microtubule-associated protein 2
MAPK	Mitogen-activated protein kinase
Met-Enk	Methionine-Enkephalin
min	Minute
mRNA	Messenger ribonucleic acid
MSN	Medium spiny neuron
n	Nano
NF-L	Neurofilament light chain
NB-medium	Neurobasal medium
NMDA-R	N-methyl-D-aspartate receptor
NT	Neurotrophin
OD	Optical density
ORBI	Orbital area
P	Postnatal (day)
p	Phospho
PBS	Phosphate buffered saline
PCR	Polymerase chain reaction
Peri	Perirhinal cortex
PFA	Paraformaldehyde
PI3K	Phosphatidylinositol-4,5-bisphosphate 3-kinase
PIP ₂	Phosphatidylinositol 4,5-bisphosphate or PtdIns(4,5)P ₂
Pir	Piriform cortex
PLC-(β)	1-Phosphatidylinositol-4,5-bisphosphate phosphodiesterase beta-1
PKA	Protein kinase A
PP-1 / PP-2	Protein-phosphatase 1 or 2
Rab5	Ras-related protein Rab-5A
Rab7	Ras-related protein Rab-7A

RNA	Ribonucleic acid
RT	Room temperature
RT-PCR	Reverse transcription polymerase chain reaction
s	Second (time)
SHP-2	Protein-Tyrosine Phosphatase 2C
SDS	Sodium-dodecyl-sulfate
SDS-Page	Sodium-dodecyl-sulfate-polyacryl-amide-gel-electrophoresis
SNc	Substantia nigra pars compacta
SNr	Substantia nigra pars reticulata
Src	SRC Proto-Oncogene, Non-Receptor Tyrosine Kinase
SSp	Primary somatosensory cortex
SSs	Secondary somatosensory cortex
STR	Striatum
STN	Nucleus Subthalamicus
TA	Temporal association area
Tab	Table
TAE	Tris-acetate-EDTA
Taq	Thermophilus aquaticus
TGN-38	Trans-Golgi network integral membrane protein 2
Th	Thalamus
TH	Tyrosine-Hydroxylase
Tris	Tris-(hydroxymethyl)-aminomethane
Trk	Tyrosine receptor kinase
TT	Taenia Tecta
V	Volt
VGluT1	Vesicular Glutamate Transporter 1
VTA	Ventral tegmental area
WB	Western Blot
WT	Wild Type
%	Percent
°C	Degrees Celsius

9. Affidavit

I hereby confirm that my thesis entitled “Effects of dopamine on BDNF / TrkB mediated signaling and plasticity on cortico-striatal synapses” is the result of my own work. I did not receive any help or support from commercial consultants. All sources and/or materials applied are listed and specified in the thesis. Furthermore, I confirm that this thesis has not yet been submitted as part of another examination process, neither in identical nor in similar form.

Place, Date:

Signature:

Eidesstaatliche Erklärung

Hiermit erkläre ich ehrenwörtlich, dass ich die vorliegende Dissertation mit dem Titel "Effekte von Dopamin auf BDNF / TrkB vermittelte Signalwege und Plastizität an cortico-striatalen Synapsen", selbständig angefertigt und keine anderen, als die angegebenen Quellen und Hilfsmittelbenutzt habe. Desweiteren, habe ich keine Hilfe von kommerziellen Beratern oder dergleichen angenommen. Diese Dissertation hat weder in gleicher, noch in anderer Form, bereits in einem anderen Prüfungsverfahren vorgelegen. Desweiteren erkläre ich, dass ich früher, außer den, mit dem Zulassungsgesuch urkundlich vorgelegten Graden, keine weiteren akademischen Grade erworben, oder zu erwerben versucht habe.

Ort, Datum:

Unterschrift:

10. Curriculum Vitae

Personal data

Name:

Date of birth:

Place of birth:

Family status:

Nationality:

Parents:

Education:

Academic Studies:

Publications

11. Acknowledgments

I want to acknowledge the members of the Michael Sendtner lab at the Institute of Clinical Neurobiology and Prof. Dr. Michael Sendtner in particular, who gave me these and other projects and the opportunity to work in his lab. This was of extraordinary value, since the equipment and technical standards are outstanding, enabling me to learn any valuable molecular biological method. During the past 6 years, Prof. Sendtner understood to recognize my strengths and further taught me about my weaknesses. During the time as his Ph.D. student, I learned a lot about science and how successful projects are designed and conducted. I am most grateful for the lesson on how scientific work is organized, in order to work efficiently and achieve project landmarks. Thank you so much for all these years and for the opportunity to work together with you. I appreciate everything I learned from you and I am grateful for your support. Finally, I learned a lot about myself and about taking on responsibility. I would also like to thank the members of my thesis committee: Prof. Dr. Asan, Prof. Dr. Volkmann, and Prof. Dr. Förster. Special thanks go to you Esther, for continuously supporting and encouraging me, for valuable conversations and discussions about the projects. Thank you, Stephanie and Robert, for your input, technical support, and discussions about my ideas and problems I had in implementing them. I am grateful for your patience and respect and also for massive help with the BDNF ELISA and qRT-PCR analysis. I have to thank Dr. Patrick Lüningschrör, who helped me a lot with the troubleshooting, regarding Western Blot analysis and surface biotinylation. Thank you, Regine, Viktor, Sven, Richard and Verena for taking care of the mice, for supporting me and being patient with sudden changes in plans. Your work is the basis for everything I have done in this thesis. Thank you Michael Skoruppa for standing at my side during so many nights in the lab and for always making me laugh. I have to thank Lena for really encouraging me in the writing process, for proof-reading and for being the best neighbor one can have on a cell culture hood. And my gratitude to my fellow lab mates: Michael, Mehri, Manju, Cora, Benjamin, Gian-Luca, Hanaa, Christian, Annalena,

Amy, Dominique, Bhuvaneish and Simon. Thank you Urveen and Judita for so much help with bureaucracy and paperwork.

Thank you, Verena Surrey. You are one of the best human beings I have ever met. Thank you for all your support, your friendship, and your kindness. All we have experienced together will never be forgotten. I have to thank my parents, who I will always love, just as they love their children. Thank you for always supporting me, financial and mental, for never doubting, for always being confident and positive all these years. You can be sure, that both of your sons will always be your biggest fans.

I need to finally thank Linda. I have no idea, where I would be without you. You always supported me, helped and carried me. I love you for taking me as I am and being crazy with me. You are my idol, my best friend, my confidant and the love of my life.